INFORMATION TO USERS

This manuscript has been reproduced from the microfilm master. UMI films the text directly from the original or copy submitted. Thus, some thesis and dissertation copies are in typewriter face, while others may be from any type of computer printer.

The quality of this reproduction is dependent upon the quality of the copy submitted. Broken or indistinct print, colored or poor quality illustrations and photographs, print bleedthrough, substandard margins, and improper alignment can adversely affect reproduction.

In the unlikely event that the author did not send UMI a complete manuscript and there are missing pages, these will be noted. Also, if unauthorized copyright material had to be removed, a note will indicate the deletion.

Oversize materials (e.g., maps, drawings, charts) are reproduced by sectioning the original, beginning at the upper left-hand corner and continuing from left to right in equal sections with small overlaps.

Photographs included in the original manuscript have been reproduced xerographically in this copy. Higher quality 6" x 9" black and white photographic prints are available for any photographs or illustrations appearing in this copy for an additional charge. Contact UMI directly to order.

Bell & Howell Information and Learning
300 North Zeeb Road, Ann Arbor, MI 48106-1346 USA
800-521-0600

Fast Shape Memory Alloy Actuators

By

Serge R. Lafontaine

A thesis submitted to
the Faculty of Graduate Studies and Research
in partial fulfillment of the requirements for the degree of
Doctor of Philosophy

Department of Biomedical Engineering
McGill University, Montréal
July 1997

Acknowledgements

I wish to express my most sincere gratitude to my thesis director, Prof. Ian W. Hunter, who has been, through his enthusiasm for science and technology, a continuing source of intellectual stimulation. I have a countless number of times called on his expertise or his breadth of knowledge overlapping all major disciplines of science. He never failed to come up with unexpected and new solutions to technical problems. He has also allowed me to work in a unique research environment with the most extraordinary instrumentation resources.

I wish to express also my gratitude to Dr. L.A. Jones who has kindly proofread this manuscript. I would also like to express my gratitude to Dr. H.L. Galiana who has been a source of support and encouragement during undertaking and completion of this thesis.

I would like similarly to acknowledge the support of my colleagues Dr. Colin Brenan, John Madden and Peter Madden who kindly proofread this thesis.

Finally I would like to express my gratitude to funding agencies who have made this research possible, including the Medical Research Council of Canada, the Natural Sciences and Engineering Research Council of Canada, the IRIS Network of Centers of Excellence and the U.S. Office of Naval Research.

Abstract

In this thesis techniques for fabricating fast contracting and relaxing shape memory alloy (SMA) fibers are presented. Shape memory alloy fibers have demonstrated the largest stress and highest power to mass ratio of any known actuator technology. However their practical application has been plagued by three major drawbacks, namely: (1) relatively slow expansion of the material despite rapid contraction; (2) problems of mechanically and electrically connecting to the material due to the violent nature of their contractions; and (3) low efficiency in the conversion of electrical energy or heat into mechanical energy. The work associated with this thesis has led to solutions to the first two problems allowing even sub-millisecond contraction-expansion cycle times, and fibers to be attached via light weight but high strength and high conductivity joints. The properties of these fibers are extensively studied. Both linear and rotary actuators are built using these fibers.

A new technique is presented to mount nickel-titanium (NiTi) SMA fibers. NiTi alloys are not readily bonded, soldered, brazed or welded to other materials. The new method employs metal deposited on the fiber or between two fibers or between fibers and other parts, creating metallic attachments that are mechanically sound and electrically conductive. Furthermore a new process for the three-dimensional microfabrication by localized electrodeposition and etching has also been developed. This latter process, combined with the first process, can be used to integrate NiTi

alloys in micro-mechanisms. The good electrical contacts as well as mechanical contact provided by the new attachment mechanisms are important, since they allow the rapid methods to be employed.

Several apparatus were built to study the response of NiTi fibers, in particular to very fast current pulses. Experimental results were obtained to describe the response of the fibers, such as their speed, hysteresis, stiffness and resistivity, and show how these variables change dynamically as a function of time, temperature and stress. Other measurements important for the design of new actuators were done, such as those of efficiency when fast actuation with large current pulses is used.

In the third part of the thesis a novel application for fast fiber actuators is presented in the form of a fast rotary motor for in-the-wheel car rotary motors.

Résumé

Cette thèse présente des nouvelles méthodes pour préparer des fibres en alliage de mémoire de forme (AMF) en nickel-titane (NiTi) qui peuvent se contracter et se rallonger rapidement. Les fibres en alliages à mémoire de forme donnent de plus grandes déformations actives et un meilleur rapport de puissance à masse que tout autre actuateur connu. Toutefois leurs applications ont été à ce jour limittées à cause de trois problèmes majeurs: (1) leur lenteur à se rallonger bien qu'elles se contractent rapidement; (2) les difficultés à surmonter lors de l'attachement mécanique ou électrique dû à la nature violente de leur contraction et (3) leur grande inefficacité dans la convertion d'énergie électrique ou thermique en travail mécanique. Les travaux de recherche de cette thèse ont résultés en solutions aux deux premiers problèmes en permettant même des cycles de contraction et d'élongation de l'ordre du milliseconde, et permettant d'attacher les fibres par un matériel léger, robuste et conductif. Les propriétés de ces fibres sont étudiées en détail. Des actuateurs linéaires et moteurs rotatifs ont été construits également à partir de ces fibres.

Dans la première partie des travaux la technique pour attacher les fibres de nickel-titane est présentée. Les fibres en nickel-titane ne peuvent pas être facilement rattachées par brasage, cimentées, soudées ou fondues à d'autres matériaux. Cette nouvelle technique emploie une déposition de métal sur une fibre, entre deux fibres

ou encore entre des fibres et d'autres pièces, servant d'attachement métallique mécaniquement fiable et électriquement conductif. Un autre nouveau procédé pour réaliser la microfabrication de pièces de géométrie arbitraire en trois dimensions a aussi été conçu. Ce procédé combiné à la technique d'attachement des fibres de nickel-titane permettent la fabrication de micro-mécanismes mûs par des fibres d'alliage à mémoire de forme. Les contacts électriques de basse résistance et la faible masse des attachements permettent également de créer des actuateurs rapides de basse inertie.

Plusieurs montages expérimentaux sont décrits pour l'étude de la réponse des fibres de nickel-titane à des pulses de courant de courte durée et de haute intensité, en fonction du temps, des contraintes et des déformations. Les résultats expérimentaux décrivant les caractéristiques des fibres, tel leur élasticité, leur résistivité et leur hystérésis et comment ces variables changent en fonction du temps, de la température et des contraintes, sont donnés. D'autres mesures aussi sont faites, tel l'efficacité electro-mécanique des fibres lors de leur actuation par des pulses électriques de haute intensité.

Dans la dernière partie expérimentale de la thèse une application des fibres rapides est presentée sous la forme d'un moteur rotatif pour la réalisation de roues motrices pour automobiles. La dernière section traite de nouveaux algorithmes de contrôle basés sur la complexité stochastique conçu pour les applications où il est préférable de les utiliser comme actuateur à contrôle continu.

Preface

The manuscript-based format was chosen for this thesis. The first Chapter provides the general background that motivated the research, the rationale and objectives.

Chapter Two provides the background material and literature review. This chapter starts with a brief historical development of shape memory alloys. Next a general overview of shape memory alloys is included. The purpose is to provide some of the background material concerning relevant properties of shape memory alloys and techniques involved in their characterization. The last part consists of a literature review of applications.

Chapter Three presents a new technique to attach mechanically and electrically NiTi fibers in order to make light and reliable actuators and sensors. Chapter Four consists of a paper that details experimental work done to characterize and better understand Nickel-Titanium (NiTi) synthetic fibers. Chapter Five presents an application of these fibers in the form of a new rotary motor. Chapter Six consists of the conclusion and the bibliography.

This thesis partially consists of several articles that have been already published in scientific journals or that will be submitted shortly for publication. In addition two U.S. patents that have been obtained by the author are included in the thesis as well as one patent pending application. The following five paragraphs must

be included to notify the external examiner of the Faculty regulations under these circumstances:

> Candidates have the option of including, as part of the thesis, a text of a paper(s) submitted or to be submitted for publication, or the clearly-duplicated text of a published paper. These texts must be bound as an integral part of the thesis.
>
> If this option is chosen, **connecting text that provides logical bridges between the different papers are mandatory**. The thesis must be written in such a way that it is more than a mere collection of manuscripts; in other words, results of a series of papers must be integrated.
>
> The thesis must still conform to all other requirements of the "Guidelines for Thesis Preparation". **The thesis must include**: A Table of Contents, an abstract in English and French, an introduction which clearly states the rationale and objectives of the study, a comprehensive review of the literature, a final conclusion and summary, and a thorough bibliography or reference list.
>
> Additional material must be provided where appropriate (e.g. in appendices) and sufficient detail to allow a clear and precise

judgment to be made of the importance and originality of the research reported in the thesis.

In the case of manuscripts co-authored by the candidate and others, **the candidate is required to make an explicit statement in the thesis as to who contributed to such work and to what extent.** Supervisors must attest to the accuracy of such statements at the doctoral oral defense. Since the task of the examiners is made more difficult in these cases, it is in the candidate's interest to make perfectly clear the responsibilities of all the authors and the co-authored papers. **Under no circumstances can a co-author of any component of such a thesis serve as an examiner for that thesis.**

Pursuant to satisfying the above Faculty requirements, given below is a list of the articles included as part of this thesis with the responsibilities of each author detailed.

1. Hunter, I.W., Lafontaine, S. Shape memory alloy fibers having rapid twitch response, U.S. Patent 5,092,901, 1992.

Contributions of each co-author:

Serge Lafontaine participated in the experiments and in the initial discovery of the fast twitch response with Prof. Hunter. He designed with Prof. Hunter the

experimental protocol to measure and quantify the fast shape memory effect. He designed the VAX-VMS computer interface and data acquisition Application Programming Interface (API). He ran with Prof. Hunter the experiments to characterize the electro-mechanical characteristics of NiTi fibers and analyzed the data. He measured the two way shape memory effect of the fast twitch NiTi fibers.

Professor Ian Hunter initially discovered and identified the process to produce the NiTi fibers having rapid twitch response. He and Serge Lafontaine designed the experimental setup for the characterization of modified NiTi fibers. He designed with Serge Lafontaine the experimental protocol and he built and assembled the mechanical components for the experimental setup. He co-developed the data acquisition software with Serge Lafontaine and analyzed the data with Serge Lafontaine.

2. Hunter, I.W., Lafontaine, S. A comparison of muscle with artificial actuators, *Technical Digest of the Fifth IEEE Solid State Sensor & Actuator Workshop*, 1992, 5, 178-175.

Contributions of each co-author:

Serge Lafontaine wrote the manuscript in collaboration with Prof. Hunter. He collected most of the experimental data included in the manuscript with Prof. Hunter. He also derived the data required for the comparison of the various muscle like artificial actuators with Prof. Hunter from available published data. He assisted Prof.

Hunter in writing the manuscript for the section on muscle.

Professor Ian W. Hunter conceived this review paper of artificial muscle actuators. He completed most of the section pertaining to muscle, and wrote the other sections with the assistance of Serge Lafontaine.

3. Hunter, I.W., Lafontaine, S., Hollerbach, J.M. and Hunter P.J. Fast reversible NiTi fibers for use in microrobotics. *IEEE Micro Electro Mechanical Systems*, 1991.

Contributions of each co-author:

Serge Lafontaine participated in the experiments and in the discovery of the fast twitch response by Prof. Hunter. He co-designed the experimental protocol and procedure to characterize the electro-mechanical characteristics of NiTi fibers with Prof. Hunter. He developed the VAX-VMS real-time data acquisition driver and Application Programming Interface (API). He also participated in the development of the data acquisition and control program as well as data analysis and participated in the writing of the manuscript.

Professor Ian Hunter discovered the process for producing the NiTi fibers having rapid twitch response described in the paper. He and Serge Lafontaine co-designed the experimental setup for the characterization of modified NiTi fibers. He co-designed with Serge Lafontaine the experimental protocol and data analysis technique for measuring the response to electrical pulses and electro-mechanical

characteristics of the modified fibers. He co-developed the data acquisition software with Serge Lafontaine.

Professor John M Hollerbach participated in useful discussions.

Professor P.J. Hunter derived the mathematical theory for the suggested actuator.

4. Lafontaine, S., Hunter, I.W. and Madden, J.D. Method for joining mechanically and electrically parts made from NiTi shape memory alloys and other materials that are not readily joined with conventional techniques, U.S. Patent application, patent pending, 1997.

Contributions of each co-author:

Serge Lafontaine invented the method and reduced it to practice.

Professor Ian. W. Hunter served in his normal capacity as thesis director and research advisor.

John D. Madden assisted Serge Lafontaine in writing the original patent disclosure and to develop the claims.

5. Hunter, I.W., Lafontaine, S.R., Madden, J.D. *Three dimensional microfabrication by localized electrodeposition and etching*, U.S. Patent 5,641,391, 1997.

Contributions of each co-author:

Serge Lafontaine and Prof. Ian Hunter reduced to practice the original 3D microfabrication process. He participated in the development of the experimental setup to verify the procedure and conducted the initial experiments in conjunction with Prof. Hunter.

Professor Ian W. Hunter invented the original process of using a micropipette as an electrode and as a means to enhance locally electrodeposition by ejecting a continuous stream of electrolyte through the tip of the micropipette. He reduced the invention to practice with the assistance of Serge Lafontaine.

John D. Madden extended the 3D microfabrication process to the situation where the tip of a metal micro-electrode is used to produce the confined electro-deposition. He also developed a finite element model of the process. He wrote the patent application.

6. Lafontaine, S., Stein, R.B. and Hunter, I.W. Experimental Study of Fast Contracting NiTi Fibers, to be submitted.

Contributions of each co-author:

Serge Lafontaine developed the various experimental apparatus used in this study together with Prof. Hunter. He also co-developed with Prof. Hunter the experimental protocol to characterize the NiTi fibers. He implemented all of the computer interfaces and data acquisition API's. He conducted most

of the experiments in collaboration with Prof. Hunter and Prof. He wrote the manuscript in collaboration with Dr. Stein. He completed by himself the resistivity measurements for the development of NiTi thermocouples.

Prof. R.B. Stein participated in the experiments and data analysis with Prof. Hunter and Serge Lafontaine. He wrote the first draft of the manuscript, which was then completed by Serge Lafontaine.

Prof. Ian W. Hunter co-developed the various experimental apparatus used in this study in conjunction with Serge Lafontaine. In his capacity as research director he developed the experimental protocol in consultation with Serge Lafontaine and R.B. Stein. He participated in the data acquisition as well as data analysis. He programmed a graphical user interface for the experimental control and data acquisition in collaboration with Serge Lafontaine.

7. Lafontaine, S., Cai, K. and Hunter, I.W. Temperature dependence of NiTi fiber impedance. 18th Canadian Medical and Biological Engineering Conference, 1992.

Contributions of each co-author:

Serge Lafontaine built the experimental setup in collaboration with Prof. Ian Hunter and K. Cai, wrote the data acquisition programs, developed the computer interface, carried the experiments, analyzed the data and wrote the article.

Kunbao Cai participated in building the experimental setup.

Professor Ian W. Hunter designed the mechanical setup,

overviewed and participated in its construction. In his normal capacity as thesis research director he defined in collaboration with Serge Lafontaine the experimental protocol and data analysis.

8. Lafontaine, S., Hunter, I.W., Jones, L.A. NiTi artificial muscles for micro-robotics and medical applications, *Proc. IA-SMA*, 1994, Quebec, Canada.

Contributions of each co-author:

Serge Lafontaine wrote the manuscript, which is an overview of the research projects involving NiTi shape-memory and super-elastic alloys.

Professor Ian W. Hunter served in his normal capacity as thesis director and research director of the various projects described in this article.

Dr. L.A. Jones proofread the manuscript and served in her normal role as principal researcher involved in projects described in the article.

Table of Contents

Table of Figures

Table of Tables

Table of Plates

Chapter 1 Introduction

This thesis deals with synthetic muscle actuator technologies with a focus on Nickel-Titanium (NiTi) artificial muscle actuators. It became clear after an extensive survey of current motor technologies that the lack of high-performance motors is one problem that limits the development of robotic devices (Hollerbach *et al.*, 1991; Hunter and Lafontaine, 1992a; Hunter *et al.*, 1991). This is also one of the main reasons why paraplegics and lower-extremity amputees still have to move in wheelchairs instead of walking with powered artificial limbs. Current motors cannot generate enough power per unit mass and enough force per unit cross-sectional area to be concealed in an artificial limb that could then actively assist in climbing stairs. It was realized after this study that NiTi fibers could fulfill this role.

Nature has developed an actuator that is used throughout the animal kingdom. Muscle fibers are nearly identical in size from the mouse to the elephant, and were developed over 300 million years ago. Their architecture is highly scalable, that is muscles consist of fibers where more fibers are used in parallel for greater force or in series for longer displacement.

In this thesis the term synthetic actuator technologies does not refer to artificial muscles that could be surgically implanted in humans or animals to replace defective muscles, but instead to a modular actuator technology in which actuators are built from smaller actuators that can be arranged in series or in parallel. The actuators consist of

individual fibers that are made from individual contractile wires, strands, ribbons or films. The synthetic muscles described in this thesis consist of individual NiTi fibers. In almost all cases, only one fiber will be used for actuation purposes. These fibers can be attached to elastic materials at either end, just as muscle fibers attach to tendons, to store energy and to protect them from rapid movements. Similarly to muscle, which include proprioceptors such as spindle receptors and Golgi tendon organs, synthetic muscles could include position and force sensors. These sensors would ideally be built from a similar class of materials.

1.1 Muscle as an Actuator

Whole muscles consist of bundles of muscle fibers. Each muscle fiber is a single cell which can be dissected and maintained in a functional state (alive) in isolation from its parent whole muscle. In comparison with other actuators, muscle cells are all basically of the same design although there are significant differences in performance (e.g., force rise-time and contraction velocity), resulting from small variations in the molecular components, architecture and kinetics.

Mammalian muscle may be broadly separated into two categories: striated and smooth. Smooth muscles are to be found controlling the diameter of various tubes (e.g., veins, arteries, colon, intestines, and the pupil in the eye). Striated muscles (so called because of the sarcomere striations readily apparent under a microscope) may be further divided into two types, cardiac and skeletal. As the name suggests, cardiac muscle is the

actuator from which the heart, a large pump, is constructed. Skeletal muscle is the actuator which drives all limbs as well as the eye, tongue and chest (for breathing).

A whole skeletal muscle is a bundle of parallel muscle fibers held together by connective tissue. Nerve fibers, blood and lymphatic vessels weave their way throughout the whole muscle. These vessels can lie beside but never inside muscle fibers. The connective tissue (collagen) at the ends of each muscle fiber join together to form the whole muscle tendon which in turn attaches to bone or fascia (connective tissue). The force generated by muscle fibers is transmitted via the tendons to the bones where it appears as a torque about some joint. If the joint torque generated by a muscle is greater than opposing torques (which may result from external loads or from opposing (antagonist) muscles) then the limb will rotate about the joint. Thus contraction of muscles produces angular displacements of limbs about joints.

The muscle fibers in large muscles are long but the diameter of muscle fibers in small and large muscles is similar. The average muscle fiber diameter in a human adult is about 50 μm whereas 100 μm diameter frog muscle fibers are common. It seems that mammals do not grow more muscle fibers as they mature (or do weight lifting), but rather the average muscle fiber diameter increases. While isolated muscle fibers can reversibly contract by over 50% it seems that during normal limb movements they only contract by 10%.

A muscle fiber is a bundle of even smaller fibers called myofibrils, which are typically about 2 μm in diameter and extend from one end of the muscle fiber to the other. Myofibrils do not have membranes but are separated from each other by a

surrounding network of tubes and sacs. This network has two parts, the transverse tubules and the sarcoplasmic reticulum.

The sarcoplasmic reticulum (SR) is a network of tubes and sacs, which contain intra-cellular fluid having a high Ca^{++} concentration. The voltage pulse which turns on a muscle fiber (called a muscle action potential) travels along the muscle fiber outer membrane (sarcolemma) (at 3 to 5 m/s in typical human skeletal muscle) and down holes into the interior (t-tubules) (at a lower velocity) where it causes Ca^{++} to be released from the lateral sacs of the SR. The Ca^{++} diffuses into the adjacent myofibrils and turns on the contractile proteins. After the action potential has passed, the Ca^{++} is actively pumped back into the SR.

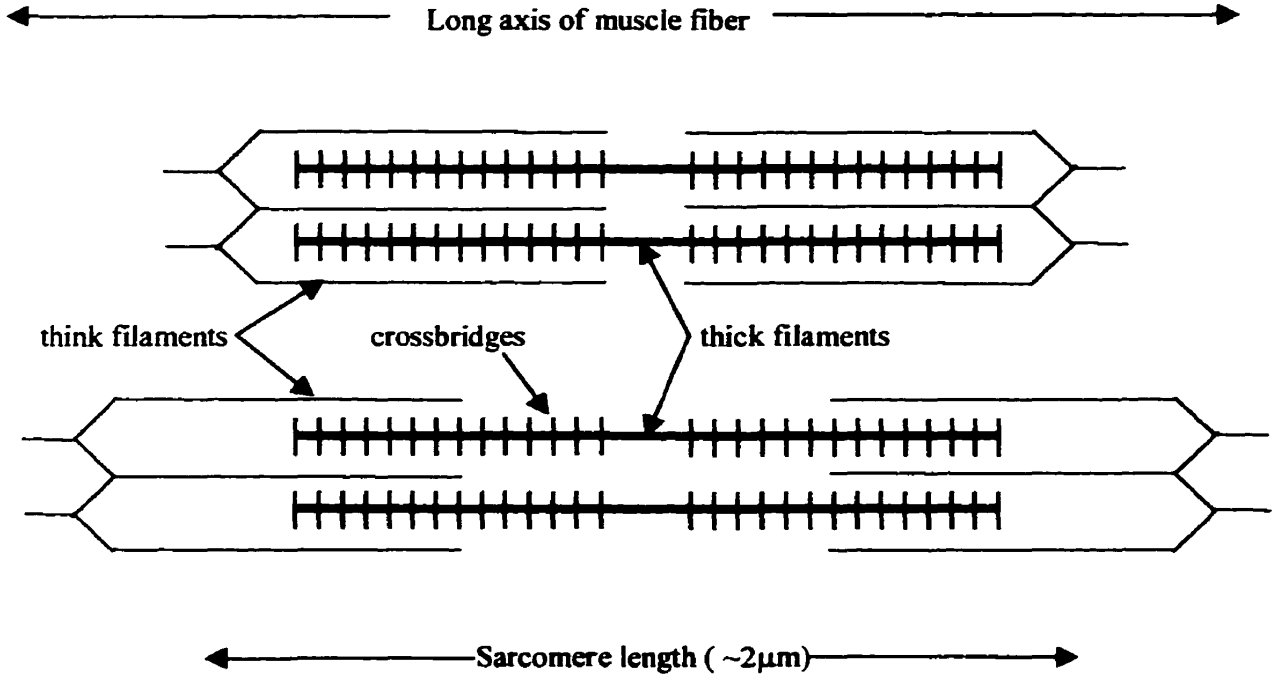

Figure 1.1 Myofilaments: The myofibril consists of a bundle of myofilaments. There are two types of myofilaments: the thin filament and the thick filament. The repeating organization of the thin and the thick filaments and the way they slide is shown here.

The myofibril is actually a bundle of even smaller fibers called myofilaments. There are two types of myofilaments, the thick and thin filaments. The thin filament consists largely of the proteins actin, troponin and tropomyosin. The thick filament consists mainly of the myosin protein. The repeating organization of the thick and thin filaments and the way they slide past one another is shown in Figure 1.1. The basic contractile unit of muscle is the sarcomere (see Figure 1.1) which in vertebrate muscle can vary in length from 1.5 to 3.6 μm with a rest length of about 2.2 μm.

The myosin protein has a large pair of heads, which protrude from the thick filament backbone. These myosin heads are called crossbridges because it appears that they reach across and attach to adjacent thin filaments during muscle contraction. There are about 300 myosin molecules per thick filament. The crossbridges periodically attach and detach from the thin filament during contraction (this is called the crossbridge theory of muscle contraction). Each crossbridge probably generates a force of about 1 pN (Ishijima *et al.*, 1991) and after a power stoke of about 12 nm (during which 1 ATP molecule is hydrolyzed) is dragged for at least 28 nm (Higuchi & Goldman, 1991). The rate of this crossbridge cycling appears to be more or less dependent on the type of muscle but it is also highly temperature dependent. For example a single myosin head appears to consume 5 ATP molecules/s during peak filament sliding at 2 m/s.

The muscle action potential (in turn generated by a single neural action potential) causes a burst of Ca^{++} to be released from the SR. The Ca^{++} binds to troponin, which in turn causes the tropomyosin molecule to "move" exposing sites on the actin chain, which attract the crossbridge. The crossbridge (initially charged with ATP (adenosine triphosphate)) rotates and generates force from the energy released as ATP splits into

ADP (adenosine diphoshate) and P_i (inorganic phosphate). The ADP and P_i are released from the crossbridge head. The crossbridge remains bound to the thin filament until an ATP molecule binds to the crossbridge head to start the cycle over again.

The number of crossbridges operating determines the total force generated by a muscle. However, the total number of crossbridges operating at a given instant is in turn dependent on the availability of an adjacent thin filament to which the thick filament can attach (as muscles are stretched the overlap of thick and thin filaments is progressively reduced) and on the availability of Ca^{++} to "turn on" the thin filament.

1.2 Synthetic Muscles

The synthetic muscles considered here are activated in a manner analogous to muscle fibers, which are activated by action potentials that travel along the nerves. Each action potential initiates one twitch response when it reaches the muscle fiber. Greater forces are obtained by summation in fibers if two or more action potentials arrive in succession, or by activating simultaneously a larger number of fibers. The control of synthetic muscle forces follows similar activation strategies.

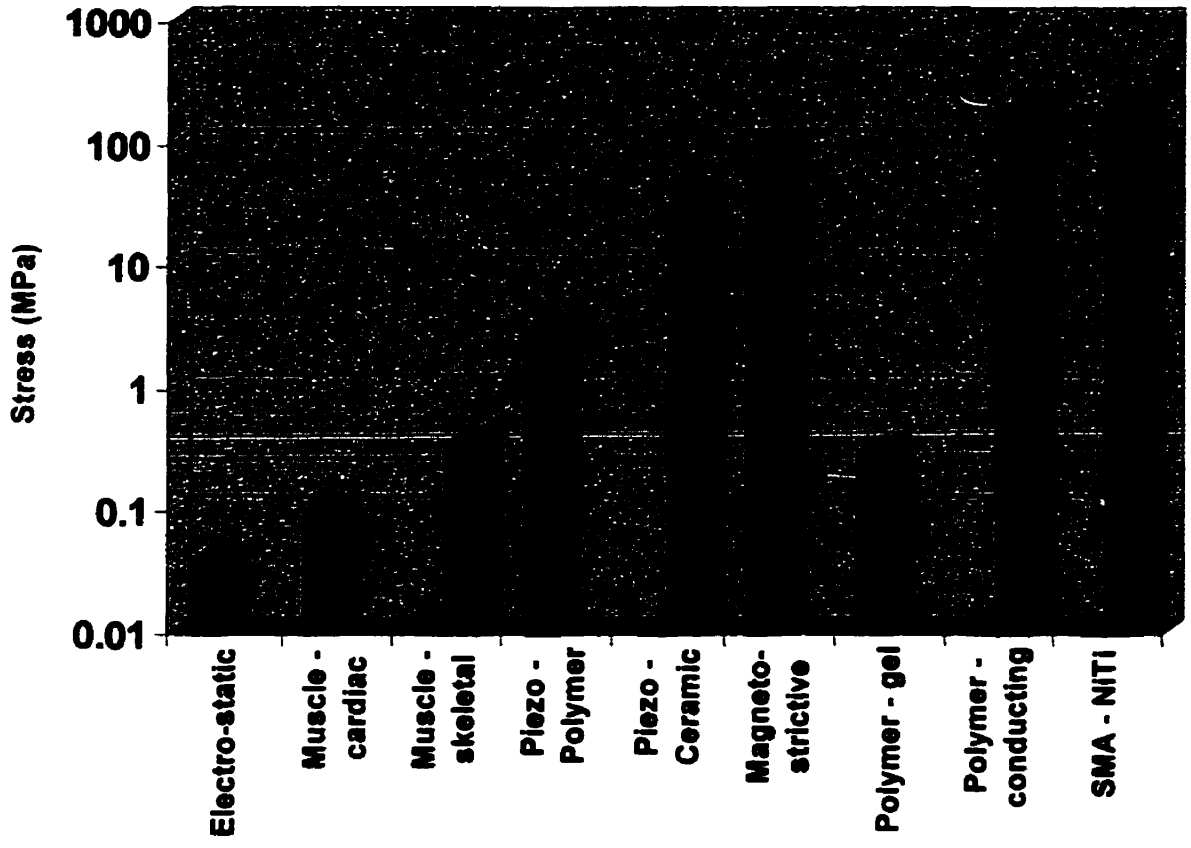

Figure 1.2 Peak stresses generated by muscle-like materials.

The actuator considered in this thesis contracts from changes in bulk material properties, which limits its contractions to approximately 8% of its total length (strain). A second limitation of the NiTi synthetic muscles is that their total lifetime, in terms of contractions that can be obtained before degradation of their response, is shortest for large contractions. This is a serious limitation for many, but not all applications. For example a micro-stepping actuator moving incrementally, using for example a ratcheting motion, can generate very great displacements, the total displacement being the sum of small strains generated by the fiber. The latter can be small, allowing long lifetimes.

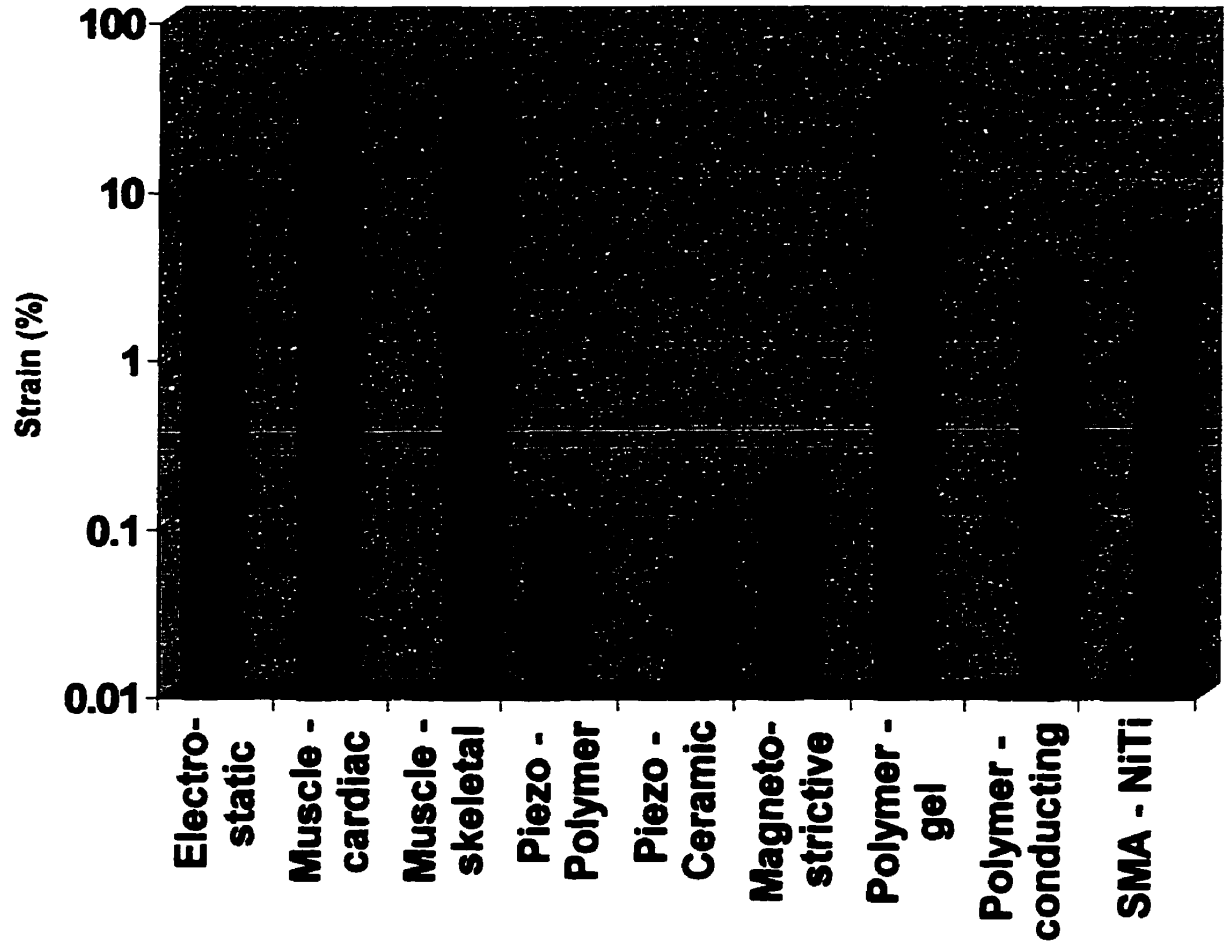

Figure 1.3 Maximum strains generated by muscle-like materials.

Before starting the work on NiTi artificial muscle presented here, a review of other actuator technologies that are in the form of contractile materials was completed (Hunter and Lafontaine, 1992a, included in Appendix II). The study results are summarized in Figure 1.2, Figure 1.3 and Figure 1.4. As can be seen particularly in Figure 1.2 and Figure 1.4 and Table 1 in Hunter and Lafontaine (1992a), muscle is a rather modest actuator. Furthermore, it cannot be used as a generator to convert mechanical energy back into electro-chemical energy. Only in some clam muscles is

there a catch state which allows it to maintain a static position without energy expenditure. Muscles on the other hand are environmentally clean, unlike several actuator technologies, such as the combustion engine, which release pollutants into the atmosphere and hydraulic engines, which regularly spill oil in the environment. Electric motors are "clean" but there is pollution created at the power plant. However, even if muscle is a rather modest actuator, its combination of high strain, power to mass, force per unit area, strain rate, efficiency and lifetime has been unmatched by any other actuator technology. Any other actuator technology, in order to be successful like muscle, should not be overly deficient in any of those areas.

From this study of new actuator technologies two materials became of interest: nickel-titanium (NiTi) shape memory alloys and electrically conducting polymers. NiTi alloys have almost reached the stage of being an engineering material that can be used in devices, although much remains to be done to improve their characteristics and understand how they operate. Figure 1.2 lists the stresses generated by each of the new materials considered. As can be immediately seen, NiTi fibers generate much larger forces per unit cross-sectional area than any other actuator technology, with the possible exception of conducting polymers (CP). NiTi fibers generate over 200 MPa, which exceeds by 600 times the largest forces per unit area that muscles can generate. Figure 1.3 lists the maximum strains that can be achieved for the same materials as a function of the number of cycles over which they can operate. The maximum recommended strain for NiTi alloys is 8% (15% for monocrystals) for this property. NiTi is second only to muscle. Figure 1.4 gives the maximum strain rates. NiTi alloys surpass by far the speeds achieved by all other materials.

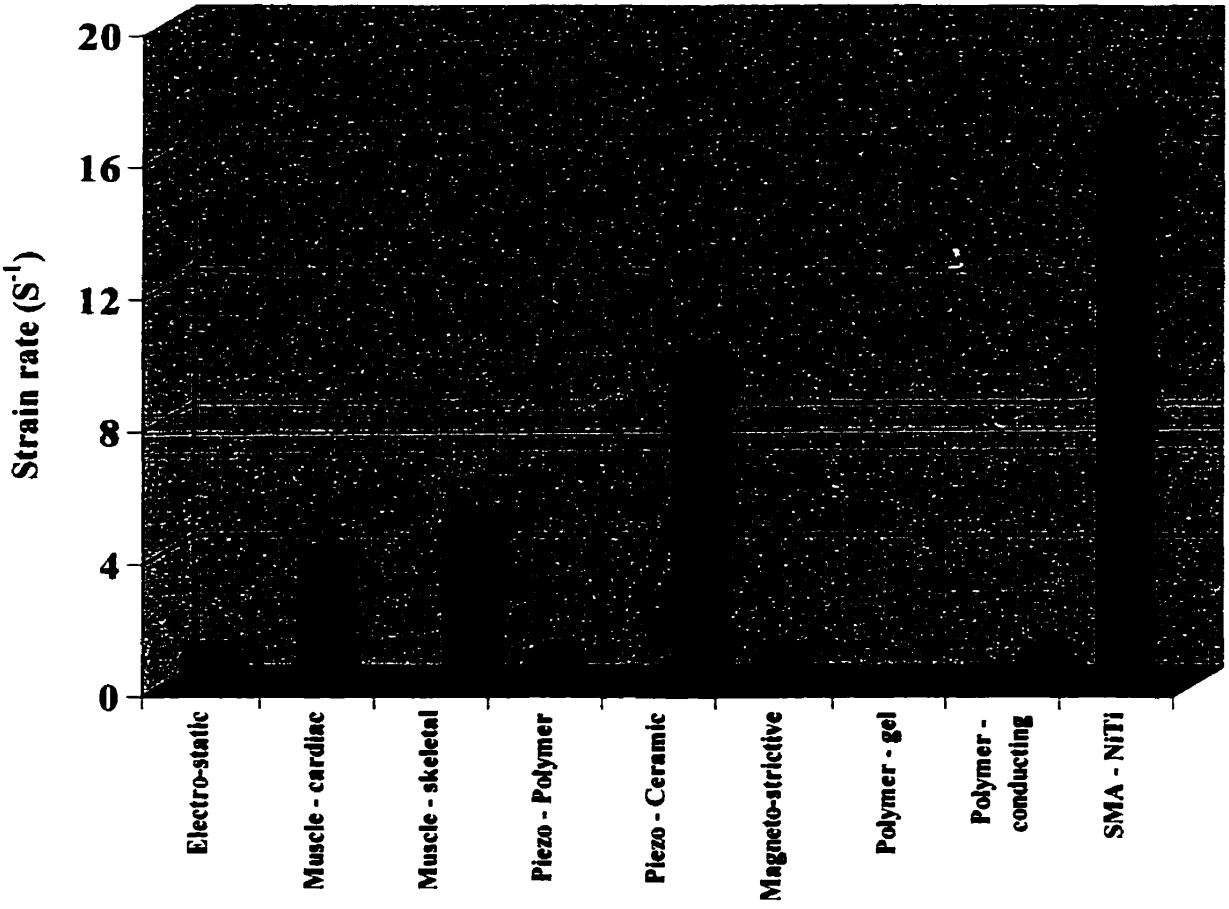

Figure 1.4 Maximum strain rates observed in muscle-like materials.

1.3 Limitations of NiTi Shape Memory Alloys

There are numerous limitations associated with using shape memory alloys that have to be taken into account in practical designs. One of their main shortcomings is their low efficiency as engines converting input energy, which can be delivered in different forms but normally results as heat in the fiber, into mechanical work. Shape memory alloy actuators are normally activated using Joule heating by passing an electrical current

through the fiber. In this case the efficiency is calculated as the ratio of work done by the fiber over the input electrical energy and it is found usually to be less than 3%. There might be in addition other losses (e.g. friction and acoustic) in the mechanism converting the mechanical work of the fiber when it contracts into useful mechanical action. However, there are numerous applications where efficiency is not a critical issue and where power is readily available. Furthermore, material research may lead to more efficient shape memory alloy actuators. Efficiencies over 5% have been measured in a new type of shape memory alloy which undergoes martensitic transformations through the application of a magnetic field (Ullakko *et al.*, 1997).

The second limitation is the useful number of contractions, active or passive, which can be achieved before the amplitude of the response decreases or failure occurs in the material. Figure 1.5 gives estimated limits for the shape memory effect in number of cycles from various sources. The lifetime however is also a function of the stress, which is not specified in Figure 1.5. The number of cycles depends on several factors such as the alloy used, the amount of strain and stress obtained in each contraction and the type of thermo-mechanical process used to achieve the final properties of the SMA. Therefore the numbers indicated in Figure 1.5 are only approximate guidelines and results may differ greatly from those. This limitation can be taken into account in system designs and circumvented in several ways. Redundancy or cycling through a number of fibers can be used in many situations given that the fibers can generate large forces per unit area and a number of them can be mounted in a small workspace. In many situations the cost of the shape memory material is relatively low compared to the final cost of the system in which they are used, and so a modular design can allow for easy replacement of the fibers

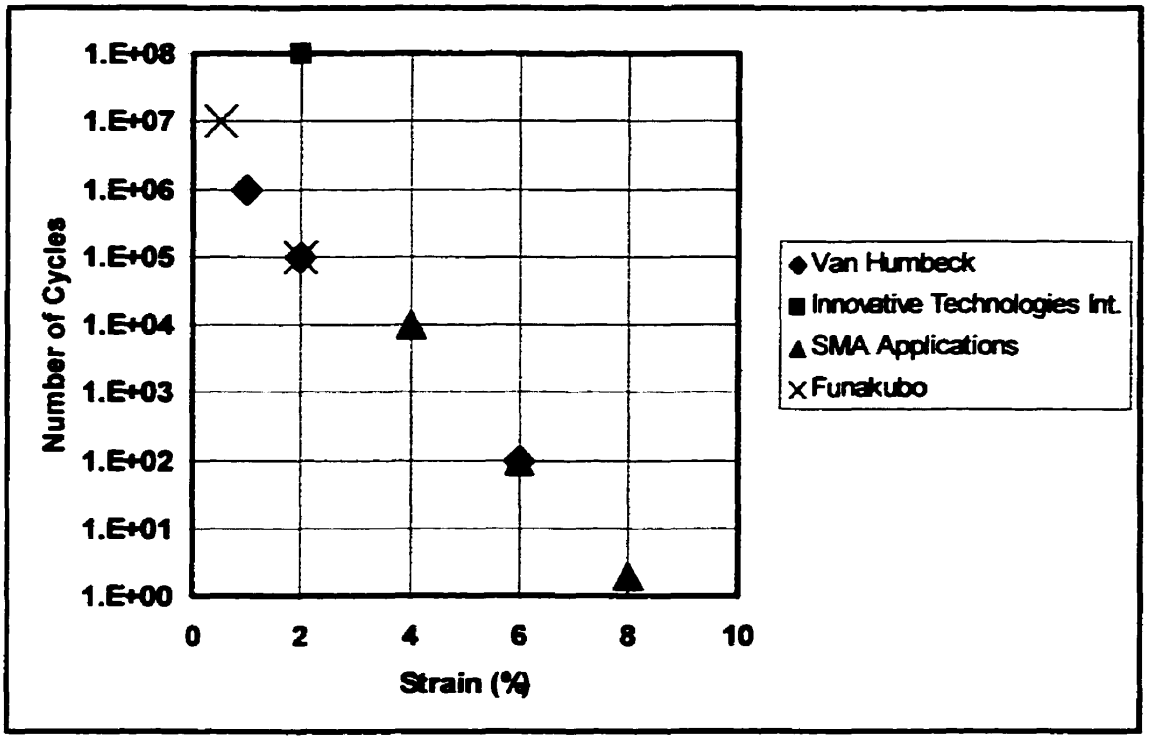

Figure 1.5 The number of complete phase transformation cycles that NiTi alloys will sustain before degradation of the shape memory effect or mechanical failure as a function of strain. The lifetime is also a function of the stress, which is unspecified, and actual results may vary considerably from those above. Data is from: (1) Van Humbeck *et al.* (1991); (2) Innovative Technology International; (3) SMA Applications Inc.; (4) Funakubo (1987).

when failure occurs. The cost of the fibers is small so that regular replacement is not usually an important consideration in the financial balance.

A third problem that occurs in using NiTi shape memory alloy fibers is the difficulty in attaching or mounting the fiber in a mechanism. It is very difficult to bond, solder, braze or weld NiTi fibers. The properties of the alloy depend critically on the exact relative concentrations of each element and any slight deviation results in very different material properties. Titanium is a highly reactive material that readily oxidizes. Soldering NiTi fibers to other materials usually results in a brittle interface due to the migration of atoms

at the interface or the oxidation of titanium and so joints readily break. It is possible using CO_2 laser welding to join together NiTi alloys, but the technique requires a fairly large laser power source. Clamps and screws normally used to attach metals and alloys rely on the forces produced by the elastic deformation of the material which is normally limited to 0.1% in most materials. Shape memory alloy materials will typically go through 8% dimensional changes when phase transformations occur and will readily release themselves from clamps and screws when they contract or will loosen their connection after a few cycles due the huge stresses generated from repeated contraction and expansion. The most commonly used technique to mount NiTi fibers consists of winding the fiber several times around an attachment to use the capstan effect such that the fiber tension itself increases the strength of the attachment.

A further problem with shape memory alloys is that they can be very fast when contracting but the relaxation speed is normally limited by the rate of heat dissipation from the fiber. The contraction process can occur in milliseconds when the fiber is quickly heated with large current pulses. In air, however, depending on the ratio of surface area to volume the relaxation will normally take several seconds in air. There have been a number of robotic hands and grippers developed with shape memory alloys but all of them are very limited in bandwidth (Iwata *et al.*, 1988; Kuribayashi, 1986; Mertmann *et al.*, 1995; Nakano *et al.*, 1984) due to the slow relaxation times. Heat dissipation can be enhanced by designing actuators with a number of small fibers that can dissipate heat more rapidly than larger fibers, by using water or other liquids for cooling, or by using thermal pumps such as Peltier devices for active cooling. A significant

contribution of this thesis deals with fibers having a fast twitch response where the material itself is modified so that it can both contract and expand rapidly.

The response of NiTi alloys to mechanical, electrical or thermal commands is highly nonlinear. The shape change occurs very rapidly over a very narrow temperature range and is difficult to control precisely. There is a hysteresis typically of 15 °C to 30 °C between the temperature at which the fiber contracts and the temperature at which expansion occurs. In addition, NiTi materials can go through one or two intermediate phases between austenite and the low-temperature martensite (Beyer, 1995). Each phase change occurs with a considerable latent heat and the martensitic transformations are highly exothermic. In all cases they generate work when contracting but no appreciable amount of mechanical work can be obtained from shape memory materials in the cooling process. In cases where only small forces and displacements are required there is an intermediate secondary phase transformation where the hysteresis is limited to approximately 1.5 °C where continuous control is more readily achieved. One objective of this thesis was to devise a control strategy for this particular situation. It is interesting to note that the response of NiTi fibers to short pulses is very similar to the twitch response of muscle fibers. Similar to muscle, precise control could be achieved in NiTi synthetic muscles by using control strategies similar to those used by nature to control muscles.

Because of the limitations outlined above, NiTi artificial muscle fibers are not the ideal actuators for robotics. However there are a number of applications where NiTi synthetic muscles are appropriate to use, in which efficiency is less important than achieving large forces in a restrained workspace, and where the lifetime of the fiber can

be compensated for by redundancy. These include a number of areas in medical tele-microrobotics, virtual reality, and the automotive industry. Shape memory materials are relatively new materials and have existed for only a short time compared to the combustion engine or the electric motor. As material science progresses, the properties of shape memory alloys will be improved and new ones will be developed.

New smart materials such as electrically conducting contractile polymers are one of the more promising actuator technologies of the future (Hunter and Lafontaine, 1992a; Madden *et al.*, 1997) not only for robotic and micro-robotic applications but also for energy storage, and information processing. It is also anticipated that the control issues will be very similar for the conducting polymer and NiTi artificial muscle technologies. Therefore any control and design advances made for NiTi devices may contribute to a faster development of the conducting polymer technology.

Two papers are included in Appendix II and Appendix III. These papers provide additional background material. The first one by Hunter and Lafontaine (Hunter and Lafontaine, 1992a) compares muscle-like actuators. The second one (Lafontaine *et al.*, 1993) overviews some applications.

1.4 Thesis Objectives

The main objective of this thesis was to develop fast shape memory alloy actuators. To this end, a new process has been developed to modify NiTi fibers so that they contract and elongate rapidly. A new technique for attaching the fibers has also been developed so that the added mass required to attach them is kept minimal. In order to

build fast micro-mechanisms using NiTi fibers, a new 3D micro-fabrication process has also been developed. It is also the objective of the thesis to study experimentally the response of NiTi fibers to large current pulses that are required to get the fast response of NiTi fibers.

Another objective of this thesis was to look at feedback control of fibers to make them useful for closed loop applications in micro-robotics. A systematic evaluation of properties that are useful for control of the fibers is done.

The final objective of this thesis was to develop a prototype of a rotary motor that could be used in automobiles. There is very little research being conducted on radically new technologies and concepts for car rotary engines. Most of the current research in the area consists of either replacing the combustion engine with an electric engine, improving the combustion engine or developing a hybrid system. A possible alternative could consist of cars using in-the-wheel rotary motors based on shape memory alloy fibers or electrically conducting polymer actuators. In this last chapter a rotary motor actuated by NiTi fibers is built and tested.

Chapter 2 Shape Memory Alloys

This chapter consists of a review of the discovery, development and applications of NiTi alloys. The second section provides an overview of shape memory materials and the third section consists of a literature review of previous applications of NiTi fibers in synthetic muscle-like actuators, rotary motors, and micro-mechanisms such as pumps and valves. The fourth section overviews some of the modeling attempts made in the past to represent NiTi shape memory materials in the form of fibers.

2.1 Brief History of Shape Memory Alloys

Arne Ölander reported the first observation of shape memory transformation in 1932 in a gold-cadmium (Au-Cd) alloy. He described the rubbery feeling of the alloy without actually observing the shape memory effect. Chang and Read discovered in 1951 that an alloy of gold and copper would return to its pre-deformed state when heated after deformation. A few years later Basinski and Christian (1954) observed the same effect in an indium-titanium alloy, as did Buehler *et al.* (1965) who worked with a nickel-titanium (50% Ni, 50%Ti) alloy. Otsuka and Shimizu (1970) showed that the shape memory effect was caused by a martensite to austenite phase transition. Numerous shape-memory-alloys (SMAs) have been studied since that time (Funakubo, 1987) with a predominant interest in NiTi alloys.

Following the discovery of NiTi alloys, a number of attempts were made to use them in practical applications (Duerig *et al.*, 1990; Funakubo, 1987; Gilbertson, 1994). NASA (Jackson, 1972) looked at their use for satellite antennas that would expand when exposed to the sun. NiTi alloys were also considered for a number of temperature controlled devices such as hot water pipe valves, greenhouse windows and automobile fan clutches. In 1974, Page and Sawyer patented an artificial heart using NiTi.

A number of experimental heat engines based on NiTi alloys have been developed (Duerig *et al.*, 1990; Funakubo, 1987; Gilbertson, 1994). R. Banks designed a sun-powered generator that was driven by an offset crank engine that ran for millions of cycles at 1 Hz (Zmuda, 1974). Cory invented a faster, scalable SMA thermal engine that was on the Chinese differential pulley (Cory, J.S., 1980). A small version of this was commercialized by the TiNi Alloy Company as the TiNi-1 Engine and it ran at 1000 RPM and generated 1 watt of power. McDonnell Douglas (McNichols, 1980) developed a 32 W engine based on 100 50 μm fibers. The rotary Banks engine developed by Glasauer and Müller (1996) based on NiTi fibers produced a torque of 15 N·m and revolved at 20 RPM.

Most of the applications described above did not go beyond the research stage due to the unreliable quality of the NiTi alloys and their low speed. In the early 1980s, Dai Homma developed an improved process for making NiTi fibers with a very uniform diameter and low deformation force (Gilbertson, 1994). The fibers were commercialized by Toki under the trade name of BioMetal. Using this material, Toki and Furukawa demonstrated many devices including a computer controlled six degrees of freedom robotic arm.

NiTi fibers and springs have frequently been proposed for use as artificial muscles because of their favorable material properties, low toxicity level, bio-compatibility, and reasonable cost (Bergamasco *et al.*, 1989; Duerig *et al.*, 1990a,b; Funakubo, 1987; Galiana and Green, in press; Hirose *et al.*, 1990, 1989a,b, 1984; Hunter *et al.*, 1991, 1990; Homma *et al.* 1989). In 1989, Oaktree Automation Inc., developed the Finger-Spelling Hand, an anthropomorphic robotic device based on 36 NiTi actuators located in the forearm and hand, which duplicated the motions of a human hand accurately enough to form the characters of the sign language (Boggs, 1993). Hitachi (Nakano *et al.*, 1984) has developed a robot hand with three fingers. Reynaerts and Van Brussel (1994) developed a two-fingered hand with five degrees of freedom. Most of these devices were too slow to be used commercially.

2.2 Shape Memory Alloys

The origin of the shape memory effect arises from martensitic transformations (MTs). The German metallurgist Adolf Martens first discovered martensite in steels (Van Humbeeck *et al.*, 1991). It was found that the transformation from the high-temperature, body-centered cubic lattice austenitic phase to the low temperature, face-centered tetragonal lattice occurs without atomic diffusion. Martensite is now used as a generic name for the product of a phase change of this kind in any material, the phase change itself being called a martensitic transformation. Such transformations are found in many metals, alloys and compounds. Martensitic transformations are at the heart of the shape memory effect.

Martensitic transformations can be defined as "a lattice transformation involving

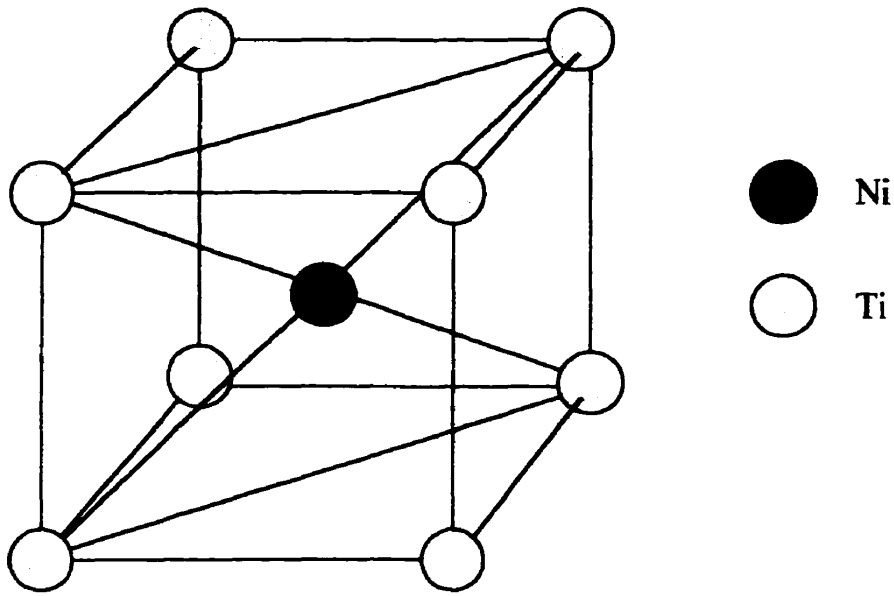

Figure 2.1 Model of the crystal structure for NiTi alloys in the austenite phase. The crystal structure for this state is BCC as for CsCl (B2).

shearing deformation and resulting from cooperative atomic movement" (Funakubo, 1987). An alternative definition is "a displacive, lattice-distortive, first order, diffusionless, athermal transformation that is accompanied by a shape change in addition to the volume change common to most phase transformations in metals and alloys" (Van Humbeeck *et al.*, 1991). There is a one-to-one correspondence between the lattice points of the parent phase and the points of the martensite phase. Therefore the martensite phase is a substitutional and interstitial solid solution, the transformation is diffusionless and accompanied by definite shape changes. When the lattice deformation is produced it occurs with complementary slip and twinning as described in Figure 2.4.

The crystal structure of the parent phase of NiTi alloys has a body centered cubic (BCC) structure like CsCl (B2), Figure 2.1. The crystal structure of the martensite phase is not fully understood. The general agreement is that of an orthorhombic crystal that has

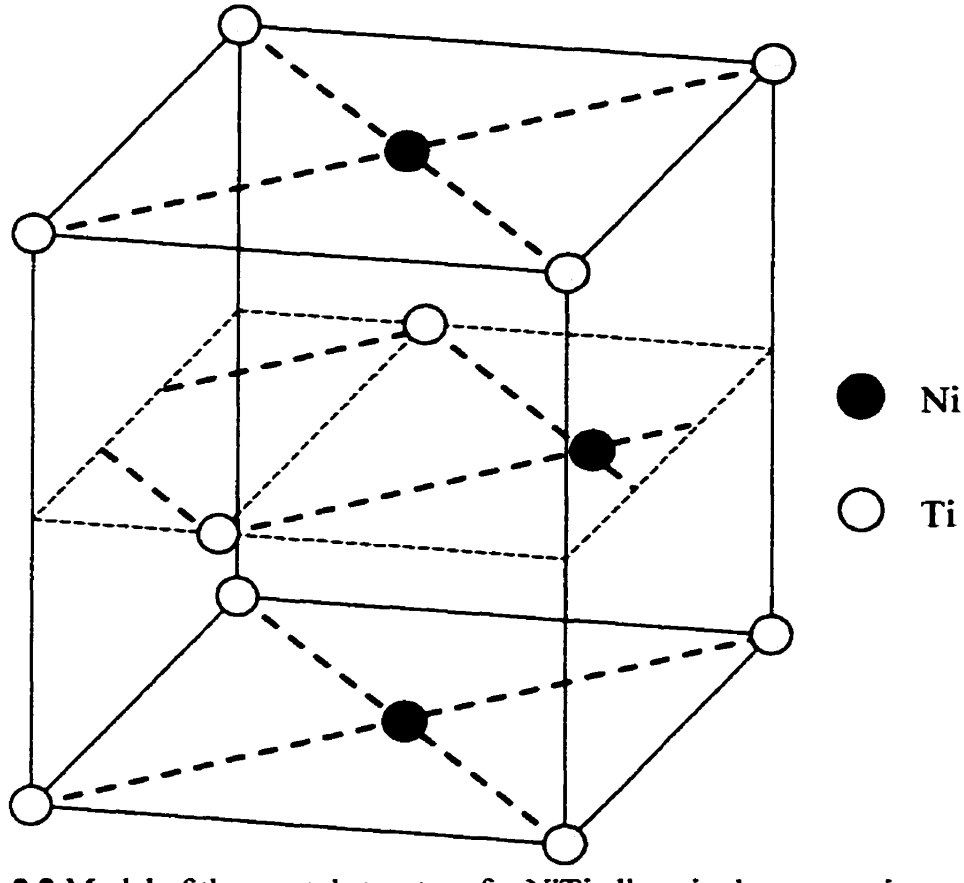

Figure 2.2 Model of the crystal structure for NiTi alloys in the martensite state

been strained to a monoclinic crystal as shown in Figure 2.2.

It has been known since 1965 that in NiTi alloys with a surplus of nickel or with nickel partly replaced by cobalt or iron that a two stage martensitic transformation occurs. The intermediate phase has a rhombohedral crystal structure. This two-phase transformation may not occur, depending on the annealing temperature among other factors. At high temperatures the alloy is in the martensite or parent phase. The material employed in the studies presented in this thesis generally exhibits such two-phase behavior.

2.2.1 The shape memory effect

As previously described, martensitic transformations occur with definite shape changes which are micro-structural changes. When the transformation occurs, no macroscopic change is observed in fibers having a polycrystalline structure, where individual crystals are small and randomly orientated. However when an external force is applied the one-way shape memory effect can be observed

Figure 2.3 describes how typically a NiTi fiber length changes with temperature when under tension. This diagram assumes a single-phase transition. When the fiber is above A_F (austenite finish) the entire alloy is in the austenite phase. In its high

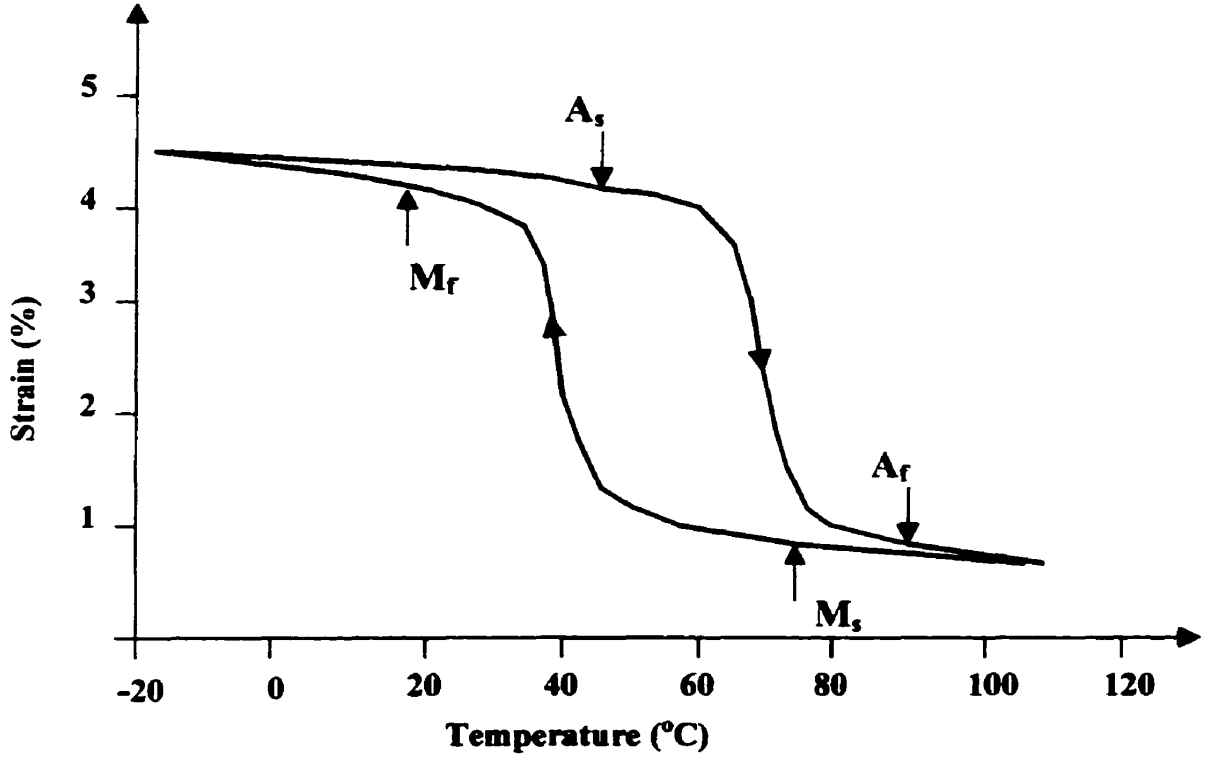

Figure 2.3 Illustration of the one way shape memory effect in a NiTi fiber subjected to a constant load. The fiber, first in the parent state, is cooled and it lengthens after it passes the point where martensitic transitions occur (M_s). When heated it contracts once the martensite reverts to the austenite form, above A_s.

temperature form, the fiber is at its shortest and in the parent (P) or austenitic state. As the fiber is cooled down below the point at which the martensite starts to form (M_s) the wire will start to. As the temperature drops below the "martensite finish" temperature (M_f) all of the martensitic transitions are completed. If the fiber is subsequently heated above the point where the phase transition to the austenite state starts (A_s), a point will be reached where the wire will shorten again. When the temperature reaches A_f most of the fiber is transformed back to the parent phase. The fiber has then returned to its original shape and length. Normally there is hysteresis as described by the stress-strain curve. This hysteresis consists of a true static nonlinearity with memory. The width of the hysteresis is normally 15 to 30 °C. There is one known exception, namely the rhombohedral (R) phase in NiTi fibers, for which the hysteresis is very small, on the order of 1.5 °C, and the transformation is considered to be reversible. Unless otherwise noted, this reversible phase is not exploited in the fibers employed in this study.

In most NiTi alloys, the shape memory effect is only observed when an external stress is applied as in the situation described above. If there is no external stress the fiber, which is a polycrystalline structure, would remain in its original shape and length. There are ways to apply thermo-mechanical treatment to the fiber such that it will return to a definite low temperature shape when cooled below M_f. This two-way shape memory effect is described below.

The process described in Figure 2.4 is similar to the one-way shape memory effect. The parent phase is highly ordered as in Figure 2.4 (A). When cooled, twinned martensite is formed, as in Figure 2.4 (C), and no shape effect occurs during cooling. If the alloy is deformed, the martensite is un-twinned as in 2.4 (B). When heated above M_f

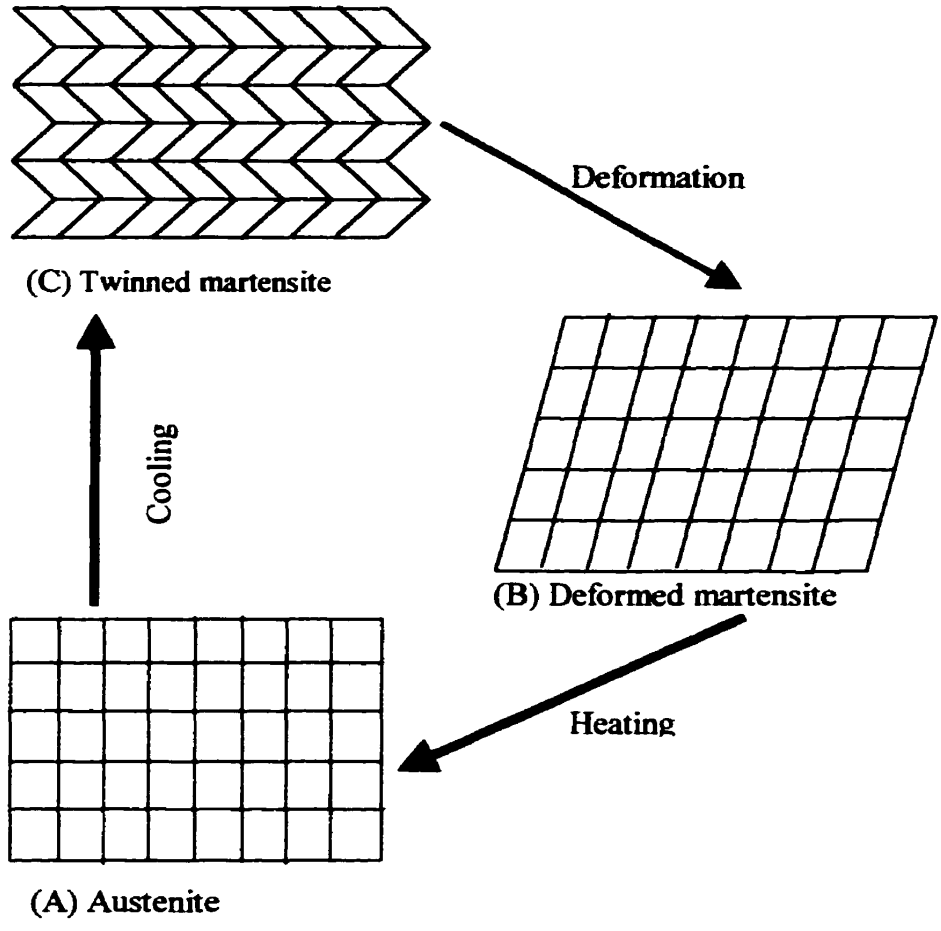

Figure 2.4 Illustration of the shape memory effect. In the shape memory effect Martensitic transformations first create a twinned martensite. As the martensite is deformed it de-twins. As it is heated again it returns to its parent phase.

the alloy returns to the highly ordered state in 2.4 (A), and contracts.

2.2.2 Kinetics

There are two main types of martensitic transformations: thermoelastic transformations and non-thermoelastic transformations. In non-thermoelastic transformations martensite crystals appear in the parent phase and develop at about one

third the speed of sound in the material. The transformation proceeds by nucleating new crystals in the parent phase. Once a crystal is nucleated, it does not change shape with time or temperature.

In thermoelastic transformations, once a martensite crystal is nucleated it grows at a velocity proportional to the cooling rate when the temperature decreases. The crystal growth can be observed under a microscope. When the temperature increases, the crystals shrink until they disappear. Nickel-Titanium alloys undergo thermoelastic transformations and it is normally assumed (Otsuka and Shimizu, 1970) that these transformations occur very rapidly in time.

2.2.3 Two-way shape memory effect

We have described the shape memory effect normally referred to as the one-way shape memory effect, in which only one shape is "remembered". There is also a two-way shape memory effect (TWSM) first reported by Delaey *et al.* in 1975 in which two shapes are "remembered", one at a high temperature and another one at a low temperature (Delaey *et al.*, 1975). In fact the material "remembers" all of the intermediate shapes between the low and high temperatures. In the one-way shape memory effect described above a force was required to deform the material at low temperature. In the TWSM no such force is required. However the strain that can be achieved and the mechanical work that can be produced with cooling are minimal in the sample in the TWSM. Special conditioning is required to achieve the TWSM; in particular thermo-mechanical treatment is required.

The origin of the TWSM is stress-biased martensite, which remains in the

austenite in the high temperature phase. There are several training routines that can be applied to introduce the TWSM. These methods can be summarized as following (Duerig *et al.*, 1990):

1. The sample is cooled below M_f and deformed well above the usual strain limit for complete recovery of the shape effect. When heated above A_f it will not return completely to its initial state. However, when cooled again below M_f the alloy will move back toward the overstrained shape.
2. The sample is submitted several times (5 to 10 times) to the normal cycle of cooling below M_f, deforming it (within the strain limit for full recovery of the shape memory effect), and subsequently heated again above A_f. After a number of these cycles the alloy spontaneously returns below M_f towards the deformed state at low temperature. The spontaneous shape change on cooling is only 20-25% of the training strain.
3. Another method consists of repeatedly loading and unloading the sample above A_f but below M_d where the superelasticity effect is expected. After a number of such cycles, typically 5 to 10, the TWSM is displayed. The spontaneous change in strain in the TWSM is here again only a small fraction of the training strain.
4. One of the most effective techniques combines the above two methods. The alloy is deformed above A_f to induce martensitic transformations, then cooled below M_f while maintaining the induced strain, and then heated up to recover the original shape. This procedure needs to be repeated a number of times.
5. The most commonly used method to obtain the TWSM consists of deforming the sample below M_f to produce a stress-biased martensitic microstructure. Then the

sample is constrained in the deformed low-temperature shape and heated above A_f. This method is relatively simple and straightforward to carry out.

2.2.4 Superelasticity

Figure 2.5 gives the stress-strain curve when the temperature is below M_f. It also illustrates the shape memory effect. The fiber can be stretched and after the stress is released a large amount of residual strain remains in the alloy. However after heating it returns to its initial state. The stress-strain curve is similar when the temperature is between M_f and A_s but a higher stress is obtained for the same deformation.

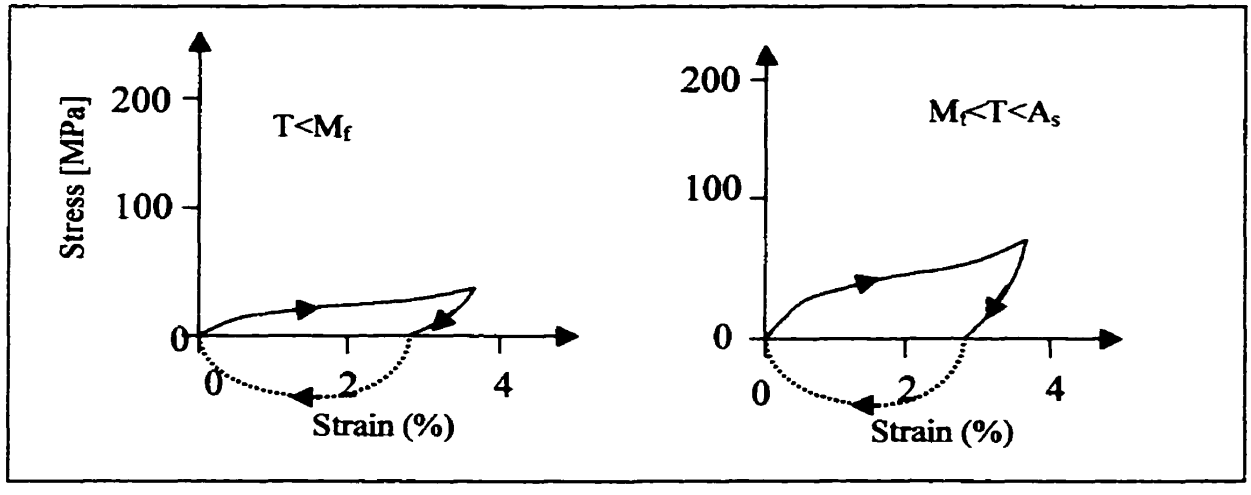

Figure 2.5 The stress strain curve is shown when the temperature is below Mf. The shape memory effect is also illustrated by dotted lines indicating the effect of heating.

Figure 2.6 displays the stress-strain relationship above A_f. The first part of the stress-strain curve is linear and the slope corresponds to the modulus of elasticity of the austenitic phase. As the strain is increased a plateau is suddenly reached. The fiber can then be stretched by as much as 6% with only a small increase in stress. Then the stress-

strain increases again. On releasing the stress a similar plateau is traversed in the opposite direction at a lower stress. As show in Figure 2.6 the fiber recovers completely from the applied stress. This nonlinear elasticity by which the fibers can be cycled

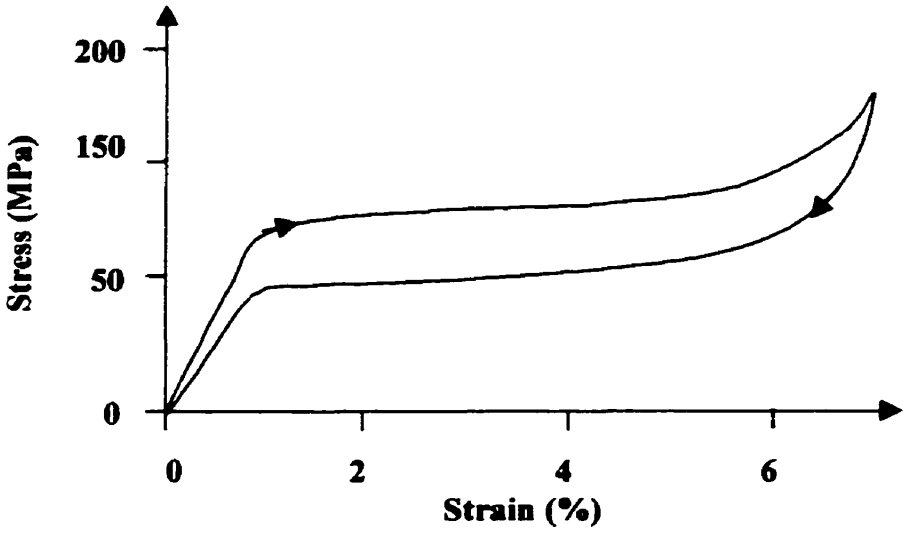

Figure 2.6 Stress-Strain curve of superelastic NiTi fiber.

reversibly to stretches as large as 7%, from which it recovers completely, is referred to as pseudoelasticity or superelasticity. As will be explained in section 2.4 the plateau corresponds to stress induced martensitic transformations.

2.3 Physical Properties of Shape Memory Alloy Phases

Each phase in a shape memory alloy has its own unique physical characteristics. Martensitic transformations are associated with changes in quantities such as resistivity, thermal conductivity, the modulus of elasticity, damping coefficient, magnetic susceptibility, and so on. Table 2.1 lists the various characteristics and physical parameters that normally differ in each phase. Each phase transition also has its own

unique characteristics. Phase transitions can be of the first or second order. They have their own characteristic latent heat and acoustic emission as well.

The acoustic emission that occurs concomitantly with phase transformations is a broadband noise that extends from low frequencies to ultrasound (Duerig, 1990). It can be used to detect the phase transformation and some of its characteristics, but it is difficult to use as a quantitative parameter to characterize the alloy.

Hardness	Roughness
Velocity of sound	Thermal expansion
Young modulus	Yield strength
Internal friction	Damping
Magnetic permeability	Resistivity
Thermoelectric power	Electromotive force
Latent heat of transformation	Thermal conductivity
Heat capacity	Hall coefficient
Poisson ratio	Density
Electron density waves	Lattice spacing

Table 2.1 List of physical properties that change with the phase in shape memory alloys.

2.3.1 Resistivity

Of the variables listed in Table 2.1, resistance is one of the easiest to measure, and is often used to study phase transitions in shape memory alloys. From the resistance and physical dimensions of the sample being characterized it is normally straightforward to determine resistivity. If there are dimensional changes that occur with the phase transition then it is important to take them into account. The Association Française de Normalisation (1991) defines phase transistion temperatures based on resistivity measurements as described below.

In the case of NiTi based alloys, the resistivity is high (0.5 to 1.1 μΩ·m) compared to that of copper (0.017 μΩ·m) and the resistance of fibers is readily measured. The electrical resistivity of copper based alloys is considerably lower than NiTi based alloys (Cu-Zn-Al: 0.07 to 0.12 μΩ·m, Cu-Al-Ni: 0.1 to 0.14 μΩ·m) and is somewhat more difficult to measure. In all cases the changes in resistance being measured are relatively small, on the order of 15%, and 4 wire resistivity measurements must be made.

The measurement of resistivity provides a qualitative description of phase transformations. It has been used (Ikuta *et al.*, 1991) as a state variable in real-time control mechanisms to determine the actual state of a NiTi fiber. However caution must be exercised as the resistivity-temperature curves vary markedly with thermal cycling history (Funakubo, 1987). NiTi alloys with R-phase exhibit complex resistivity changes with temperature as three phases may simultaneously coexist (Riva and Airoldi, 1995). Other NiTi based alloys may even have 2 or more intermediate phases (see Section 2.3.2).

Unfortunately a fair amount of confusion exists on resistivity in the literature. The experimental conditions under which resistivity is measured are rarely described, and what is typically measured is the resistance of a straight or coiled fiber. Either the percentage change in resistance is given with respect to a resistance at a given temperature or resistivity is obtained from the length and area of the fiber at room temperature. Dimensional changes are almost never measured with temperature and martensitic phase changes.

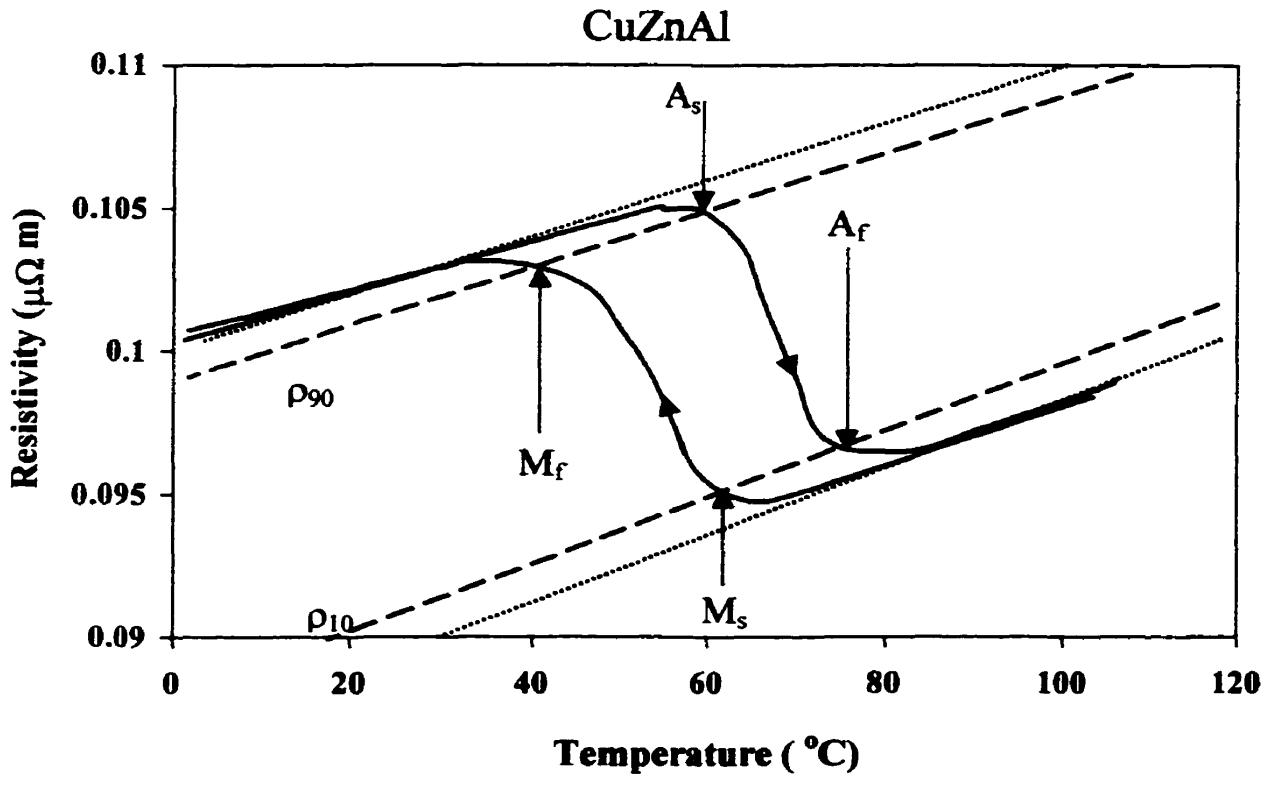

Figure 2.7 Resistivity curve diagram with one phase transition. The hysteresis is well defined. In NiTi alloys there can be intermediate phases that complicate the diagram.

The change in resistivity with temperature can be sketched as shown in Figure 2.7 for a Cu-Zn-Al-Ni alloy. Above A_f (Austenitic finish), the sample is in the parent phase, and the quasi-linear increase of resistivity with temperature is observed. At temperatures below M_f (Martensitic finish) the resistivity is that of the martensitic form, and the linear increase in resistivity with temperature is observed. Therefore if ρ_p is the resistivity in the parent phase and ρ_m is the resistivity in the martensitic phase, we can write as a first order approximation:

$$\rho_p(T) = \rho_p(T_0) + C_p \cdot (T-T_0), \quad (2.1)$$

$$\rho_m(T) = \rho_m(T_0) + C_m \cdot (T-T_0). \quad (2.2)$$

When going from A_s (Austenitic start) to A_f or from M_s (Martensitic start) to M_f large nonlinear changes can be observed with temperature. The "law of partial fractions" can express these:

$$\rho = R_m \cdot \rho_m + R_p \cdot \rho_p, \quad (2.3)$$

Conversely, the resistivity plot can be used to estimate the various transition temperatures: A_s, A_f, M_s, M_f. This is done by drawing the lines described by estimating the four coefficients of equations (2.1) and (2.2). The two additional lines are drawn:

$$\rho_{10}(T) = (0.9 \cdot \rho_p + 0.1 \cdot \rho_m)) \cdot (T_0) + (0.9 \cdot C_p + 0.1 \cdot Cm) \cdot (T-T_0), \quad (2.4)$$

$$\rho_{90}(T) = (0.1 \cdot \rho_p + 0.9 \cdot \rho_m)) \cdot (T_0) + (0.1 \cdot C_p + 0.9 \cdot Cm) \cdot (T-T_0) \quad (2.5)$$

A_s is estimated from the intersection of the $\rho_{90}(T)$ line and the curve ascending in temperature, while A_f is found from the intersection of ρ_{10} and the resistivity curve. Similarly M_s is found from the intersection of ρ_{10} and the resistivity curve corresponding to decreasing temperatures, and M_f is found from the intersection with the line.

2.3.2 Intermediate phases

In fully annealed binary NiTi alloys the B_2 parent phase transforms directly to the $B_{19'}$ monoclinic-phase. Recent advances in the study of martensitic transformations of

NiTi alloys indicate that there are two possible intermediate phases that may be formed. In binary NiTi alloys which have been subjected to thermo-mechanical treatment or thermally cycled, a two step transformation occurs: B_2 parent phase → trigonal R-phase → $B_{19'}$ monoclinic phase (Beyer, 1995). Addition of a third element such as Cu or Pd can result in a different two-step transformation from B2 → B_{19} orthorombic → $B_{19'}$ monoclinic phase. Therefore the possible transformations include all of the following possibilities (Beyer, 1995):

1. B_2 (body cubic centered) →$B_{19'}$ (monoclinic).
2. B_2 →R-phase (rhombohedral) →$B_{19'}$.
3. B_2 →orthorombic B_{19} →$B_{19'}$,
4. B_2 →R-phase →B_{19} →$B_{19'}$.

In NiTi alloys with nickel exceeding 50.5 at % (percent atomic ratio) the parent phase slowly decomposes with slow cooling or aging at lower temperatures (after quenching from high temperatures). The process involves two metastable phases Ti_3Ni_4 and Ti_2Ni_3 and the stable $TiNi_3$. The Ti_3Ni_4 is important for the all-around shape memory effect. A three-step transformation is also possible: $B_2 \rightarrow R \rightarrow B_{19} \rightarrow B_{19'}$.

In NiTi alloys undergoing the R-phase, resistivity curves are more complex to interpret. Figure 2.8 illustrates the resistivity in a NiTi alloy that displays an intermediate R-phase. As the temperature cools down and point 1 is reached the R-phase starts to appear. The resistance of the R-phase is much larger than for any other phase. With further cooling when point "2" is reached the orthorhombic martensite appears and the resistance falls until point 3. At that point all of the R-phase has been transformed.

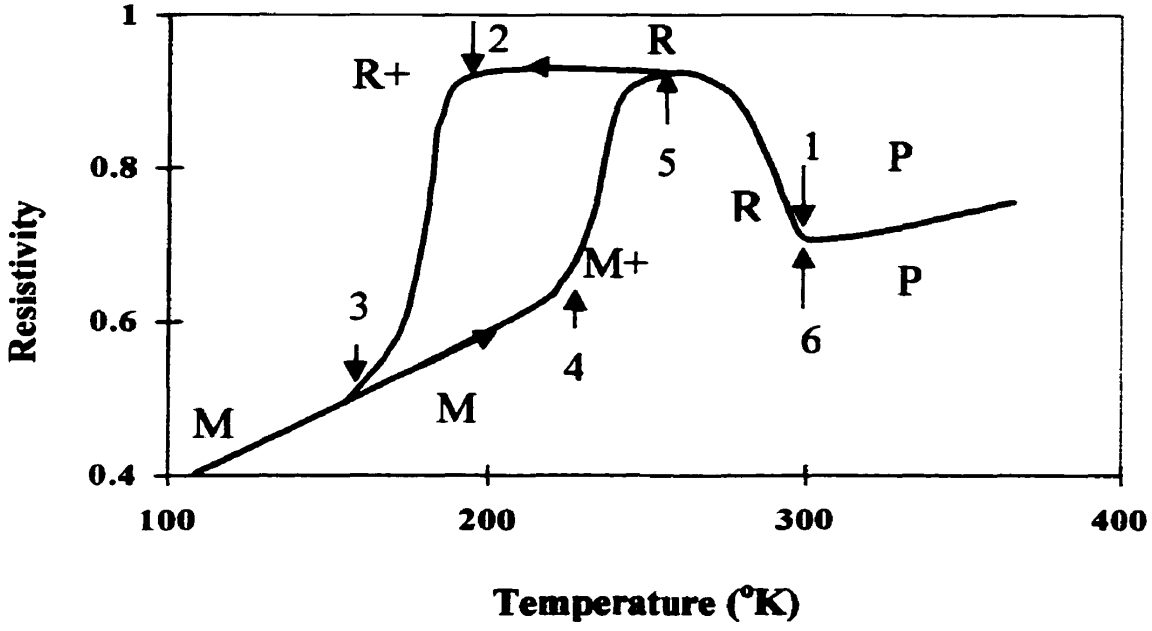

Figure 2.8 Resistivity curve of a NiTi alloy exhibiting one intermediate phase between the M-Phase and the R-phase. One or two intermediate phases may appear in NiTi alloys.

When the specimen is heated above point 4, part of the martensite transforms itself in the intermediate state. The two coexist until point 5 where most of the sample consists of the R-phase and then after point 6 the parent phase has been restored. The transformation P $\rightarrow$R is almost completely reversible, and is associated with an hysteresis in the order of 1.5 °C only.

The resistivity curves measured in this thesis were all acquired for NiTi alloys under no tension. As a consequence there were only negligible changes in either the length or the diameter of the fiber.

The R-phase has been known to occur in NiTi alloys with a surplus of Ni or where Ni has been replaced with a third element (such as Fe or Co). Dautobich and Purder (1965) first reported the appearance of the R-phase. This intermediate phase

appears when the NiTi alloy is annealed at a low temperature, which is between 300 °C and 550 °C.

Study of the transformation phases using differential scanning calorimetry (DSC) shows that the inverse transformation from the martensitic phase to the parent phase may occur with one or two peaks. Thus the martensite can transform directly to the austenite phase without going through the R-phase (Jordan *et al.*, 1995).

The presence of the R-phase is also affected by cold working. The R-phase will occur when the martensitic transformations are suppressed relative to the R-phase. This is normally achieved in three possible ways:

1. The introduction of dislocations by cold-working the alloy, followed by low-temperature annealing.
2. The introduction of precipitates in the solution and subsequently aging an alloy rich in Ni at low temperatures.
3. The addition of a third element that suppresses the martensitic transformations (e.g. Fe or Al).

The recoverable strain from the R-phase is limited to approximately 1%. Although this is small, it is extremely useful for accurate thermal actuators given its reversibility. It can readily be used in proportional control devices since its hysteresis is under two degrees. Furthermore the stress-strain curve is highly stable under cycling for a million cycles or more.

2.3.3 Thermoelectric effect

The parent and martensite phases have different thermoelectric potentials. Therefore if a shape memory alloy fiber is clamped at its ends to two metallic reference connectors and a temperature difference is maintained between the two connectors, a potential difference will be recorded which is a function of the temperature difference. The thermoelectric power of NiTi has been reported by Wasilewski *et al* (1967) and by Hanlon *et al.* (1967). The usual technique to measure the thermoelectric effect consists of using two metal blocks of the same metal and fixing the sample between the two blocks. One block is maintained at a reference temperature and the temperature of the second block is varied. The potential is then recorded as a function of the temperature difference. Plots of the thermoelectric effect versus temperature are similar to those of resistivity and the interpretation is the same.

2.4 Thermodynamics

If T_0 is the temperature at which the chemical free energy of the P phase and M phase are equal, the alloy must be supercooled below T_0 before martensitic transitions start to occur. In other words the transformation requires an excess of non-chemical free energy such as strain energy and interface energy for the transformation to begin. Similarly a driving force is also required for the reverse transformation to occur. If we assume cylindrical crystals with a radius, r, and a thickness, t, change in chemical free energy density, Δg_c, and A(t/r) is the elastic strain energy per unit volume, the total energy change due to nucleation is:

$$\Delta G = \pi r^2 t \Delta g_c + \pi r^2 t A. \qquad (2.6)$$

When reaching M_s the first term on the right will exceed the second term and the crystal will grow. However the crystal will grow even if the temperature is above M_s as shown by the superelastic effect. This occurs because an applied stress contributes to the nucleation of the M crystals. If $\Delta G^S(\sigma)$ is the amount of energy introduced by a stress σ, nucleation will start when the first term on the right of Equation 2.6 is now:

$$\pi r^2 t \Delta g_c = \Delta G^S(\sigma) - \pi r t^2 A. \qquad (2.7)$$

The transformation will start at a higher temperature, which is a function of the applied stress. In fact the transformation temperatures follow the Clausius-Clapeyron equation (Duerig *et al.*, 1990):

$$dP/dT = \Delta H/T\Delta V, \qquad (2.8)$$

where P is the pressure, T is the temperature, ΔH is the transformation latent heat and ΔV is the transformation volume change. For metallurgical purposes the equation can be rewritten as:

$$d\sigma/dM_s = -\Delta H/T\varepsilon_0, \qquad (2.9)$$

where σ is the applied stress, M_s is the shifted temperature and ε_0 is the strain. Therefore the transition temperatures will normally vary almost linearly with the applied stress.

2.5 Latent Heat, Specific Heat and Efficiency

Associated with each phase transformation is a corresponding latent heat, specific heat, and also thermal conductivity. Appendix IV lists values for both the latent heat and specific heat. The specific heat of transformation for NiTi is 31.5 kJ/kg (Funakubo, 1987). For NiTi with an intermediate R-phase, (Ti-51 at % Ni) the specific heat for the transformation from the low temperature martensite to the high temperature is 24.3, and

for the intermediate phase to high-temperature it is 6.43 kJ/kg. Those have been measured for most alloys by differential scanning calorimetry (DSC). For $Ni_{47.5}Ti_{50}Fe_{2.5}$ alloys they have been found to be 7.79 kJ/kg for the II->I transformation and 15.5 kJ/kg for the III->II transformation. The specific heat (Q_M) is 837 J/kg/°C.

Values for the latent and specific heat can be used to calculate the amount of energy required for a transformation to occur. They can give some estimates for the efficiency and energy required to produce a contraction. Given the resistivity diagram for the NiTi material used in this thesis, the fiber is in the R-phase at room temperature (20° C). A stress of approximately 50 MPa starts to induce martensitic transformations. If a 100 MPa stress is applied, the stress induced change in transition temperature would raise M_s by 23 °C (Ikuta, 1990), which would introduce stress induced martensitic transformations. M_s is raised from 5 °C to 28 °C and A_f from 70 °C to 93 °C. In order to contract the fiber the temperature must be raised from room temperature to A_f, which is near 73 °C. The amount of energy, W_1, in Joules, required for this is equal to:

$$W_1 = Q_M \cdot (A_f - T), \tag{2.8}$$

$$W_1 = 61 \text{ kJ/kg}. \tag{2.9}$$

Next an amount of energy W_2 equal to the latent heat must be supplied:

$$W_2 = (24.3+6.4) \text{ kJ/kg}. \tag{2.10}$$

Therefore the total amount of energy, W, to produce a contraction would be:

$$W = 91.8 \text{ kJ/kg/cycle}. \tag{2.11}$$

If we assume the fiber dimensions to be 100 mm in length, L, and with a diameter, d, of 250 μm, and given a density of 6,450 kg/m^3, the weight, ω, of the fiber would be:

$$\omega = (\pi d^2/4) \times L \times (6450 \text{ kg/m}^3) = 31.6 \text{ μg}, \tag{2.12}$$

and the amount of energy in Joules to contract the fiber is:

$$W = 91.8 \text{ kJ/kg} \times 0.0316\text{x}10^{-3} \text{ kg} = 2.9 \text{ J.} \quad (2.13)$$

Next if we assume that the fiber contracts by 5% at 5N (100 MPa) the mechanical work, W_m done is:

$$W_m = F \cdot d = 25 \text{ mJ} \quad (2.14)$$

The efficiency in this case is 24 mJ/2.8 J = 0.8%.

This is a theoretical example. However values are quite close to those obtained in laboratory tests (Gilbertson 1994; Lafontaine *et al.*, to be published, appended to chapter 4) and it demonstrates the origin of the low efficiency of the fibers quite well.

2.6 Applications of NiTi Shape Memory Alloys

Shape memory alloys have been used in a number of fields, such as medicine, electronics and textiles. Table 2.2 describes past applications or prototypes that have been built with SMA's (Duerig et al., 1990, Funakubo, 1987, Patoor and Berveiller, 1994, Van Humbeeck, 1992, Weynant *et al.*, 1993).

NiTi alloys have been used in preference to other shape memory alloys in industrial applications because of their larger recovery strain and stress, their longer repetition life, their excellent resistance to corrosion, and relatively low cost. They have a very good bio-compatibility but in-situ applications in medicine are restricted by the slow diffusion of nickel which is highly cytotoxic (Funakubo, 1987).

Field	Application
Electronic Equipment	Circuit breakers Zero force insertion connectors (ZIF) Memory elements Disk-drive heads Pen recorder Cell phones antennas
Automotive	Head lights actuation Noise reduction (damping) Radiator thermostat
Arts	Moving sculptures
Home and Textile	Circuit breakers (coffee makers, etc.) Underwire bra Permanent press shirts Air conditioners (louver actuation) Toys, ashtrays, etc. Ashtrays (low hot cigarette butts) Eyeglass frames
Food	Temperature extrema marker (thermomarker)
Smart Materials	Composite materials, building dampers
Robotics	Robotic actuators (grippers, arms, hands) Sealing ring Actuator for camera
Machinery	Pipe joints Fixation mechanisms Valves
Medicine	Artificial joins, spines Vascular, esophageal and biliary stents Artificial heart Micro-pumps Guide wires for catheters Guidepins, localization hooks Actuated catheters Mammelak breast hook Blood clot filter
Dentistry	Orthodontic wires
Space	Antenna releasing system Release mechanism and bolts Vibration damping during launching
Photography	Shutter mechanism for telescope CCDs.
Security Systems	Fire alarm and extinction actuators Anti-scald device Gas-valve lock

Table 2.2 – Applications of Shape Memory Materials

2.6.1 Muscle-like actuators

A number of robot limbs have been constructed using NiTi fibers. For example, Hitachi has produced a robot hand (Nakano *et al.*, 1984), and Homma *et al.* (1989) have built a small 5 degree-of-freedom robot arm. Bergamasco *et al.* (1989) have described experiments using an agonist-antagonist NiTi actuator for robotic applications. A NiTi actuated worm-like endoscope has been built (Hirose *et al.*, 1990; Ikuta *et al.*, 1988).

A number of robotic end effectors were built (Stoddard and Schiferl, 1986; Reynaerts, 1991). Iwata *et al.* (1988) developed a four fingered "anemone-like" gripper for space applications, and more recently Mertmann *et al.* (1995) have built a flexible robotic gripper. While the developments to date have been impressive, a major problem with all current SMA-based robot actuator designs is that the total contraction and relaxation time is slower than muscle and most electromagnetic actuators.

Many applications of NiTi use the fibers wound in the form of a coil spring. The maximum shear strain is usually limited to 1% to avoid fatigue (Tamura and Suzuki, 1988). For applications requiring rotation (e.g., robotic limbs) the two NiTi coil springs are often attached to a circular pulley to form an agonist-antagonist pair. A problem with this design is that as the NiTi spring shortens, the force it generates, and hence the torque delivered by the joint, varies. Recently, Hirose *et al.* (1989) have proposed a non-circular pulley that is designed to enable the maximum generated torque to be held constant with rotation. Van Moorleghem discusses other applications based on SMA springs, including a robotic finger actuator, a micro-actuator and a space gripper actuator.

Mertmann *et al.* (1995) used a different approach in designing flexible robotic grippers where the NiTi fiber was imbedded in a flexible silicone matrix with a steel leaf

spring to provide a restoring force. The robotic hand included four fingers made from these grippers.

More recently Grant and Hayward (1995, 1997) developed a high-strain NiTi actuator for robotic applications and used it to control a camera platform. The main originality of the actuator came from the weaving geometry of a NiTi mesh that provided a mechanical gain to amplify the limited displacements of the NiTi fibers.

2.6.2 Miniature actuators

Ikuta (1990) has developed a small (30 mm × 40 mm × 14 mm, 27 g) gripper having NiTi coil spring actuators (1 mm diameter coil, 0.2 mm diameter fiber). The gripper response time is >700 ms. An innovation in this work (see also Ikuta *et al.*, 1988) is the use of the change in resistance (which accompanies the martensite to autenite transformation) to control the NiTi directly.

2.6.3 Valves

Kohl *et al.* (1995) have developed prototypes of membrane microvalves using microstructures made from 157 μm NiTi sheets, reduced by HF and HNO_3, and cut with a Nd-YAG laser or electrolytic photoetching. The NiTi sheets displayed an R-phase upon cooling but returned directly to the parent phase on heating. For their tests, only the R-phase transformation was used which resulted in a very low hysteresis. An array of eight NiTi beam-cantilever devices of 1.5 mm in length, 0.1 mm in width and 0.15 mm thick were used to realize the first microvalve. These devices controlled the deflection of a

polyimide membrane on a valve chamber, which was biased by an external pressure.

The TiNi Alloy Company (San Leandro, CA) also fabricates thin film shape memory alloy minivalves ranging between 0.1 to 10 mm in size. These valves are fabricated with micromachining and microelectronic processes and materials. They are proportional control valves where the flow, of up to 1 liter per minute, is almost proportional to the current used to control the valve.

2.7 Models of NiTi actuators

There have been a very large number of models developed in the literature to simulate the electro-mechanical and thermodynamic response of NiTi shape memory fibers. They fall in the following categories: (1) models of the thermodynamics of martensitic transformations (Achenbach, 1989; Gillet *et al.*, 1995; Müller, 1995; Lexcellent et al., 1993; McNichols, J.L. (1987); Thuillier *et al.*, 1995), (2) development of the constitutive equations and solution by finite element modeling of the stress-strain cuves of springs and and fibers (Patoor and Berveiller, 1994; Trochu and Yuan-Yao, 1997; Leclercq *et al.*, 1996), (3) models of hysteresis including Preisach models developed for the ferromagnetic magnetization curve (Hugues and Wen, 1995; Likhachev, 1995), (4) electro-thermo-mechanical models representing the bulk properties for control purposes (Ikuta, 1990; Ikuta *et al.*, 1991; Ikuta *et al.*, 1988; Liang and Robers, 1992; Malygin, 1993).

What is more relevant to fast shape memory actuators are lumped models that are simple and efficient to use for real-time control purposes. For simulation of mechanisms Ikuta *et al.* (1990, 1991) developed one of the most complete models to date. The "variable sub-layer model" includes either 2 layers or three layers when there are intermediate R-phase transformations. The model includes the heat transfer function of the fiber, the hysteresis in the phase transformation, the nonlinear stress-strain relationship of the martensitic and rhombohedral phase, and the thermoelastic transformation including the stress dependence of the transformation temperatures. However Ikuta did not properly apply the variable sublayer model to calculate changes in resistance. While in a variable sublayer model the resistances of the various layers are effectively in parallel, he added the resistances to represent the total resistivity of the wire as if the layers were in series. As shown in Figure 2.9, the currents of the different sublayers add. Given a voltage V, the total current will be:

$$I = V \cdot A_p/(L \cdot \rho_p) + V \cdot A_i/(L \cdot \rho_i) + V \cdot A_m/(L \cdot \rho_m), \qquad 2.15$$

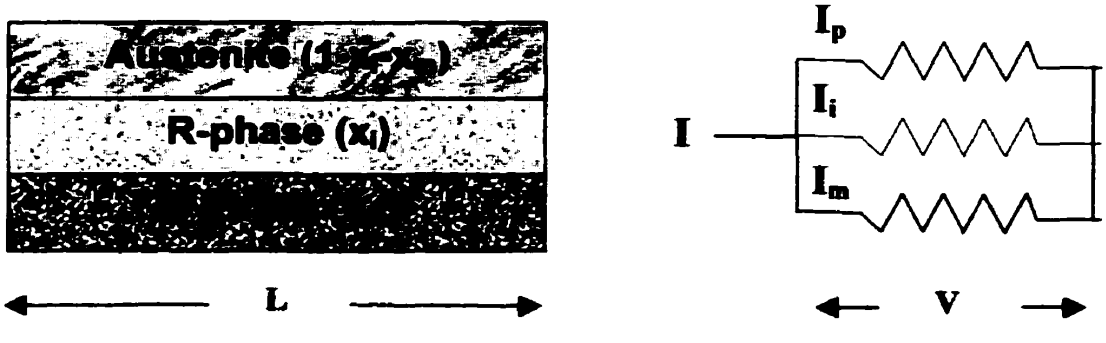

Figure 2.9 Variable sublayer model.

where ρ_p, ρ_i and ρ_m are the resistivities of the parent (austenite), intermediate (R) and martensite phases, L is the length of the sub-layer, V the voltage, I the total current, A_p, A_i and A_m are the respective areas of the parent, intermediate and martensite phases. However the ratios of the different areas, A_p, A_i and A_m to the total area A are the same as the fractions of the respective phases (by volume, or weight given that the densities of the various phases do not differ markedly). Assuming that x_i is the fraction in the intermediate phase and x_m the fraction in the martensite phase, we get:

$$1/R = (A/L)\cdot((1-x_i - x_m)/ \rho_p + x_i/\rho_i + x_m/\rho_m). \qquad 2.16$$

Or if σ_p, σ_i, and σ_m are the conductivities of the parent, intermediate and martensite phases we get:

$$1/R = (A/L)\cdot(1 - x_i - x_m)\cdot\sigma_p + x_i\cdot\sigma_i + x_m\cdot\sigma_m). \qquad 2.17$$

In other words, the variable sublayer model predicts that the additive rule of mixing in solids should apply to the conductivities and not the resistivities (like they apply to stiffness but not compliance).

More recently Lu (1997) improved the parallel two-layer model of Ikuta's variable sub-layer model to incorporate the temperature-current relationship of the NiTi fibers and improved the representation of the hysteresis that occurs in the martensitic transformations.

2.8 Conclusion

Three documents are included to complement the material given in this chapter. The first one (Appendix I) is a U.S. patent entitled "Shape memory alloy having fast

twitch response" (#5,092,901) which describes the process for creating NiTi fibers with a fast twitch response. Normally NiTi fibers will contract very rapidly. The rate at which they can be heated and the speed of sound in NiTi mainly limits the rate at which they contract. However they take a long time to elongate back to the original length. As will be shown in chapter 4, we have developed a process that modifies NiTi fibers so that they can contract and elongate more quickly. In addition fibers that are modified with this process have a strong two-way shape memory effect.

The second document (Appendix II) is a conference paper by Hunter and Lafontaine (1992a) that reviews artificial muscle actuators. The content of the paper is briefly summarized at the beginning of this chapter.

The third document (Appendix III) is a conference abstract that describes some of the research projects related to NiTi alloys.

Chapter 3 Growing and Attaching NiTi fibers

The main technical difficulties in bringing NiTi artificial muscle fibers to real engineering applications have been described in the Introduction. The difficulties are also outlined in Funakubo (1987) and are:

1. SMA's can actively contract and expand by 2 to 8%, while typically appropriate contact materials are limited to 0.2%. (In particular, for the case of fibers activated by current pulses, metals are sought as joining materials because of their combination of high stiffness and conductivity.) Hence even if SMA's can be clamped, they normally will easily free themselves.
2. The properties of shape memory alloys critically depend on the exact ratio of elements, nickel and titanium in the case of NiTi alloys. Even a slight deviation from the required stoichiometric ratio can lead to a brittle material. In brazing an alloy formation occurs between the braze and the substrate. Therefore brazing usually does not work well because of the brittle interface formed at the surface of the NiTi alloy.
3. Titanium is a highly reactive material that readily oxidizes. A clean surface oxidizes in air in less than a second. Many operations require working in an inert gas. Otherwise, a titanium oxide layer rapidly forms at the surface of the fiber and prevents fluxes from wetting the surface and the solder from flowing.

4. The capstan effect can be used to effectively attach NiTi alloys. In this case as the tension builds in the fiber it further tightens inner loops of NiTi fiber which then hold better in place. However in many applications the fiber expands rapidly and becomes loose. Therefore some additional mechanisms must be used to prevent it from unwinding when it expands. Furthermore a capstan tends to consume a large amount of space and mass relative to the fibers it holds.
5. It is impossible to glue, cement or bond NiTi alloys. After a few cycles of contraction and expansion they will crack and fracture all known adhesives.
6. When a NiTi alloy is heated well above its temperature A_f, its shape memory effect or superelastic effect is normally lost. It is therefore difficult to use any high temperature process to join them. Welding, brazing or soldering involves heating the NiTi alloys whose properties end up being severely degraded. Brazing can be effective however in joining two NiTi alloys, providing of course that the shape memory effect is not lost, because diffusion of metal atoms between parts does not change the net stochiometry. Hence embrittlement is not an insurmountable problem.

Soldering when used in electrical devices is only safe for electrical connections, components having to be mechanically held in place by some other means. Otherwise, soldered joints fail if subjected to cycling stresses. Therefore soldering as a means to hold electrical wires for example is not allowed by industry standards.

It is also difficult to effectively make use of NiTi in micro-mechanical parts. Such parts are becoming increasingly popular as micro-switches and sensors (e.g. airbag accelerometers). The most widely known and used micro-fabrication techniques are based on silicon lithography or related methods such as LIGA (a German acronymn

Lithographie-Galvanofurmung-Abformung, meaning lithography, electrodeposition and molding). They allow fabricating only parts in two dimensions with thickness. They are also restricted to a few materials such as silicon and gallium arsenide, and do not lend themselves to micro-fabrication using metals, although LIGA allows fabricating 2D parts with a high aspect ratio from nickel. Three-dimensional structures can often be built by stacking 2D layers but applications of this technique are limited. If for example it was required to build a hollow sphere none of these techniques would allow it.

We have included a U.S. patent application with this chapter that addresses the first issue. It is a new process that allows mechanical and or electrical attachment to NiTi alloys. This process is currently patent pending. The second document included with this Chapter is U.S. patent #5,641,391 entitled "Three dimensional microfabrication by localized electrodeposition and etching". This latter U.S. patent addresses directly the issue of microfabrication. The two processes are fully compatible with each other, so that NiTi alloys can be joined with the first process to micro-structures or micro-mechanisms formed with the second process, all in one combined apparatus.

3.1 Joining NiTi alloys

The technique for joining NiTi alloys is described in the US Patent application entitled "Method for joining mechanically and electrically parts made from NiTi shape memory alloys and other materials that are not readily joined together with conventional techniques".

Fibers may either be joined together by an electrodeposit, in which case they are

placed in close proximity in an electrochemical bath, and a plating potential is applied to both, or a layer of material is grown onto the fiber which can then be connected to using traditional joining methods. The technique developed to join NiTi alloys can be summarized as follows: (1) the shape memory effect is inhibited or destroyed locally on all areas where the fiber or fibers need to be joined (heating the fiber for example); (2) the surfaces are cleaned; (3) some areas may be protected using an insulating material painted or applied otherwise on the surfaces; (4) the fibers are positioned in a specially shaped electrolytic bath in order to maximize the current density where joining is required; (5) the metal or other substance that can be electrodeposited is formed electrolytically by passing a current between an appropriate anode and the fibers which are all electrically connected together as cathodes.

The process normally involves deposition of a thickness comparable to the thickness of the fiber or fibers to be joined. The current may also be reversed to etch certain areas as well. Etching and depositing can also be repeated until the desired result is obtained.

3.2 Spatially Confined Electrodeposition

We have developed a new process based on spatially confined electrodeposition (SCED) to build 3D components and structures. The technique has been demonstrated on objects such as a spring, which would be impossible to build with LIGA or silicon photolithography. The process was designed to fabricate objects by electrodeposition and also to machine parts by electrochemically etching material. The process is described in

the US Patent 5,641,391.

The technique cannot be used to directly form NiTi alloys with sufficiently high Ti content to demonstrate the shape memory effect, and fibers will have to be fabricated using conventional techniques. However the two processes are inherently compatible and SCED could be used to form metal around the fibers to be mounted in a micro-mechanism fabricated with SCED. In other words, metals, such as Ni, and conducting polymers, such as polypyrrole and polyaniline, could be grown directly onto fibers, and in arbitrary geometries, forming micro-devices.

3.3 Results

Figure 3.1 is a photograph of a NiTi fiber, which has been "grown" electrolytically at both ends (only one is shown). The fiber was mounted for mechanical testing by soldering the nickel ends to hollow hexagonal rods. None of the fibers tested in this manner failed at normal operating stress levels (<200 Mpa). This technique allows dynamic measurements at high frequencies since the added mass of the nickel is small compared to the total mass of the fiber. If other means of clamping the fibers are used, their mass is so large that it must be included in a lengthy calibration procedure to get at the dynamics of the fiber. Other groups (e.g. Hall, 1993) have tried electroplating and soldering the plated fibers but the results were not satisfactory. In our tests the fibers often broke before the joints, and the joints typically failed at stresses greater than 500 MPa.

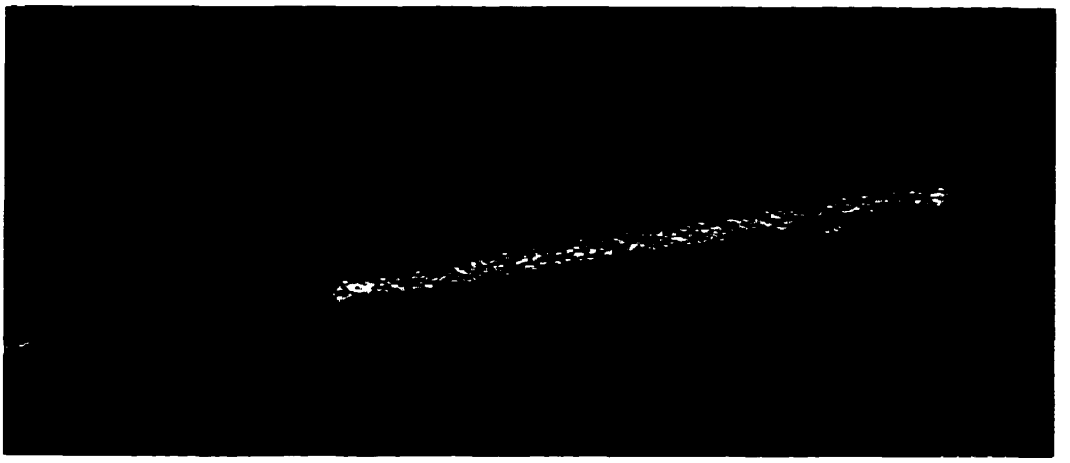

Figure 3.1 NiTi fiber grown at one end for attachment.

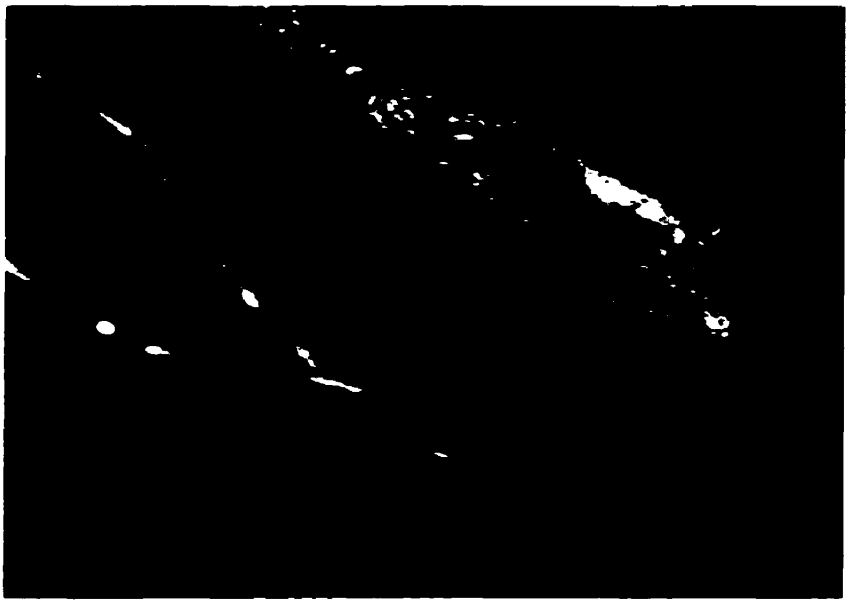

Figure 3.2 The fibers at the top were embedded together in copper using electrodeposition. The fibers at the bottom form a copper-constantan thermocouple.

Figure 3.2 illustrates another application of the process. In this case a copper wire has been directly joined to a NiTi fiber using copper electrodeposition. In this way the thermocouple effect can be directly recorded from the two pieces. It is the only known technique that allows the creation of a NiTi thermocouple having a very small volume.

Figure 3.3 Example of a NiTi fiber first twisted in a loop and subsequently fixed in place by coating the fiber in electrodeposited nickel.

Otherwise the two pieces must be attached together to metal blocks that have intrinsically a very long thermal equilibrium time.

Figure 3.3 gives one more illustration of the process. In this case the fiber was wrapped around itself to make a loop at the end. It was subsequently coated in a nickel sulfamate bath for embedding the loop in nickel. Although it is difficult to see in this picture a copper wire was soldered to the loop at the bottom left for electrical stimulation. The unevenness of the nickel layer was caused by an excessively large deposition rate.

3.4 Conclusions

The new technique employing electrodeposition to grow mechanical attachments has been extremely useful for most measurements in this thesis and should prove

invaluable to applications in general. It is novel in that a step is used to remove locally the shape memory effect and in that a large thickness of deposited material is used. Electrodeposition has been used in the past to make electrical connections to NiTi parts. However this has not been successfully used for mechanical attachments because the deposited material fails after a few cycles as the NiTi part goes through the expansion and contraction associated with phase transitions. This has never been the case for the electrodeposition method reported here.

The main disadvantage of this technique is that few metals have the exact mechanical characteristics of NiTi alloys. Nickel for example is much stiffer than NiTi. As a result if stresses are not in line and if the forces generated at the point of junction with the nickel generate points of concentration of stresses, then the NiTi fiber will break earlier than normally expected.

Although full characterization has not been done, the force at which the nickel interface detached from the NiTi fiber was in some tests 27 N for a 250 μm fiber, which corresponds to a 540 MPa stress. Although not as high as the yield stress of NiTi fiber, this is still 2.7 times higher than the maximum recommended stress for this fiber size in normal applications. Methods have also been reported to directly electrodeposit onto fibers parts of arbritrary geometry. This ability could lead to the development of many novel electromechanical parts. This technique has been used extensively to test the mechanical properties of NiTi fibers (see chapter 4) and in our experiments none of the joints ever failed.

DOCKETED

Attorney's Docket No. 1964/115 PATENT

IN THE UNITED STATES PATENT AND TRADEMARK OFFICE

Box Patent Application
Assistant Commissioner for Patents
Washington, D.C. 20231

NEW APPLICATION TRANSMITTAL

Transmitted herewith for filing is the patent application of

Inventor(s): Serge R. Lafontaine
Ian W. Hunter
John D. Madden

WARNING: Patent must be applied for in the name(s) of all of the actual inventor(s). 37 CFR 1.41(a) and 1.53(b).

For (title): Method for Joining Mechanically and Electrically Parts Made from NiTi Shape Memory Alloys and Other Materials that are not Readily Joined with Conventional Techniques

---

CERTIFICATION UNDER 37 CFR 1.10

I hereby certify that this New Application Transmittal and the documents referred to as enclosed therein are being deposited with the United States Postal Service on this date March 5, 1997 in an envelope as "Express Mail Post Office to Addressee" Mailing Label Number EM557102133US addressed to the: Assistant Commissioner for Patents, Washington, D.C. 20231.

Samuel J. Petuchowski
(type or print name of person mailing paper)

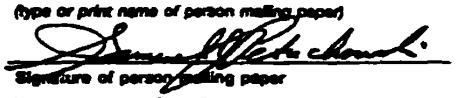

Signature of person mailing paper

NOTE: Each paper or fee referred to as enclosed herein has the number of the "Express Mail" mailing label placed thereon prior to mailing. 37 CFR 1.10(b).

WARNING: Certificate of mailing (first class) or facsimile transmission procedures of 37 CFR 1.8 cannot be used to obtain a date of mailing or transmission for this correspondence.

Background of Invention

1. Field of Invention

The present invention relates to an electrodeposition process whereby a part of a mechanical or electrical component is grown directly on a shape memory alloy component. Conventional techniques can then be used to join or mount the resulting part by joining to the electrodeposited material. This process can include also etching and machining to obtain the desired shape of the final product. The present invention consists also of a technique to join several discrete parts together when one or more part must be made from a shape memory alloy. For this purpose electrodeposition is done simultaneously on two or more parts until they are joined by the electrodeposited material.

The invention was first conceived and put to practice by the two inventors in June 1994 and subsequently continuously improved and developed. This document describes the concept and development to date.

2. Description of Prior Art

Shape Memory Alloys[3] (SMA), such as NiTi alloys, consist of a class of materials which undergo diffusionless martensitic transformations accompanied by definite shape changes. The shape memory effect occurs when a SMA alloy which is deformed in the Martensite temperature range returns to its original undeformed shape when heated above the Martensite inverse transformation temperature and returns to its Parent (austenitic) phase. The superelasticity effect is one of stress induced martensitic transformations. The material is deformed in its Austenite temperature range and internal stresses in the material cause martensitic transformations which are associated with large elastic deformations. These deformations are typically at least an order of magnitude greater than what would be expected from thermal expansion over the applied range of temperature or the maximum elastic deformation in a metal.

Wires made from NiTi shape memory alloys, often referred to as muscle wires, can contract by as much as 8% when heated to the austenite temperature range and in the process exert external forces

exceeding 150MN/m^2. The external forces per cross-sectional area exerted by NiTi wires exceed by a factor of 500 or more those generated by human skeletal muscles. The heating process can occur in less than a millisecond when using Joule heating and the contraction in NiTi wires can be completed within 10-20 milliseconds. Typically it takes a long time for the wire to return to its original length. When using NiTi wires modified by very large current pulses during stretching (see ref. 1) the authors completed twitches including both contraction and relaxation 10 times faster than muscle. NiTi wires can potentially find a large range of applications as actuators in robotics and micro-robotics devices.

NiTi SMA alloys consist of intermetallic compounds which have an atomic composition ratio close to 1:1 and may include a very small percentage of a third element. The atomic composition ratio over which the shape memory effect is observed is very narrow and the alloys very rapidly become very brittle as this range is exceeded. These alloys also have a very high chemical activity and react readily with metals such as Ni, Cu and Fe to produce a brittle reaction phase. For these reasons it is difficult to solder NiTi alloys or to weld them to different metals.

During phase transitions SMA alloys may undergo large dimensional changes. This effect is particularly great in NiTi alloys. As a result if a surface is bonded or joined to another material which does not go through similar dimensional changes very large stresses are generated at the interface that break or weaken the joint. Large external forces can also be generated by martensitic transformations. When mechanical attachments the parts may become loose through cycling. For this reason it is difficult to make reliable mechanical attachments to SMA alloys by the means of clamps, rivets or tightening with screws. In order to generate enough force and compression clamps used to secure NiTi wires must therefore be extremely large and heavy compared to the wires. One of the most

reliable method to attach a NiTi wire is to to wind the wire several times on an anchor and utiiize the capstaneffect.

NiTi alloys can be joined together using fusion welding techniques such as laser welding[4], TIG welding, pressure welding. electron beam welding, pressure welding methods, flash butt welding and friction pressure welding. There is still left the problem of joining NiTi alloys to a dissimilar alloy or metal.

A technique has recently been developed to join SMA alloys to other metals[2]. One of the method for joining parts consists of contacting the surface of the NiTi alloy to the surface of the other metal to be joined, forming a melt-forged structure interface by heating the parts to cause a reactive fusion of the NiTi alloy and the other metal. With the application of sufficient heat and pressure to the NiTi alloy and the other metal hot-forged structures are formed on the two sides of the interface.

Another known method[2] of joining NiTi alloys to other metals consist of a sequence of plating and soldering. The joining surface of the NiTi part to be joined is first plated with a metal which is easily solderable and demonstrates a good adhesion to the NiTi alloy. The part to be joined is then soldered at the plated metal. The plating whose thickness typically does not exceed 10 microns prevents a reaction between the NiTi alloy and the brazing material. It was found impossible however to subject the joined parts to high stresses because of the dependence of the joint strength on the adhesive strength of the solder and of the plating substrate[2]. Soldering is known to provide poor mechanical mounting properties, and it is an industry practice and an electrical standard to provide secure mechanical attachments of components such as electrical wires before soldering.

Summary of Invention

The invention consists in electrochemically growing the parts to be joined until they are linked by the electrodeposited material or to grow one part to form a section which can then be used for mounting. The formation process can also include electrochemical etching of the electrodeposited material or of the original part.

The electrodeposition technique can consist of conventional electrodeposition, spatially constrained electrodeposition[1], laser enhanced electrodeposition (LEEP) used alone or in combination of other methods to control the rate of plating and spatial distribution of the electrolytic currents. The electric field which drives the electrolytic currents can be spatially controlled in three dimensions with the use of masks and resists, and designing the shape of electrodes and container holding the plating solution. Other techniques can be used to accelerate electrodeposition such as local heating, ultra-sound and controlling the flow and replenishment of the plating solution.

Electrochemical etching can also be used as described in the patent on spatially constrained electrodeposition[1]. The electrodeposition can be reversed and material can be removed by reversing the polarity of electrodes and the direction of the currents. The spatial distribution of electrolytic currents can be controlled with the design of electrodes and electrolytic bath, with masks and resists, by controlling the temperature and local flow of electrolytes. Other etching techniques, being chemical, electrical or electrochemical and mechanical machining can also be used to create the desired final shape. Ultimately, the process may only involve etching or machining of the SMA component without any electrodeposition.

This technique can also be used to join directly SMA and non-SMA parts. For example, two NiTi wires with different transition temperatures and properties can be joined by bringing two ends close together other and locally depositing nickel to fill the gap. Alternatively one of the wires could be a copper wire providing an electrical contact.

The robustness of the joints using this technique is mainly a function of the mechanical properties of the deposited material and of the adhesion strength of the deposited material on the SMA alloy. Thermal or mechanical processes may be used to change the properties of the SMA alloy around the interface of the electrodeposited material to prevent phase transformations and high stresses that are induced at the interface.

The reduction in size and weight afforded by the mechanical and electrical connection method of this invention is particularly valuable in building micro-devices, where size and weight are critical. The ability to electrodeposit onto the fibers allows mechanical parts to be electrochemically grown from the fibers. In one microfabrication method, described in U.S. patent application number 08/440949[1], Hunter et al. describe a process in which three dimensional micro-structures are created by localized electrochemical deposition. By localizing electric field in a plating solution to a region on a substrate, deposition is also localized. In this method, fields can be spatially constrained on a substrate by placing a small electrode close to the substrate surface. A potential is applied between the electrode and the substrate to generate a field and induce localized deposition. Three dimensional structures are formed by moving the electrode appropriately relative to the surface to build up deposits. Thus wires and mechanical linkages can be connected directly to the artificial muscle fibers. Among other materials, copper, chrome and nickel can readily be deposited onto plated nickel, thus allowing mechanical and electrical connections. The combination of the localized electrodeposition technology and the method of this invention thus allows the fabrication of actuated micro-electro-mechanical devices. The ratio of force to cross-sectional area provided by the artificial muscle fibers and their rapid contraction times make them very well suited to incorporation in micro-structures.

BRIEF DESCRIPTION OF THE PROCESS

Figure 1 describes a method of embodiment which permits to attach a NiTi wire to a rod or another NiTi wire. A NiTi wire 2 is joined to a nickel rod 3. An electrodeposition bath 1 consists of a rectangular section of plastic with a chamber in the center to the plating solution. There are two slits in the wall of the chamber where the wire and the rod can be inserted. These slits are covered with a thin latex membrane to prevent leakage of the electrolitic solution. On the right side the left end of a NiTi wire 2 enters the chamber and comes in close contact with the rod. On the left the right end of the nickel rod 3 enters the chamber. A nickel anode 4 with a circular hole in the center is positioned vertically in the center of the chamber. The rod and NiTi wire are centered along a line which goes through the center of the hole. The electrodeposition is therefore concentrated around the gap between the NiTi wire and the nickel rod. Both the nickel rod and the NiTi wire are connected to the negative side of a current source and serve as cathodes. The

electrodeposited nickel grows simultaneously on the two ends which come in physical contact and subsequently nickel grows in the form of a spindle joining the two wires.

The NiTi surface of the sample must first be prepared for the electrodeposition as described in Johnson[5]. The surface is first cleaned with alcohol and a silicon carbide abrasive. The final removal of the oxyde layer and other impurities is achieved by chemical etching in a solution of 16% nitric acid and 4% hydrofluoric acid. The part subsquently washed with distilled or deionized water.

The prefered plating solution consists of approximately 1M nickel fulmanate. The sulfamate is chosen because it produces nickel deposits with a high tensile strength (620 Mpa), low residual stress (3.5Mpa) and even distribution. The anode normally consists of pure nickel but can also consist of other materials.

Figure 2 depicts a NiTi wire 1 after a bulk electrodeposition of Nickel 4 at one end. Typically the diameter of the wire 250μ and the diameter which is grown to approximately 750μ. Such a wire can then be mechanically mounted by inserted in a holder 2 which has a slit of 275μ at the bottom and a cylindrical cavity of 800μ where the enlarged end of the NiTi fiber is deposited. A screw 3 secures mechanically the NiTi wire in place.

In its simples form, one end of the wire is grown with bulk electrodeposition of Nickel. The end of the fiber is then soldered or brazed on the nickel for electrical connection. Soldering can be used to mount the electrodeposited nickel mechanically for temporary use or for applications which do not involve any electrical safety hazard if the connection breaks. The main difference between this method and the already known method consisting of plating and soldering is that in the known method a nickel coating of a few microns only is used. We used a sufficiently large amount of electrodeposited nickel is to increase the diameter of the NiTi fiber by a significan amount, typically by a factor of 4 and more. Our tests show that the force required to pull the NiTi wire out of the nickel is much greater than the force required to break the NiTi fiber. Our tests show also that it resists to repeated cycling of the temperature between the Martensite temperature range and the Austenite temperature range.

Claims:

1. A method for electrically and mechanically coupling elements comprising the steps of
(a) providing two or more elements positioned close to each other;
(b) providing a solution that will, in an electrochemical reaction, deposit a desired product on the elements;
(c) providing a counter electrode;
(d) depositing the product on the elements by passing a current between the elements and the counterelectrode and through the solution, thereby inducing electrodeposition of the product onto the elements;
(e) continuing the deposition of step (d) such that the product bridges the gap between the elements;
whereby a mechanical and electrical coupling is formed between the elements.

2. The method of claim 1 wherein the product is at least in part a material selected from the group consisting of electrodepositable metals, alloys, polymers and semiconductors.

3. The method of claim 2 wherein the product is at least in part nickel.

4. The method of claim 1 wherein the elements are at least in part materials selected from the group consisting of metals, alloys, polymers and semiconductors onto which electrodeposition is achievable.

5. The method of claim 4 wherein the elements are at least in part a material selected from the group consisting of titanium and titanium alloys.

6. The method of claim 4 wherein the elements are at least in part composed of nickel titanium alloy.

7. The method of claim 1 wherein the spacing between the elements is between contact and 0.2 mm.

8. The method of claim 1 where mandrels are used to constrain the electrodeposited metal in space.

9. The method of claim 1 or claim 6 where the electrodeposited metal is then attached to another piece using any other know technique.

10. The method of claim 9 where only one element is used.

11. The method of claim 1 or claim 10 where first the current is to etch part of the elements and then reversed to electrodoposit material.

12 The method of claim 11 repeated a number of times.

13. A method of claim 10 where the deposited materail exceeds a thickness of 10 μm.

Abstract

This disclosure describes a process which permits the mechanical and electrical joining of parts made from nickel-titanium shape memory alloys (SMA) and other materials that are difficult to join using conventional techniques such as welding, brazing, soldering, bonding, clamping and pressure assembly.

This process was developed more particularly for nickel titanium (NiTi) shape memory alloys (often referred to as nitinol) and superelastic alloys whose range of applications as actuators and flexible joints is severely limited by the difficulties encountered in mounting them using known techniques. The new process consists of using electrodeposition or spatially constrained deposition (see ref. 1) to grow a material such as nickel on the parts to be joined until it connects physically the parts together or until it forms a new section of the part that can then be used for attachments. This process has a wide range of applications and can be used to join a very large range of materials including Titanium alloys in general and other materials such as synthetic metals.

The following references are incorporated herein by reference:

1. Hunter, Ian, Lafontaine, Serge R. and Madden, John D Three dimensional microfabrication by localized electrodeposition and etching, U.S. Patent 08/440949.

2. Hall, Todd A. Joint, A laminate, and a method of preparing a nickel-titanium alloy member surface for bonding to another layer of metal. U.S. Patent 08/05354623.

3. Funakubo, H. Shape Memory Alloys, Gordon and Breach Science Publishers, 1987.

4. Hirose, A., Uchihara, M., Araki, T., Honda, K., Kondoh, M., Laser welding of Ti-Ni type shape shape memory alloy, Journal of the Japan Institute of Metals, vol 54, no. 3, p 262-269.

5. Johnson, A.D. and P.I. Katz, Spontaneous emf associated with shape memory effect in TiTi, Journal of Applied Physics, Vol 48, No 1, January 1977.

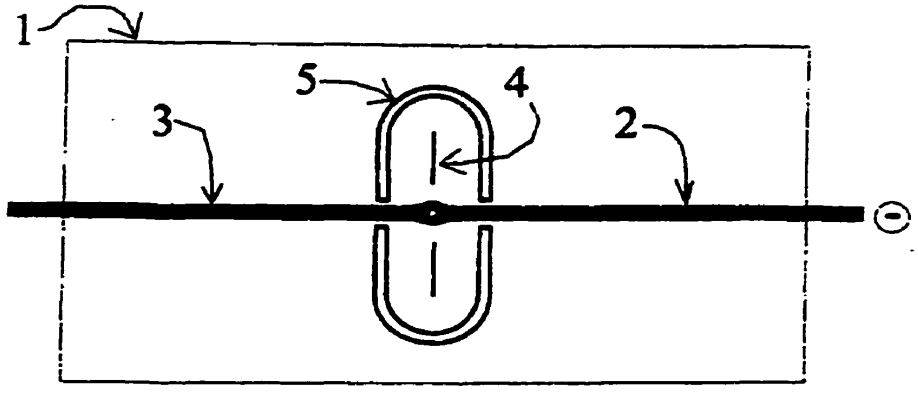

Figure 1 Joining a NiTi wire to another wire.

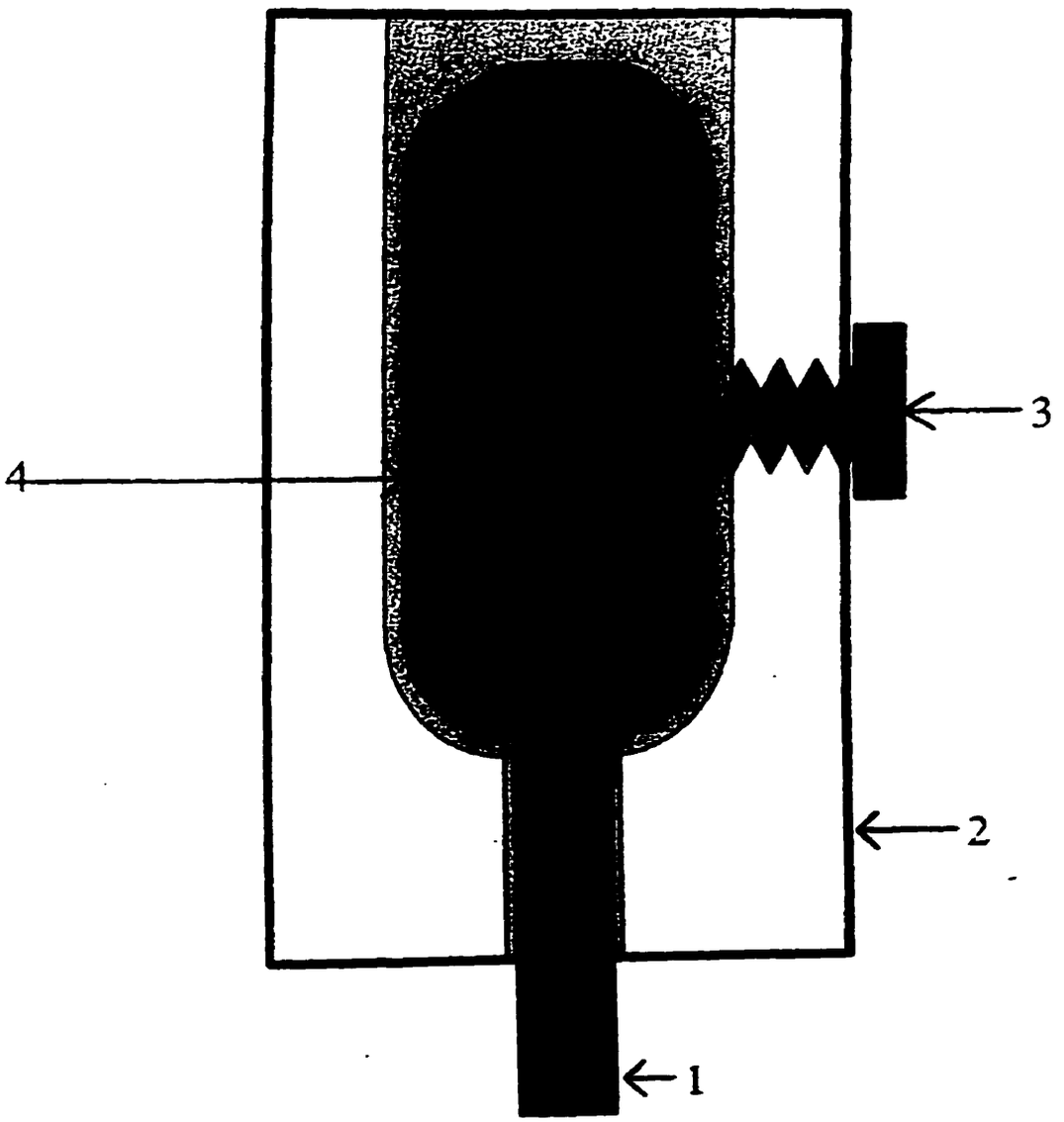

Figure 2 **Example of an attachment of a NiTi wire.**

US005641391A

United States Patent [19]

Hunter et al.

[11] Patent Number: 5,641,391

[45] Date of Patent: Jun. 24, 1997

[54] **THREE DIMENSIONAL MICROFABRICATION BY LOCALIZED ELECTRODEPOSITION AND ETCHING**

[76] Inventors: **Ian W. Hunter**, 6 Oakdale La.; **Serge R. Lafontaine**, 11 Mill St. Extension, both of Lincoln, Mass. 01773; **John D. Madden**, 3290 Cypress St., Vancouver B.C., Canada, V6J 3N6

[21] Appl. No.: **440,949**

[22] Filed: **May 15, 1995**

[51] Int. Cl.[6] C25D 5/00; C25D 5/08; C25D 7/06; C25F 3/00

[52] U.S. Cl. 205/80; 205/133; 205/137; 205/138; 205/139; 205/140; 205/141; 205/142; 205/640; 205/652; 205/654; 205/668; 205/670; 205/672; 205/686

[58] Field of Search 205/80, 118, 133, 205/137, 138, 139, 140, 141, 142, 640, 652, 668, 670, 672, 686, 654; 204/129.1, 129.5

[56] **References Cited**

U.S. PATENT DOCUMENTS

3,267,014	8/1966	Sanders	205/670
4,349,583	9/1982	Kalyuych	427/53.1
4,364,802	12/1982	Inoue	205/118
4,432,855	2/1984	Romankiw	204/207
4,497,692	2/1985	Ganchaski	204/15
4,929,402	5/1990	Hall	264/401
4,968,390	11/1990	Bard et al.	205/118
5,149,404	9/1992	Blonder et al.	205/686
5,162,078	11/1992	Bley	205/75
5,389,196	2/1995	Blomstrom	156/643

FOREIGN PATENT DOCUMENTS

563 744	10/1993	European Pat. Off. .
57-120692	7/1982	Japan .

OTHER PUBLICATIONS

Uhlir, Jr., "Micromachining with Virtual Electrodes", Rev. of Sci. Instr., vol. 26, No. 10, pp. 965–968 Oct. 1955.

Liu et al., "High Resolution Photoelectrochemical Etching of n-GaAs with the Scanning Electrochemical and Tunneling Microscope", J. of Electrochem. Soc., vol. 134, No. 4, pp. 1038–1039 1987.

Jean M. Hagenhorst et. al. Focussed Excimer Laser Beams: A Technique for Selective Micropatterning, SPIE vol. 998 pp. 105–112 (No Month, 1988).

K. Ikuta, "Three Dimensional Integrated Fluid Systems . . . ", Proceedings—IEEE Micro Mechanical Systems, pp. 1–6, 1994 (No Month).

(List continued on next page.)

Primary Examiner—Kathryn L. Gorgos
Assistant Examiner—Edna Wong

[57] **ABSTRACT**

Embodiments of the present invention provide a new method for producing a three dimensional object, particularly suited to microfabrication applications. The method includes the steps of providing a substrate with a conducting interface, an electrode having a feature or features that are small relative to the substrate, and a solution. The solution has a reactant that will either etch the substrate or deposit a selected material in an electrochemical reaction. The electrode feature is placed close to but spaced from the interface. A current is passed between the electrode and the interface, through the solution, inducing a localized electrochemical reaction at the interface, resulting in either the deposition of material or the etching of the substrate. Relatively moving the electrode and the substrate along a selected trajectory, including motion normal to the interface, enables the fabrication of a three dimensional object. In an alternative embodiment, current is passed through an orifice placed close to but spaced from the substrate surface, and may be accompanied by forced convection through the orifice. The method provides the potential to fabricate using many materials, including metals, alloys, polymers and semiconductors in three dimensional forms and with sub-micrometer spatial resolution.

17 Claims, 7 Drawing Sheets

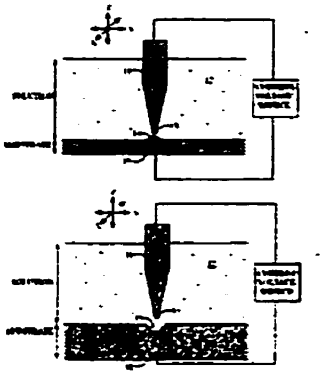

OTHER PUBLICATIONS

M. Boman, "Helical Microstructures Grown by Laser Assisted Chemical Vapour Deposition", Proceedings—IEEE Micro Electro Mechanical Systems, pp. 162–167 1992 (No Month).

W.H. Bruenger, "E-Beam Induced Fabrication of Microstructures" Micro Electro Mechanical Systems, pp. 168–170, 1992 (No Month).

C.W. Lin, "High Resolution Photoelectrochemical Etching of n-GaAs . . . " J. of Electrochemical Society, vol. 134 pp. 1038–1039, 1987 (No Month).

Schein, "Creating and Observing Surface Features with a Scanning Tunneling Microscope" SPIE vol. 897 pp. 16–19 1988 (No Month).

A.A. Gewirth, "Fabrication and Characterization of Microtips . . . " Journal of Electroanalytical Chemistry vol. 261, pp. 477–482, 1989.

Nagahara "Preparation and Characterization of STM Tips for Electrochemical Studies", Review of Scientific Instruments vol. 60 pp. 3128–3139 Oct., 1989.

FIG. 1a

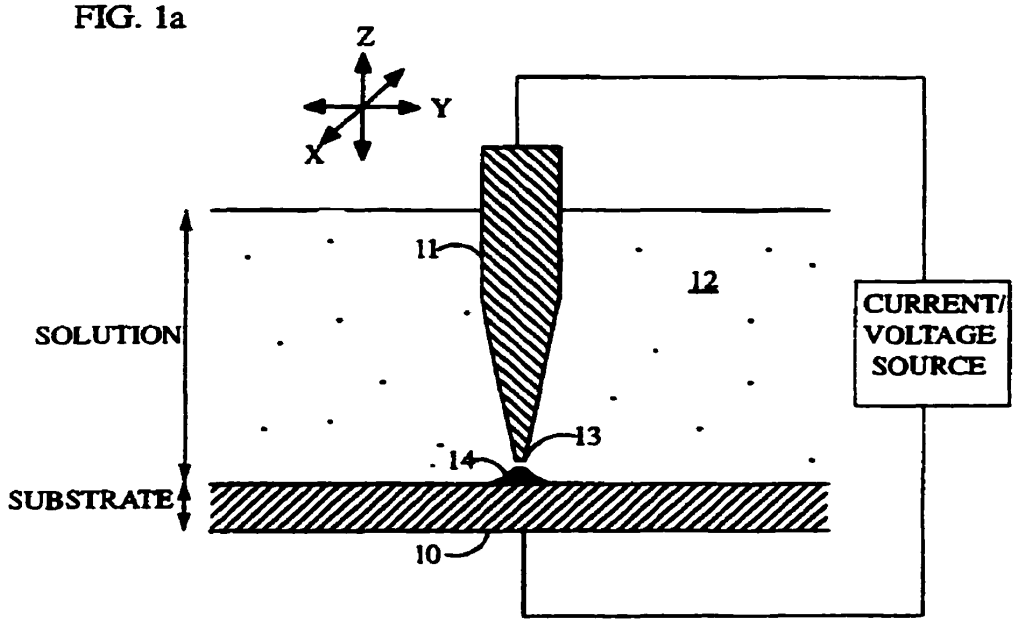
Z
Y
X
11
12
SOLUTION
CURRENT/
VOLTAGE
SOURCE
13
14
SUBSTRATE
10

FIG. 1b

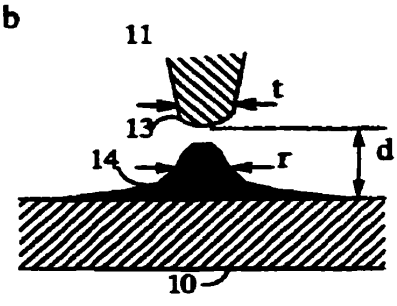
11
t
13
14
r
d
10

FIG. 1c

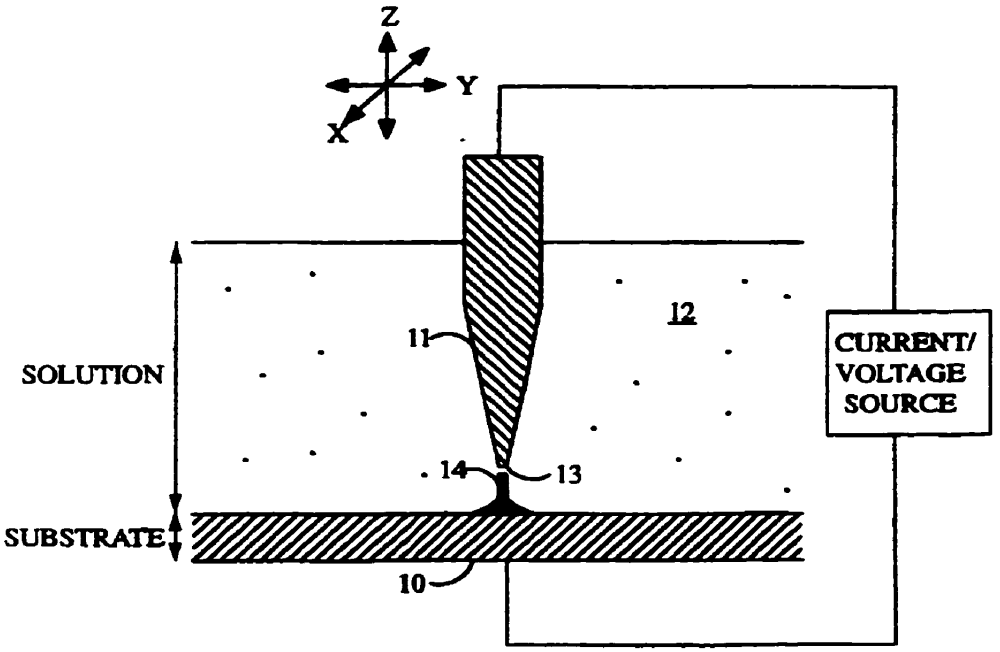
Z
Y
X
SOLUTION
SUBSTRATE
11
12
13
14
10
CURRENT/
VOLTAGE
SOURCE

FIG. 1d

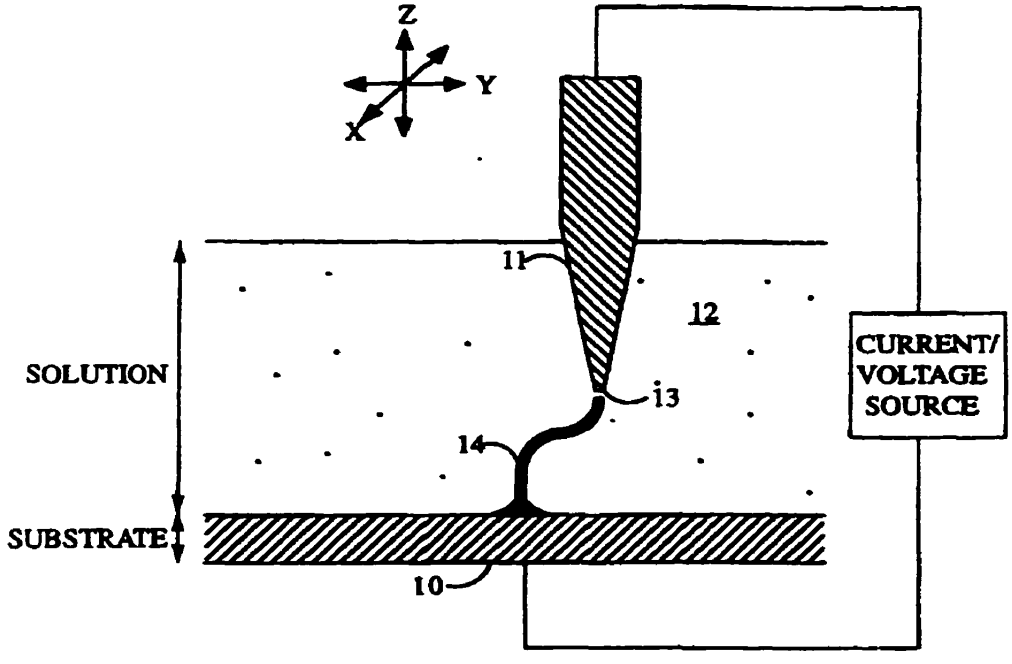
Z
Y
X
11
12
13
14
SOLUTION
SUBSTRATE
10
CURRENT/
VOLTAGE
SOURCE

FIG. 2a

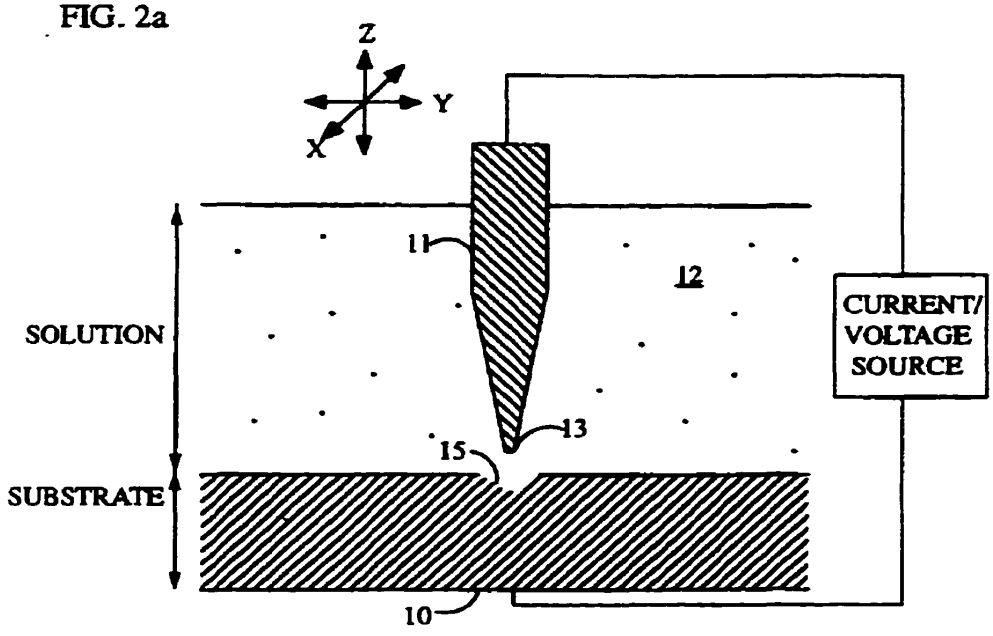
Z
Y
X
11
12
SOLUTION
CURRENT/
VOLTAGE
SOURCE
13
15
SUBSTRATE
10

FIG. 2b

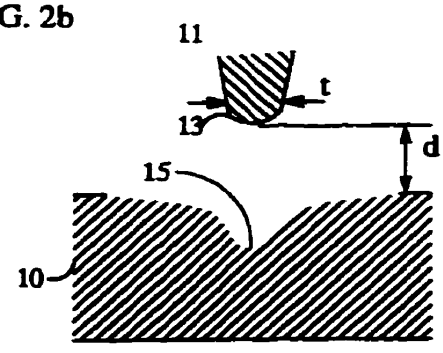
11
t
13
d
15
10

FIG. 2c

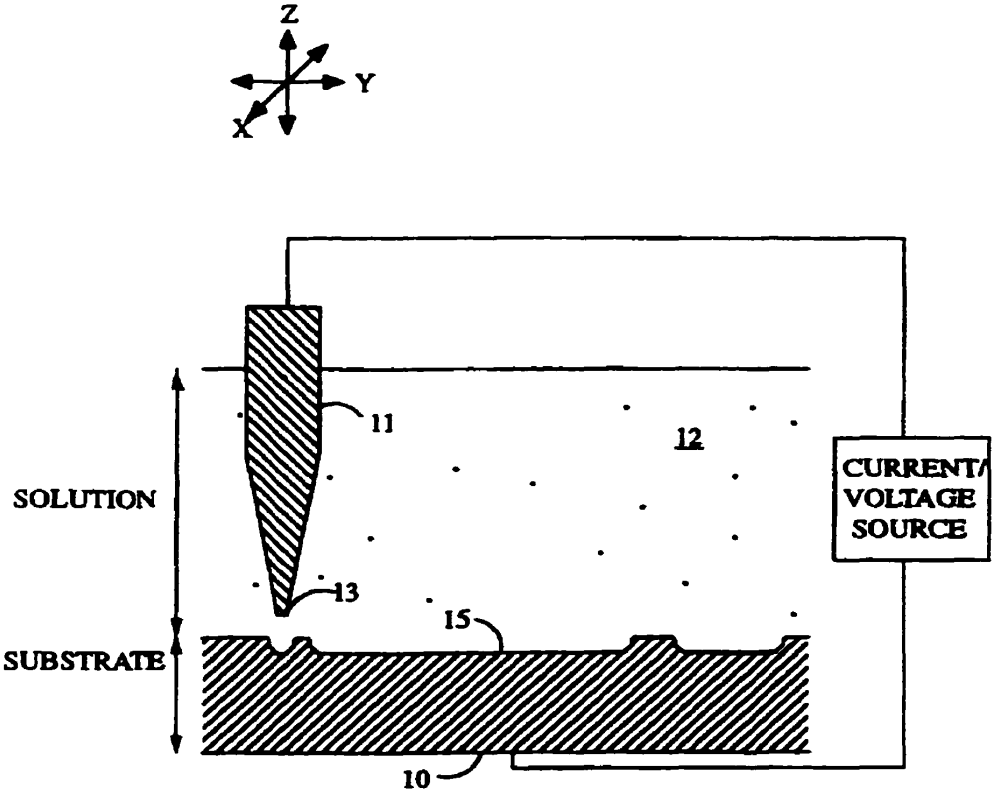
Z
Y
X
11
12
13
15
SOLUTION
SUBSTRATE
CURRENT/
VOLTAGE
SOURCE
10

FIG. 2d

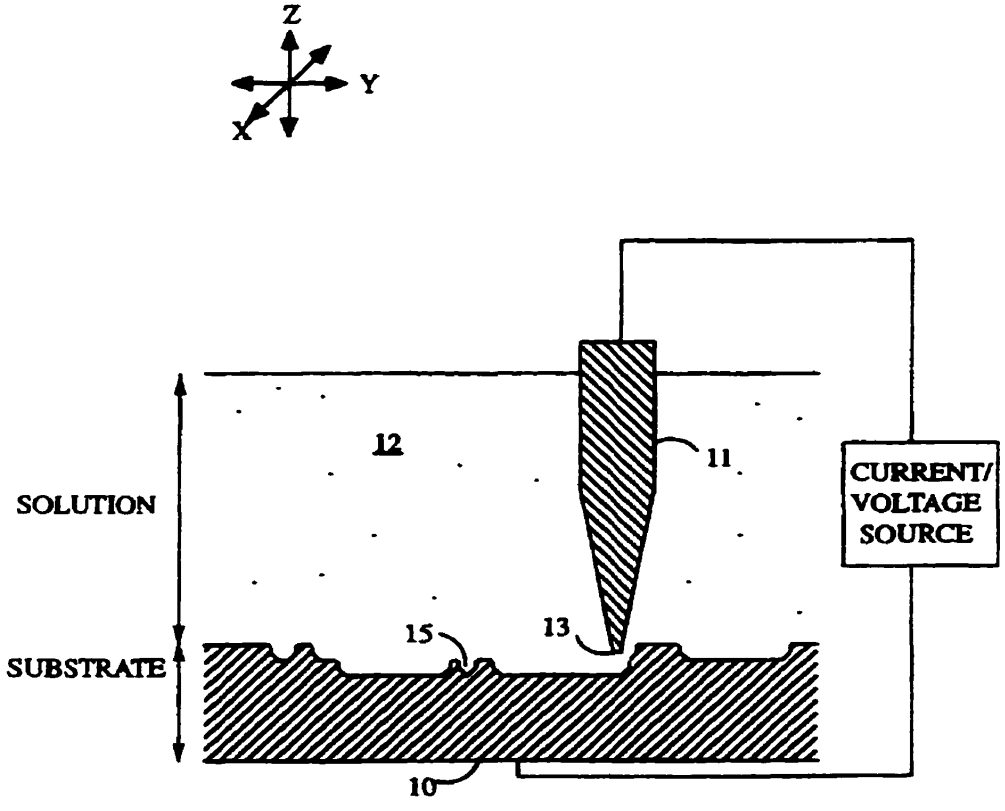
Z
Y
X
12
11
SOLUTION
CURRENT/
VOLTAGE
SOURCE
15
13
SUBSTRATE
10

FIG. 3

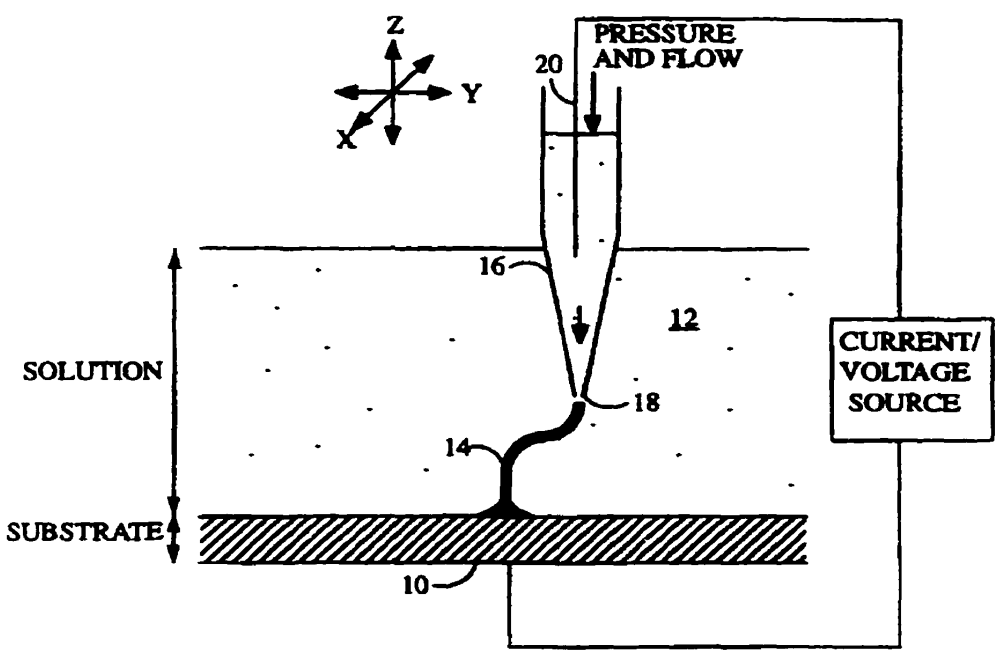
Z
Y
X
PRESSURE
AND FLOW
20
16
12
18
14
SOLUTION
SUBSTRATE
10
CURRENT/
VOLTAGE
SOURCE

THREE DIMENSIONAL MICROFABRICATION BY LOCALIZED ELECTRODEPOSITION AND ETCHING

TECHNICAL FIELD

This invention relates to the fabrication of three dimensional microstructures by a process of localized electrochemical deposition and localized electrochemical etching.

BACKGROUND OF INVENTION

The miniaturization of electronics has led to devices that are faster, cheaper, and more versatile with every new generation. Building micromechanical devices offers similar benefits. For example, resonant frequencies increase as dimensions are reduced, allowing high bandwidth accelerometers and pressure sensors to be built. Miniature devices integrating actuators, limbs, sensors, computing and energy supplies offer, among other things, the potential to access microscopic spaces, with major implications for medicine. In large scale devices, nature offers many examples of what can be achieved by fabricating macroscopic systems with nanoscopic precision, including ourselves.

In order to realize the potential offered by micro and nanotechnology, it is necessary to manipulate material on micrometer and nanometer scales. Important characteristics of fabrication technologies include (1) spatial resolution, (2) achievable geometry, (3) available materials, (4) fabrication rate and (5) cost. Spatial resolution is defined by the dimensions of the smallest feature that can be produced by a given fabrication method. Achievable geometry refers to the range of shapes a method is capable of producing. The ability to incorporate a wide range of materials is particularly important because microdevices, like macrosystems, in general require actuators, energy delivery and storage, mechanical elements, circuits, and sensors. These functions are unlikely to be optimized using a limited range of materials. The difficulty in assembling and fastening parts on micrometer scales make geometric versatility and wide range of materials particularly desirable properties of a fabrication process.

Traditional milling, welding and fastening technologies do not have the spatial resolution required to generate microdevices. Integrated circuit technology is increasingly being applied to fabricate mechanical, electro-mechanical and electro-opto-mechanical devices on millimeter and micrometer scales, including miniaturized accelerometers and pressure sensors. However, the nearly two-dimensional regime of this technology restricts applications and performance. In general, the low aspect ratio (height to width) structures of uniform thickness produced do not optimize functionality. While multiple layers have been employed to add thickness and features in a third dimension, the long development times, low yields and high costs involved restrict the number of layers which are practical. Furthermore, the materials used are primarily silicon-based.

Lithography-related techniques such as LIGA (from the German for lithography, electroplating and molding) allow aspect ratios to be increased substantially (see for example U.S. Pat. No. 5,162,078 in the name of P. Bley et. al. issued Nov. 10 1992). In these techniques two dimensional mask patterns are etched into resist layers that can be more than 300 micrometers thick. The resist layers are often used as molds. While lithography-related techniques produce high aspect ratio structures with high lateral resolution, these structures are of uniform thickness, or essentially two dimensional structures with added thickness.

Several three dimensional microfabrication technologies are under development, the most notable being focussed beam excimer laser machining, stereo lithography and laser-assisted chemical vapour deposition.

A three dimensional fabrication technology is defined as one that can be employed to generate objects of virtually arbitrary geometry. In general, achievable geometries are limited only by the requirements of material continuity with a supporting substrate and mechanical stability of the objects being constructed. Three dimensional fabrication technologies are capable of generating objects such as helically coiled springs and hollow spheres. Two classes of three dimensional fabrication technologies exist, namely those in which material is removed from an existing body, as in milling and sculpting, and those in which material is added to build up a structure, as in brick laying and stereo lithography. Material addition methods generally require few or no assembly steps. For example, the fabrication of a hollow sphere can be achieved in one process, without assembly, by the method of this invention, whereas with a machining process at least one assembly step is necessary. The minimization of assembly steps is especially important in microfabrication because manipulation of parts is particularly challenging. The ability to combine material removal and addition in one technology is very valuable because large numbers of part geometries can be constructed and modified, either by addition or removal of material.

Fabrication methods wherein patterns of relatively uniform depth are generated on a surface are not considered three dimensional. These include methods of patterning uneven and contoured surfaces.

Focussed excimer laser beams have been used to ablate a wide range of materials, including polymers, ceramics and metals (see for example J. M. Hagenhorst et. al. "Focussed Excimer Laser Beams: A Technique for Micropatterning", SPIE, vol. 52, pp.299–304, 1992.). Resolution of focussed beams is diffraction limited to approximately ~0.2 micrometers. However, there is a tradeoff between depth of focus and resolution since high resolution requires high numerical aperture beams. Hence high aspect ratio is only practical with micrometer or larger features. Material removal technologies, such as excimer machining, are in general limited in their geometrical versatility, in part because they access through the outer surface of an existing substance.

In U.S. Pat. No. 4,929,402, issued May 29, 1990, C. H. Hull teaches a stereolithography method which has been employed by Ikuta et. al. to build microstructures ("Three Dimensional Micro Integrated Fluid Systems Fabricated by Stereo Lithography", Proceedings—IEEE Micro Electro Mechanical Systems, pp. 1–6, 1994.). In stereo lithography a beam of radiant energy interacts with a photo-sensitive polymer, causing it to harden. Controlled volumetric irradiation of the polymer allows structures of virtually arbitrary geometry to be fabricated. Materials are limited to a selection of photosensitive polymers, however. Resolution is restricted by diffraction limits and viscous forces from the unhardened polymer on the hardened material. The best resolution achieved to date is about 10 micrometers.

M.Boman et. al. describe a microfabrication method employing laser assisted chemical vapour deposition (LCVD) to fabricate three dimensional structures ("Helical Microstructures Grown by Laser Assisted Chemical Vapour Deposition", Proceedings—IEEE Micro Electro Mechanical Systems, pp. 162–167, 1992.). T. M. Bloomstein et. al. describe a similar method for depositing and etching material in U.S. Pat. No. 5,389,196, issued Feb. 14, 1995. A

focussed photon, ion or electron beam interacts with a substrate surface in a vapour atmosphere, inducing a local chemical reaction, and resulting in material being deposited from the vapour or etched from the substrate. Reported resolutions using photon beams are ≦10 micrometers, limited by diffraction and thermal conduction at the substrate surface. Electron beams have enabled 0.2 micrometer resolution, but at the expense of deposition rate, which is on the order of 0.02 micrometers per second (see W. H. Brunger et. al., "E-beam Induced Fabrication of Microstructures", Proceedings—IEEE Micro Electro Mechanical Systems, pp. 168–170, 1992). Photon beam induced deposition rates of several micrometers per second are achieved in building three dimensional structures. In the deposition process, materials are restricted to those that can be grown on a substrate from vapour phase via a chemical reaction. Common materials are tungsten, boron and silicon.

Electrochemical deposition and Etching

A wide range of materials can be electrodeposited, including many metals and alloys, some polymers (such as polyaniline and polypyrrole), and semiconductors (such as cadmium chalcogenides). Electrochemical etching enables many of the same materials to be machined as well as others such as gallium arsenide. However, in conventional electroplating deposition occurs indiscriminately on a substrate, forming thin films rather than three dimensional structures. Rates of deposition are generally slow (e.g. about 100 micrometers per hour). Electroforming is used to build three dimensional structures. There is still the difficulty of fabricating the mold however.

Three basic approaches have been taken to create lateral features in deposits. The first makes use of lithography to selectively etch features in a deposited film. This method is used to make electrical connections for integrated circuits, for example. The aspect ratios achieved are particularly low due to etching undercut. Two other approaches involve either locally enhancing deposition rate by local heating, or placing a small electrode near the substrate to localize the reaction.

In laser enhanced electroplating and etching, laser light is focussed on a substrate, heating a local region, as taught by U.S. Pat. No. 4,497,692 (Gelchinski et. al., Feb. 5, 1985) U.S. Pat. No. 4,432,855 (L. T. Romankiw, issued Feb. 21, 1984), and U.S. Pat. No. 4,497,692 (D. R. Vigliotti et. al., issued Feb. 5, 1985) The heating locally enhances deposition and etching rates by as much as three to four orders of magnitude. Jet-plating and etching, in which a jet of plating or etching solution locally impinges on a substrate, is combined with laser enhanced electroplating, as described in U.S. Pat. No. 4,349,583, to improve deposit and etch properties, and to further enhance reaction rate. Laser enhanced electroplating (etching) produces two dimensional patterns deposited (etched) by scanning the beam parallel to the substrate surface. Resolution is again limited by diffraction as well as the substrate thermal conductivity. Reported resolutions are ≧2 μm. Deposition rates, however, are high (about 10 micrometers per second)

Liu et. al. describe a method whereby placing a sharp-tipped electrode (scanning tunneling microscope tip) close to a substrate surface in a conducting solution, and applying a selected potential between the tip and the substrate, local etching is induced ("High Resolution Photochemical Etching of n-GaAs with the Scanning Electrochemical and Tunneling Microscope", Journal of the Electrochemical Society", vol. 134, pp.1038–1039, 1987). They use an approximately 0.1 micrometer diameter electrode in close proximity (<1 micrometer) to a GaAs substrate to etch 0.3 micrometer wide lines. The GaAs substrate is uniformly irradiated by alight source to make it conductive. An electrochemical reaction is induced on the substrate whose spatial distribution is a function of the surface current distribution, which in turn depends on the applied potential, and the tip to substrate distance. The tip was scanned parallel to the substrate to form lines. No attempt was made to build a three dimensional object.

U.S. Pat. No. 4,968,390 describes a method to electrochemically deposit conducting substances on the surfaces of conducting objects (Bard et.al., issued Nov. 6, 1990). The invention involves coating a substrate with a thin, ionically conducting film containing the reactant to be deposited, and scanning laterally across the film to deposit and etch lines of widths as small as ~0.2 micrometers, where the feature size is limited by the sharpness of the tip. Deposition and etching in three dimensions is not possible using this method since the solid electrolyte effectively fixes the tip to substrate spacing.

Schneir et. al. describe a similar method wherein an electrode is placed 1 micrometer from a gold substrate in a liquid plating solution and a potential is applied across the gap ("Creating and Observing Surface Features with a Scanning Tunneling Microscope", SPIE vol. 897, pp. 16–19, 1988). Positioning of the tip relative to the substrate is achieved by first finding the substrate surface using the tip in tunneling mode. In their method the tip and the substrate are immersed in an electroplating solution. The applied potential induces electrodeposition at the surface. The tip was moved back and forth in a line parallel to the gold substrate to produce a line of electrodeposited gold about 0.3 micrometers wide. There is no description or discussion of using this technique to build three dimensional objects.

It is the object of the invention to provide a process for producing three dimensional structures with sub-micrometer spatial resolution employing a range of materials selected from metals, polymers, and semi-conductors that will attempt to overcome the lack of fabrication methods capable of producing three dimensional objects from a wide range of materials and with sub-micrometer spatial resolution.

Further objects and advantages will become apparent from a consideration of the drawings and ensuing descriptions.

SUMMARY OF INVENTION

These and other objects of the invention are achieved by a method which in one aspect features a method for producing a three dimensional object. The method includes the steps of providing a suitable conducting substrate, an electrode and a solution. The outer surface of the substrate defines an interface. The electrode must have at least a feature with at least a dimension that is small relative to the dimensions of the interface. The solution contains a reactant that will, in an electrochemical reaction, deposit a desired material. The electrode feature or features are placed close to but not contacting the interface. Local deposition of the material is achieved by passing a current between the electrode and the substrate through the solution. Relatively moving the electrode and the substrate along a selected trajectory, and locally depositing in the process, enables the fabrication of a three dimensional object, given that part of the trajectory and some corresponding deposition occurs normal to the surface. In etching the surface to form a three dimensional object, the procedure is almost the same as described for deposition. The solution is chosen such that, in

an electrochemical reaction, the substrate is etched, rather than material deposited. Furthermore, etching is performed along a trajectory that contains a component normal to and towards the substrate surface.

In the method described, more than one reactant may be provided in the solution. Varying the potential can then be caused to selectively deposit the different materials as chosen, or a combination of them together (in an alloy for example). The deposited material may be a pure metal, an alloy, a polymer or a semiconductor. Similarly, more than one reactant may be provided to selectively etch various materials that comprise the substrate individually, or simultaneously. The substrate materials may also be metals, alloys, semiconductors or polymers.

An example electrode is a sharp conducting wire with a tip diameter of between about 5 and 200,000 nm. The tip provides the feature mentioned above. Another example electrode is an approximately disk-like or hemispherical electrode having about the same range of dimensions as the tip. More general shapes and patterns are also possible. As an illustrative example, the feature may be placed within approximately its own smallest dimension of the interface in order to localize the deposit or etch. Multiple electrodes can also be provided, as opposed to just one, providing that they each have at least a feature with a dimension that is small relative to the substrate. Each electrode is used just as described for a single electrode.

Injecting fresh solution into the region of the localized electrochemical reaction (etching or deposition) can improve mass transfer and thereby increase the rate. In the case of deposition, the quality may also be improved. Therefore the invention provides for the optional addition of a nozzle, through which the solution is pumped into the region between the electrode and the interface during deposition or etching.

In accordance with an aspect of the invention there is further provided a method for producing a localized deposit of material comprising the steps of providing a substrate, an electrode, a nozzle, and a solution. The substrate has an outer conducting surface defining an interface. The solution contains a reactant which will, through an electrochemical reaction, lead to the deposit of a desired material. The nozzle is electrically isolated from the electrode and the substrate. The nozzle is placed between the electrode and the interface such that any current between them will pass through the nozzle. A flow is generated through the nozzle's orifice, which is positioned close to, but not in contact with, the substrate. Passing a current between the electrode and the substrate, and therfore through the orifice, induces a spatially localized electrochemical reaction at the interface. The product of the reaction is the deposited material and thus material is locally deposited. Localized etching is achieved in the same manner, with the following exceptions. The solution contains a reactant which will, through an electrochemical reaction, lead to the etching of a selected material. Thus the step of passing a current through the orifice leads to localized etching of the substrate.

Following the same steps described in the previous paragraph, with the added step of relatively moving the electrode and the substrate along a selected trajectory, and locally depositing in the process, enables the fabrication of a three dimensional object, given that part of the trajectory and some corresponding deposition occurs normal to the surface. The same applies to etching the surface, where local deposition is replaced by local etching.

Advantageously, the method of the current invention range of possible geometries, and composed of a wide variety of materials to be constructed with a resolution dependent only on the ability to localize electrochemical deposition or etching.

BRIEF DESCRIPTION OF DRAWINGS

Exemplary embodiments of the invention will now be described in conjunction with the drawings in which:

FIG. 1*a* shows a schematic representation of a method to locally electrodeposit material on a conducting substrate;

FIG. 1*b* shows a schematic representation of a sharp electrode placed close to but spaced from a conducting substrate;

FIG. 1*c* shows a schematic representation of the result of the tip being translated vertically with simultaneous deposition as an illustration of a trajectory leading to the fabrication of a three dimensional object;

FIG. 1*d* shows a schematic representation of the result of the tip being further translated from the situation shown in FIG. 1*c* leading to the fabrication of a three dimensional object;

FIG. 2*a* shows a schematic representation of a method to locally electrochemically etch material on a conducting substrate;

FIG. 2*b* shows a schematic representation of a sharp electrode placed close to but spaced from a conducting substrate;

FIG. 2*c* shows a schematic representation of material being selectively removed from a layer of the substrate;

FIG. 2*d* shows a schematic representation of material being selectively removed from a second layer of the substrate leading to the fabrication of a three dimensional object;

FIG. 3 shows a schematic representation of an embodiment in the deposition configuration wherein current is channelled through an orifice, through which solution is being forced.

DETAILED DESCRIPTION

The present invention involves a new method of depositing metals, polymers and semiconductors and of etching metals, semiconductors, ceramics and polymers with high resolution and in three dimensions. Deposition and etching are achieved by electrochemical reactions which are localized on a conducting surface.

The method involves choosing a suitable conducting substrate and a liquid solution that contains reactant(s) that will deposit the desired product(s) upon electrochemical oxidation or reduction. In the etching case the reactant(s) are chosen so that they will etch the substrate. An electrode is provided with characteristic features that are small relative to the size of the substrate. By placing these features close to the substrate, and applying an appropriate potential, current and thus either etching or deposition on the substrate are localized. The electrode is then moved relative to the substrate in three dimensions to form structures, either building up material from the substrate, or etching it away.

An illustrative system for carrying out the process is schematically shown in FIG. 1. The etching case is shown in FIG. 2. A conducting substrate 10 and an electrode 11 are immersed in a solution containing reactant(s) 12. The substrate 10 is prepared for deposition such that the surface roughness is significantly less than the desired fabrication

glass slides or other materials. Alternatively, mechanical polishing or electropolishing can be employed. In the etching case, surface roughness on the order of etching resolution can be smoothed as part of the process. The electrode 11 has a sharp tip 13 and is typically made of platinum or platinum iridium, whose preparation has been previously described in scanning tunneling microscopy related literature. However, the electrode 11 can potentially be made of any electrically conducting material, including, but not limited to metals, carbon, and conducting polymers. The tip 13 dimensions range between about 5 and 200 000 nm in diameter. Motors drive the tip relative to the substrate in X, Y and Z directions. In the exemplary embodiment microstepping motors were used. However voice coil actuators and other motors capable of producing sub-micrometer scale displacements are also appropriate. Rotational degrees of freedom can be added, allowing the direction of growth or etching to be perpendicular to the electrode surface. Degrees of freedom can be attached to either the electrode, the substrate or both since it is the relative motion that is important. An example combination of substrate 10 and solution 12 for deposition is copper in a sulfamate nickel plating solution.

The tip 13 is positioned close to the substrate 10 in order to localize deposition or etching. The appropriate tip to substrate separation in order to achieve a given localization, or spatial resolution, depends on tip geometry, the solution and reactant(s) used, the applied potential between the tip and the substrate and to some extent on the tip and substrate materials. In general to achieve a given resolution, r, the distance, d, between the tip and the substrate should be $\leq r$, with a tip diameter, $t \leq r$. For a given tip, the best achievable resolution is $\geq t$ given $t \geq d$.

Electrode geometries other than sharp tips can be employed to generate a spatially modulated field distribution. Disk or hemispherical electrodes can be used, for example. Given an electrode diameter, d, resolution is again obtained as described in the previous paragraph. Electrodes of virtually arbitrary geometry can be used to effect localized etching and deposition, providing a dimension of some feature is small relative to the interface size. A razor blade geometry, for example, can be employed, with the sharp edge aligned parallel to the interface. Moving the electrode vertically allows the construction of a wall. In order to deposit or etch a given electrode pattern the smallest dimensions of the pattern should be approximately its own width away from the surface. The advantage of using non-tip geometries is that structures are then effectively being built-up in parallel. However, the tip electrode described above is both the simplest to fabricate and implement, and can generate the widest range of structure geometries. The use of several electrodes acting in parallel offers the possibility of both maximum resolution and parallel fabrication. These electrodes can move together, or independently. The potentials of all electrodes need not be the same, such that etching and deposition can be effected simultaneously. Two or more materials might also be etched or deposited and etched simultaneously, as controlled by electrode potentials. Having multiple electrodes of different sizes and shapes could be used to optimize fabrication rates.

There are several means of setting the initial tip position relative to the substrate, including using feedback on Faradaic current (see for example A. A. Gewirth et. al., "Fabrication and Characterization of Microtips for in situ Scanning Tunneling Micorscopy", Jounal of Electroanalytical Chemistry", vol. 261, pp. 477–482, 1989) and bringing the tip within tunneling current range and then retracting it as Schneir et. al. do, referenced above. A tip to substrate potential can also be applied and the tip lowered until a sharp rise in current is observed, indicating electrode to substrate contact. In order to use the later procedure for tip diameters, $t \leq 30$ μm, it is preferred that the electrode 11 be insulated, leaving the tip area exposed. This is because the impedance on tip to substrate contact apparently becomes comparable to the impedance between the rest of the exposed wire, through the solution, to the tip. Several methods for coating sharp electrodes are listed in the following two references: A. A. Gewirth et. al. above; Nagahara et. al., "Preparation and Characterization of STM Tips for Electrochemical Studies", Review of Scientific Instruments, vol. 60, pp. 3128–3130, 1989. Furthermore, by insulating the tip the spatial resolution is improved somewhat. However it appears to be the concentration of field provided by the sharp tip combined with the tip to substrate distance, d, that most affects resolution, rather than the level of insulation. For positioning purposes the tip need not be coated right to the end, but rather such that the impedance offered by the electrode to substrate contact is much the solution impedance.

An oxidation or reduction potential is applied to induce deposition, FIG. 1, or etching, FIG. 2, once the electrode 11 is properly positioned. Either a voltage supply or a current source connected between the electrode 11 and the substrate 10 may be employed. The appropriate potential depends on the reactant(s) and results in a deposition 14 or etching 15. If nickel is to be deposited from a sulfamate solution onto a copper substrate using a platinum electrode, for example, a voltage between about 2.5 V and 5.0 V is appropriate. At high voltages deposition rates are observed to be ≥ 10 μm/s.

In order to generate three dimensional objects the electrode is translated along a three dimensional trajectory. A number of such trajectories are possible. For example, the electrode can be raster scanned over the substrate surface, moving normal to the surface by a fixed increment after each scan. Potential or current can be varied as a function of position in order to produce lateral and vertical features. A random access mode is also possible. FIG. 2 shows a sequential layer etching approach, while FIG. 1 illustrates continuous deposition. The deposition of certain structures, including helical springs for example, are well suited to continuous deposition, as shown in FIG. 1. These are but a few of the possible trajectories.

In order to fabricate in three dimensions material deposited must be conductive and electrically continuous with the substrate. Also, as deposition proceeds the electrode position relative to the interface must be maintained as described above for the initial positioning to maintain resolution.

There are several methods of maintaining the appropriate tip to surface separation, d. For deposition the most straightforward is to move at a rate slower than the deposit growth rate. Deposited material can grow to contact the electrode, at which point deposition will cease as electrons flow through the low resistance contact region. The reaction is effectively self-limiting. Alternatively, the contact between the deposit and the electrode can be detected, either by a rise in current or a reduction in current fluctuations. Current fluctuations are particularly large when bubble formation is occuring, which stops on contact. The contacting is then used to signal further motion or to increase speed, for example. Other control methods exist including periodically moving to contact the surface and then retracting, moving to within tunneling range to check the surface location (Schneir et. al., "Creating and Observing Surface Features with a Scanning Tunneling Microscope", SPIE vol. 897, pp. 16–19, 1988).

using Faradaic current to determine the separation distance (A. A. Gewirth et. al., "Fabrication and Characterization of Microtips for in situ Scanning Tunneling Microscopy", Jounal of Electroanalytical Chemistry", vol. 261, pp. 477-482, 1989), and measuring impedance changes at sensistive frequencies. The Faradaic current and impedance methods are not very reliable in the presence of noise, as occurs, for example, during bubble formation. The noise can be useful in determining distance from the substrate. The release of bubbles from the electrode is affected by the tip to substrate distance, which in turn changes the nature of current fluctuations. This method is somewhat complex because the frequency and amplitude of bubble release is not solely related to distance to the substrate. The same control schemes are used with etching, except that in the contact method substrate to electrode contact is used as a signal to stop the relative motion rather than to continue.

An alternative embodiment combines the localization of deposition or etching with localized solution flow. As in jet-plating and jet-etching a solution stream is focussed onto the substrate, increasing rates of mass transfer. Deposited structures are found to exhibit superior properties, including density and adhesion.

The embodiment is schematically shown in FIG. 3. The two principal differences between this embodiment and those shown in previous figures are that current is channelled from the electrode 20 to the substrate surface 10 through a pipette 16 and that flow is induced. Standard techniques are used to pull quartz and glass pipettes with orifice diameters between 0.02 and 10 μm. Pressure is applied to induce flows of up to 0.05 m/s or more. The appropriate distance, d, between the orifice 18 and the surface in order to achieve a given resolution, r, is as before and the scanning methods are the same. Note that flow can be directed out of the pipette or into it. Normally it is directed outward to locally inject a fresh supply of plating solution, thereby increasing mass transfer.

The technique is not limited to deposition of metals. Semiconductors (such as cadmium chalcogenides) and polymers (such as polyaniline and polypyrrole) can also be electrodeposited. For example, polyaniline can be deposited on stainless steel from 0.1M aniline and 1.0M H_2SO_4 by cycling the potential between −100 mV and 750 mV vs. SCE. Once deposited, conductivity of polyaniline and other conducting polymers, can be switched by up to 11 orders of magnitude by changing oxidation state. Changes in oxidation state can also be accompanied by dimensional changes, making them useful actuators. CdTe can be deposited from $CdSO_4$ and TeO_2. The conductivity can be changed from n to p type by changing or manipulating the potential.

Actual and likely future advantages of embodiments of the present invention include the following examples:

1. The deposition of many materials including Al, Ag, As, Au, Bi, Cd, Co, Cr, Cu, Fe, In, Ir, Mn, Ni, Os, Pb, Pd, Pt, Re, Rh, Ru, Sb, Se, Sn, Te, Te, Tl and Zn.

2. Depositing alloys including brass, bronze, electrodepositable gold alloys, Cd-Tl, Co-W, Zn-Ni, Sn-Ni, Ag-Pb, Ni-Co, Ni-P, Ni-Fe, Ni-Tl, Sn-Pb and other electrodepositable alloys.

3. The deposition of conducting polymers such as polyaniline and polypyrrole. These materials have many applications including use in batteries, actuators, capacitors, transistors, chemical sensors and electrochromic devices.

4. The control of potential such that either deposition or etching of a given material, without changing solution, is possible.

5. Semiconductors such as GaAs can be irradiated to make them conductive, thereby making them suitable as substrates for etching and deposition.

6. The use of multiple electrodes providing the following advantages:

(a) Increasing the speed of fabrication by depositing and etching in parallel;

(b) Allowing for multiple electrode geometries and sizes;

(c) Enabling different reactants to be simultaneously deposited and etched by independently controlling the potentials at each electrode and using multiple reactants.

7. The ability to achieve sub-micrometer resolution by spatially localizing an electrochemical reaction. Resolution is not diffraction limited, as in many other processes, among other advantages and embodiments.

Conclusion

As previously stated, important properties on which microfabrication technologies are judged include the range of achievable structure geometries, spatial resolution, the range of materials available, rate and cost. The invention described enables three dimensional metal, polymer and ceramic structures to be rapidly formed. Unlike other three dimensional fabrication processes, spatial resolution is not restricted by the diffraction limit of light. Finally, the apparatus is relatively simple and inexpensive, especially when compared with microelectronics technology.

While the above description contains many specificities, these should not be construed as limitations on the scope of the invention, but rather as exemplifications of preferred embodiments thereof. Accordingly the scope of the invention should be determined not by the embodiments illustrated, but by the appended claims and their legal equivalents.

We claim:

1. A method for producing a three dimensional object comprising the steps of

(a) providing a substrate having an outer conducting surface defining an interface;

(b) providing an electrode having at least a feature having at least a dimension that is small relative to the dimensions of the interface;

(c) providing a solution having a selected reactant that will, in an electrochemical reaction, deposit a desired product;

(d) positioning the feature at a starting distance from the substrate such that the feature is close to but spaced from the interface;

(e) selecting a trajectory for relatively moving the electrode and the substrate, at least part of the trajectory having a directional component normal to the substrate surface, such that when the trajectory is followed a feature to substrate separation of at least several times the starting distance is generated somewhere along the trajectory;

(f) depositing the product by passing a current between the electrode and the substrate and through the solution to induce a spatially localized electrochemical reaction at the interface;

(g) relatively moving the electrode and the substrate along the trajectory; and

(h) repeating step (f) along the trajectory;

where the depositing of the product along the trajectory, including at one or more locations several times the starting distance away from the substrate, forms the three dimensional object.

2. The method of claim 1, further comprising the step of providing further reactants in step (c) that will, in an electrochemical reaction, deposit a desired product.

3. The method of claim 1, wherein the deposited product is at least in part selected from the group consisting of comprising electrodepositable metals, alloys, polymers and semiconductors.

4. The method of claim 1, wherein the electrode provided in step (b) is a sharp conducting wire having a tip having a diameter between about 5 and 200 000 nm, the tip providing the feature in step (b).

5. The method of claim 1, wherein the smaller feature dimension provided in step (b) is a distance, d; and wherein step (d) in claim 1 is performed such that the smaller dimension of the feature provided in step (b) is placed within about a distance, d, of the surface defined by the interface.

6. The method of claim 1 wherein the electrode is approximately disk-shaped or hemispherical having a diameter between about 5 and 200 000 nm.

7. The method of claim 1, further comprising the steps of providing a plurality of electrodes in step (b) each having at least a feature having at least a dimension that is small relative to the dimensions of the interface; and wherein each electrode is subject to the remaining steps of claim 1.

8. The method of claim 1, further comprising the steps of providing an orifice; and generating a flow of the solution provided in step (c) of claim 1 directed by the orifice to the region between the electrode and the interface.

9. A method for producing a three dimensional object comprising the steps of

(a) providing a substrate having an outer conducting surface defining an interface;

(b) providing an electrode having at least a feature having at least a dimension that is small relative to the dimensions of the interface;

(c) providing a solution having a selected reactant that will, in an electrochemical reaction, etch the substrate;

(d) positioning the feature at a starting distance from the substrate such that the feature is close to but spaced from the interface;

(e) selecting a trajectory for relatively moving the electrode and the substrate, at least part of the trajectory having a directional component normal to the substrate surface, such that when the trajectory is followed while etching the electrode feature penetrates at least several times the starting distance into the etched substrate somewhere along the trajectory;

(f) etching the substrate by passing a current between the electrode and the substrate and through the solution to induce a spatially localized electrochemical reaction at the interface;

(g) relatively moving the electrode and the substrate along the trajectory; and

(h) repeating step (f) along the trajectory;

where the etching of the substrate along the trajectory, including at one or more locations penetrating several times the starting distance into the substrate, forms the object.

10. The method of claim 9, wherein the substrate material is at least in part a material selected from the group consisting of metals, alloys, polymers and semiconductors.

11. The method of claim 9, wherein the electrode provided in step (b) is a sharp conducting wire having a tip having a diameter between about 5 and 200 000 nm, the tip providing the feature in step (b).

12. The method of claim 9, further comprising the steps of defining the smaller feature dimension provided in step (b) as a distance, d; and

placing the smaller dimension of the feature provided in step (b) within about a distance, d, of the surface defined by the interface.

13. The method of claim 9, wherein the electrode is approximately disk-shaped or hemispherical having a diameter between about 5 and 200 000 nm.

14. The method of claim 9, further comprising the steps of providing a plurality of electrodes in step (b) each having at least a feature having at least a dimension that is small relative to the dimensions of the interface; and wherein each electrode is subject to the remaining steps of claim 9.

15. The method of claim 9, further comprising the steps of providing an orifice; and generating a flow of the solution provided in step (c) of claim 9 directed by the orifice to the region between the electrode and the interface.

16. A method for producing a three dimensional object comprising the steps of

(a) providing a substrate having an outer conducting surface defining and interface;

(b) providing an electrode;

(c) providing an orifice that is electrically isolated from the electrode and the substrate;

(d) providing a solution having at least a selected reactant that will, in an electrochemical reaction, deposit a desired product;

(e) placing the orifice in the solution and between the electrode and the interface such that current between the electrode and the interface will pass through the orifice;

(f) positioning the orifice at a starting distance from the substrate such that the feature is close to but spaced from the interface;

(g) generating a flow of solution through the orifice sufficient to greatly increase mass transport of the reactant to the surface;

(h) selecting a trajectory for relatively moving the orifice and the substrate, at least part of the trajectory having a directional component normal to the substrate surface, such that when the trajectory is followed an orifice to substrate separation of at least several times the starting distance is generated somewhere along the trajectory.;

(i) depositing the product by passing a current between the electrode and the substrate and through the solution to induce a spatially localized electrochemical reaction at the interface; and

(j) repeating step (i) along the trajectory;

where the depositing of the product along the trajectory, including at one or more locations several times the starting distance away from the substrate, forms the three dimensional object.

17. A method for producing a three dimensional object comprising the steps of

(a) providing a substrate having an outer conducting surface defining and interface;

(b) providing an electrode;

(c) providing an orifice that is electrically isolated from the electrode and the substrate;

(d) providing a solution having at least a selected reactant that will, in an electrochemical reaction, etch the substrate;

(e) placing the orifice in the solution and between the electrode and the interface such that current between the electrode and the interface will pass through the orifice;

(f) positioning the orifice at a starting distance from the substrate such that the feature is close to but spaced from the interface;

(g) generating a flow of solution through the orifice sufficient to greatly increase mass transport of the reactant to the surface;

(h) selecting a trajectory for relatively moving the orifice and the substrate, at least part of the trajectory having a directional component normal to the substrate surface, such that when the trajectory is followed while etching the orifice penetrates at least several times the starting distance into the etched substrate somewhere along the trajectory;

(i) etching the substrate by passing a current between the electrode and the substrate and through the solution to induce a spatially localized electrochemical reaction at the interface; and

(j) repeating step (i) along the trajectory;

whereby the etching of the substrate along the trajectory, including at one or more locations penetrating several times the starting distance into the substrate, forms the object.

* * * * *

Chapter 4 Experimental Characterization of NiTi Fibers

This chapter describes the experimental procedure and the analysis of the data acquired to characterize the NiTi shape memory alloy fibers. Over six different experimental setups have been constructed to characterize different aspects of the material properties or the dynamic response of the fibers. Most of the experimental results are outlined in a paper included after this chapter. Section 3 of this chapter gives additional information on the results. Section 4 concludes the chapter.

4.1 Experimental Setups

The mechanical and dynamic properties of the NiTi shape memory alloys as described before are complex, highly nonlinear, and are functions of temperature, time, stress, strain and the past history of the fiber. It is not possible with one experimental setup to characterize all of the different properties. Over six different experimental setups were used to obtain the results described in this chapter. The first setup was used to test the response of the fast twitch NiTi fibers. The second setup was designed to study the electrical resistivity of the fibers since it has been suggested that resistivity can be used for control purposes. The third setup was designed to study the mechanical properties as a

function of temperature and rate of change of the temperature. The other setups were designed to look at the mechanical properties of the fibers.

4.1.1 Study of NiTi fibers with fast twitch response

The NiTi fiber was bathed in a 50% methanol-water mix, which was pumped through a 1200 W refrigeration unit (Polyscience, model KR-60A) in series with a variable voltage heater (peak 3 kW). The temperature of the NiTi bath was controlled over a temperature range of 10 °C to 70 °C using a semiconductor temperature transducer (National Semiconductor LM35) and a variable voltage heater. One end of the fiber was attached to a strain gauged proving ring with a flat bandwidth of 1 kHz, later replaced with a Bruël & Kjaer load cell and Bruël & Kjaer charge amplifier model 2635. The other end of the fiber was attached to a voice-coil electromagnetic motor. A photodiode and lateral effect photodiode (LEPD) measured displacements of the voice coil. A United Detector Technologies analog processor was used to obtain a signal proportional to the displacement of the photodiode. A digital micrometer (Mitutoyo, 1 μm increment) was used to adjust the static force in the fiber.

The setup was controlled by a MicroVAX computer system running VAX-VMS and the experiments were run from the LISP programming language. A Data Translation multifunction board was used to sample the position and force signals and to control pulses applied to the NiTi fiber with a D/A converter controlling the gate voltage of IRC HEXFETS (200 A peak). A detailed photograph of the setup is given in Plate 4.1.

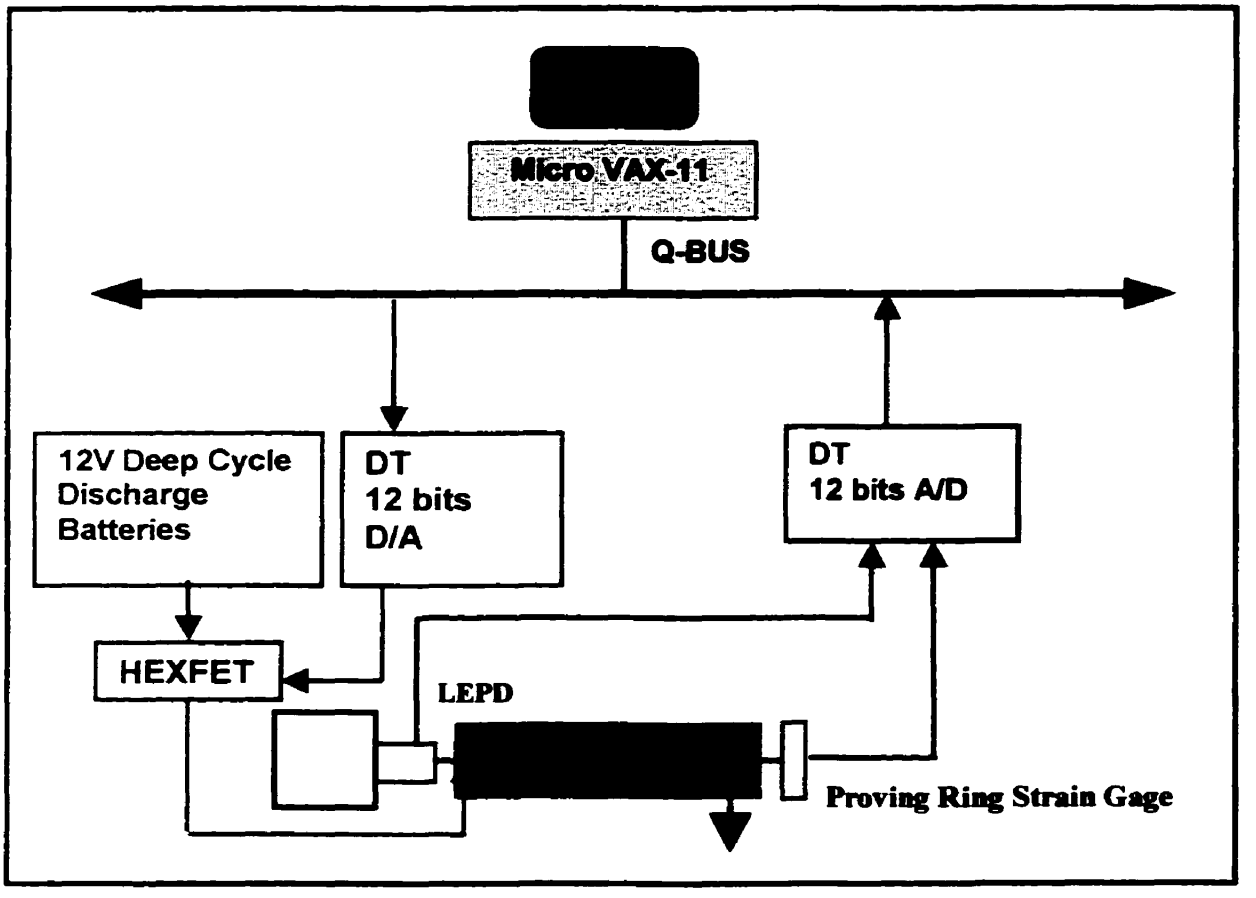

Figure 4.1 First experimental setup for data acquisition and control for modifying NiTi fibers. A Micro-VAX 11 was used for the experiments. A Data Translation Q-BUS multifunction board was used to acquire data and control the HEXFETS.

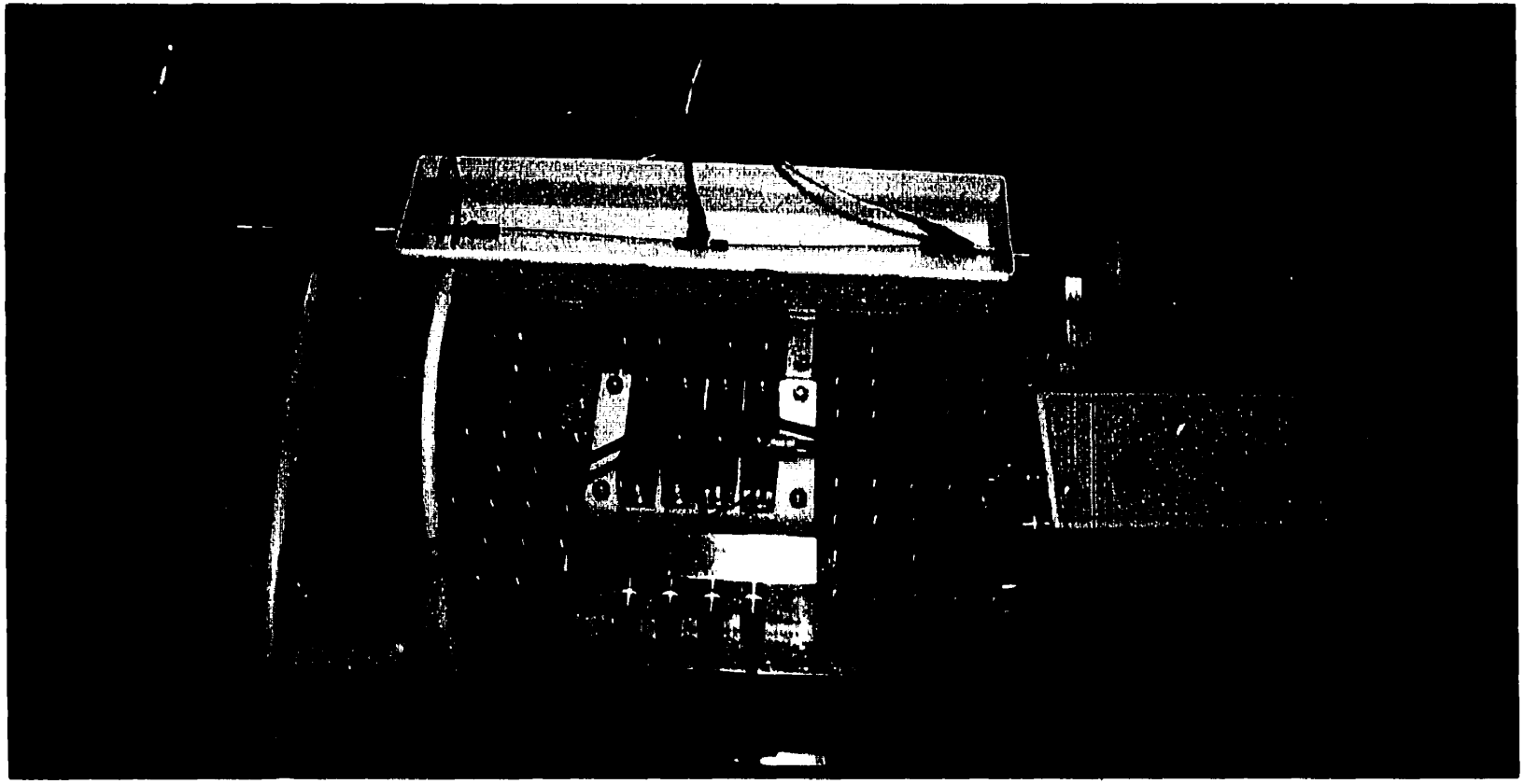

Plate 4.1 Experimental setup built to characterize the NiTi fibers with fast twitch response.

4.1.2 Resistivity and modulus of elasticity measurements

The previous setup was redesigned to use a much more powerful electromagnetic motor required to run experiments on 0.8 mm diameter NiTi fiber capable of actively generating over 100 N of force. A Bruël & Kjaër (model 4808) linear electromagnetic voice-coil motor capable of generating 180 N peak force was mounted on an optical table. The position of the voice coil assembly was measured with a variable inductance displacement transducer (Data Instruments FASTAR FS380) and a signal processor (Data Instruments SP300A) provided the position signal. A connecting rod was mounted to the motor shaft and at the other end crimped to the NiTi fiber. The other end of the NiTi fiber was attached to a strain gauge force transducer (Omega Engineering Inc., LCC200 shear beam type). The fiber was mounted horizontally and was enclosed by a clear plastic tube where a 50% methanol-water mix was circulating. The temperature inside the chamber was measured using a 100 Ω RTD platinum wire. The temperature of the methanol-water mix was controlled by a 1200 W refrigeration unit (Polyscience, model KR-60A) in series with a 3 kW variable heater. The refrigeration unit and the variable heater could be individually turned On or Off using semiconductor AC switches.

The system was controlled with an IBM RISC SYSTEM/6000 (Model 320) using FORTRAN-90 as a programming language. External devices were controlled from a National Instruments NI-GPIB (IEEE488) interface using the IEEE 488 bus. The NiTi fiber resistance and impedance was measured using the standard four wire (Kelvin) technique using an HP 3458A $8^1/_2$ digit precision multimeter. For impedance measurements the HP4194 Impedance Gain/Phase instrument was used. Impedance frequency response functions were taken with a 2 °C temperature increment and the

resistance every 1 °C. Force and displacement were read using HP34401 multimeters and read via the IEEE 488 bus. Temperature measurements were obtained from the resistance and using an 8th order polynomial giving the relationship between resistance and temperature.

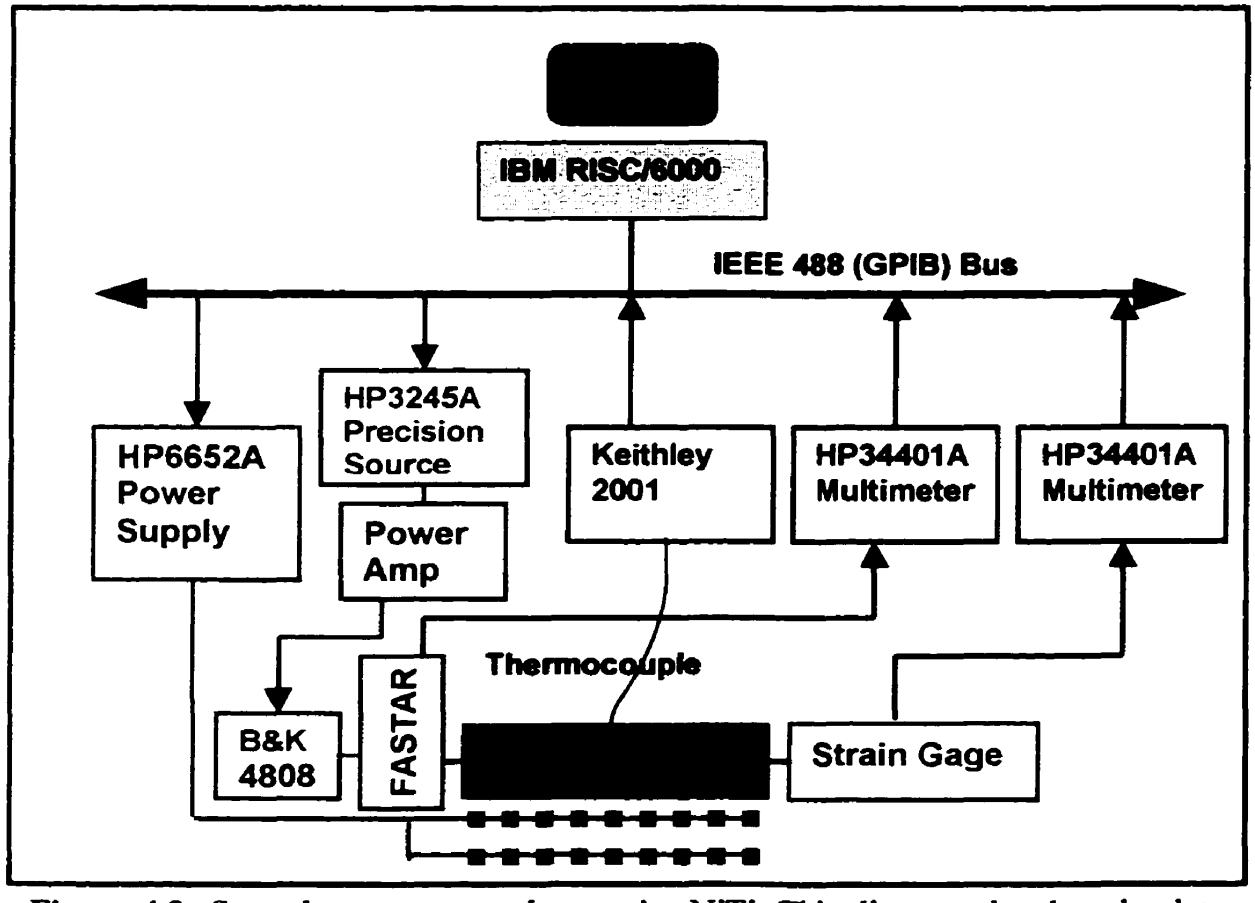

Figure 4.2: Second apparatus to characterize NiTi. This diagram sketches the data acquisition and control system used to characterize stiffness and resistivity as a function of temperature.

Plate 4.2 Experimental setup developed to do resistivity and stiffness measurements as a function of temperature.

4.1.3 Study of the stress-strain response as a function of temperature

This experimental setup was designed to study the dynamic properties of the fibers as a function of temperature, stress and electrical pulses. The NiTi fibers 0.1 mm in diameter and 100 mm long were clamped between two General Scanning (GT350) galvanometer motors. The NiTi fibers were mounted horizontally between the motors in a water bath machined into a copper bar (see Plate 4.3). The top surfaces of 14 Peltier effect heat pumps (Marlow Industries MI1064T) were attached to the copper bar to provide temperature control of the bath and hence the NiTi fibers. The other faces of the Peltier devices were attached to another copper bar which in turn was bolted to a 19 mm thick water-cooled aluminum plate which served as a water-cooled heat sink. Two parallel water channels were machined inside the bottom plate and water entering one input port flowed to the other extremity of the bar where it was re-circulated through the second channel and collected at an output port. Each heat pump could carry up to 5.3 A, at up to 4 V, which was supplied from a Hewlett Packard HP6652A DC power supply. Each motor was capable of producing 0.2 N·m peak torque or 10 N peak force on the fiber via a lever extending 20 mm from the shaft.

An IBM-RISC Model 6000 computer was used to control the experiments via a National Instruments Microchannel IEEE 488 interface. The bath temperature was controlled via the HP6652A DC Power Supply (25 A) by a PI (proportional & integral) controller running at 5 Hz. A relay controlled by the HP6652A relay control output was used to reverse current. Temperature as measured by a Keithley 2001 5.5 digit multimeter via a type K thermocouple was sampled at 5 Hz.

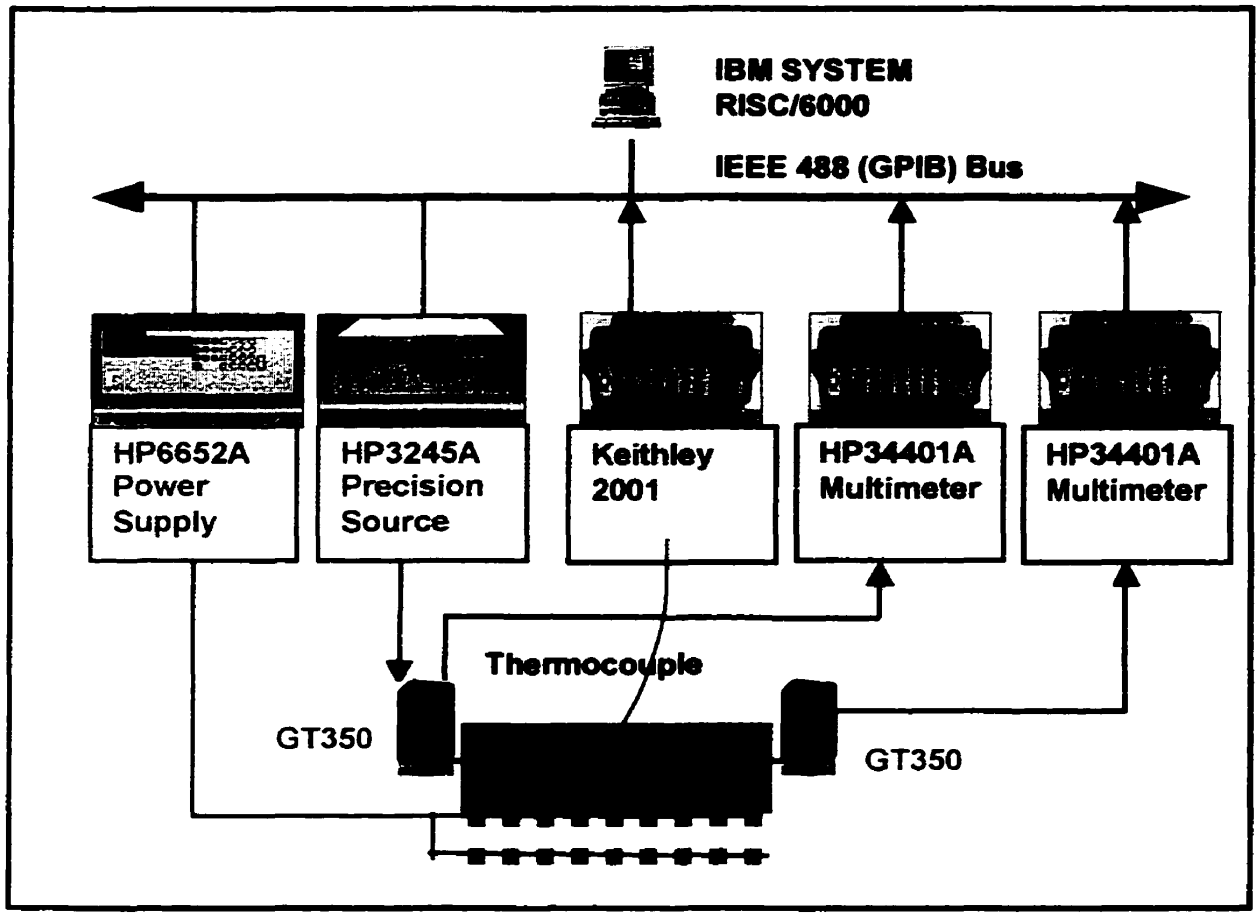

Figure 4.3 Diagram describing the experimental control and data acquisition method used for a first set of resistivity measurements.

For the first series of experiments, where the stress-strain response was analyzed as a function of temperature, the setup was as described in Figure 4.3. HP34401A multimeters measured the force and position signals and the samples were downloaded to the host via the IEEE 488 interface. The HP3245A precision source and arbitrary function generator was used to generate a triangular force command signal to the GT350DT galvanometer.

In a second series of experiments designed to look at the pulse responses of the

NiTi fibers the data acquisition and control setup was as described in Figure 4.4. The position and force signals from the General Scanning GT350DT galvanometer were sampled by a HP54501A digitizing scope and the sampled signals were read via the GPIB bus.

The HP6652A was programmed to provide the required output voltage and the HP3245A was programmed to generate 10V pulses to switch ON/OFF an insulated gate bipolar transistor (IGBT) that delivered the current from the HP6652A voltage supply to the NiTi fiber.

This setup has also been used for resistivity measurements. In this case a 4 wire (Kelvin) resistivity measurement was taken either with the HP3458A $8^1/_2$ multimeter, or for fast measurements a 10 mA constant current source was injected in the fiber and the potential difference measured with an instrumentation amplifier (Analog Devices AMP-02).

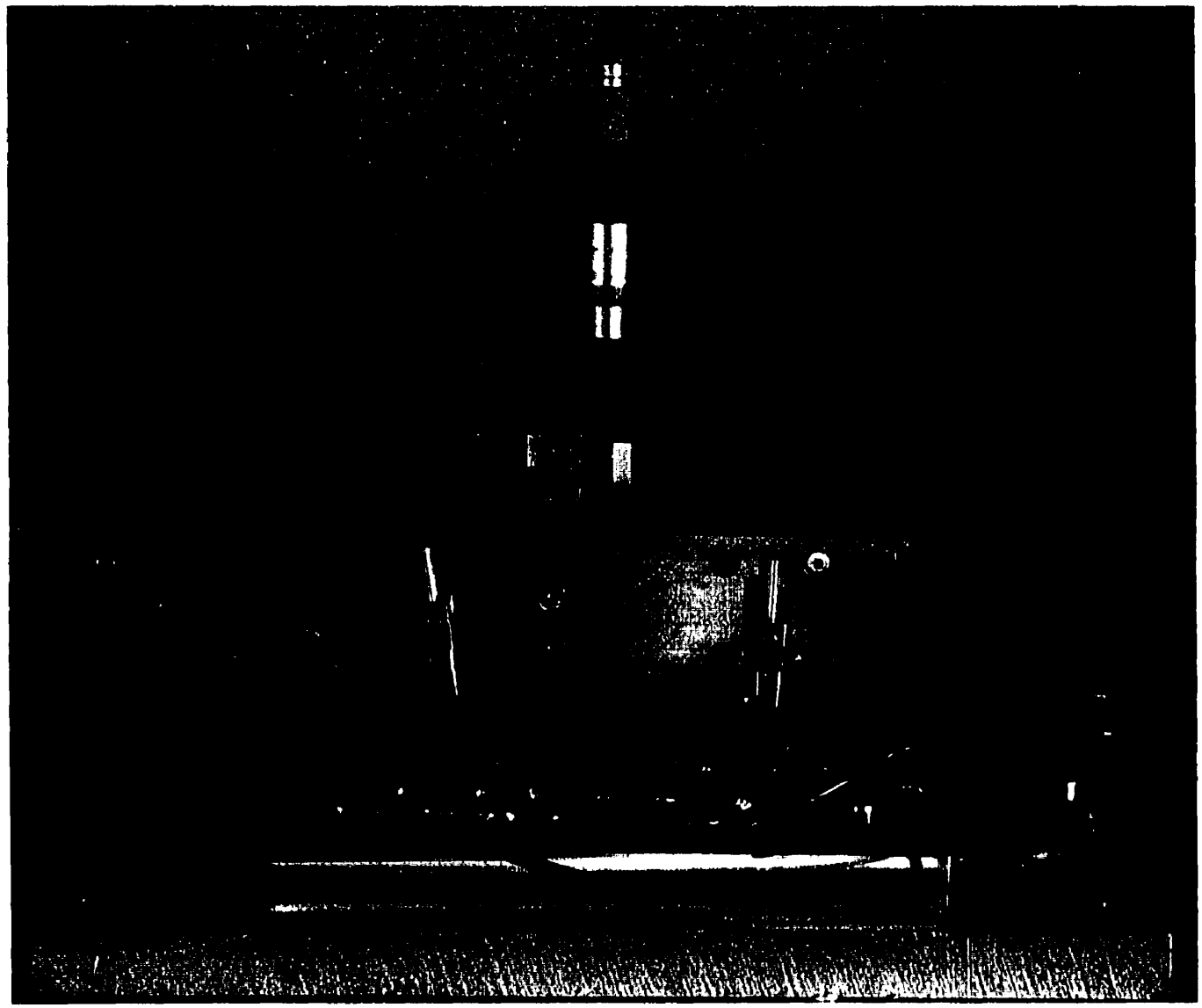

Plate 4.3 Experimental setup used for studying NiTi fibers as a function of temperature.

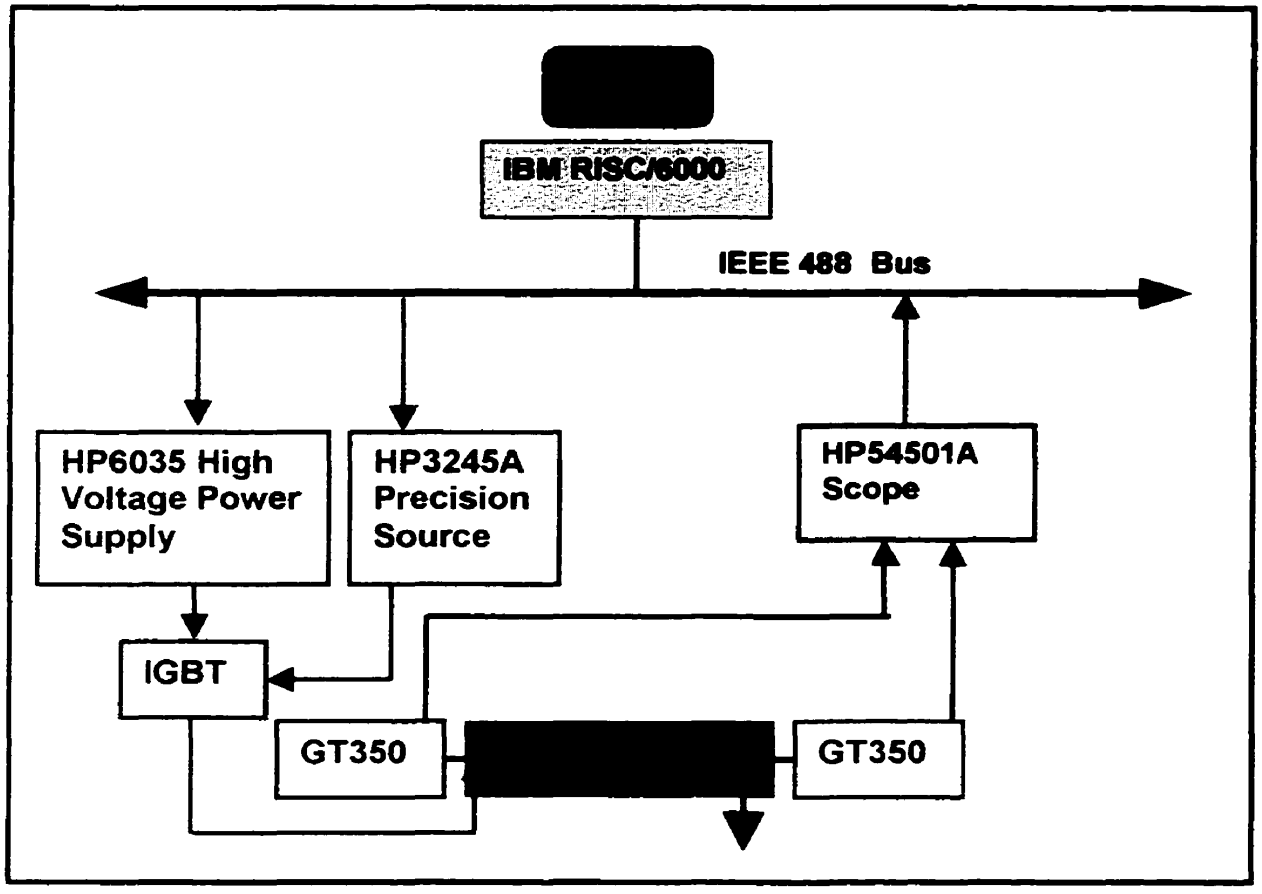

Figure 4.4 Description of the experimental system used for data acquisition and control of data acquired to study the response of NiTi fibers to electrical pulses.

In these experiments a current with proportional, integral and derivative feedback (PID) servo was used to cycle the motor force with a 1 N amplitude, 10 s triangular wave. The motors have inbuilt capacitive angular position transducers with a noise level of 0.01 mdeg rms at 10 Hz. The force was obtained from the current running through the galvanometers. The sensitivity was obtained from calibration with known weights. The temperature of the bath was regulated by a proportional-integral (PI) controller, based on temperature measurements taken at 5 Hz by a platinum thin RTD element (Omega 100W30 thick film sensor) via a Keithley 2001 5½ digit multimeter. HP34401A

multimeters were used to digitize the outputs from the position and force signals. A HP3245A Universal Source was used to generate the command to the motors. An IBM RISC/6000 with National Instruments GPIB microchannel card was used for bi-directional communication with the multimeters and universal source.

4.1.4 Experimental setup for agonist-antagonist double pulses.

An experimental setup was designed to study the response of NiTi fibers configured in an agonist-antagonist pair where each fiber provides a direction of motion opposite to the other. For these experiments 100 μm diameter and 150 mm long fibers were attached at one end to a Sigma force transducer and at the other end to a Mitutoyo micrometer used to set the initial tension in the fiber. In its middle the fiber was attached to a brass metal sheet which in turn carried a lateral effect photodiode (United Detector Technology (California)) used to generate a signal proportional to the location of the photodiode. The brass sheet was connected to ground. Each fiber was connected at one end to the brass sheet and at the other end to an IGBT. The IGBT's were controlled by an HP3245A precision source. The HP 54501 digitizing scope acquired the measured force signal from the Sigma force transducer and position signal from the diode.

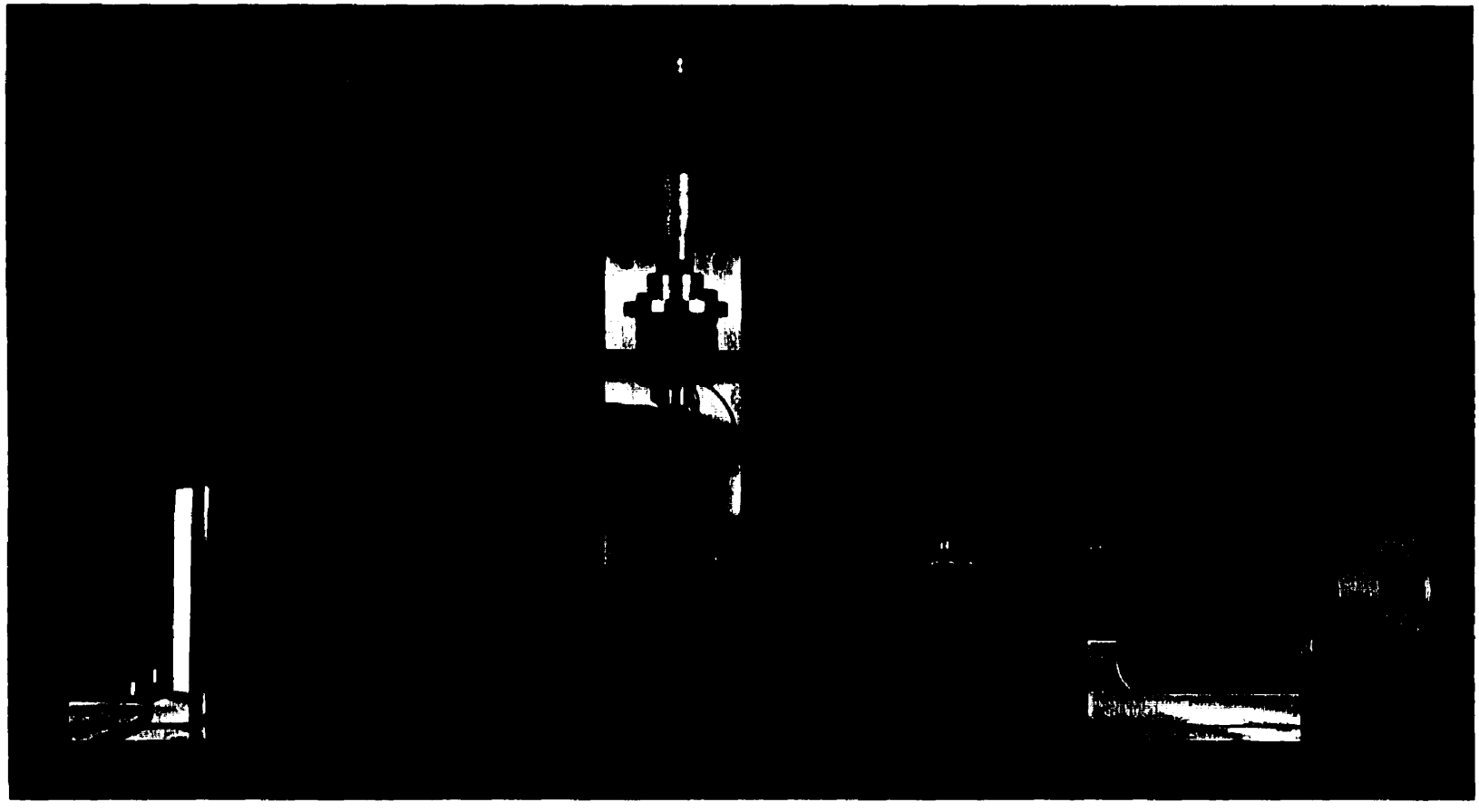

Plate 4.4 Experimental setup to study the pulse response of NiTi fibers configured as agonist-antagonist pairs.

4.1.5 Experimental setup for pulse and heat trans fer experiments

In a fourth series of experiments fibers with 250 μm diameters and 50 mm nominal lengths were grown electrolytically at each end to a nominal diameter of 400 μm. The ends were then soldered to brass hexagonal rods for both electrical and mechanical attachment. One rod was mounted to an Entran force transducer (model ELF-TC13-25). The other end was attached to a Bruël & Kjaer mini-shaker (type 4810) with 10 N maximum force and ±3 mm range. A FASTAR SP200A and FS380 linear position transducer, mounted between the Bruël & Kjaer mini-shaker and an hexagonal rod, was used to measure the changes in fiber length. The fiber was kept in a distilled water bath as shown in Figure 1. The hexagonal rods were extending outside the bath through two round windows at each end. No seal was used between the rods and glass plates so that friction was minimized. Water from the middle chamber freely ran through the windows to be collected and re-circulated in the middle chamber. The ENTRAN force transducer was mounted on a New-England stage motorized by a Compumotor LN57-51-MO stepping motor and controlled by a Compumotor LN-Drive for large adjustment of the distance between rods and for initial tension in the NiTi fiber.

An IBM RISC/6000 model 520 with VXI data acquisition and control modules was used for experimental control and data acquisition. VXI modules include a Hewlett-Packard HP1413A 16 bits (18 bits internal calibration), 64 channel A/D module for A/D conversion. A TASCO VXI/DAC16 16 channel 16 bit analog output module and C&H Engineering model 441C digital I/O module were used for D/A conversion and digital outputs respectively. Digital pulses from the C&H 441C were first converted to 15 V

pulses which were then used to switch current from an 60 V APEX PA04 power amplifier (whose output voltage was controlled by a D/A) through an IGBT (model IRCPC50U). A PID control loop, implemented digitally by the IBM RISC-6000 computer at 5 kHz, controlled the motor. Pulses from the C&H 441C were used to control the LN57 stepping motor. In some experiments the current going through the NiTi fiber was measured from the voltage drop in a 0.1 Ω inline resistor.

In another series of experiments using the same setup the stiffness of the fiber was measured as a function of the temperature. For these experiments a type K chromel-alumel thermocouple was bonded directly on the NiTi fiber using a thermally conductive

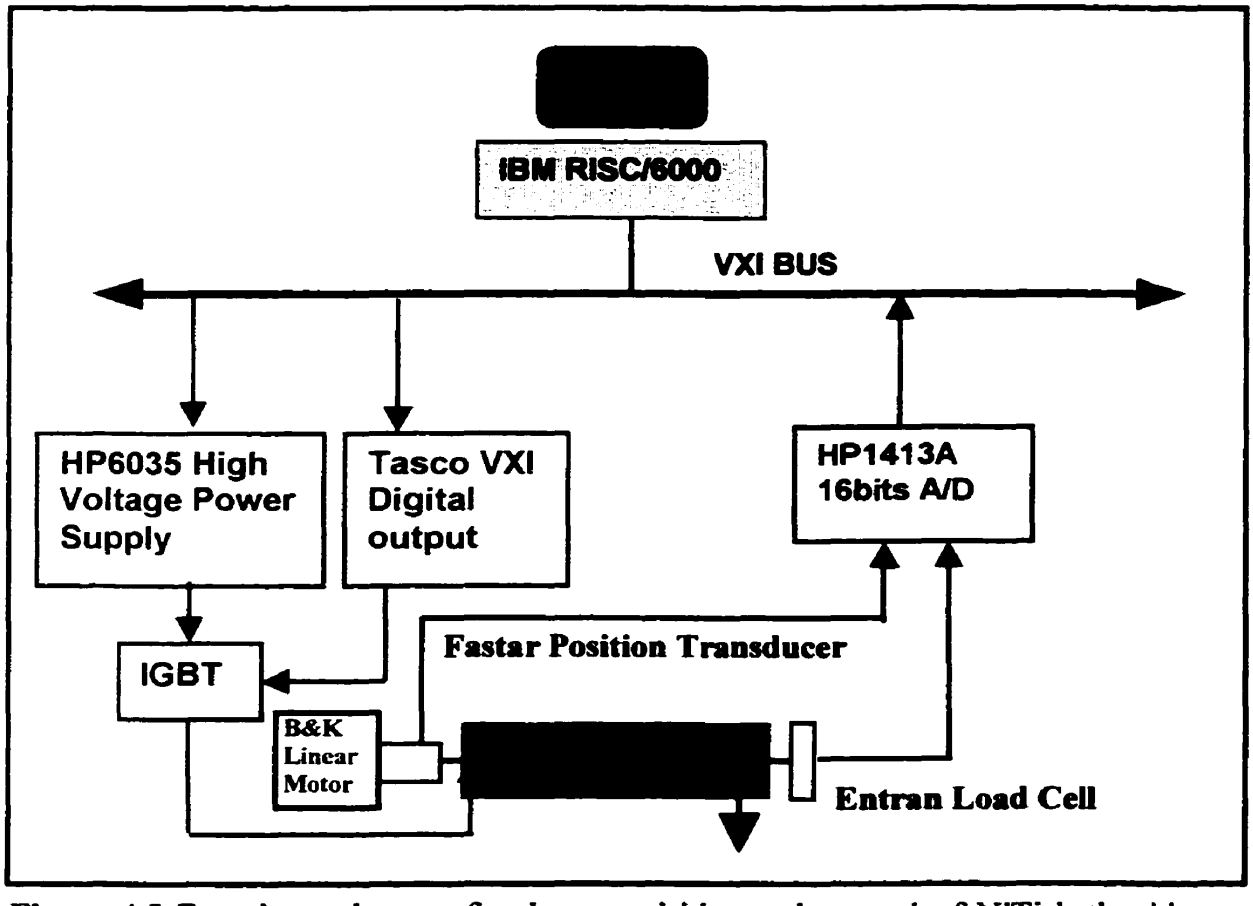

Figure 4.5 Experimental setup for data acquisition and control of NiTi bath with an IBM RISC SYSTEM/6000 and VXI data acquisition instruments.

epoxy cement (Wakefield Laboratories). The thermocouple junction consisted of a welded ball of metal that was 250 μm in diameter, the same diameter as the NiTi fiber used for these experiments. All of the experiments were carried out in air. Assuming that the thermal conductivity of metal is much higher than air and that only a thin layer of epoxy separated the thermocouple junction from the NiTi fiber, the temperature measured via the thermocouple can be assumed to be close to that of the fiber. The fiber was directly heated using an electrical current that could also be used to measure the resistance of the NiTi fiber. The temperature was varied quasi-statically in these experiments. Using a pseudo-random perturbation in the stress applied to the fiber dynamic measurements of the stiffness were made. For these experiments a Keithley 2001 multimeter was used to record the temperature.

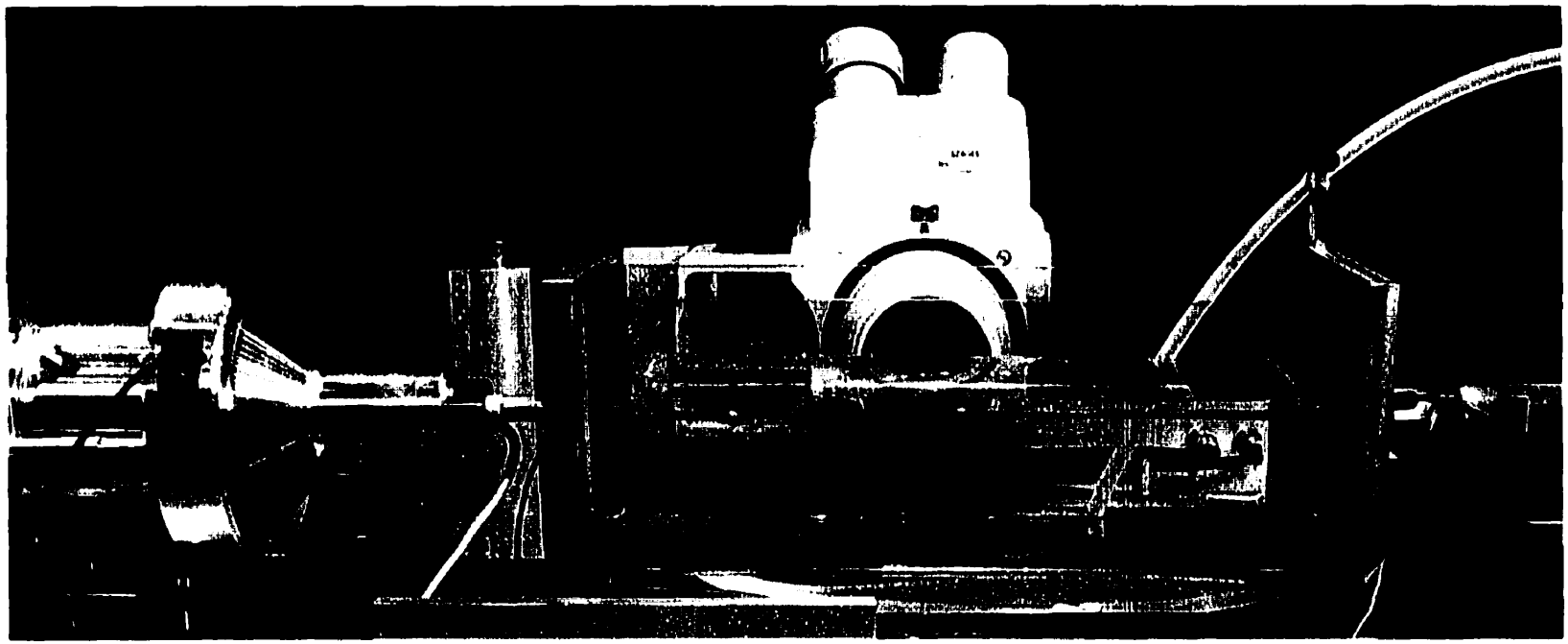

Plate 4.5 Experimental setup to study the pulse response of NiTi fibers in water and to study nucleation and heat transfer phenomena at the surface of the fiber.

4.2 Experimental Results

Most of the experimental results are given in the publications included with this thesis. However some of the results will be outlined here with additional results, background and justification. Where appropriate the results are also discussed in more detail. However some results (i.e. resistivity) were taken with more than one setup and justify a discussion in themselves.

4.2.1 NiTi fibers with a fast twitch response

The basic results are outlined in as the U.S. patent 5,092,901 (Hunter and Lafontaine, 1992b) and in the paper "Fast reversible NiTi fibers for use in microrobotics" (Hunter *et al.*, 1991) as well. These two documents describe a technique to modify the characteristics of NiTi fibers using brief current pulses while the fiber is stretched. After modification the fiber shows a much faster twitch response. That is, a fiber's response to an electrical pulse will cause a much more rapid contraction and elongation than in a normal unmodified fiber.

The basic results are described in Figure 1, Figure 2 and Figure 3 of the US Patent 5,092,901 (Hunter and Lafontaine, 1992b; Appendix I) and Figure 2, Figure 3 and Figure 4 of Hunter *et al.* (1991) included with this chapter. Figure 1 of Hunter and Lafontaine (1992b) displays the response of a 0.8 mm diameter 100 mm long NiTi fiber following a very brief, large current pulse. This figure gives the absolute change in strain as a function of time. The fiber contracts rapidly but takes over 300 ms to return to 50% of the maximum strain and the full recovery takes over 1 second.

The process to modify the fiber consists of applying short pulses (1 to10 ms) of voltages of high enough amplitude to cause the fiber to fully contract while subjected to a constant stress (e.g. 40 MPa) . The stress is maintained so that the fiber elongates under the externally applied stress after the pulse. After the process has been repeated 10 to 20 times it is observed that the fiber recovers 50% of the strain in less than 40 ms and the fall time (10%-90%) is under 130 ms as show in Figure 2 of Hunter and Lafontaine (1992b).

It is unclear what causes this phenomenon. Shape memory alloys are complex materials whose properties can be greatly modified by a number of thermal and mechanical processes. There are a number of thermo-mechanical processes leading to new properties such as the two-way shape memory effect (Duerig *et al.*, 1990) or the introduction of the R-phase.

There is an important effect of this modification process that has not been reported elsewhere, which is that modified NiTi fibers display a very strong two-way shape memory effect. When heated above A_f and then cooled down below M_f, their length increases actively by over 4% without the application of an external stress. This can partially account for the fast twitch response, in that there is an active re-lengthening of the fiber and less energy losses in friction between internal surfaces

It is unclear also why large current pulses produce such a modification. It is known that electric current can modify the properties of the fibers. In NiTi alloys various phenomena such as precipitation and oxidation occur in a complex manner and there is no clear understanding of how best to mechanically process the fibers for optimal performance and no satisfactory heat and mechanical treatment has been established yet.

Furthermore the exact process is normally kept as a trade secret and not made generally known.

Normally NiTi fibers available commercially have been obtained from an ingot of NiTi alloy which is hot worked around 800 °C into a shape close to the desired final product. Next cold working and stress relief annealing are repeated until the final shape is obtained. Subsequently three different methods are normally used to give the as-drawn NiTi alloy its shape memory effect. A first method consists of annealing it at a temperature between 400 °C and 500 °C for approximately 15 minutes to 1 hour with its shape restrained. A second technique consists of heating at 800 °C, rapidly cooling to normalize its structure, then cold working and annealing at a low temperature (200 °C to 300 °C) with it shape restrained. The third technique consists of heating it to 1000 °C so that it becomes a homogeneous solid solution, quenching and aging at 400 °C. The last method is preferred for NiTi alloys with more than 50.5% Ni.

In all these cases when the as-drawn alloy is produced and delivered without further processing the crystal grains within the fiber are randomly orientated. NiTi fibers consist of polycrystalline materials where transformations occur within the grains themselves. In large reason because of this random orientation a maximum of 2% length change can be obtained from commercially available fibers that are straight annealed without further processing.

In 1990, Homma *et al.* were granted a US patent for a process based on heating NiTi fibers with a current in order to improve their characteristics such as improved lifetime, stability of the shape memory effect, maximum achievable strain, as well as efficiency of conversion of electrical energy to mechanical work. In this process the fiber

is first kept below M_f and under a moderate load (100 MPa). Then an electrical pulse generating very large currents and very rapid heating of the fiber is applied until the fiber displays a plastic deformation, at a temperature close to M_f. At this point the current is stopped and the fiber is cooled at a high rate using forced air. Then the stress is rapidly increased to 200 MPa for the time needed to extend the fiber (and decrease the diameter) into super-plastic deformation. At that point the stress is reduced to 100 MPa.

Homma *et al.*'s theory of modification was based on the hypothesis that the resistivity of the fiber is small within the crystal grains and large between the randomly orientated crystals of the polycrystalline fiber. By rapidly heating the fiber, the temperature would consequently increase first at the grain boundaries, without significantly heating the grains if the pulse is kept shorter than the time for heat diffusion to take place. With the grain boundaries heated and under stress, the crystals reorient in the fiber along the direction of the stress. The improved characteristics of the fiber would therefore be related to the orientation of the crystals within the fiber. This technique was developed for NiTi alloys which have a greater concentration of Ti and where the transition temperature is close to 100 °C.

Homma *et al.*'s technique differs from the process developed by Hunter and Lafontaine (1992b) in that the fiber does not actively contract under the heat generated by the current pulse and that the stress must be increased in a controlled manner at the end of the pulse. The technique also has been developed for NiTi alloys where the alloy had a slightly larger content of Ti than the 50-50% concentrations, while the technique described in Hunter and Lafontaine (1992b) worked with alloys having a very large Ni concentration (55%). Nevertheless one of the possible explanations for the fast twitch

fiber response described here could also be related to the reorientation of the crystals within the fiber. In addition the technique described here allows the fibers to actively expand as well as contract as in the two-way shape memory effect.

To properly understand the mechanism responsible for the observed changes in properties, other studies such as time-resolved X-ray diffraction and neutron diffraction would be required.

4.2.2 Resistivity measurements

The first resistivity measurements are included from a conference abstract (Lafontaine *et al.*, 1992). The abstract outlines early resistivity measurements. More important are the measurements of impedance. Figure 4.6 shows a typical result. The electrical impedance of a NiTi fiber was measured in a frequency range extending from 100 Hz to 40 MHz. The data indicates that the NiTi fiber was purely resistive up to several hundred kHz. The implication of this result is that if the resistance of the fiber can be measured at the same time as the fiber is electrically heated for control purposes, a high frequency electrical signal can be used for impedance measurements in a frequency band outside the frequency band used to control the fiber.

Other typical resistivity measurements are given in Figure 4.7. The first curve in Figure 4.7A covers a temperature range from 20 °C to 95 °C. These measurements were made using 250 μm fibers, under zero external load. The resistivity versus temperature shows only a small hysteresis of less than 2 °C. The resistivity is quite high at lower temperatures which is indicative of the R-phase. Therefore under small load and above room temperature the fibers change only between the parent phase and the intermediate phase. The transition temperature A_f is 70 °C.

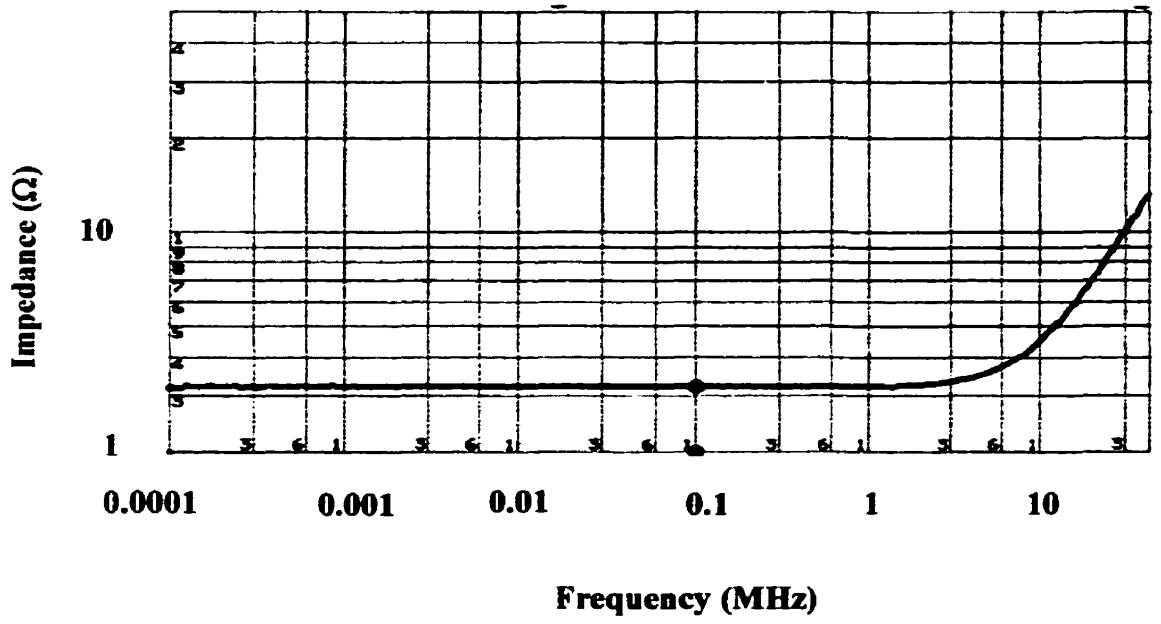

Figure 4.6 Impedance measurement of NiTi fiber at 20 °C.

The resistivity curve given in Figure 4.7B was taken over a larger temperature range, from –30 °C to 95 °C. In this case the resistivity curve displays a very large hysteresis. Below 20 °C the resistivity drops rapidly as the R-phase transforms into martensite. This curve indicates that M_s is close to 10 °C. Unfortunately it was not possible to lower the temperature enough to find accurately M_f and A_s which are at a temperature below –20 °C. The next salient feature from this curve is that on the heating side of the resistivity curve (the lower curve), the R-phase transition did not fully complete as the resistance remained much lower than 0.91 μΩ·m. Therefore some of the martensite transforms directly to the parent phase without going through the intermediate phase.

The resistivity curve given in the conference proceedings is quite different again.

In this case the resistivity remains almost constant, the minimum value being 1.005 μΩ·m and the maximum is 1.034 μΩ·m. The total relative change is only 2.8%, while for the previous results the change was greater than 16%. As described in Lafontaine *et al.* (1992) the most likely reason is that the fiber was clamped and could not change in length. As a result stress induced martensitic transformations prevented the parent phase from forming and there probably was very little phase transformation.

Figure 4.8 (A) gives a resistance curve of a NiTi fiber under constant load (40 MPa) as a function of temperature. The length changes by 3%, and the resistivity curve is estimated based on the assumption that the volume remains constant. The resistance curve shows a small hysteresis as the fiber contracts and lengthens. Figure 4.9B gives the hypothetical resistivity as a function of temperature, taking into consideration the change in length and diameter, assuming that martensitic transformations don't cause large volume changes and that Poisson's ratio is 0.33. Under such assumptions there are marked differences between the resistance and the resistivity curves.

This change is significant considering that the resistance has been proposed as a "state variable" for control purposes (Ikuta, 1990). From these considerations it is expected that the NiTi fiber properties would change in a complex manner with resistance. In order to get the resistivity, the length and area of the fiber must be known. Riva and Airoldi (1995) also conclude from different considerations that it would be difficult to use resistance as a "state variable" in situations where the load changes in time, and that it would only be appropriate when the NiTi fiber is under constant load.

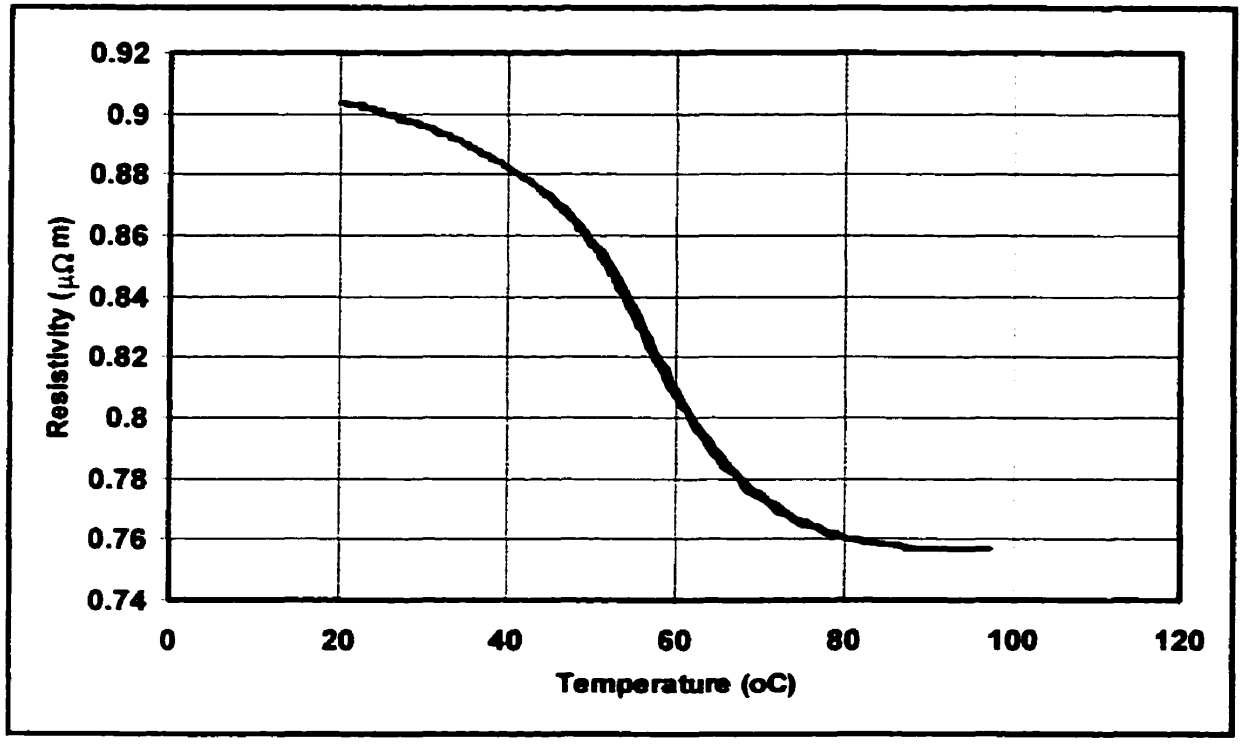

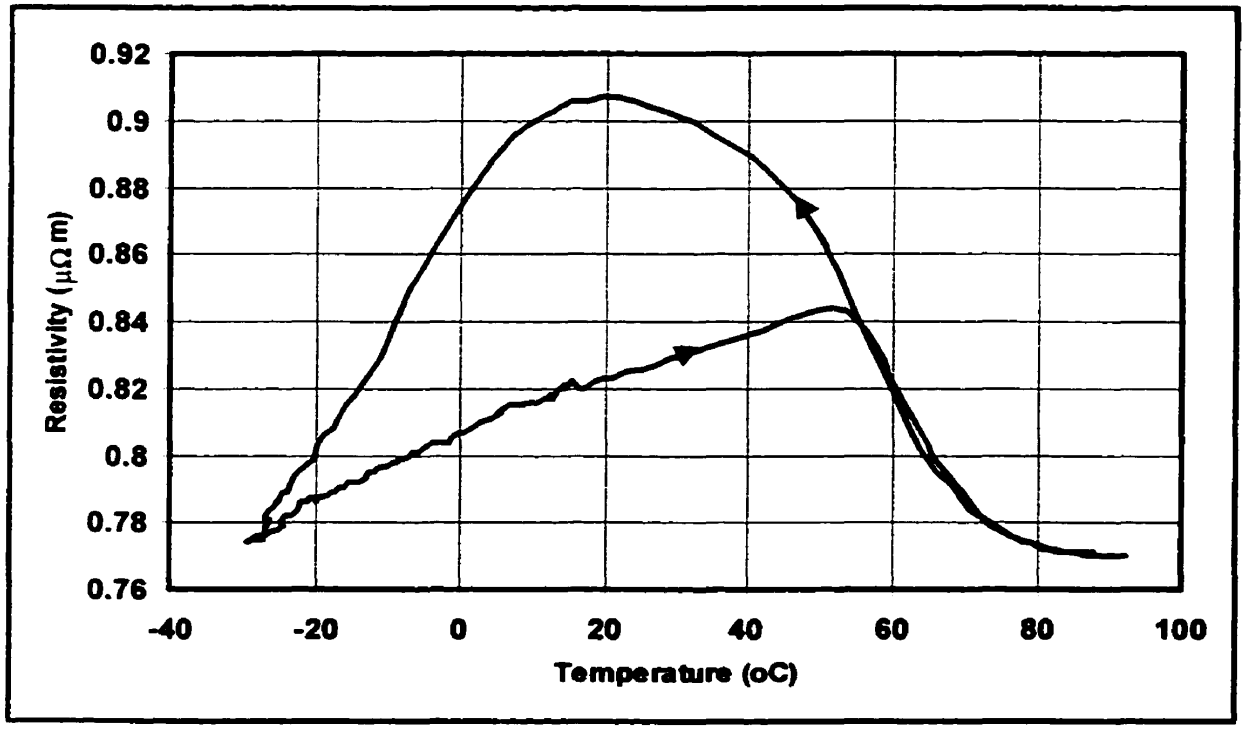

Figure 4.7 Resistivity curves of a commercially available NiTi alloy. The top curve(A) is for the portion of the R-phase only, and the lower curve (B) is includes transitions to the M phase.

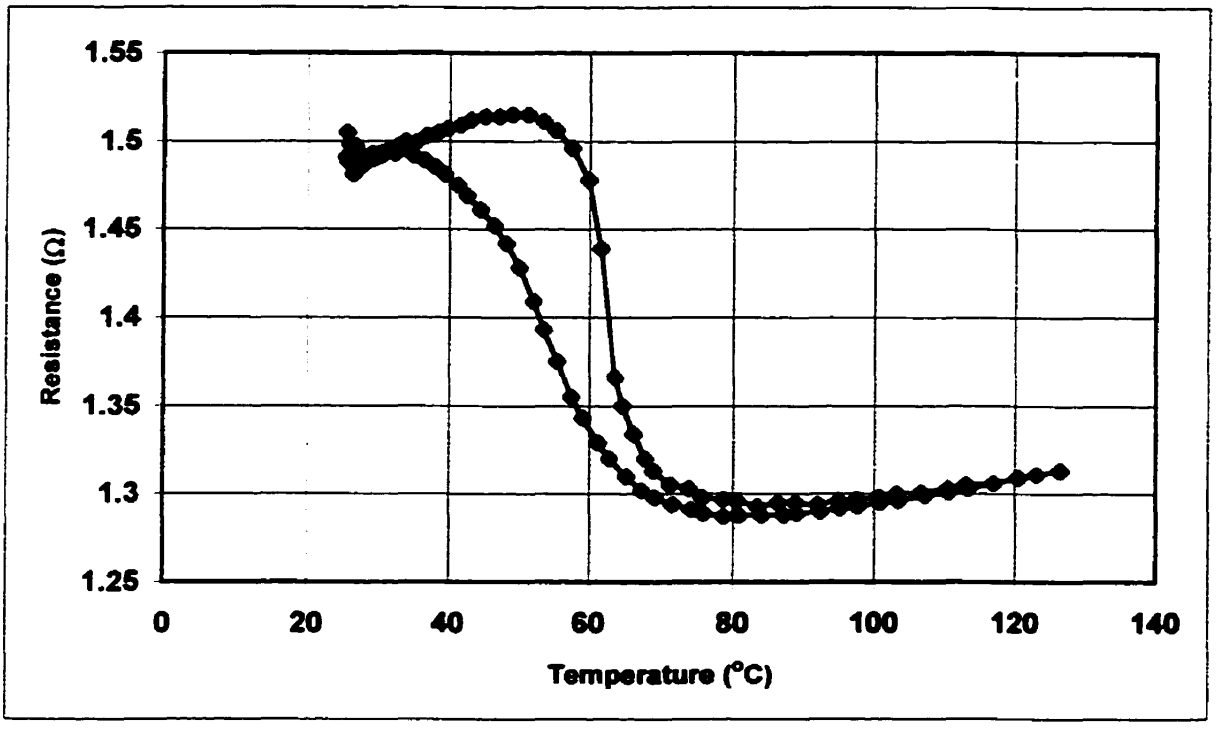

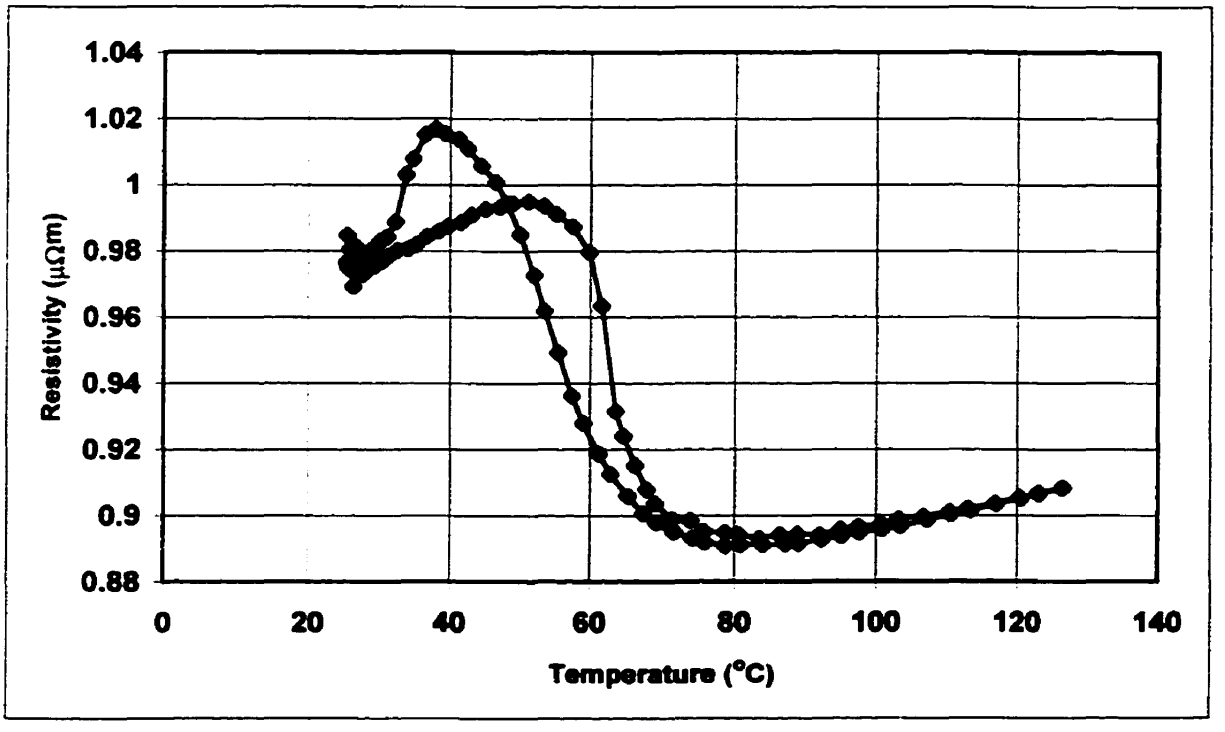

Figure 4.8 Resistivity curves for a NiTi fiber under load. At room temperatures the resistivity curve clearly indicates a wide hysteresis characteristic of the M-phase.

4.2.3 Changes in the fiber stiffness as a function of temperature

The main results are reported in the manuscript (Lafontaine *et al.*, to be submitted) included at the end of this chapter. It is first reported in this manuscript that the hysteresis in the change in fiber length versus temperature was a function of the rate at which the temperature was changed. The significance of this result is further discussed in the manuscript. In these experiments the stiffness (Young's modulus) was estimated as a function of temperature. A stress that varied triangularly in time and with a peak to peak amplitude of 60 MPa was used in these experiments. The measured strain was fitted to the measured stress using a general procedure to fit a straight line with errors in both coordinates (Press *et al.*, 1992). Figure 2B (Lafontaine *et al.*, to be submitted) gives the "variance accounted for" (VAF) as a function of temperature. The VAF is defined from the variance of a signal and the variance of residuals after fitting the signal:

$$VAF = (\Sigma y_i^2 - \Sigma e_i^2)/\Sigma y_i^2. \qquad 4.1$$

When the VAF is close to one the fit is very good. It can be seen here that the VAF was close to one everywhere except where the stiffness went down. The estimated stiffness curve showed a very large decrease in stiffness at the transition temperatures, larger than what is found in published data. It has been reported that there is a decrease in stiffness associated with the intermediate R-phase transition. A 35-50% decrease in stiffness is reported (Wu *et al.*, 1995; Jordan *et al.*, 1994; Duerig *et al.*, 1990; Funakubo, 1987). After inspection of the data it was found that large deformations occur in the material. Figure 3 (Lafontaine et al., to be submitted) illustrates one stress-strain cycle on the cooling part of the cycle. When the stress exceeds a certain threshold the fiber

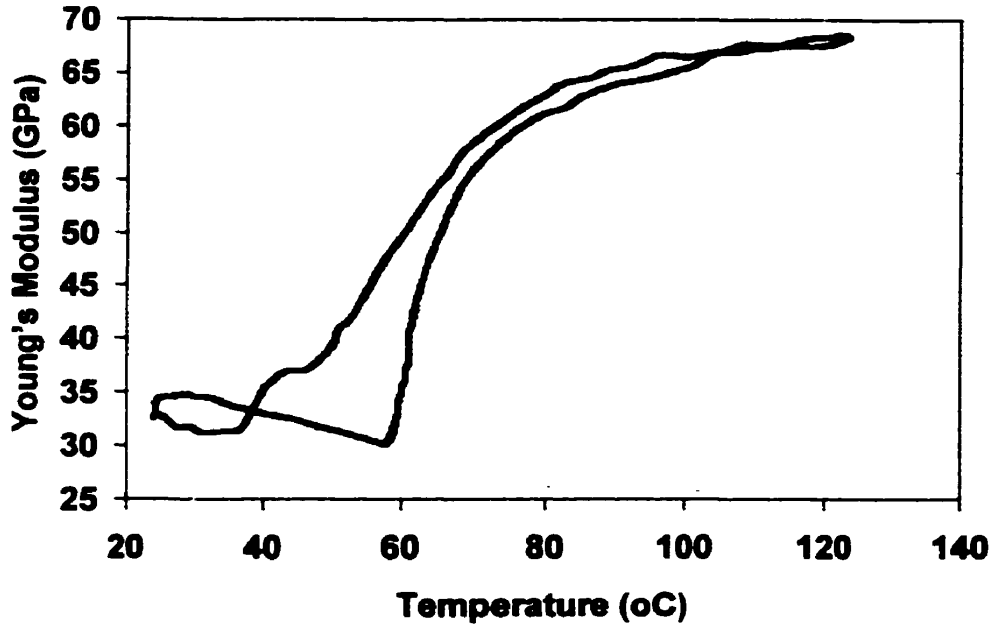

Figure 4.9 Young's modulus computed using a system identification technique.

suddenly elongates.

In the presence of large nonlinearities, non-stationarities or time-varying dynamics an adequate model is essential before estimating the stiffness. In the absence of an adequate model, the best alternative technique is to use nonparametric system identification. A series of experiments were performed using a pseudo-random binary sequence to vary the stress. Then the strain, considered as the output signal, is deconvolved from the input to find the nonparametric linear relationship between the input and the output. If the impulse response is then integrated the steady-state stiffness is found. Figure 4.9 shows the stiffness as a function of temperature. In this experiment a decrease in stiffness was still observed but it was of a much smaller magnitude (<20%).

4.2.4 Response of the fiber to short electrical pulses

Here again the main results are outlined in the manuscript appended to this chapter. The manuscript analyzes important issues such as efficiency of the fibers as a function of stress and duration of the pulses. It is found generally that the greatest efficiency is reached when larger energy pulses are used.

4.3 Discussion and Conclusion

One rationale for using short electrical pulses is that for very long current pulses more heat would be dissipated before the contraction occurs than for short pulses. On the other hand if the pulses are extremely short there might be a surface effect where the current would travel only at the surface of the fiber and local heating would occur. Furthermore the fibers consist of a polycrystalline material where the conductivity and hence heating would change across the fiber. An estimate of the time required to reach thermal equilibrium within the fiber is given by:

$$T = d^2/(4\alpha), \qquad 4.2$$

where T is the thermalisation time, d is the distance, and α is the thermal diffusivity and is given by,

$$\alpha = k/\rho c, \qquad 4.3$$

where k is the thermal conductivity, ρ the material density and c is the specific heat. The thermalisation time for a 250 μm diameter fiber is calculated to be 3.5 ms. This number is

only an approximate value but it matches well with the experimental results that pulses longer than 5 ms did not produce as much contraction for the same energy. It also explains why for pulses shorter than 5 ms, there was no significant variation in efficiency. Furthermore, if the explanation of the process to modify fibers given by Homma *et al.* (1990) is related in some manner to the process developed for this thesis, it means that pulses shorter than 5 ms would be best to modify the fibers.

Experimental Study of Fast Contracting NiTi Fibers

Lafontaine, Serge, Stein, R.B., Hunter, I.W.

To be Submitted.

Introduction

None of the current actuators satisfactorily meet the design requirements essential for robotic and prosthetic applications. Muscles, on the other hand, have been in widespread use for over 300 million years throughout the animal kingdom, even though their overall performance is rather modest in many respects. Muscles are exceptional for their large range of motion (approximately 20% of their body length in-situ) and very long life time (over 2.5 billion cycles). The efficiency of conversion of chemical to mechanical energy is moderately low (35%), as are the force per unit area (350 kPa), power to mass ratio (50 W/kg, 200 W/kg peak) and bandwidth (10 to 20 Hz) (Hunter and Lafontaine, 1992). They are scaleable in design such that more force or displacement can be obtained by adding muscle fibers in parallel or series. Their stiffness changes over a range of 100:1 and can be modulated by co-contraction. Muscles have local energy storage for about 35 full contractions so an external energy supply does not need to be provided for a high-speed low delay muscle response. On the other hand they have no "catch state" and require continuous energy expenditure to maintain a fixed position even though no mechanical work is done. Finally muscles cannot be used as a generator to recover energy from mechanical work.

In a review of new actuator technologies Hunter and Lafontaine (1992) evaluated a number of materials that could be used in artificial muscle-like actuators as fibers, films or rods and that could be assembled in a series or in a parallel configuration and controlled like muscle fibers. Out of that study two materials became of great interest: nickel-titanium (NiTi) shape memory alloys and electrically conducting polymers. NiTi alloys have reached the stage of being an engineering material that can be used in actual designs (Funakubo 1987; Duerig *et al.*, 1990). They generate huge forces of more than180 MN/m^2, about 700 greater than muscle, large displacements (>7%), and have very large power to mass ratios (>100 kW/kg). The main limitations are their very low efficiency (<2%) and a limited lifetime that can be compensated by redundancy given high power-to-mass ratio and force per unit area.

New smart materials such as electrically conducting contractile polymers are one of the most promising actuator technologies of the future (Hunter and Lafontaine, 1992), not only for robotic and micro-robotic applications, but also for energy storage and information processing. While we are actively pursuing research in polymer actuators, we are working on practical applications using our fast contracting NiTi artificial muscle fibers for immediate use such as in haptic interfaces. Similarities in control and design considerations between the two technologies are anticipated.

Methods

In the first series of experiments, designed to characterize the properties of NiTi fibers as a function of temperature, NiTi fibers 0.1 mm in diameter and 100 mm long were clamped between two General Scanning (GT350) galvanometer motors. One General

Scanning AE1000 analog control board was used to maintain one end of the fiber at a fixed location and a second modified AE1000 board applied a force proportional to the input voltage. Each motor was capable of producing 5 N of force on the fiber via a lever extending from the shaft. In these experiments a current servo-control system with proportional, integral, and derivative feedback (PID) was used to apply a triangularly varying force of 1 N with a 10 s period. The motors have inbuilt capacitive angular position transducers with a noise level of 0.01 mdeg rms at 10 Hz. The force was calculated from the current running through the galvanometers. The sensitivity was obtained from calibration with known weights. The ratio of force change to length change was used to calculate the stiffness of the fibers. The NiTi fibers were mounted horizontally between the motors in a water bath machined into a copper bar. The top surfaces of 14 Peltier effect heat pumps (Marlow Industries MI1064T) were attached to the copper bar to provide temperature control of the bath and hence the NiTi fibers. The other faces of the Peltier devices were attached to another copper bar which in turn was bolted to a 19 mm thick water-cooled aluminum plate which served as a heat sink. Each heat pump could carry up to 5.3 A at up to 4 V supplied by a Hewlett Packard HP6652A DC power supply. The temperature of the bath was regulated by a proportional-integral (PI) controller, based on temperature measurements taken at 5 Hz by a type K thermocouple using a Keithley 2001 5.5 digits precision multimeter. HP34401A multimeters were used to digitize the outputs from the position and force signals. A HP3245A Universal Source was used to generate the command to the motors. An IBM RISC/6000 with National Instruments GPIB microchannel card was used for bi-directional communication with

multimeters and the universal source.

In a second series of experiments, designed to characterize the pulse response of NiTi fibers, the HP3245A precision source was connected to the gate of an Insulated Gate Bipolar Transistor (IGBT) to switch the high voltage from an HP6035 high voltage power supply. Pulses generated by the HP3245A precision source controlled the gate of the IGBT. As before all devices were controlled via the IEEE488 data bus. The output voltage of the HP6035 power supply was controlled via the IEEE488 bus under program control. The position and force signals from the AE1000 galvanometer control boards were acquired by the HP54501 digitizing scope and were subsequently uploaded to the IBM RISC/6000 and saved to disk.

In a third series of experiments, whose purpose was to look at the response of NiTi fibers to very large current pulses, 100 μm diameter and150 mm long fibers were attached at one end to an InterTechnology force transducer (model 9363-D1-100-20P3) and at the other end to a Mitutoyo 164-152 micrometer used to set the initial tension in the fiber. In its middle the fiber was attached to a brass metal sheet which in turn carried a miniature HP photodiode. A lateral effect photodiode and United Detector Technologies (UDT) processor generated a signal proportional to the location of the photodiode. The brass sheet was connected to ground and each end of the fiber was connected to an IGBT. The collectors of the IGBT's were connected to an HP6035A power supply and the emitters to the fiber. The IGBT's were gated from an HP3245A precision source. The force signal from the force transducer and position of the diode were acquired by the HP54501 digitizing scope and read via the IEEE 488 bus.

In a fourth series of experiments, performed to investigate resistivity, 100 mm long fibers with a diameter of 250 μm were electrodeposited with nickel to a diameter of 500 μm at each end. Two wires were connected at each end for four wire ohm measurements. A type K chromel-alumel thermocouple with a 250 μm welded ball at its end was used to measure the temperature right at the surface in the middle of the NiTi fiber. Approximately 10 mm of thermocouple wire was wrapped around the fiber and bonded with the thermocouple ball. A constant current of 10 mA was passed through the fiber and an instrumentation amplifier with a gain of 10,200 amplified the voltage recorded by two sense leads. A Fisher 2101 heater and NESLAB cooler were used to provided two water baths at different temperatures between which the fiber was quickly switched. A Pentium based Windows NT system with a National Instruments PCI-MIO-16XE multifunction board was used to acquire the temperature and resistance data.

Results

Figure 1A shows the mean length changes for a 100 mm long NiTi fiber when the temperature was increased and decreased slowly from -10 to +110 °C. When the temperature increased, the fiber shortened abruptly by more than 2.5 mm (>2.5% strain) at about 72 °C and when it decreased, the fiber relengthened at about 42 °C. Thus, there was a considerable hysteresis in the transitions. Figure 1B shows how the hysteresis changes with the rate of cooling and heating. The hysteresis in temperature was markedly smaller for faster rates of temperature changes. This topic is considered further in the discussion.

(Figure 1 near here)

It is now well established that in the phase transitions of NiTi alloys, there are one or two intermediate phases as described by Beyer (1995). It is often assumed that there is a large change in stiffness associated with R phase transformations as described by Jordan *et al.* (1994) and Wu *et al.* (1995). Using a linear fitting procedure between stress and strain to estimate the stiffness showed a much larger drop in the stiffness than previously reported for the R phase. However the apparent decrease in stiffness shown in Figure 2A seemed an artifact of the poor fit as indicated by the variance accounted for (VAF) in Figure 2B. Inspection of the data showed large nonlinearities in the response such as a large plastic deformation on the cooling part of the curve as shown in Figure 3. This could be partly accounted for by fitting only the sections of the stress-strain curve, which lie on a straight line. Figure 4A shows the corrected stiffness that remained large over all temperatures and is in agreement with other reported values. Figure 4B shows the VAF. Transitions to either the high (Austenite) or low (Martensite) temperature states were associated with a moderate decrease (<30%) in the fiber stiffness (see Methods for details of the measurement). This suggests that there is also a third state in the sample, which is confirmed by the resistivity curve shown in Figure 5. The resistivity curve clearly indicates an R phase with low hysteresis at intermediate temperatures (between 20 °C and 70 °C), and the martensite phase at lower temperatures.

(Figure 2, 3, 4, and 5 near here)

Figure 6A shows the effect of a 0.5 ms 60 V pulse of current on a fiber that was maintained at room temperature in air. The pulse is sufficient to heat the fiber above its transition temperature and there is a 4% change in length that then decays exponentially with a time constant of about 0.5 s. With larger pulses (80 V) the response saturates at a length change near 9 mm for several hundred milliseconds, but then decays more rapidly. A similar experiment is shown in Figure 6B in water. The cooling and the relengthening associated with the pulse of current is much quicker, even though the pulse is longer (5 ms, 36 V). The 6.4 mm shortening and relengthening is all completed in about 100 ms.

(Figure 6 near here)

Using two fibers in series and activating them sequentially produced even better temporal resolution. Figure 7A shows the effect of pulses separated by 100 ms. Both pulses were 80 V, but the pulse to the second fiber was longer than that to the first (1.3 vs 1.0 ms). Although the length changes cancel out, the force from each pulse will sum as shown in Figure 7B. The speed of shortening and lengthening that is possible is seen in Figure 7C in which the interval between the two pulses was shortened to 1 ms. The width of the response is only 1.6 ms, which is more than an order of magnitude better than fast twitch muscle fibers. The velocity of shortening was nearly 1.7 m/s or 17 fiber lengths/s, which again is an extraordinarily high value, compared to muscle.

(Figure 7 near here)

The use of very short pulses has other important consequences. Figure 8A shows the effect of different duration pulses in terms of the energy requirements in VA ms. There is little difference in the length change produced for a given energy input with inputs briefer than about 2 ms, but the efficiency is less with longer pulses (5 or 10 ms). Efficiency was studied more carefully in a second series of experiments. The integral of force times length represents the work done which can be compared to the electrical energy input. The efficiency is low (little work is done) for energy inputs less than 1 Joule, but increases rapidly to between 2 and 3% for larger energy inputs. A steady stress of 40 MPa was applied in this series of experiments, which were conducted with the fibers in water at room temperature. The energy efficiency was relatively constant for pulses below 5 ms, but declined abruptly for longer duration pulses (not shown).

(Figure 8 near here)

The energy efficiency is relatively low, but was not optimized in these experiments. Two factors could be varied to improve efficiency: first the force could be altered since the length change depends on force. Figure 9A shows the effect of varying the force on the length change and the product of force and length. The optimal efficiency was obtained at a force level of 4. N in this experiment, but was only 1.3%. The speed of shortening is also reduced at higher force levels as shown in Figure 9B. Secondly, the temperature of the bath could be maintained nearer to the transition temperature so that less energy than the 1 Joule, shown in Figure 8 would be required. Of course, some energy

will be required to maintain a higher bath temperature and the reverse transition will be slower. The dissipation of the applied energy into air will also be less than into water, but this severely restricts the speed, as described above.

(Figure 9 near here)

One final point of interest is the response of the system to series of pulses. In Figure 10 responses are superimposed for 1, 2, 5, 10, 15 and 25 pulses at 5 ms intervals. Each pulse was 55 V and 1 ms in duration. With the fiber in water, the total response to one pulse was quite brief (20 ms), but subsequent pulses could add to the response and maintain a partially fused contraction. At higher rates the response would be completely fused. This behavior is reminiscent of the twitch and tetanic behavior of muscle fibers when stimulated with a brief pulse (the action potential) and a series of such pulses at various frequencies. This pulse code modulation may be a more efficient way of activating NiTi fibers, as well as muscle fibers.

(Figure 10 near here)

Discussion

The thermodynamics of martensitic transformations is complex and not fully understood yet. There have been many modeling attempts and it is generally assumed that martensitic transformations occur at close to the speed of sound in the alloy and that the

temperature completely determines the thermodynamic state of the martensitic transformations. Hirose *et al.* (1989) and Ikuta *et al.* (1991) assumed in their lumped model that the martensitic transformations occur instantaneously and any dynamics are related to heat exchanges to heat or cool the fiber. More recently Lu (1997) used a similar approach and combined Ikuta's model with the thermal time constant of the NiTi fiber. Experimentally Leo et al. (1992) have found that the hysteresis curve of superelastic alloys depends on the strain rate. Similarly Shaw (1997) recorded thermal images of the nucleation and propagation of phase transformation fronts in a NiTi alloy and illustrated a process in which the latent heat released or absorbed in a superelastic alloy in air is sufficient to heat or cool the metal and contribute to the martensitic transformations. However this process does not occur when the fiber is immersed in a liquid and the stress-strain curve of superelastic alloys is well defined.

In real alloy crystals the martensitic transformations depend on several factors such as plasticity. Silling (1992) developed a mathematical model where he showed that martensitic plates can propagate at subsonic speeds. The results observed in Figure 1 however clearly indicate hysteresis in the stress-strain curve of a shape memory alloy material which depends on the heating or cooling rate. This indicates a dynamic process by which martensitic transformations occur at a low speed. To further test this possibility, the state of martensitic transformations was measured by resistivity when the alloy was subjected very rapidly to a large temperature change and then kept at a constant temperature. There was a very rapid change in resistivity over temperatures where only transitions to the intermediate R-phase are expected. The results for larger changes are

given in Figure 11, where the NiTi alloy temperature was between 95 °C and –16 °C. It can be clearly seen that the resistivity decreases almost instantaneously when the fiber is heated to 95 °C. However when the fiber is cooled down to –16 °C the resistivity changes very slowly which indicates that even after 20 seconds the transformations are not fully completed yet. In this alloy the resistivity of the parent phase is 0.78 $\mu\Omega$·m, the resistivity of the R phase is .92 $\mu\Omega$·m and the resistivity of the martensitic state is .86 $\mu\Omega$·m. When cooled, the R phase appears very quickly and rapidly transforms into the M phase. When heated, however, the R phase does not seem to reappear completely and there is a significant portion of the M phase that transforms directly to the parent phase. Based on these considerations a model of the transformations is being developed to explain the results displayed in Figure 1 and will be presented in a future paper.

(Figure 11 near here)

Bibliography

Beyer, J. Recent advances in the martensitic transformations of Ti-Ni alloys. *Journal de Physique IV*, 1995, *5(Colloque C2)*, C2-433-443.

Duerig, T.W., Melton, K.N., Stöckel, D. and Wayman, C.M. *Engineering aspects of shape memory alloys.* Boston: Butterworth-Heinemann, 1990.

Funakubo, H. *Shape memory alloys.* New York, NY: Gordon and Breach, 1987.

Hunter, I.W. and Lafontaine, S. Shape memory alloy fibres having rapid twitch response. US patent 5,092,901, 1992.

Hirose, S., Ikua, K. and Umetani, Y. Development of shape-memory alloy actuators. *RoManSy '84, the 5th CISM-IFTOMM Symposium*, 1984.

Ikuta, K., Tsukamoto, M. and Hirose, S. Mathematical model and experimental verification of shape memory alloy for designing micro actuator. *Proceedings of IEEE Micro Electro Mechanical Systems*, 1991.

Jordan, L., Chandrasekaran, M., Masse, M. and Bouquet, G. Study of Phase Transformations in Ni-Ti based shape memory alloys. *Journal de Physique IV*, 1995, *5(Colloque C2)*, C2-489-494.

Lu, X. A systems approach to modelling and design of high strain shape memory alloy actuators. Master of Engineering Thesis, Department of Electrical Engineering, McGill University, Montreal, 1997.

Shaw, J.A., Kyriakides, S. On the nucleation and propagation of phase transformation fronts in a NiTi alloy. *Acta Materialia*, 1997, 45(2), 683-700.

Silling, S.A. Dynamic growth of martensitic plates in an elastic material. *Journal of Elasticity*, 1992, 28(2), 143-64.

Wu, K., Dalip, S.K., Liu, Y. and Pu, Z. Damping characteristics of R-phase NiTi shape memory alloys. *Smart Structures and Materials SP IE-Int. Soc. Opt. Eng.*, 1995.

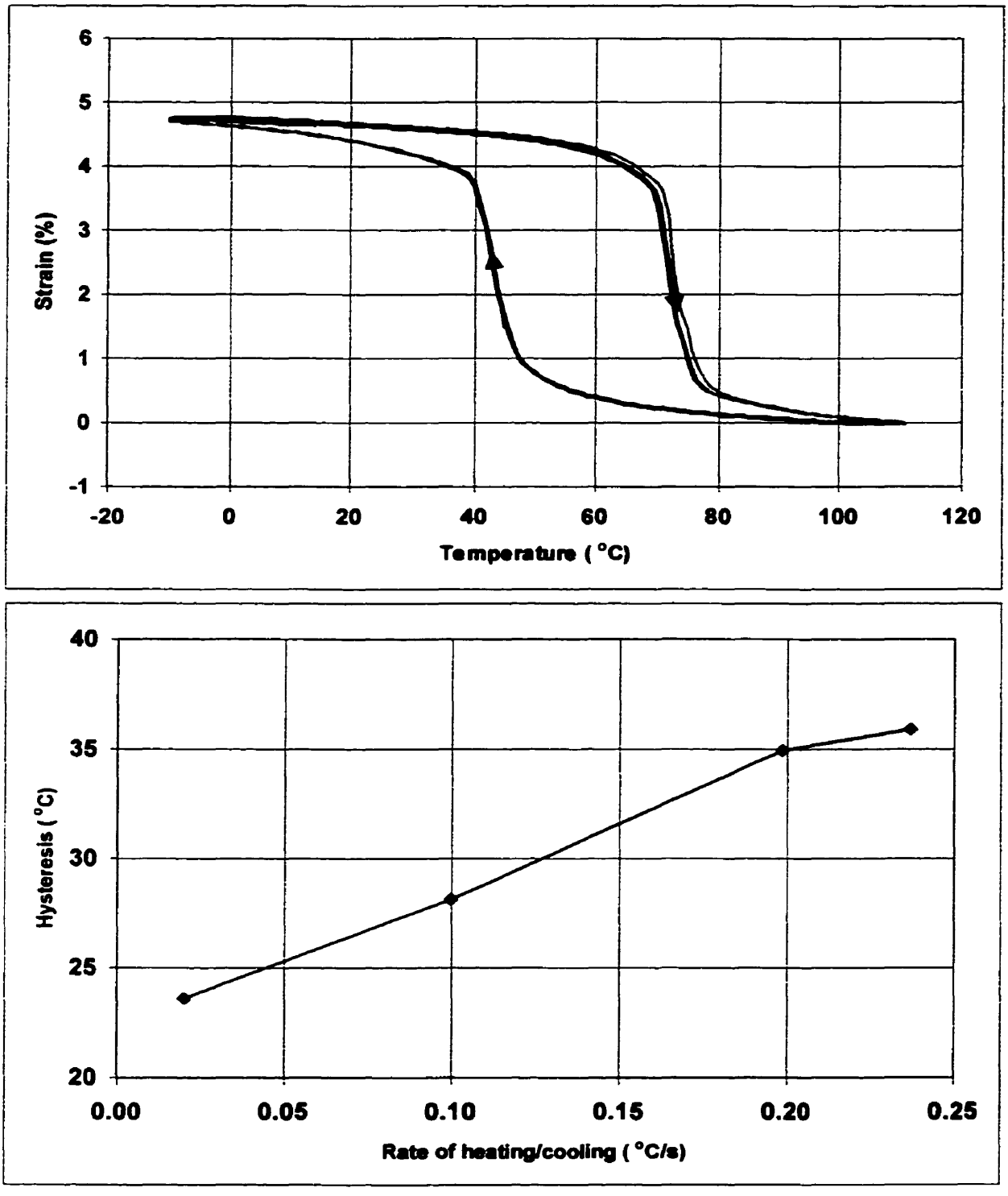

Figure 1 Hysteresis in length versus rate of change in Temperature. Top curve (A) shows how the relative fiber length changes as the temperature is cycled between –20 °C and 120 °C. The bottom curve (B) shows the hysteresis width as a function of the temperature rate change.

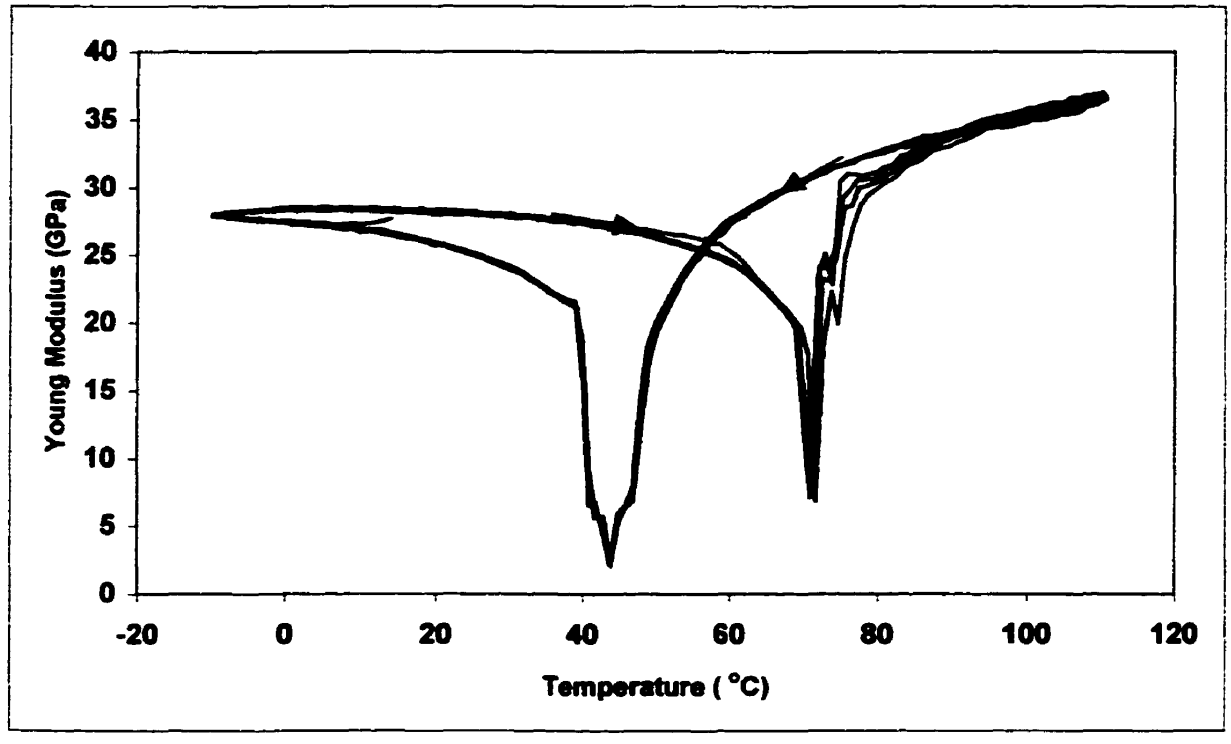

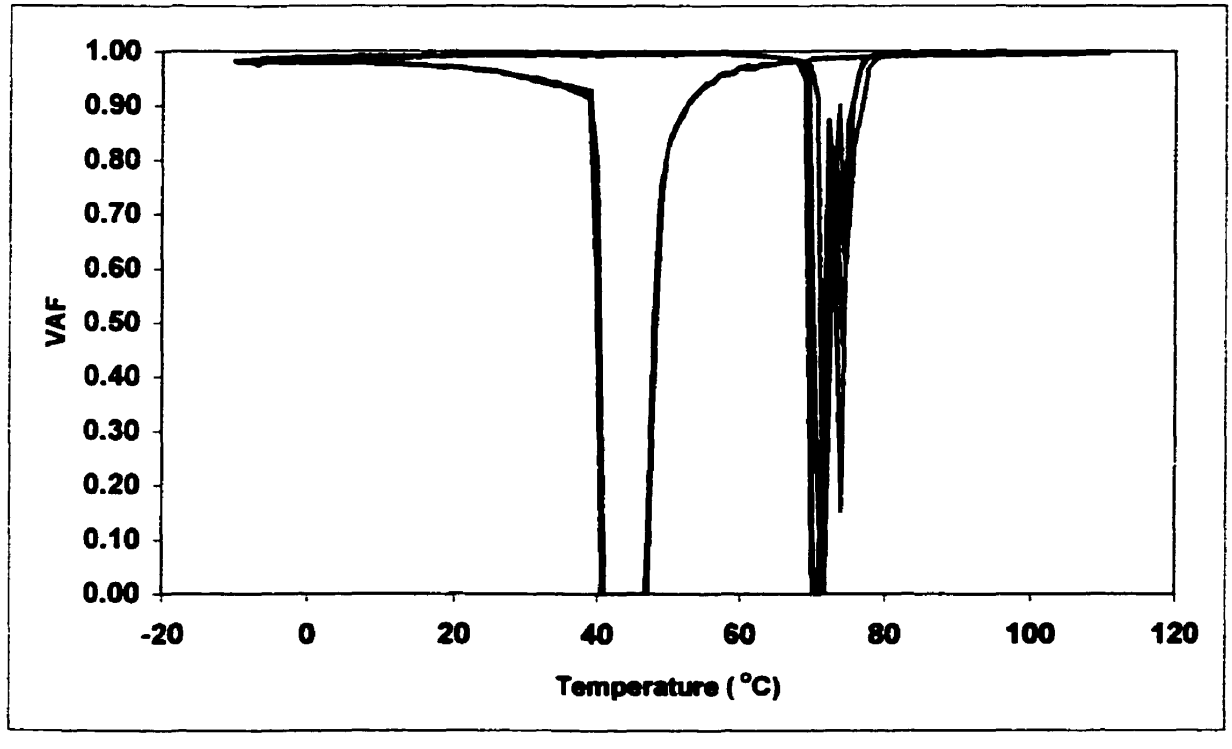

Figure 2 Modulus of elasticity of the NiTi fiber as a function of temperature obtained from a triangular change in stress. Figure 2A (top) gives Young Modulus obtained from fitting the input stress to the measured strain. Figure 2B (bottom) gives the Variance Accounted For (VAF) which indicates the goodness of fit.

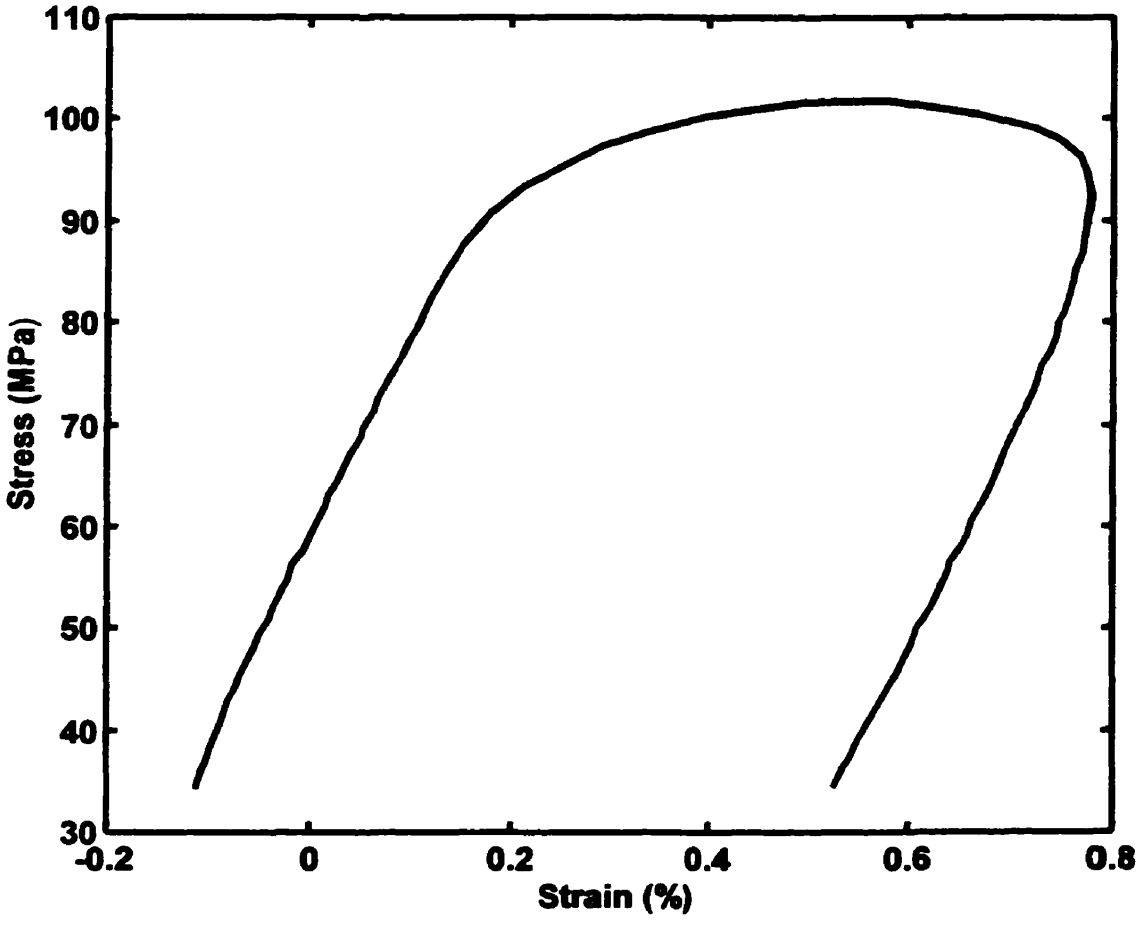

Figure 3. Illustration of the plastic deformation which occurs on the cooling cycle when the parent phase transforms into the intermediate R-phase.

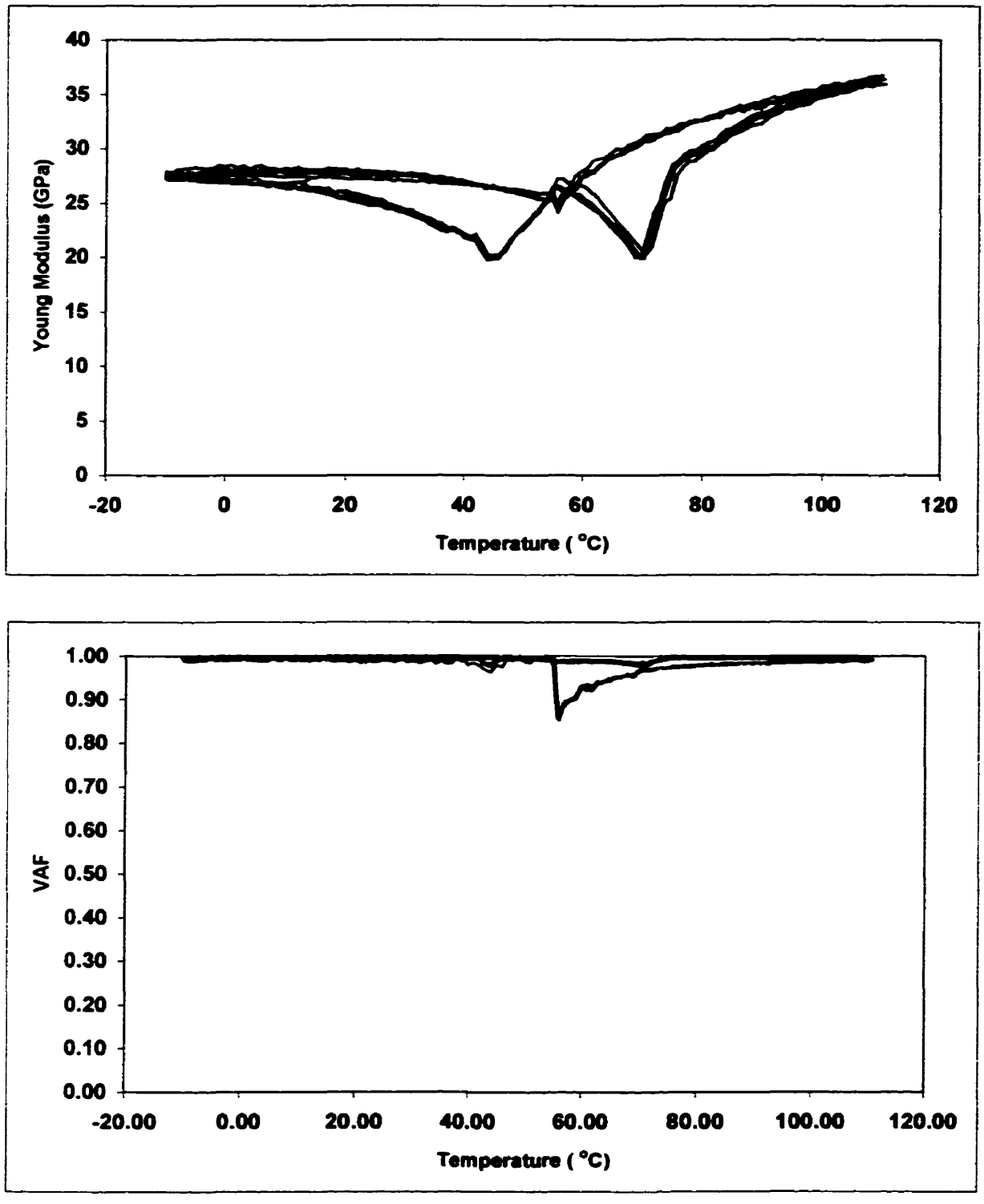

Figure 4 Modulus of elasticity of the NiTi fiber as a function of temperature. Figure 4A (top) gives Young Modulus after correction. Figure 4B (bottom) gives the variance accounted for which indicates the goodness of fit.

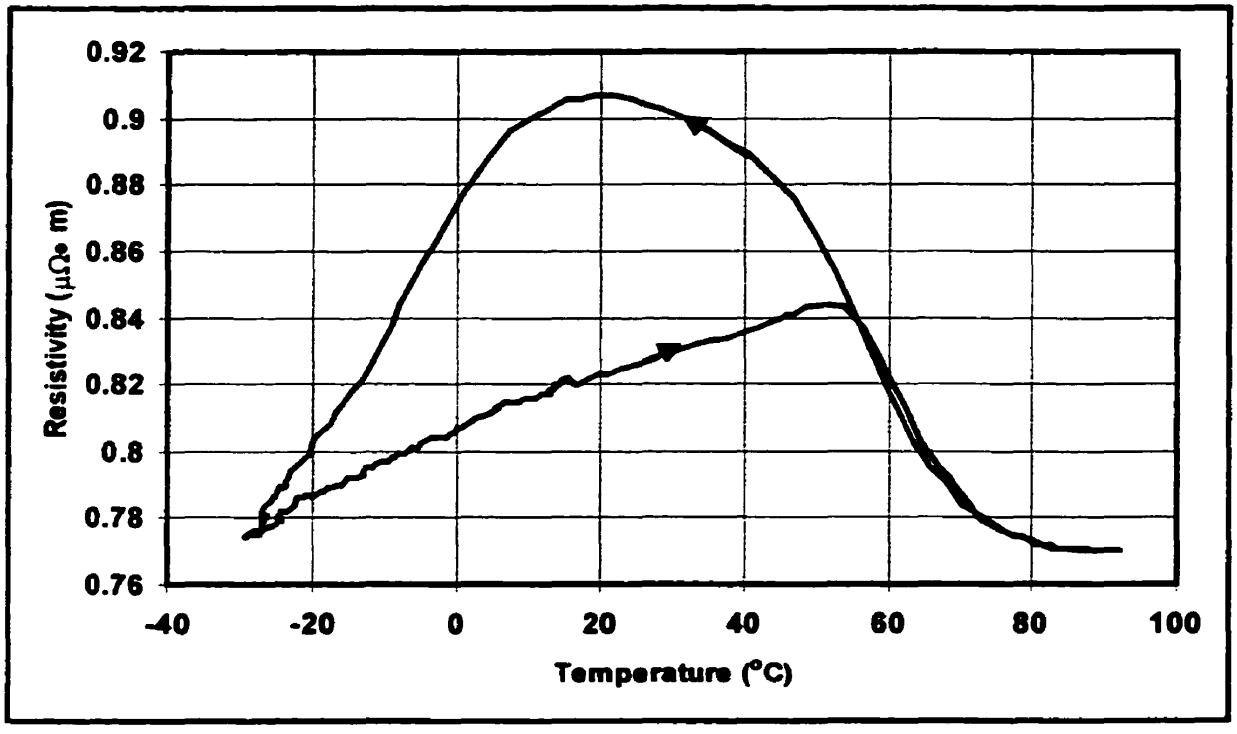

Figure 5 The resistivity curve for the NiTi sample clearly shows a large resistivity characteristic of an intermediate R phase between 20 °C and 70 °C, as well as its very small hysteresis.

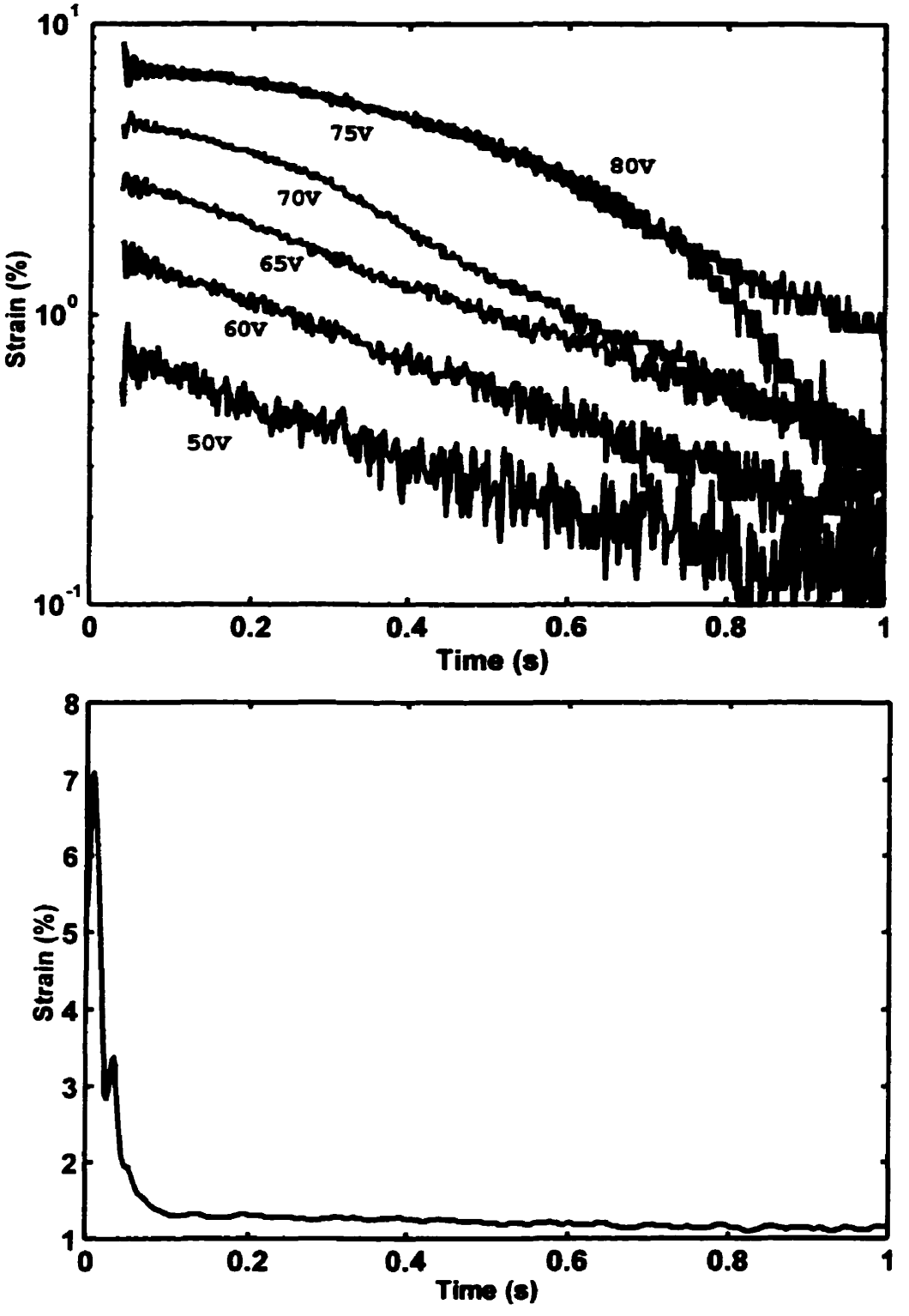

Figure 6 The relaxation times of NiTi fibers are displayed in the two plots above. The curves at the top (A) show relaxation times in air for different voltages applied to the fiber. The relaxation time shown below (B) is much shorter and is typical of relaxation times observed in water.

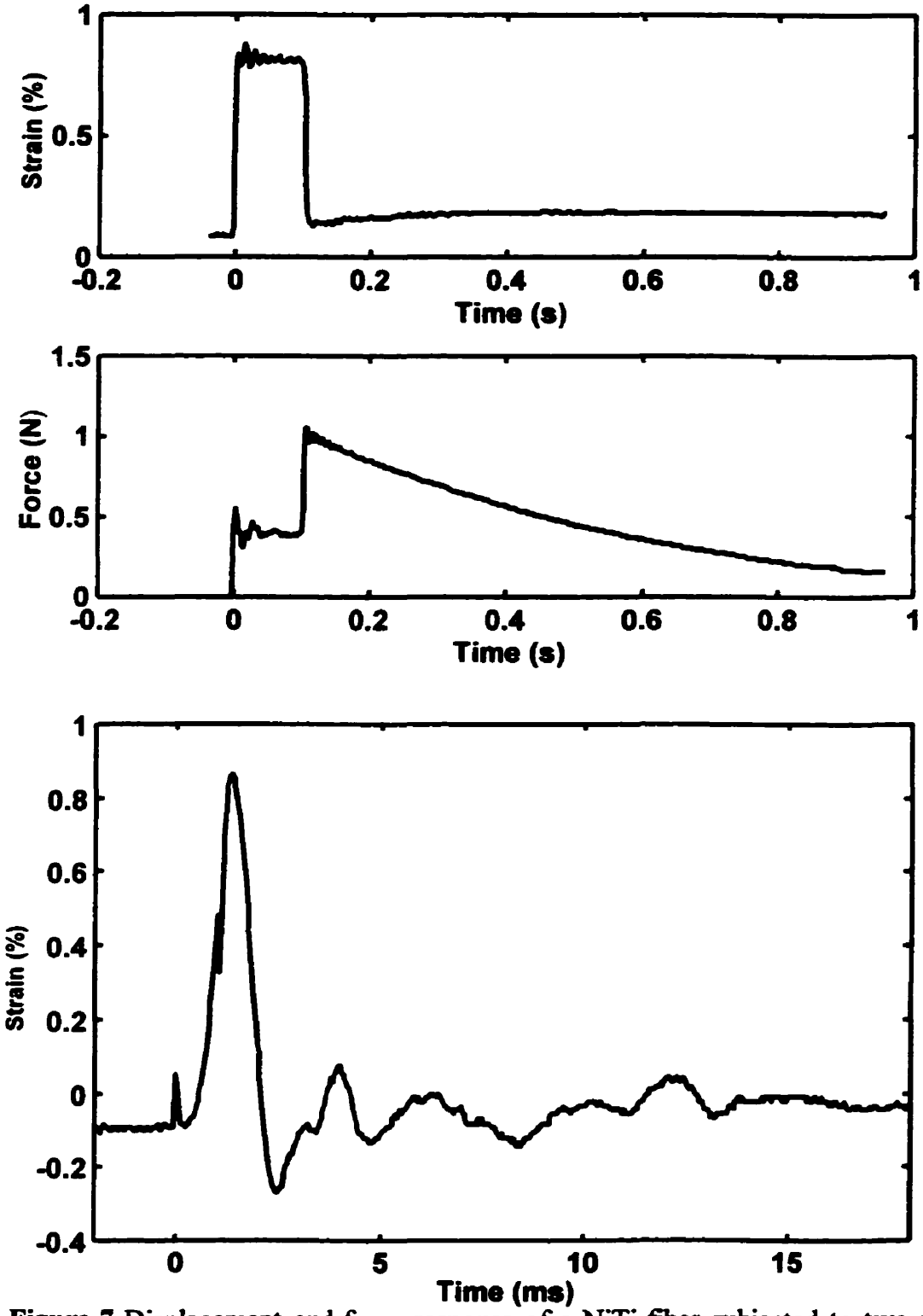

Figure 7 Displacement and force response of a NiTi fiber subjected to two pulses stimulating opposite halves of the fiber. Figure 7A at the top shows the rapid displacement. Figure 7B in the middle displays the force and Figure 7C at the bottom displays the fiber displacement when the pulses are separated by 1ms.

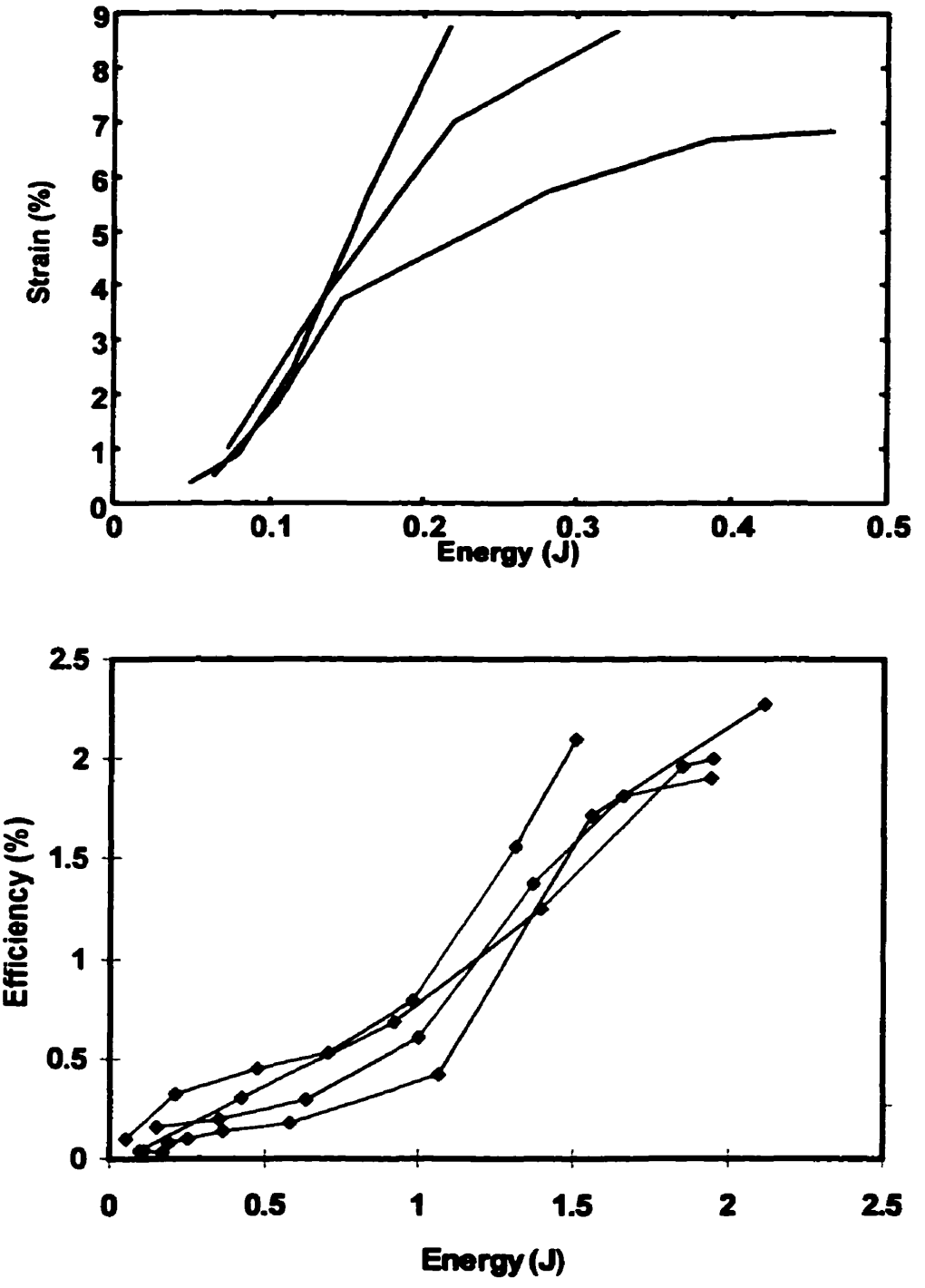

Figure 8 The mechanical work done by a NiTi fiber is a function of the force against which it is acting as show in Figure 8A at the top. Figure 8B at the bottom shows the efficiency of conversion from electrical energy to mechanical work.

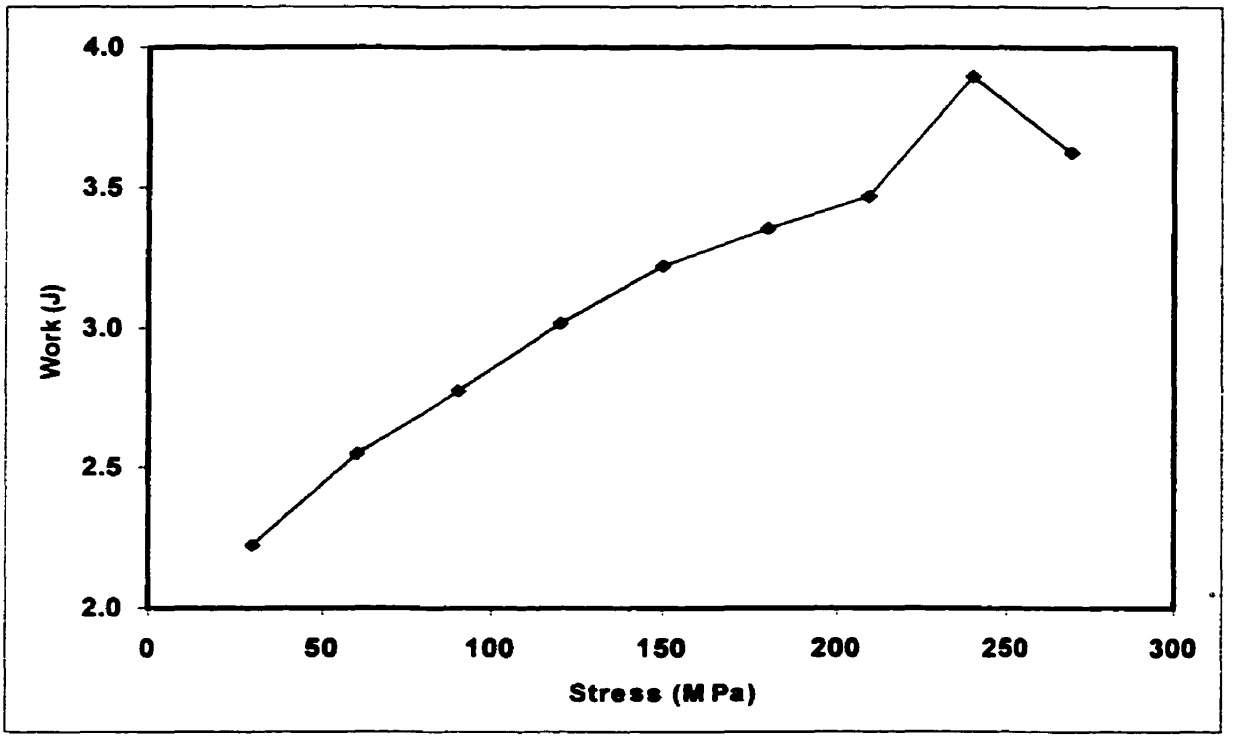

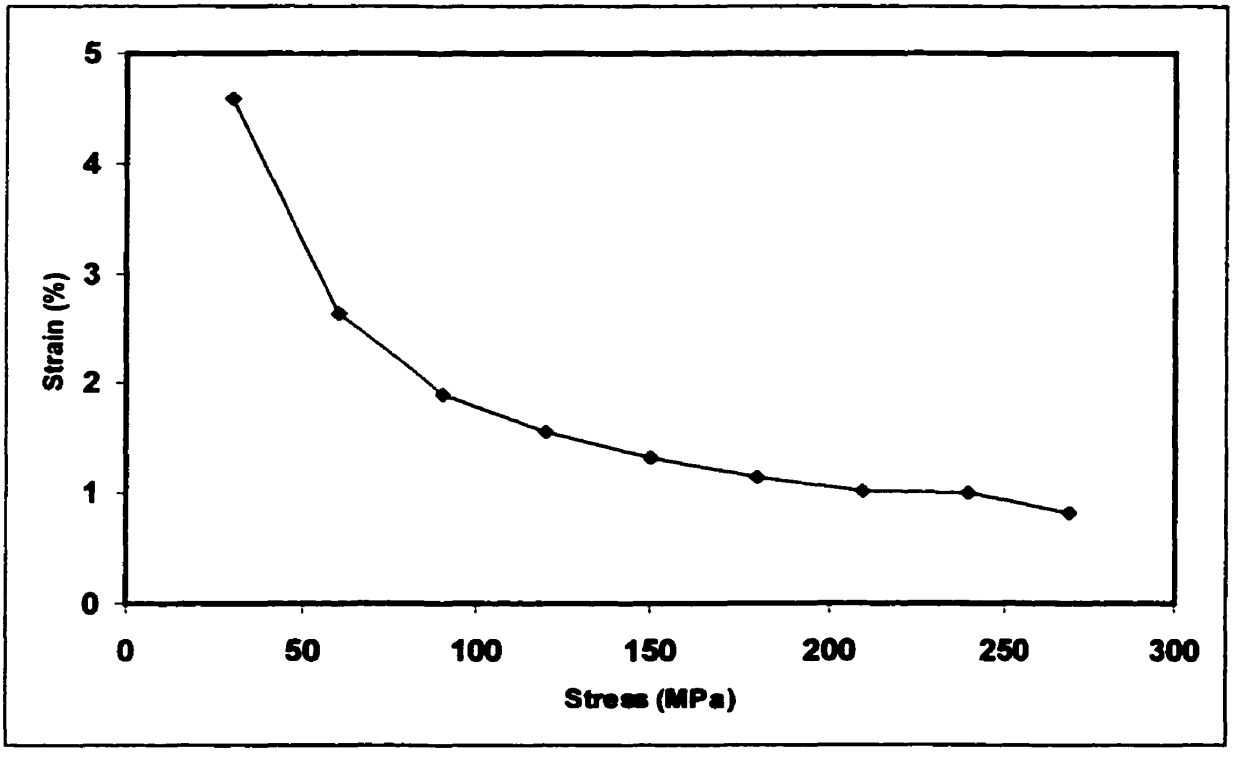

Figure 9 The amount of mechanical work done by the fiber depends on the stress maintained in the fiber and the strain in the fiber. Figure 9A at the top displays the mechanical work as a function of the stress. Figure 9B at the bottom displays the corresponding change in length.

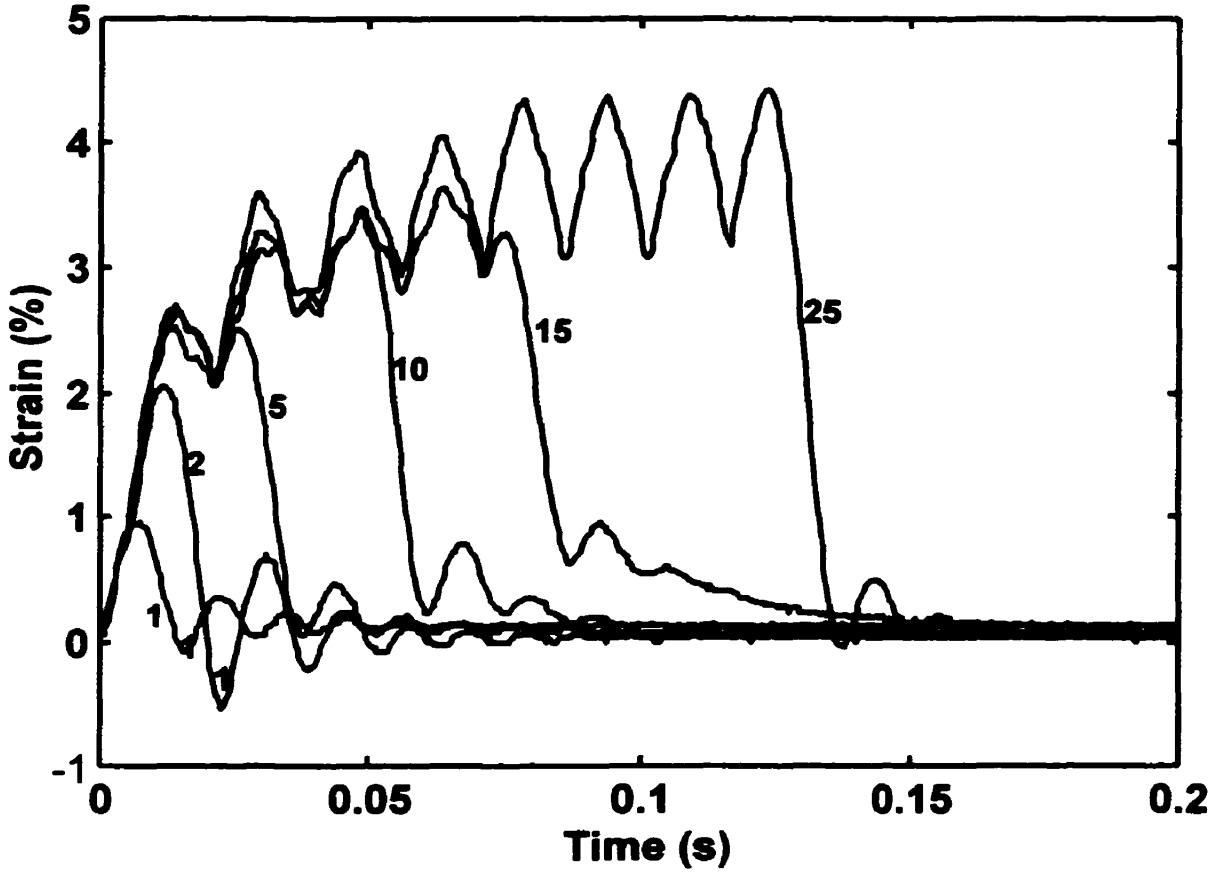

Figure 10 The curves above correspond to the displacement of a NiTi fiber when subjected to a number of pulses applied at 20ms intervals. The individual pulse responses fuse together like in muscle. At shorter intervals the individual responses would be completely fused.

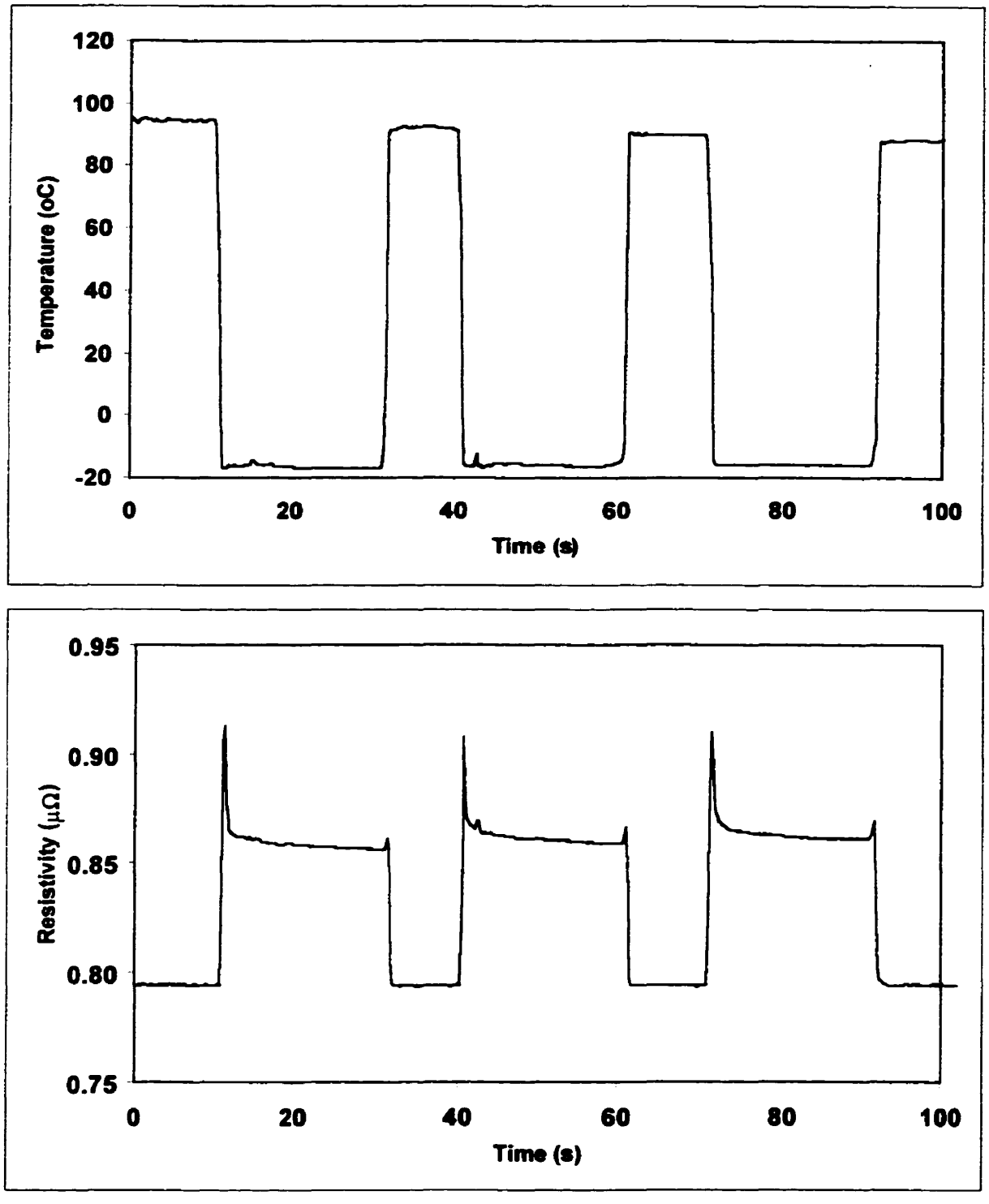

Figure 11 The temperature of a NiTi fiber was suddenly changed by transferring the fiber quickly between a hot water bath at 95oC and a cold water bath at –16 °C. The corresponding temperature changes as measured by a thermocouple are indicated in Figure 10A above and the corresponding resistivity changes are shown in Figure 10B below.

FAST REVERSIBLE NiTi FIBERS FOR USE IN MICROROBOTICS

Ian W. Hunter, Serge Lafontaine, John M. Hollerbach and Peter J. Hunter
Biorobotics Laboratory, Department of Biomedical Engineering,
McGill University, 3775 University Street, Montreal, Canada H3A 2B4

ABSTRACT

We report the experimentally determined characteristics of NiTi fibers which have been modified using a preparation procedure in which the fibers were subjected to brief very large current pulses during forced stretching. The modified fibers contract and relax fast enough to be of use in micro–robotics. The modified fibers generate a maximum extrapolated stress of 230 MN/m^2 and yield a peak measured power/mass approaching 50 kW/kg. The theory of a micro–actuator incorporating the modified fibers is presented.

INTRODUCTION

The shape memory alloy NiTi generates large forces (>100 MN/m^2) with substantial displacements (up to 10% strain), and appears to hold considerable promise as an actuator either in fiber form in robotics [1] or in thin film form in micro–mechanics [2][3][4]. Two drawbacks that have limited the usefulness of NiTi actuators are (1) low bandwidth (around 1 Hz in fiber form [1] and 5 Hz in thin film form [4]) and (2) nonlinear dynamics. The low bandwidth is due to the long relaxation time which is usually assumed to be determined by the relatively long cooling thermal time constant.

EXPERIMENTAL APPARATUS

Figure 1 shows a sketch of the apparatus used to perform

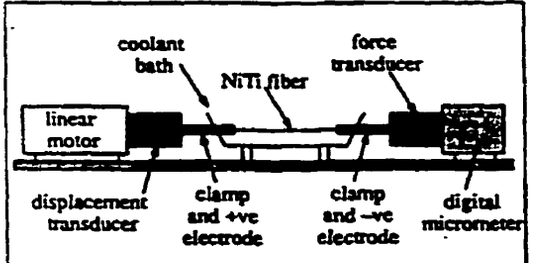

Figure 1. Experimental apparatus used to determine NiTi fiber properties.

mechanical experiments on the NiTi fibers. A NiTi fiber is clamped between a force transducer at one end and a linear motor and displacement transducer at the other end. The displacement transducer was a lateral effect photodiode with a flat bandwidth to 1 kHz. The force transducer was a strain gaged proving ring with a flat bandwidth to 1 kHz. External forces were applied using a servo–controlled electromagnetic linear (voice–coil) motor. The NiTi fibers were immersed in recirculating methanol which was stirred and cooled to –10°C. All experiments were under computer control and force and displacement data were sampled via 12 bit A/Ds. The NiTi fibers were subjected to either sustained constant currents or computer controlled current pulses delivered using 200 A power–MOSFETS.

NiTi Fiber Modification

Figure 2 shows the contraction of a 100 mm long 0.8 mm

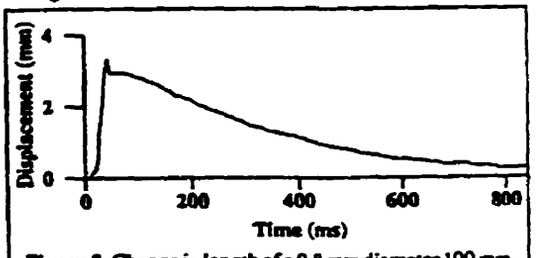

Figure 2. Change in length of a 0.8 mm diameter 100 mm long NiTi fiber following a brief current pulse.

diameter NiTi fiber following a single brief current pulse. The relaxation back to it original length is slow compared with the contraction time. Indeed in robotic applications the time taken to relax is usually much longer than this because cooling conditions were very favorable here. We tried a variety of cooling methods including vortex cooling and Peltier effect heat pumps without significant improvements.

We have attempted to shorten the relaxation time and have found that by exposing NiTi fibers to very large brief current pulses (> 10^9 A/m^2 which may be generated for example using 2000 A radar thyristers) during externally imposed shortening and lengthening cycles we can change their properties. The altered NiTi now will both shorten and lengthen very rapidly as shown in Figure 3. The time course of this twitch response is shown in more detail in Figure 4. It is unclear to us why the relaxation time has changed so dramatically. It could be that the material properties have been altered in some way and/or that mechanical recoil via the NiTi stiffness is involved.

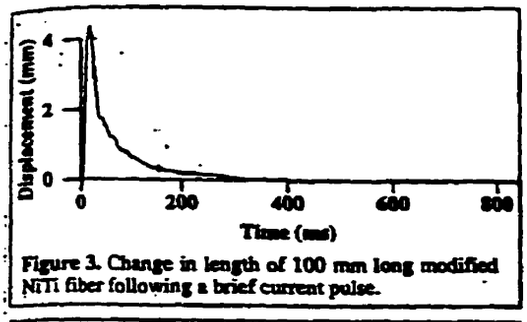

Figure 3. Change in length of 100 mm long modified NiTi fiber following a brief current pulse.

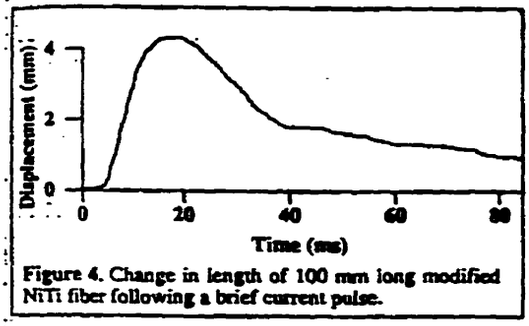

Figure 4. Change in length of 100 mm long modified NiTi fiber following a brief current pulse.

CHARACTERISTICS

We now present the result of experiments performed to characterize the mechanical properties of the modified NiTi fibers.

Force

When the modified NiTi fibers are subjected to a constant load (via the linear motor) they produce a peak force which if greater than the imposed load causes shortening. The difference between the peak force generated and the imposed load (i.e., incremental stress) is a function of the imposed load (i.e., applied stress) as shown in Figure 5. This figure also shows that the linear extrapolated force at which the load force equals the force generated (i.e., incremental force is zero) corresponds to a stress of 235 MN/m^2. For comparison the peak stress generated by human skeletal muscle is about 350 kN/m^2.

Power/Mass

The peak power/mass of these modified NiTi fibers is a function of externally imposed stress as shown in Figure 6. When loaded to a stress of 100 MN/m^2 the modified fibers produce a power/mass of nearly 50 kW/kg. For comparison the peak power/mass generated by human skeletal muscle is about 200 W/kg (about 50 W/kg sustained).

% Contraction

When heated with constant amplitude and duration current pulses the maximum shortening strain achieved by the modified fibers is a function of externally imposed stress as shown in Figure 7. Note that even with a load of 100 MN/m^2 the fibers shorten by over 1%.

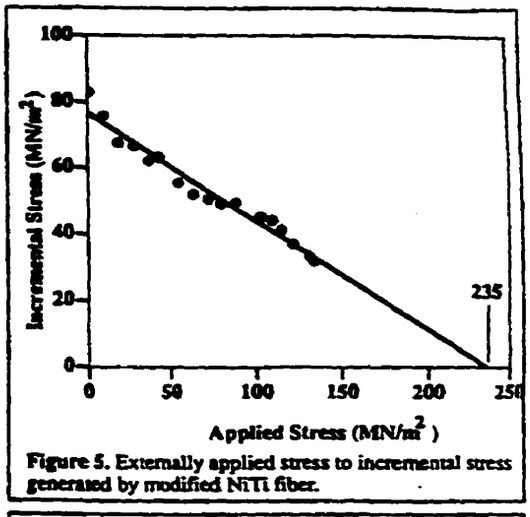

Figure 5. Externally applied stress to incremental stress generated by modified NiTi fiber.

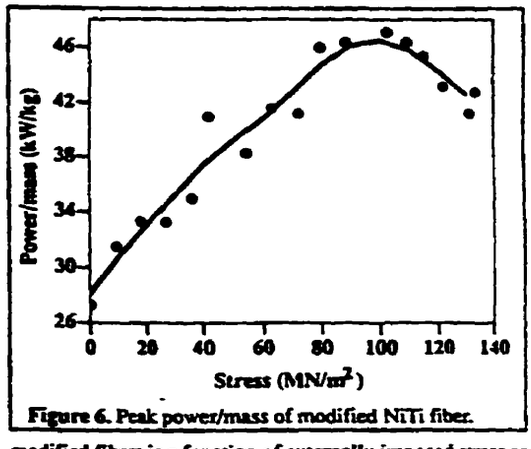

Figure 6. Peak power/mass of modified NiTi fiber.

Shortening Velocity

The strain rate (shortening velocity) is a monotonically decreasing function of load as shown in Figure 8. Note that at zero imposed load the strain rate is 3 s^{-1} and even with an imposed load of 100 MN/m^2 is still 1 s^{-1}.

Comparisons

Hence it now appears that NiTi can be made fast enough as a macro or micro actuator, with impressive force/mass and power/mass ratios. Figure 9 shows a comparison of the power/mass of nature's actuator muscle, modified NiTi and a range of aircraft internal combustion engines. The modified NiTi has a peak power/mass about 100 times greater than muscle. However the comparison does not take into consider-

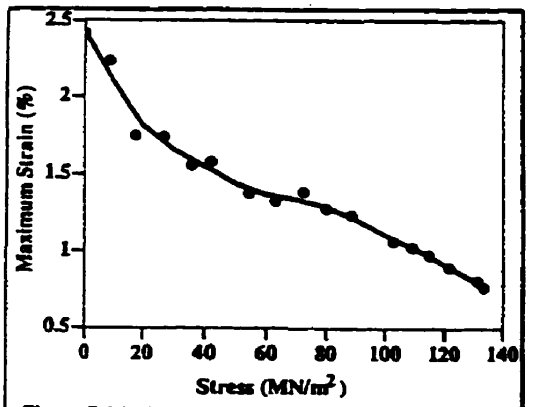

Figure 7. Maximum shortening (strain) of modified NiTi fiber as a function of externally applied stress.

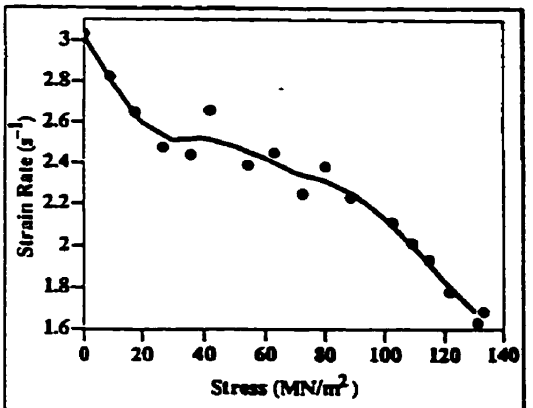

Figure 8. Peak shortening velocity (strain rate) of modified NiTi fiber as a function of stress generated.

ation the mass of the cooling system surrounding the NiTi fiber. When this is done both the peak stress generated and power/mass of muscle and modified NiTi are similar.

The Table shows a comparison of some properties of modified NiTi and muscle (human skeletal). It is important to remember that some of the values for the NiTi shown in the Table will be considerably less when the mass and volume of the cooling system is included.

NONLINEAR PROPERTIES AND CONTROL

The electromechanical properties of the NiTi fibers are dynamically nonlinear and time-varying [10]. For effective control of the fibers for fast movements we have found that it is necessary to characterize these properties experimentally using nonlinear time-varying system identification techniques. These techniques [6,7] also hold considerable promise for use in characterizing the properties of other micro-actuator technologies.

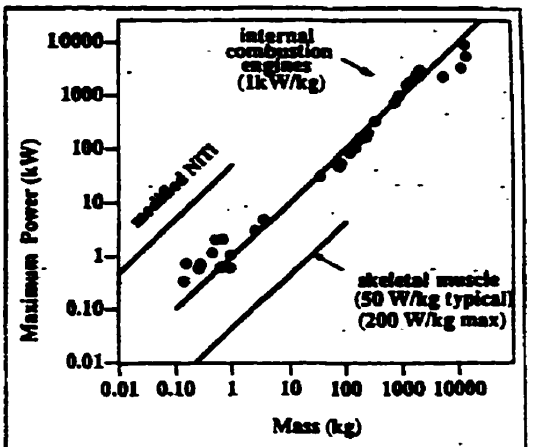

Figure 9. The peak powers produced by modified NiTi fibers, a range of aircraft internal combustion engines and human muscle.

Table: Comparison of Modified NiTi and Muscle

	NiTi	Muscle
Maximum tension (kN/m²)	>200,000	350
Maximum power/mass (W/kg)	>30,000	<500
Maximum strain rate (s⁻¹)	>3	<2
Typical max. displacement (%)	5	20
Power efficiency (%)	>1	>35

Various control schemes have been used to control NiTi fibers [8,9,10]. When forces larger than a single fiber can produce must be generated the NiTi fiber are arranged in parallel mechanically. When this is done we have found that a combination of pulse rate modulation and recruitment of fibers may be used to control force. This same scheme is used in nature in the neuromuscular control of whole muscle (muscle fiber bundles) force. Indeed for high bandwidth applications any single NiTi fiber should not be restimulated for a few hundred milliseconds to enable it to fully recover to its original state (see Figure 4 where it may be observed that the fiber rapidly lengthens only by about 2/3 and then for the remaining 1/3 recovers more slowly).

CONTRACTION OF FIBRE WOUND CYLINDER

We now consider a microactuator design which can make use of the properties of the modified NiTi fibers. We propose using small controlled length changes of the NiTi fibers to produce a large displacement, large force microactuator as follows. The NiTi fiber is wound around a cylindrical tube of length l, radius r and constant volume

$$V = \pi r^2 l \qquad (1)$$

as shown in Figure 10. If the pitch of the helix is p, one turn

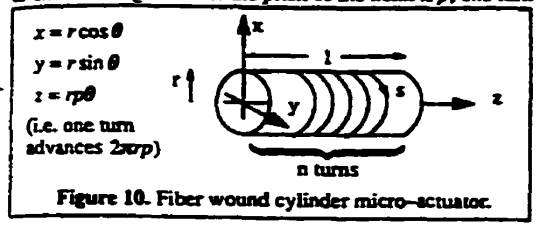

Figure 10. Fiber wound cylinder micro–actuator.

corresponds to an axial distance of $2\pi rp$, and the length for n turns is

$$l = rpn2\pi \tag{2}$$

The length of fibre in one turn is

$$s = \int_0^{2\pi} \sqrt{dx^2 + dy^2 + dz^2} = r\int_0^{2\pi} \sqrt{1+p^2}\,d\theta = 2\pi r\sqrt{1+p^2} \tag{3}$$

using the rectangular cartesian coordinates $x = r\cos\theta$, $y = r\sin\theta$ and $z = rp\theta$ shown in Figure 10.

From Equation 1, with V constant,

$$\frac{dl}{dr} = -\frac{2V}{\pi r^3} \tag{4}$$

and from Equations 1 and 2

$$p = \frac{V}{2\pi n^2 r^3} \tag{5}$$

The rate of change of cylinder length l with respect to radius r is

$$\frac{dl}{ds} = \frac{dl}{dr}\cdot\frac{dr}{ds} = -\frac{\frac{2V}{\pi r^3}}{\frac{ds}{dr}} \tag{6}$$

where, from Equations 2 and 3,

$$\frac{ds}{dr} = \frac{\delta s}{\delta r}\bigg|_p + \frac{\delta s}{\delta p}\bigg|_r \frac{dp}{dr} = 2\pi\sqrt{1+p^2} + \frac{2\pi rp}{\sqrt{1+p^2}}\cdot\frac{dp}{dr}$$

where $\frac{dp}{dr} = -\frac{3V}{2\pi n^2 r^4} = -\frac{3p}{r}$

gives

$$\frac{ds}{dr} = 2\pi\left[\sqrt{1+p^2} - \frac{3p^2}{\sqrt{1+p^2}}\right] = 2\pi\frac{1-2p^2}{\sqrt{1+p^2}}$$

and hence Equation 6 becomes

$$\frac{dl}{ds} = -\frac{2V}{\pi r^3}\cdot\frac{\sqrt{1+p^2}}{2\pi(1-2p^2)} = -2np\frac{\sqrt{1+p^2}}{1-2p^2} \tag{7}$$

This relationship is plotted in Figure 11, which shows the singular behavior occurring at $p = \frac{1}{\sqrt{2}}$.

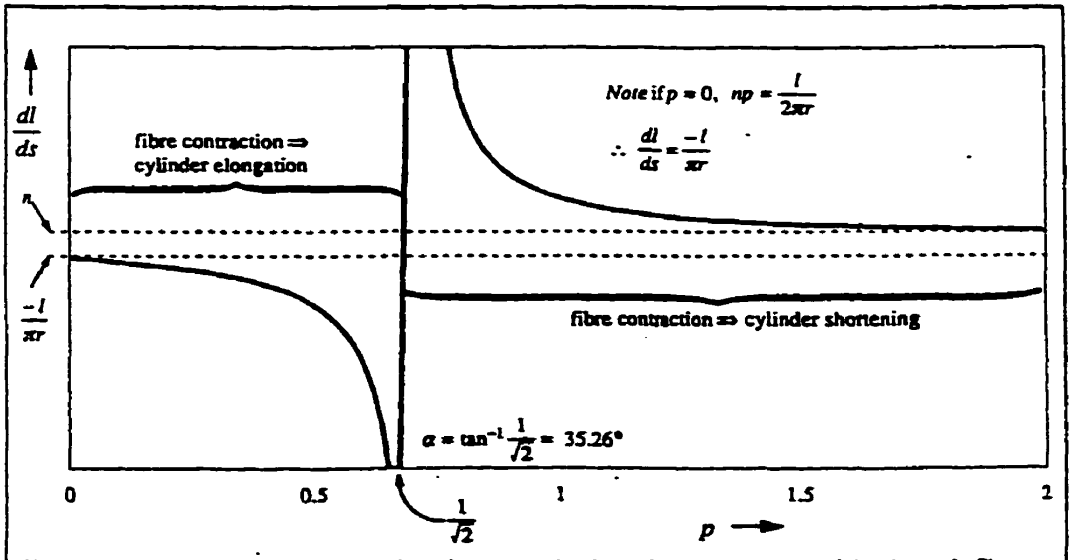

Figure 11. The effect of fibre pitch, p, on the ratio between the change in cylinder length and the change in fiber length (i.e., amplification factor).

For a given constant volume V, fiber-turn length s, and number of turns n, the radius, length and pitch of the cylinder can be calculated as follows: From Equations 1, 3 and 5

$$r^3 = \left(\frac{s}{2\pi\sqrt{1+p^2}}\right)^3 = \frac{V}{2n\pi^2 p}$$

gives

$$np s^3 = 4\pi(1+p^2)^{\frac{1}{2}}V \qquad (8)$$

Putting $p = \tan\alpha$, where α is the angle subtended by the tangent to the fiber in the circumferential direction, Equation 8 becomes

$$(1+p^2)^{\frac{1}{2}} = \sec^3\alpha$$

and Equation 8 becomes

$$ns^3 \tan\alpha = 4\pi\sec^3\alpha\ V \quad or \quad \sin\alpha\cos^2\alpha = \frac{4\pi V}{ns^3}$$

Now if we put $\sin\alpha = x$

$$x - x^3 = \frac{4\pi V}{ns^3}$$

or

$$x^3 - x + a = 0 \quad where\ a = \frac{4\pi V}{ns^3}$$

Solving this cubic equation for x yields the pitch p, for a given volume V and fiber length s. The cylinder radius and length then follow from Equations 2 and 3.

At $p = \frac{1}{\sqrt{2}}$, corresponding to the fiber making an angle $\alpha = \tan^{-1}p = 35.26°$ with the circumferential direction, the fiber length s, is a minimum and the rate of cylindrical length change with fiber length change is infinite (here we are considering kinematics only – of course the forces required to achieve this length change would be correspondingly large). When the pitch is less than this critical value contraction of the fiber causes the cylinder to lengthen and the pitch to increase. Similarly, for an initial pitch greater than the critical value, fiber contraction leads to cylinder contraction or fiber lengthening to cylinder lengthening. Thus, by suitably adjusting the shape of the cylinder and hence the initial pitch prior to controlled fiber contraction or lengthening, the cylinder length can be controlled with a desired mechanical amplification factor.

ACKNOWLEDGEMENTS

This work was partly supported by the Natural Sciences and Engineering Research Council of Canada (NSERC) through the Strategic Grant STR-0040872. Personal support for IWH was provided by a Canadian Institute for Advanced Research (CIAR)/ General Motors (GM) Fellowship and for JMH by an NSERC/CIAR Industrial Research Chair.

REFERENCES

[1] Bergamasco, M., Salsedo, F. and Dario, P. A linear SMA motor as direct-drive robotic actuator. Proc. IEEE Int. Conf. on Robotics and Automation, 1989, *1*, 618–623.

[2] Ikuta, K., Fujita, H., Ikeda, M. and Yamashita, S. Crystallographic analysis of TiNi shape memory alloy thin film for micro actuator. Proc. IEEE Micro Electro Mechanical Systems, Napa Valley, CA, Feb. 11–14, 1990, pp. 38–39.

[3] Busch, J.D. and Johnson, D.A. Prototype micro-valve actuator. Proc. IEEE Micro Electro Mechanical Systems, Napa Valley, CA, Feb. 11–14, 1990, pp. 40–41.

[4] Kuribayashi, K. Yoshitake, M. and Ogawa, S. Reversible SMA actuator for micron sized robot. Proc. IEEE Micro Electro Mechanical Systems, Napa Valley, CA, Feb. 11–14, 1990, pp. 217–221.

[5] Hunter, I.W., Lafontaine, S., Nielsen, P.M.F., Hunter, P.J. and Hollerbach, J.M. Manipulation and dynamic mechanical testing of microscopic objects using a tele-micro-robot system. IEEE Control Systems Magazine, 1990, *10*, 3–9.

[6] Korenberg, M.J. and Hunter, I.W. The identification of nonlinear biological systems: Wiener kernel approaches. Annals of Biomedical Engineering, 1990, *in press*.

[7] Korenberg, M.J. and Hunter, I.W. The identification of nonlinear biological systems: Volterra kernel approaches. Annals of Biomedical Engineering, 1990, in press.

[8] Homma, D., Miwa, Y., and Iguchi, N. Micro robots and micro mechanisms using shape memory alloy. 3rd Toyota Conf. Integrated Micro Motion Systems, Tokyo, Oct. 22–25, 1989, pp. 22–1 – 22–21.

[9] Ikuta, K. Micro/mimiature shape memory alloy actuator. Proc. IEEE Intl. Conf. Robotics and Automation, Cincinnati, May 13–18, 1990, pp. 2156–2161.

[10] Kuribayashi, K. A new actuator of a joint mechanism using TiNi alloy wire. Int. J. Robotics Research, 1986, *4*, 47–58.

TEMPERATURE DEPENDENCE OF NiTi FIBER IMPEDANCE

Serge Lafontaine, Kunbao Cai and Ian W. Hunter,
Biorobotics Laboratory, Department of Biomedical Engineering,
McGill University, Montréal, Québec, Canada H3A 2B4

INTRODUCTION

We (Hunter and Lafontaine) have recently developed a technique to produce NiTi shape–memory alloy fibers which are faster and more powerful than fast twitch skeletal muscle fibers. Some of the characteristics of these "artificial muscle" fibers have been reported in Hunter et al. (1,2). However much research needs to be undertaken before these fibers will be understood sufficiently to control them effectively. In this paper we examine the dependence of the electrical impedance of these fibers on temperature. The original goal of this work was to find a method to control the length and force of these fibers under dynamic conditions using electrical impedance as a state variable. The motivation comes from previous studies in which the resistance change of NiTi fibers has been measured during the reversible martinsite to austenite metallic transformation which occurs with temperature change. A companion paper explores the change in stiffness of these NiTi fibers over the same temperature range(3).

APPARATUS AND PROCEDURE

Our original NiTi testing apparatus used a linear actuator having a rather limited peak continuous force generation capacity. We have recently rebuilt this apparatus using a much more powerful linear electromagnetic actuator (Brüel and Kjær, model 4808) with a 187 N continuous force capability. This actuator is driven by custom built dual 2000 W water–cooled low–noise (class A/B) power amplifiers (100 kHz bandwidth). Movement of the actuator is measured by an inductive displacement transducer (Data Instruments, Fastar FS380) which has a flat frequency response to 15 kHz. The strain gage force transducer (Omega Engineering, Inc. LCC200 shear beam type) and associated amplifier has a similar frequency response. Static changes in the length of the NiTi fibers are made via the digital micrometer (Mitutoyo, 1 μm increment). The NiTi fiber resistance is measured by an 8.5 digit multimeter (HP 3458A) and its impedance over a 100 Hz to 15 MHz range by an impedance analyzer (HP4194). Both resistance and impedance are measured using the standard four wire (Kelvin) technique.

The NiTi is bathed in a 50% methanol–water mix which is pumped through a 1200 W refrigeration unit (Polyscience, model KR–60A). The temperature of the methanol immediately adjacent to the NiTi fiber is measured with a semiconductor temperature transducer (LM35) with a linearity better than 0.3 °C. The temperature of the NiTi bath is controlled over a –10 to 70 °C range by a variable voltage heater (peak 3000 W) in series with the refrigeration unit. The apparatus is controlled by an IBM RISC System/6000–320 workstation running an early version of Fortran90. The various instruments are controlled via an IEEE488 bus connected to the computer. Impedance frequency response functions were taken every 2 °C temperature increment and the resistance every 1 °C.

RESULTS

Figure 1 shows the impedance frequency response (magnitude only) function obtained at 20 °C. Notice that the impedance is flat to about 300 kHz above which it abruptly increases. Figure 2 shows the impedance at DC (i.e., resistance) plotted as a function of temperature. For the dimensions of the NiTi fiber used here (177 mm long, 0.8 mm diameter) a resistance of 0.36 Ω corresponds to a resistivity of 1 μΩ·m. We find that changes in impedance with temperature below 300 kHz closely follow changes in resistance.

CONCLUSIONS

We have made the first detailed measurements of NiTi impedance as a function of frequency and temperature and observed that the impedance does not differ markedly from the resistance up to a few hundred kHz. Impedance measurements should therefore reflect as well changes in the martensite to austenite transformation as DC measurements. It has been suggested (4) that there is a one–to–one correspondence between resistance and transformation ratio from a martensite to austenite phase, and that resistance can be used as

a state variable in NiTi actuator control. The change in resistance reported by others (e.g., 4) is typically in the order of 15–30% for NiTi wire wound in the shape of a coil spring. Unlike taught wires (as used here), coil springs are free to change dimension during temperature changes. If the cross-sectional area and length of a material are free to change with temperature (via thermal expansion or otherwise), the measured resistance will be found to change even when the material has a constant resistivity. The change in resistance observed here should reflect more closely the change in resistivity of NiTi than most other measurements.

In an actuator where the NiTi fiber is submitted to stresses, like those caused by external loads and disturbances, stress induced martensitic transformations occur. The resistance of NiTi is a function of resistivity, dimensions, temperature and the transformation ratio of martensite to austenite phases (5). The reason why the resistance change reported here is smaller is probably due to stress induce martensitic transformation and also because of more tightly controlled dimensions. It may be that the resistivity, even in loosely constrained fibers, may not change as much as the resistance. In order to better understand these results and to gather a more informative set of measurements for control purposes we are currently performing experiments to measure the impedance as a function of temperature at different levels of stresses, and also measure the impedance as a function of stress at different temperatures, measuring continuously dimensional changes.

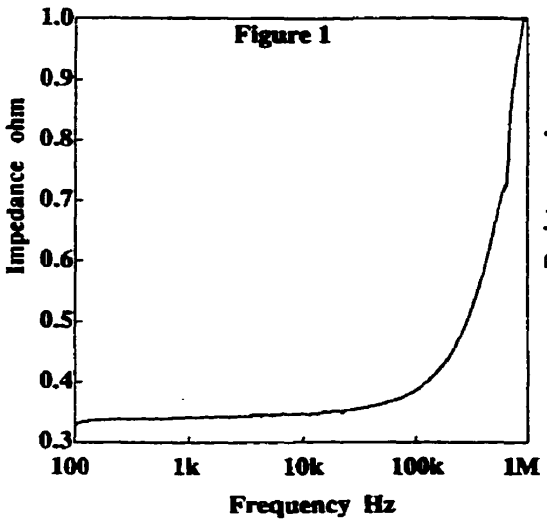

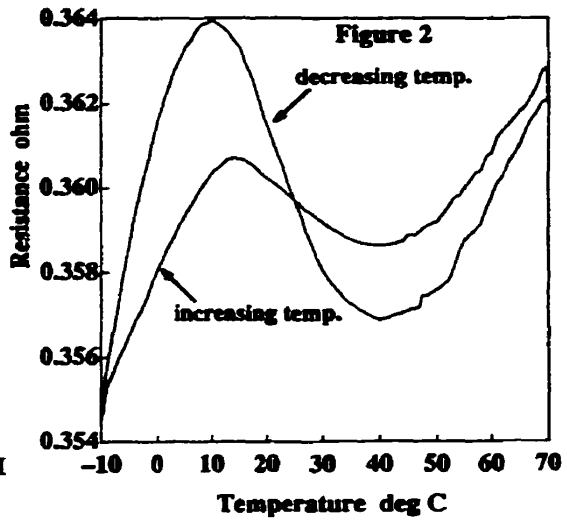

Acknowledgements

This work was supported by the Canadian Natural Sciences and Engineering Research Council (NSERC), the Medical Research Council (MRC) of Canada, and the Institute for Robotics and Intelligent Systems (IRIS) a Canadian Network of Centres of Excellence.

References

(1) Hunter, I.W., Lafontaine, S., Hollerbach, J.M. and Hunter, P.J. Fast reversible NiTi fibers for use in microrobotics. *Proceedings IEEE Micro Electro Mechanical Systems*, 1991, 2, 166–170.

(2) Hunter, I.W., Lafontaine, S. and Hollerbach, J.M. Artificial muscle prototype for use in robotic and prosthetic limbs. *Proceedings of the 16th Canadian Medical and Biological Engineering Conference*, 1990, 16, 35–36.

(3) Rohling, R.N., Lafontaine, S., Hunter, I.W. and Hollerbach, J.M. Changes in NiTi fiber stiffness with temperature. *Proceedings of the 18th Canadian Medical and Biological Engineering Conference*, 1992, submitted.

(4) Ikuta K. Micro/miniature shape memory alloy actuator, *Proceedings of the IEEE International Conference on Robotics & Automation*, 1990, 2156–2161.

(5) Funakubo H. (ed.), *Shape Memory Alloys*, Gordon and Breach Science Publishers, 1987.

Chapter 5 An Application: A Rotary SMA Motor

Currently the electric motor is the major alternative being developed to replace the internal combustion engine in automobiles. Internal combustion engines have power/mass ratios in the order of 1 kW/kg and utilize the 43 MJ/kg energy density of gasoline with about 35% efficiency at the crankshaft, or 25% efficiency at the driving wheels. Thus, the effective energy density of gasoline engines is about 10 MJ/kg. By comparison, high-revving electric motors can be over 90% efficient, but generate considerably less power/mass and typically draw on low energy density battery technology, e.g. lead-acid at 0.15 MJ/kg. We have developed powerful novel contractile-fiber technologies; they could potentially lead to a superior alternative to the use of electric motors for automotive propulsion.

As discussed in earlier chapters, this contractile fiber technology is an electrically-activated, shape-memory, contractile alloy actuator, which generates over 235 MN/m^2, and contracts by up to 8% of its rest length. We have measured power/mass ratios exceeding 100 kW/kg and have developed a demonstration rotary motor that spins at more than 15 revolutions per second (i.e. 900 RPM). Unlike an internal combustion engine and a high-revving electric motor, our shape-memory alloy rotary motor generates peak torque at 0 revs, and can accelerate very quickly. Furthermore, the torque/mass ratio of this motor is orders of magnitude higher than that of a direct-drive electric motor.

Indeed, the motor is sufficiently small and light to be mounted *inside* the wheels of a vehicle. With all four wheels so-equipped, traction control, variable four-wheel drive, independent wheel-speed control, etc. become largely software control issues. With this engine-in-the-wheel approach, engine replacement could be as simple as changing the wheel. Unfortunately, the efficiencies of these shape-memory alloy motors is currently low, which in part motivates development of an alternative contractile material fabricated from conducting polymers and new types of shape memory alloys. The results of this materials research will not be conclusive for at least 2 to 3 years (Madden *et al.*, 1996). In the meantime, the memory-alloy offers the potential to at least match the efficiencies of the gas combustion engine. In other words, while the efficiencies of NiTi actuators are not yet high enough to justify application in an autonomous vehicle, there are two principal reasons for pursuing this research. (1) The feasibility of the concept is demonstrated, allowing future versions to incorporate higher efficiency fiber actuators (either improved efficiency NiTi fibers, or conducting polymer actuators), and improved battery technology (e.g. Li polyaniline batteries having 10 times the energy density of lead acid batteries). (2) There are a number of non-autonomous or non-continuously running applications where the high torque to mass and high power to mass of the NiTi actuators are beneficial and where efficiency is not critical. Some of the latter are mentioned below under automotive applications.

In this project we have developed an early prototype of a NiTi rotary engine which could be used to study issues such geometric design and control strategies common to the new wheel design, regardless of the selected contractile material. Knowledge of the contractile impulse response should be sufficient to adapt the new

wheel to various actuator-fiber materials.

Plate 5.1 shows our first early prototype of a rotary engine. It used only one NiTi fiber to activate a water wheel. We have observed rates as high as 20 RPM with this wheel. Given that there was only one fiber it had to be started manually. A Hall effect sensor detected the position of the wheel which then triggered at the right moment either a HEXFET or IGBT to send a current pulse to the fiber.

A second prototype was subsequently built. This prototype, with 8 dual fibers can self-start and is described in this chapter.

5.1 Automotive Applications

Besides replacing combustion engines there are a number of other applications of shape memory alloys in cars. In a modern car there are more than 100 actuators used to control the engine, the transmission, suspension, seats, and windshield wipers. Shape memory alloy actuators been considered for a number of thermal control and management systems, including the radiator shutter, fan clutch, climate control, engine radiator control and brake ventilation. Table 5.2 lists the main thermal actuators in a car that could be controlled with shape memory alloys.

Doors in an automobile for example are extremely difficult to manufacture because of the large number of motors and amount of electrical cabling that must be included. They include actuators for lifting the windows, moving the external mirror and locking the doors. Shape memory actuators would offer the benefit of actuation in a very small space and hence greatly facilitate the design of cars.

Another potential application involves the safety belt. The main reason why people die from a car accident is the sudden deceleration of the body. The heart is not firmly attached inside the torso and the seat belt always has a certain amount of slack. In the case of a collision it therefore takes some time before the body is decelerated by the safety belt. When the torso hits the safety belt and after the belt is locked, enormous forces stop the body. The heart is already in motion and is only retained by arteries and blood vessels that can rip apart under the tremendous forces required to decelerate the heart. Shape memory alloy fibers could pretension the safety belt very quickly in case of impact and save many lives.

Other applications include adjusting body seats to conform to the driver's morphology. There are over 6 actuators right now in a car seat. Shape memory alloys could allow many more degrees of freedom. Another important application is windshield wipers. Current motors are large, bulky and consume large currents. Shape memory alloys could also serve in highly efficient windshield washer fluid pump.

5.2 Rotary Motor for Car Engines

The main application considered here is for in-wheel rotary motors. There is currently no research on completely new design technologies for automotive engines. Most car manufacturers work on electric vehicles. Electric motors have been in existence for a long time and most of the new vehicles will consist of hybrid vehicles where a standard gas engine or Sterling engine will activate an electric generator that will in turn power a central electric motor. A large amount of research also goes into improving

existing combustion engines from incremental improvements such as actuating each piston valve independently with electric actuators for example.

What we advocate however is that research should be done on completely different rotary motor technologies for cars. One such design is a rotary motor with synthetic muscle actuators inside the wheel. The artificial muscle actuators would be fixed at one end to a crankshaft and at the other end fixed circularly around the shaft. The shaft would then power the wheel. The ideal design would also include the control electronics right inside the wheels. IGBT's can switch extremely large currents in a very small space and power to the wheel could be transmitted inductively above 100 kHz for a totally wireless assembly.

We already referred in Chapter 2 to heat engines that ran rotary motors from NiTi shape memory alloy fibers or springs (Funakubo, 1987; Duerig *et al.*, 1990; Gilbertson, 1994). Banks designed a sun-powered motor that used an offset crank engine and ran for millions of cycles at 1 Hz (Zmuda, 1974). Other rotary engines mentioned by Funakubo (1987) include Johnson's thermal engine that was scalable and was based on the Chinese differential pulley. A small version of this was commercialized as the TiNi-1 generated 1 watt of power. McDonnell Douglas developed a 32 W engine based on one hundred 50 μm diameter fibers. The rotative Banks engine developed by Glasauer and Müller (1996) based on NiTi fibers produced a torque of 15 N·m and revolved at 20 RPM.

NiTi rotary engines with offset cranks have been designed previously (Funakubo, 1987). Ginel's offset crank engine that used coiled NiTi springs was extremely limited in the torque that could be produced. A reciprocal offset crank engine has also been designed based again on coiled-springs. The main disadvantage of this design is that

fibers are arranged inline like pistons and activate individually a different segment of the crankshaft. The only rotary motors that have been designed that were not thermal engines were the "Kick" engine and the "Stepping" Engine (Funakubo, 1987) which also made use of coiled springs. Gabriel *et al.* (1988) developed a micro-rotary engine where a twisted fiber rotated by changing the state of the shape memory alloy. This motor is not easily scalable nor can it turn continuously in the same direction.

Wiper pressure control	Foglamp Louver
Seat-belt adjustment	Engine hood lock
Shock absorbers	Retractable head-light
Trunk Lock	Fuel management
Suspension Adjustment	Engine control
Central locking system	Transmission control
Filler inlet lock	Climate control
Windshield Wipers	Rear-view mirror adjustment
Wheel lateral control	

Table 5.1 List of possible applications of shape memory alloy actuators in a car.

The limitations of shape memory alloys as actuators have been discussed in Chapter Two. Large improvements in material properties and or battery technology need to be made before considering seriously NiTi as a viable technology for car engines. NiTi is however only one artificial muscle technology. There are projects on alternate

materials, and recently rapid advances have been made on conducting polymer actuators (Madden *et al*, 1996). One of the most promising classes of materials is electrically conducting polymers. In the meantime, knowing that better technology is on the horizon, research can be done on new designs, control strategies and applications.

5.3 Requirements

There are a number of requirements for the design of a car engine. Some useful general guidelines are listed below.

5.3.1 Peak torque and acceleration.

The peak torque to be generated at the wheel should be approximately 450 N·m. Given four wheels and a wheel radius of 375 mm, the total force at the wheels should be 4800 N. Assuming a nominal weight of 1000 kg (the typical weight of an electric vehicle (EV) without the power train), the peak acceleration should be about 0.5 g. Cars are normally designed to provide an acceleration of 0.5 g for 0.5 s (personal communication from GM engineers). A sports car such as the Corvette can accelerate at 0.7 g for 0.8 s.

5.3.2 Lifetime

Current combustion engines have an extremely long useful life, exceeding several hundred thousand kilometers for a car and over 720×10^6 cycles assuming an average speed of 50 km/h and 3000 RPM. This greatly exceeds the capability of shape memory alloys. However the cost of shape memory alloy is quite low. The motors could be designed to have a number of redundant fibers in case of breakage. Furthermore the wheels could be designed to be replaced like tires and serviced at regular intervals, like

10,000 km, or roughly 5,000,000 cycles. By cycling fibers once every tenth tire rotation, such performance could be achieved. Note that the fiber redundancy will not cause a mass problem – the power to mass is so large that the motor itself is a negligible portion of the mass.

5.3.3 Active braking

All of the new electric vehicles will use active braking and convert kinetic energy back into electric energy when the driver brakes. Approximately 25% of the car

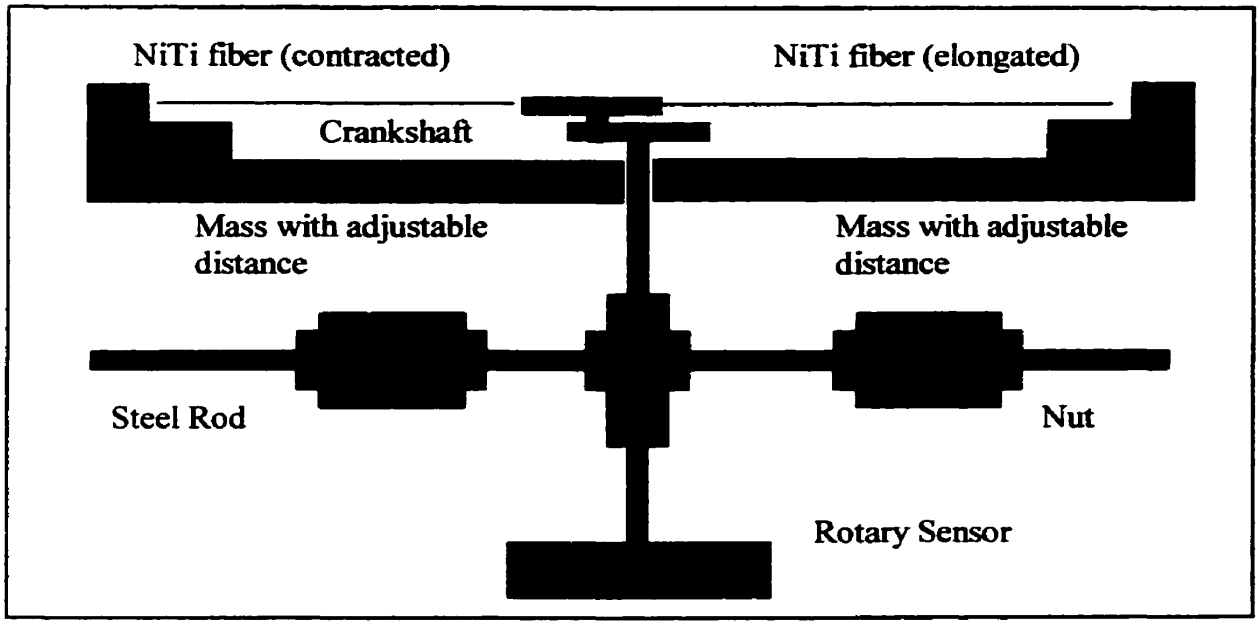

Figure 5.1 Diagram of the R8 motor flywheel.

inefficiencies when driving in traffic arise from constantly accelerating and decelerating a car. It is not currently possible to use shape memory materials to convert mechanical energy into electrical energy. However this will be possible for conducting polymer actuators.

It is possible to use active braking with NiTi motors and achieve very high

deceleration rates. Furthermore the braking could be closed-loop as in ABS brakes.

5.4 Experimental Setup

The experimental setup is shown in Plates 5.3 and 5.4. It consists of an R8 engine. There are 8 pairs of fibers arranged circularly as can be seen in Plate 5.2. They all extend from the periphery where they have individual connections to electronic power switches (HEXFETs). At the other end they are all connected to a crank (Plate 5.2). The fibers are electrically connected to the crankshaft where they receive electrical power from a common source. The motor is designed to work horizontally and the fibers are kept in water for rapid cooling. On the bottom side of the motor there is a flywheel with a variable moment of inertia to regulate the motion of the fibers.

A Pentium Pro computer running Windows NT controlled the system. The National Instruments PCI-MIO-16XE digital I/O port was used to control the motor. Each port was individually connected to a HEXFET that switched the voltage to the motor. The control was done closed loop and the position of the wheel was acquired from a potentiometer with output between 0 and 5 V over 360 ° of motion.

Plate 5.1 First Rotary NiTi motor. This flywheel ran from a single NiTi fiber at up to 1200 RPM.

Inertia of Flywheel	0.004 kg-m^2
Flywheel steel rod length	0.25 m
Flywheel steel rod diameter	7.8 mm
External Weights	Hex Al sections, 25.5 mm OD, 20.4 mm in length
Nuts: hexagonal	Steel OD=13 mm, ID=6.7 mm, L=6.34 mm
Center connecting piece	Al Hexagonal rod OD= 21.7 mm, L= 36.8 mm
Crankshaft eccentricity	5 mm (adjustable to 4,5,6 mm)
Fiber electrical resistance	4.8 Ω (2 in parallel for 2.4 Ω)
Fiber length	215 mm
Peak force per NiTi fiber pair	20 N
NiTi fiber diameter	250 μm
Peak Torque (per pair of fibers)	0.1 Nm
Distance of weights in tests	65 mm
Operating Voltage	24 to 48 V

Table 5.2 Characteristics of R8 NiTi motor

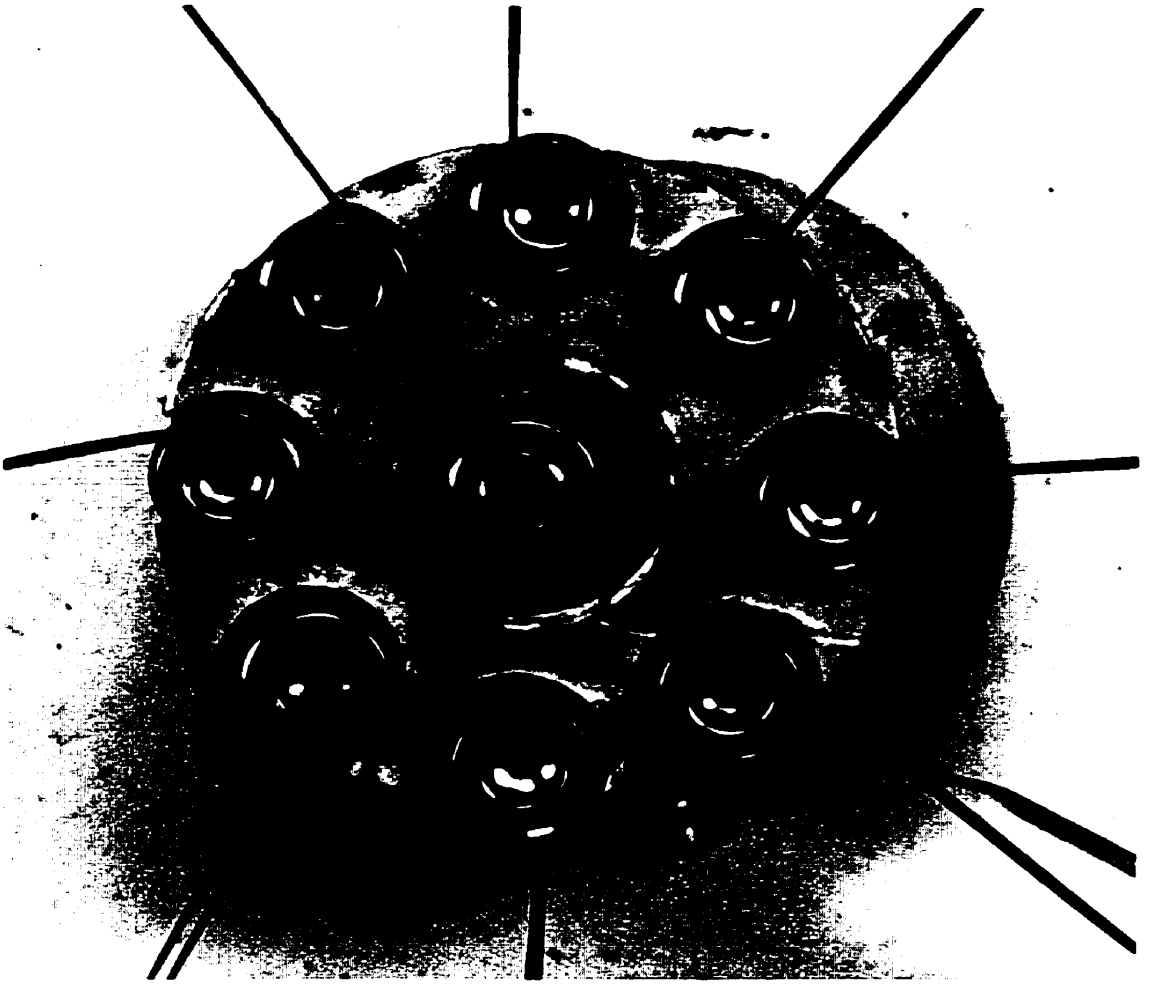

Plate 5.2 Crankshaft of the R8 engine. The eight fibers terminate on the crankshaft mounted eccentrically on the main shaft. They are all electrically connected to a common electrical power source.

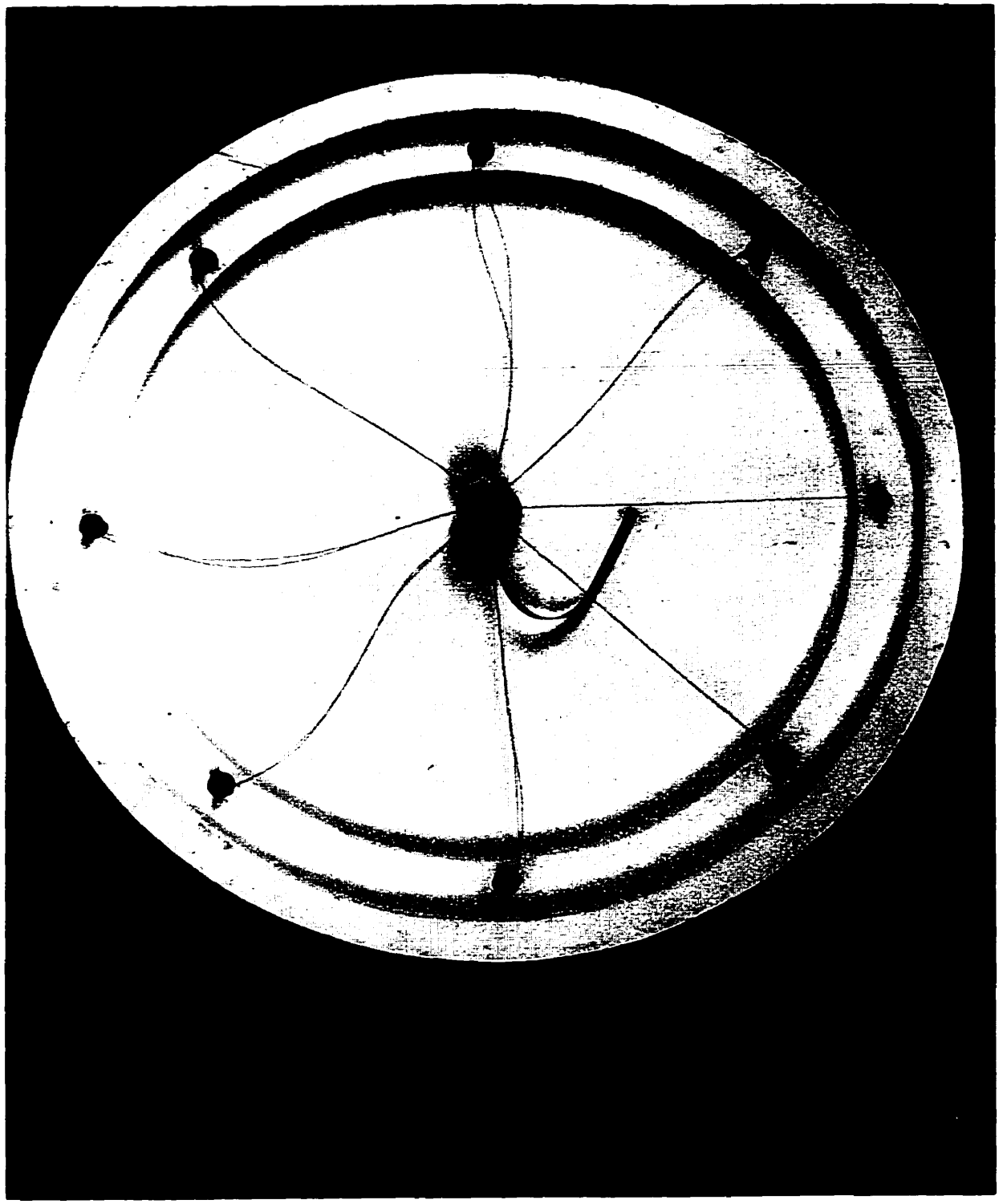

Plate 5.3 R8 NiTi prototype rotary motor.

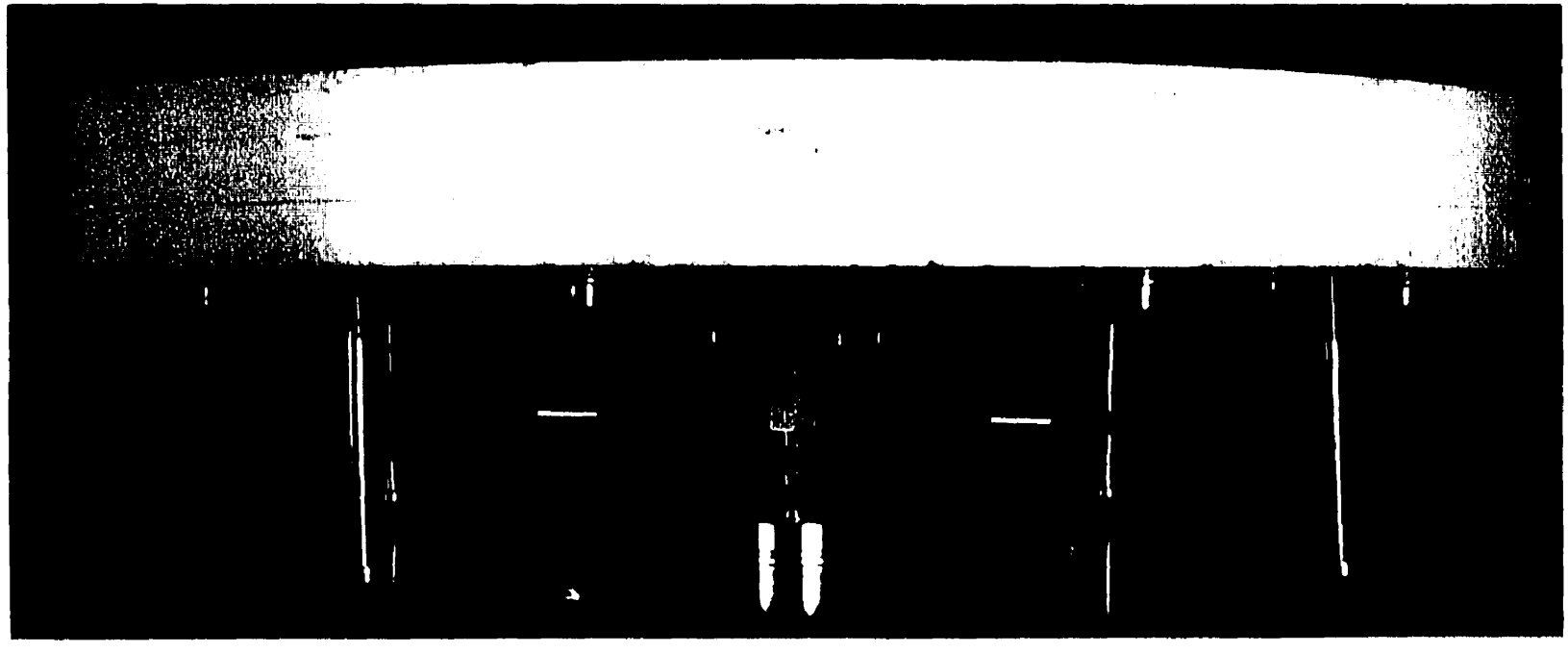

Plate 5.4 NiTi rotary motor bottom view of the adjustable flywheel.

5.5 Results

The resulting motor characteristics are shown in Figures 5.2, 5.3 and 5.4, and Table 5.2 outlines the motor's physical properties. The peak acceleration recorded was 4 revs/s^2 which corresponds to 0.96 g if the wheel had been moving and the radius of wheel from the axle to the ground was 750 mm. The peak speed that was achieved was 6.5 rotations/s, which corresponds to 55 km/h under similar assumptions. The efficiency recorded however was very low, in the order of 0.27%. This can be explained partly by friction in the mechanism. What further contributes to the inefficiencies is that one way shape memory alloy fibers are used, which had to be stretched passively after their contraction. Also, even if we recorded theoretical efficiencies of 3% observed in pulse experiments, there are always losses in the transmission of that power.

The next step in the rotary motor development will be to construct an R128 shape memory alloy rotary actuator, with 128 fibers, integrated IGBT's and sensors.

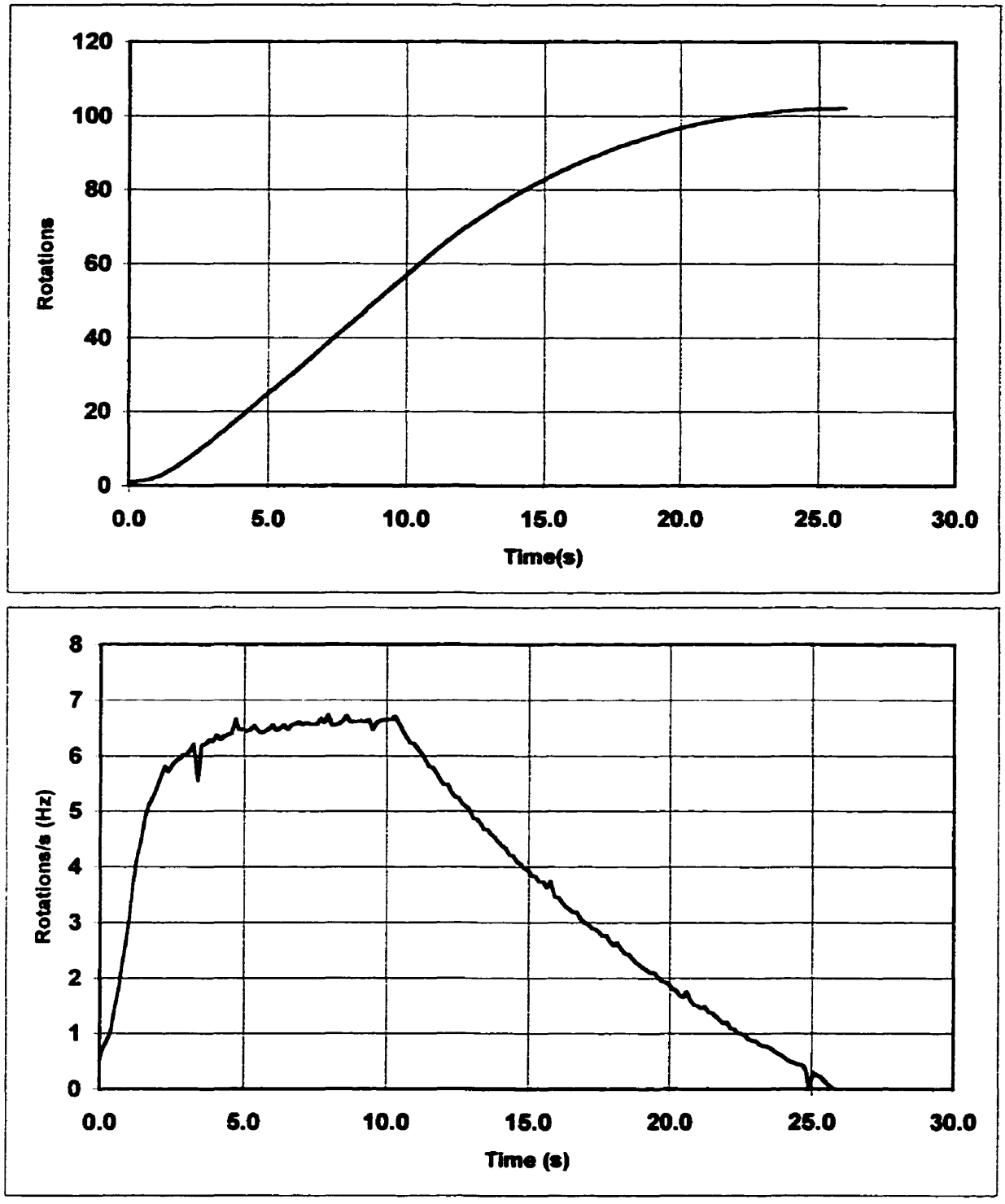

Figure 5.2 Position signal (A) at the top and speed (B) at the bottom achieved by the R8 motor. The peak velocity was 6.7 rotations per second.

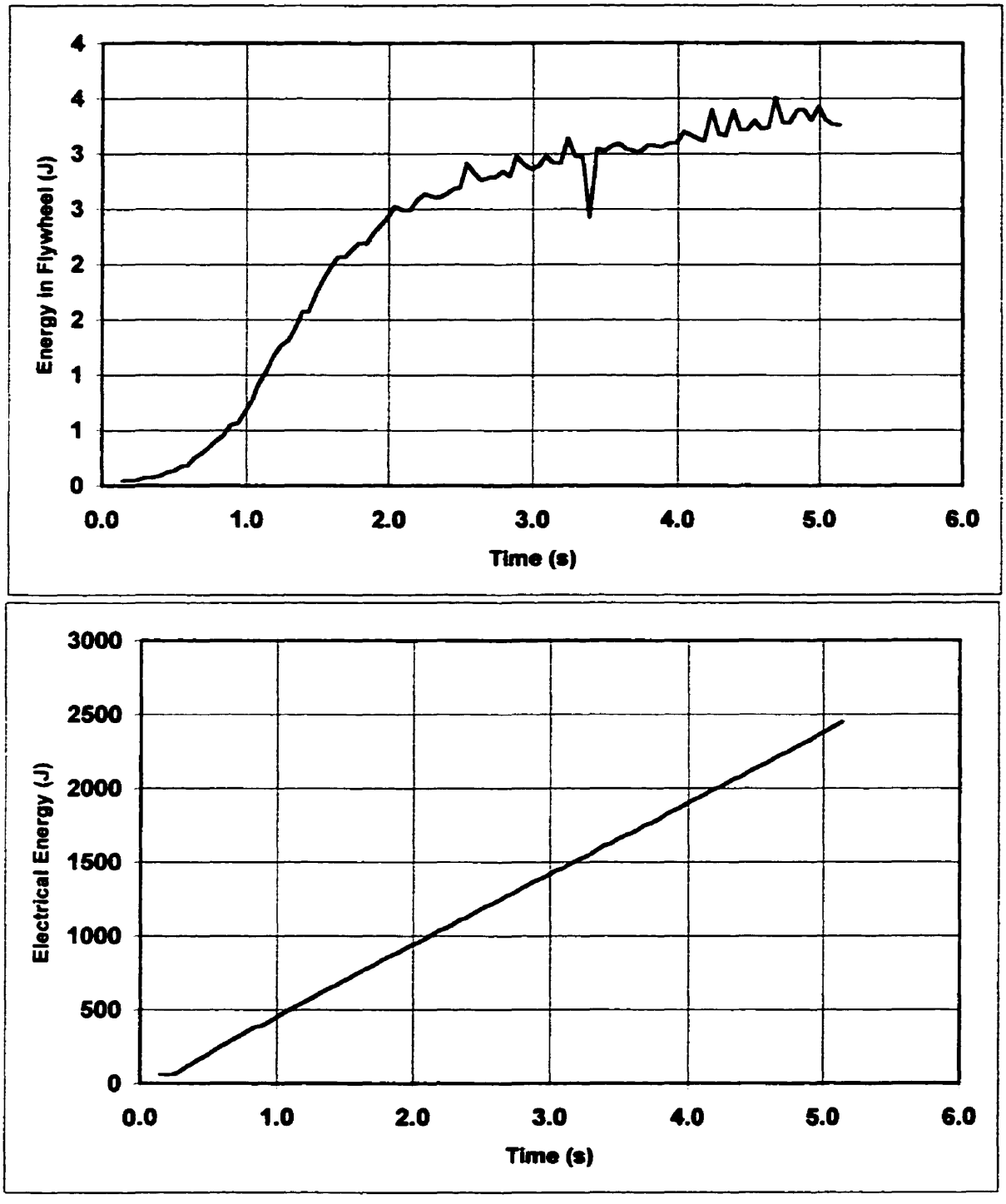

Figure 5.3 The top diagram (A) gives the total energy in the flywheel with time. The bottom curve indicates the total amount of electrical work delivered to the motor as a function of time.

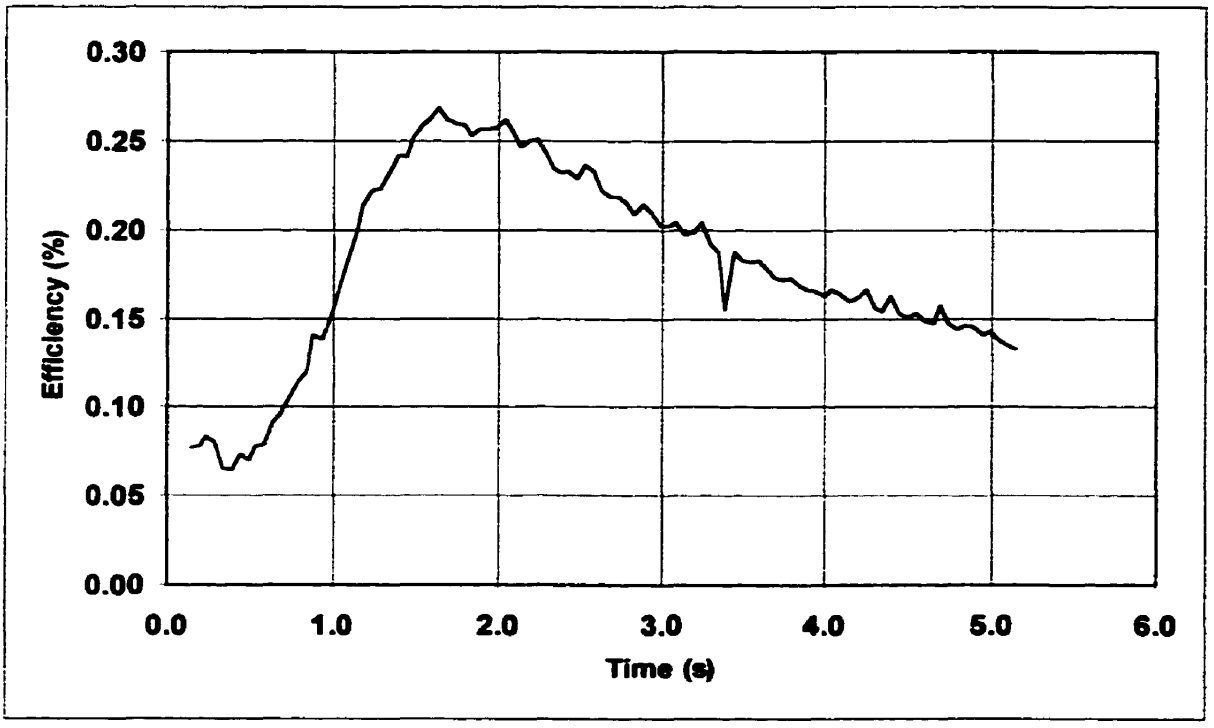

Figure 5.4 Efficiency achieved at the beginning of the acceleration. Initially most of the energy goes into the flywheel. As speed is gained most of the electrical energy goes into friction and the efficiency drops.

5.6 Conclusions

We have built a new rotary motor. This motor will not be used in the near future in cars. However it is a prototype that can be used to make further tests on control algorithms and to look at methods for improving the geometry of future engines. It was computer controlled and hence speed, acceleration and braking all become software control issues. This type of motor is self-starting which is a large advantage over the combustion engine. .

Chapter 6 Conclusions and Future Work

I have in the previous chapters described some advances towards the development of a synthetic muscle. Much remains to be done however. It was not possible within the time limits to actually build a synthetic muscle with a large number of fibers, with individual control, having tendons, thermal, strain and force sensors all of the same material. The building blocks are in place for the future. In this chapter areas of future research will be discussed first then the original contributions will be stated.

6.1 Areas of Future Research

The ultimate goal of synthetic muscle technology is to imitate muscle by building larger actuators from many smaller (ultimately nano-scale) devices. The actuator considered in this thesis contracts from changes in bulk material properties, which limits its contractions to approximately 8% of its total length (strain). A second limitation of the NiTi synthetic muscles is the total lifetime in terms of contractions that can be obtained before degradation of their response is shortest for large contractions. This is a serious limitation for many applications but a micro-stepping actuator (like muscle) could potentially move over much longer strains, and this could be achieved without impairing

their useable lifetime.

Compared with other actuators (e.g. combustion engine) shape memory alloys were discovered only recently (Chang and Read,1951). They are complex materials and much remains to be done to properly understand them. New types of shape memory alloys have been discovered, such as amorphous forms of shape memory alloys (Shi, J.D. *et al.*, 1996) and shape memory alloys activated electro-magnetically (Ullako *et al.*, 1997). From a materials science viewpoint, control, modeling, optimal control purposes are all areas that will require more investigation.

More directly related to the research reported in this thesis, further work is required to understand the mechanism of fast contraction in the fibers that I co-developed. Time-resolved X-ray diffraction would enable changes in the crystal structure to be followed as the NiTi is modified and would enable a better understanding of the contraction mechanism Other measurements, such as differential scanning calorimetry, additional resistivity measurements, and optical and electron microscopy would be required to further elucidate the phenomena.

Several new areas of research are suggested by this thesis. Some results strongly suggest slow dynamics in martensitic transformations. These are extremely relevant from a control and modeling viewpoint as they may affect the stability of closed-loop systems. Although there is a strong indication that they exist, as they should be expected from a material that shows primary phase transformations, more experiments should be performed to confirm that these are not artifacts and the result of spontaneous nucleation from energy liberated from the latent heat. This could be revealed by thermal imaging of the fibers inside the water.

Further work will be required to complete a mathematical model for control purposes. This model will need to incorporate all of the major phenomena that are part of the shape memory effect, such as friction of interfaces, the thermodynamics of the hysteresis, heat latencies, heat transfer, intermediate transformations, etc.

The R8 NiTi rotary engine has been developed to investigate the geometry, control and eventual performance of this class of motor. The R8 engine developed in this thesis has been done in order to develop a tool for further research and it was not the immediate objective to fully characterize it. The performance under varying voltages, pulse width, and pulse sequence strategies should be investigated. Optimization could be done after a proper control model has been fully developed. The immediate next step (currently underway) will be to build a R128 engine, with more fibers, integrated power electronics, sensors and control system. This new rotary motor will include also redundant fibers and will used to test different control algorithms.

Finally one of the most exciting research area for the future is that of conducting polymers. Out of this single class of materials it is possible to co-fabricate all of the basic elements required for synthetic actuators and synthetic life forms. These include actuators, high quantum efficiency light sensors, gas detectors, position sensors, force sensors, very high energy rechargeable batteries, super-capacitors, transistors (chemfets), light emitting diodes, wires with very low resistivity in one direction and insulating in the others, electrochromic windows, electro-magnetic shielding and memory elements.

It will therefore be possible to fabricate all of the building elements of artificial life forms, including synthetic muscles, nerves, neurons, spindles (length sensors), Golgi tendon organs (force sensors), for chemical energy storage (like ATP), artificial eyes and

retina, artificial ears, artificial bones as structural elements, tendons, skin, arteries. Actuators surpassing a frequency response of 10 Hz have been reported (Madden *et al.*, 1997). These actuators do not have the same theoretical low efficiency limitations or limited lifetime as NiTi fibers. Conducting polymers will be one of the most exciting research areas in the years to come.

6.2 Micro-actuators and their Control.

6.2.1 R-phase based micro-actuators.

Muscle like actuators with enough artificial muscle fibers should be as accurate in motion as human fingers. However technology has to be improved before we will be able to build synthetic muscles with a large population of fibers that can be controlled either individually or in small groups as they are in muscles.

There is another large range of applications where NiTi fibers could be used individually, in pairs or in small numbers if each one of them could be operated in a continuous precise manner. One of the great difficulties encountered in this type of application is that martensitic transformations are first order phase transformations. Properties change discontinuously during the phase transition and there is a large hysteresis in temperature at which the transitions occur. Most existing control strategies fail in this situation.

There is however the intermediate R-phase transition that is a second-order phase transformation with almost no hysteresis. It is therefore possible to accurately control NiTi fibers in a graded manner using the R-phase transition. There are limitations to

these applications because the range of motion that can be achieved from the R-phase is only 0.5% to 1%. Maximum forces are also smaller. However, for in micro-robotics or microsurgery large motions are not required. A 100 mm long fiber concealed in a scalpel could provide motion over 500 μm. This is enough to remove tremor from a surgeon's hand, to manipulate individual cells or to assemble structures at the micrometer level.

6.2.2 Stochastic control.

There are a number of problems that occur in digital control when high accuracy is required. Numerical instability often occurs because of ill-conditioned numerical procedures. A major source of inaccuracies in traditional approaches of the systems theory literature arises from fitting discrete-time models to sampled data (Pintelon and Kollar, 1991). At high sampling rates the design of accurate digital controllers also becomes increasingly difficult. As sampling rates increase, all the poles of difference equations tend to unity. When the poles differ by a value that is too small to be represented accurately by the computer's numerical precision, the difference equation no longer represents the continuous time system and the system can no longer be identified accurately. Furthermore as the sampling rate increases the number of floating point operations also increases and numerical roundoff errors accumulate. This is particularly the case for many real-time controllers based on embedded digital signal processors, which currently support only single-precision, or in rare cases extended precision (40 bits).

High sampling rates, typically 5 kHz and above, are used in digital controllers for most of our control systems. At lower sampling rates, transients caused by discrete changes in the control signals can be perceived by the human operator either as a

vibration, a sound (due to mechanical vibrations) or jumps in the trajectory. Lower control rates can also limit system stability due to additional delays introduced in feedback loops.

In a preliminary study of this problem, it was shown that numerical instability is not inherent, and that it can be eliminated using continuous-time models (Gerencsér *et al*, 1994; Gerencser and Rissanen, 1986). However the full potential of continuous-time modeling is still to be explored. The diversity of the literature indicates that continuous-time identification remains a challenge.

The superiority of continuous-time models over discrete-time models can be restated as the superiority of one parameterization over another one. Parameterization issues in connection with system identification have been studied for a long time. An attractive parameterization with a simple range for the parameters is considered in Ober (1991, 1987). New ways of balancing are also of considerable interest for high-accuracy control.

One problem in controlling NiTi fibers is their nonlinearity and their time-varying dynamics. Therefore for accurate control a continuous identification and control strategy is required. Normally it is difficult to identify a system at the same time that it is controlled. However it has been shown that identifiability can be obtained at the same time as control provided that a dither is added to the input signal. The covariance matrix must be controlled however.

On the other hand, adding a dither degrades the performance of the control scheme. Therefore there is a balance between identifiability and control that must be achieved, where a large enough perturbation must be added to achieve identification but

it has to be kept small in order to preserve the accuracy in control.

In recent years it has been shown that the stochastic complexity theory developed by J. Rissanen, IBM Research, San Jose, can be successfully applied to the above problem of interaction. It has been observed that the problem of computing the effect of statistical uncertainty on control performance is analogous to computing excess in mean-codelength when estimated frequencies of the letters of an alphabet are used in an encoding procedure. The basic problem of applying information theory of stochastic complexity to the statistical analysis of linear stochastic systems has been previously studied.

The stochastic complexity theory is close to real world testing. One of the major remaining issues is that simulations have been done for first order systems only. Additional work remains to be performed for the implementation of the theory. Additional measurements should be taken to characterize more accurately the thermocouple effect in shape memory alloys.

6.3 Originality of the Research

The research done in this thesis was original from many viewpoints. The major areas of originality are listed below.

6.3.1 Fibers with fast twitch response

I have co-developed a completely new way to produce fibers that have a fast twitch response. The same simple technique can also be used to induce the two-way

shape memory effect in NiTi fibers.

6.3.2 Fibers with two way shape memory effect

The process described in the patent application presents also a new and simple technique that can be used to induce the two way shape memory effect in NiTi fibers. Other techniques exist but the process described in the patent is simple compared to most other techniques.

6.3.3 Stiffness Through in Modulus of Elasticity

I have observed that very large nonlinearities and non-stationarities occur in the stress-strain relationship when there are sudden decreases in the modulus of elasticity. I have shown that these can be partly compensated by proper stiffness measurements.

6.3.4 Time dynamics of Martensitic Transformations

I have observed a very large change in hysteresis with changes in the rate at which the temperature is changed. These measurements indicate that martensitic transformations can occur much below the speed of sound in the material.

6.3.5 Growing and Attaching NiTi fibers

I have developed a new process to attach NiTi fibers. The new method employs metal deposits on the fiber or between two fibers or between fibers and other parts, creating metallic attachments that are mechanically sound and electrically conductive.

6.3.6 Thermo-electric measurements

I have developed a new practical technique to use the thermo-electric effect to study the state of the martensitic transformations through the new method of attachment of NiTi fibers. With this technique we were able to record large potential differences

between copper and NiTi fibers of 10 μV/°C.

Bibliography

Achenbach, M. A model for an alloy with shape memory. *International Journal of Plasticity*, 1989, *3*, 371-395.

Basinski, Z. S. and Christian, J. W. Crystallography of deformation by twin boundary movements in Indium-Thallium alloys. *Acta Metallurgica*, 1954, *2*, 101-116.

Bergamasco, M., Salsedo, F. and Dario, P. A linear SMA motor as direct-drive robotic actuator. *IEEE International Conference on Robotics and Automation*, 1989a, *1*, 618-623.

Bergamasco, M., Salsedo, F. and Dario, P. Shape memory alloy micromotors for direct-drive actuation of dexterous artificial hands. *Sensors and Actuators*, 1989b, *17*, 115-119.

Beyer, J. Recent advances in the martensitic transformations of Ti-Ni alloys. *Journal de Physique IV (Colloque)*, 1995, *5*, C2-433-443.

Boggs, R.N. How memory metals shape product designs. *Design News*, 1993, *6-21-93*, 72-74.

Buehler, W.J., Gilfrich, J.V. and Wiley, R.C. Nickel-Base Alloys. *U.S. patent* 3,174,851, 1965.

Chang, L.C. and Read, T.A. The Gold-Cadmium Beta Phase. *Trans. AIME*, 1951, *189*, 47.

Cory, J.S. Solid state engine, *U.S. Patent* 4,305,250, 1980.

Dautobich, D.P. and Purder, G.R. *Canadian Met. Quart.* 1965, *4*, 129.

Delaey, L, Thienel, J. Shape Memory Effects in Alloys, Jeff Perkins (ed), Plenum, 1975, New York, 341-350.

Duerig, T.W., Melton, K.N., Stöckel, D. and Wayman, C.M. *Engineering aspects of shape memory alloys.* Boston: Butterworth-Heinemann, 1990.

Funakubo, H. Shape memory alloys. New York, NY: Gordon and Breach, 1987.

Gabriel, K.J., Trimmer, W.S.N. and Walker, J.A. A micro rotary actuator using shape memory alloys. *Sensors and Actuators*, 1988, *15*, 95-102.

Galiana, H.L. and Green, A.M. Vestibular adaptation: how models can affect data interpretation. Special Issue on Vestibular Adaptation, Otolaryngol. *Head & Neck Surgery*, in press 1997.

Gerencsér, L., Lafontaine, S., Hunter, I.W., Hetthéssy, J., Jones, L, Vágó, Z. High accuracy stochastic adaptive control with applications to master-slave tele-micro-surgical robots. *SYSID'97, 11th IFAC Symposium on System Identification*, 1997, Fukuoka, Japan.

Gerencsér, L., van Schupper, J.J., Rissanen, J. and Vágò, Z. Stochastic complexity, selftuning and optimality. *Proceedings of the 33rd Conference on Decision and Control, Lake BuenaVista*, 1994, 652-654.

Gerencser, L., Vago, Z., Hunter, I.W., Lafontaine, S. and Horvath, A. Stochastic complexity of continuous time processes. *Proceedings of the 1994 American Control Conference*, 1994b.

Gerencser, L. and Rissanen, J. A prediction bound for Gaussian ARMA processes. *Proceedings of the 25th IEEE Conference on Decision and Control*, 1986.

Gillet, Y., Meunier, M.A., Brailovski, V., Trochu, F., Patoor, E., Berveiller, M. Comparison of thermomechanical models for shape memory springs. *Journal de Physique IV (Colloque)*, 1995, *5*, 1165-1170.

Gilbertson, R.B. Muscle Wires as Project Book: A Hands-on Guide to Amazing Robotic Muscles that Shorten When Electrically Powered. *Mondo-tronics, Inc.*, 1994, San Anselmo, CA.

Glasauer, F.-U. and Müller, I. Drum- and -disc-engine with shape memory wires. *Journal de Physique*, 1996, *IV 6(c1)*, 301-307.

Grant, D. and Hayward, V. Design of shape memory alloy actuator with high strain and variable structure control. *Proceedings of 1995 IEEE International Conference on Robotics and Automation*, 1995.

Grant, D. and Hayward, V. Variable structure control of shape memory alloy actuators. *IEEE Control Systems Magazine*, 1997, *17(3)*, 80-88 .

Haas, T. Laser beam welding of NiTi – shape memory alloys. *Report No. FZKA 5709, Forschungszentrum Karlsruhe GmbH*, 1996.

Hall, T.A. Joint, a laminate, and a method of preparing a nickel-titanium alloy member surface for bonding to another layer of metal. *U.S. patent* 5,354,623, 1993.

Hanlon, J.E., Butler, S.R. and Wasilewski, R.J. Effect of Martensitic Transformation on the Electrical and Magnetic Properties of NiTi. *Transactions of the Metallurgical Society of AIME*, 1967, *239*, 1323-1327.

Higuchi, H., Goldman, Y.E. Sliding distance between actin and myosin filaments per ATP molecule hydrolysed in skinned muscle fibers. *Nature*, 1991, 352-354.

Hirose, S., Ikuta, K. and Tsukamoto, M. Development of a shape memory alloy actuator. Measurement of material characteristics and development of active endoscopes. *Advanced Robotics*, 1990, *4(1)*, 3-27.

Hirose, S., Ikuta, K. and Umetani, Y. A new design method of servo-actuators based on the shape memory effect, in Theory and Practice of Robots and Manipulators. *RoManSy '84, the 5th CISM-IFTOMM Symposium*, 1984.

Hirose, S., Ikuta, K and Umetani, Y. Development of shape-memory alloy actuators. Performance assessment and introduction of a new composing approach. *Advanced Robotics*, 1989a, *3(1)*, 3-16.

Hirose, S., Ikuta, K. and Sato, K. Development of a shape memory alloy actuator. Improvement of output performance by the introduction of a s-mechanism. *Advanced Robotics*, 1989b, *3(2)*, 89-108.

Hirose, S., Ikua, K. and Umetani, Y. Development of shape-memory alloy actuators. *RoManSy '84, the 5th CISM-IFTOMM Symposium*, 1984.

Hollerbach, J.M. and Hunter, I.W. Macro and Micro Robotics, *Proceedings of the Second International Symposium on Measurement and Control in Robotics*, 1992, Tsukuba Science City, Japan, 3-9.

Hollerbach, J.M., Hunter, I.W. and Ballantyne, J. A comparative analysis of actuator technologies for robots. *Robotics Review*, 1991, 301-345.

Homma, D., Horiguchi, K.-s. and Yokohama-shi, K.-k. Method of treating Ti-Ni shape memory alloy. *US Patent* 4,919,177, 1990.

Homma, D., Miwa, Y. and Igushi, N. Micro robots and micro mechanisms using shape memory alloy. *The 3rd Toyota Conference: Integrated Micro Motion Systems Micromachining, Control & Application*, 1989.

Hunter, I.W. and Lafontaine, S. A comparison of muscle with artificial actuators. *Technical Digest of the Fifth IEEE Solid State Sensor & Actuator Workshop*, 1992a, 5, 178-185.

Hunter, I.W. Novel actuators for use in robotics and tele-robotics. *Report Prepared for the US Office of Naval Research*, 1990.

Hunter, I.W. and Lafontaine, S. Shape memory alloy fibres having rapid twitch response. *US patent* 5,092,901, 1992b.

Hunter, I.W., Lafontaine, S., Hollerbach, J.M. and Hunter P.J. Fast reversible NiTi fibers for use in microrobotics. *IEEE Micro Electro Mechanical Systems*, 1991, *2*, 166-170.

Hugues, D. and Wen, J.T. Preisach Modeling of piezoceramic and shape memory alloy hysteresis, *Smart Materials and Structures*, 1995, *6(3)*, 1086-1091.

Ikuta, K., Tsukamoto, M. and Hirose, S. Mathematical model and experimental verification of shape memory alloy for designing micro actuator. *Proceedings of IEEE Micro Electro Mechanical Systems*, 1991, 103-8.

Ikuta, K. Micro/miniature shape memory alloy actuator. *IEEE Micro Electro Mechanical Systems,* 1990, *3,* 2156-2161.

Ikuta, K., Tsukamoto, M. and Hirose, S. Shape memory alloy servo actuator system with electric resistance feedback and application for active endoscope. *Proceedings of the IEEE International Conference on Robotics and Automation*, 1988, 427-430.

Ishijima, A., Doi, T., Sakurada, K. and Yanagida, T. (1991). Sub-piconewton force fluctuations of actomyosin in vitro. *Nature,* 1991, *352*, 301-306.

Iwata, T., Machida, K., Toda, Y., Kurita, Y. and Honda, T. Active holding mechanism using shape memory alloy for space application - Space Anemone. *Proceedings of the International Symposium on Space Tech. & Science*, 1988, *2* 1641-1648.

Jackson, C.M., Wagner, H.J., Wasilewski, R.J. *55-Nitinol – the alloy with a memory: its physical metallurgy, properties, and applications; a report.* Washington: Technology Utilization Office, National Aeronautics and Space Administration, 1972.

Jordan, L., Chandrasekaran, M., Masse, M. and Bouquet, G. Study of Phase Transformations in Ni-Ti based shape memory alloys. *Journal de Physique IV(Colloque)*, 1995, *5*, C2-489-494.

Kohl, M., Skrobanek, K.D., Quandt, E., Schloßmacher, S.I. and Allen, D.M. Development of microactuators based on the shape memory effect. *Journal de Physique IV (Colloque)*, 1995, *5,* C8-1187-1192.

Kuribayashi, K. Millimeter-sized actuator using a shape memory alloy. *Sensors and Actuators*, 1989, 20, 57-64.

Kuribayashi, K. A new actuator of a joint mechanism using TiNi alloy wire. *The International Journal of Robotics Research*, 1986, *4(4),* 47-57.

Lafontaine, S.R., Hunter, I.W., Belanger, P. and Stein, R.B. Time resolved properties of NiTi fibers during twitches. *The 5th Annual Conference of the Institute for Robotics and Intelligent Systems (IRIS)*, 1995.

Lafontaine, S.R. and Hunter, I.W. Time resolved stiffness of fast NiTi artificial muscle fibers. *IRIS – PRECARN IV Annual Conference*, 1994.

Lafontaine, S.R., Hunter, I.W. and Jones, L.A. NiTi artificial muscles for micro-robotics and medical applications. *Proceedings of the International Conference on Industrial Applications of Shape Memory Alloys*, Quebec City, 1994.

Lafontaine, S., Cai, K. and Hunter, I.W. Temperature dependence of NiTi fiber impedance. *18th Canadian Medical and Biological Engineering Conference*, 1992.

Leclercq, S., Lexcellent, C. and Gelin, J.C. A finite element calculation for the design of devices made of shape memory alloy. *Journal de Physique IV (Colloque)*, 6, C1-225-234.

Liang, C. and Robers, C.A. Design of Shape Memory Alloy Actuators. *Journal of Mechanical Design*, 1992, *114*, 223-230.

Lexcellent, C., Torra, V. and Raniecki, B. Hystérésis d'alliages thermoélastiques, étude comparative de quelques modèles de comportement des alliages à mémoire de forme. *Journal de Physique III*, 1993, *3*, 1463-1477.

Likachev, A.A. Differential equation of hysteresis: application to partial martensitic transformation in shape-memory alloys. *Journal de Physique III (Colloque)*, 1995, *5*, C2-465-469.

Lu, X. A systems approach to modelling and design of high strain shape memory alloy actuators. Master of Engineering Thesis, Department of Electrical Engineering, McGill University, Montreal, 1997.

Madden, J.D., Madden, P.G., Hunter, I.W., Lafontaine, S.R. and Brenan, C.J.H. Microrobots: Present and Future. *IEEE/RSJ International Conference on Intelligent Robots and Systems*, 1996.

Malygin, G.A. Kinetic model of superelastic deformation effects and of the shape memory in martensitic transformations. *Physics of the Solid State*, 1993, *35(1)*, 127-137.

McNichols, J.L. and Cory, J.S. *Thermodynamics of Nitinol. Journal of Applied Physics*, 1987, *61(3)*, 972-984.

McNichols, J.L. Final report – prototype nitinol heat engine, MDC G9290, *McDonnell Doublas Company*, Huntington , 1980, Beach, CA.

Mertmann, M., Bracke, A. and Hornbogen, E. Influence of the thermal treatment on the stability of partially constrained recovery of NiTi actuator wire. *Supplément au Journal de Physique III*, 1995, *5*, C8-1259-1264.

Müller, I. Thermodynamics of ideal pseudoelasticity. *Journal de Physique IV (Colloque)*, 1995, *5*, C2-423-431.

Nakano, Y., Fujie, M. and Hosada, Y. Hitachi's robot hand. *Robotics Age*, July 1984, 18-20.

Ober, R. Balanced parametrization of classes of linear systems. *SIAM J. Control and Optimization*, 1991, *29*, 1251-1287.

Ober, R. Balanced realizations: canonical form, parametrization, model reduction. *International Journal of Control*, 1987, *46*, 643-670.

Olander, A. *J. Am. Chem. Soc.*, 1932, 3819.

Otsuka, K. and Shimizu, K. Memory effect and thermoelastic martensite transformation in Cu-Al-Ni alloy. *Scripta Metallurgica*, 1970, *4(6)*, 469-472.

Page, M. and Sawyer, P.N. Prosthetic Pump. *US Patent* 3,827,426, 1974.

Patoor, E. and Berveiller, M. Technologie des alliages à mémoire de forme, 1994, Hermès, 289p.

Pintelon, R. and Kollar, I. Exact discrete time representation of continuous time systems. *Proceedings of the 9th IFAC/IFORS Symposium on Identification and System Parameter Estimation*, 1991.

Press, W.H., Teukosky, S.A., Vetterling, W.T. and Flannery, B.P. Numerical Recipes in C. Cambridge, UK: *Cambridge University Press*, 1992.

Reynaerts, D. and Van Brussel, H. Development of a SMA high performance robotic actuator. *Proceedings of the International Conference on Advanced Robotics*, Pisa, 1991, 61-66.

Reynaerts, D. and Van Brussel, H. Design and transputer based control of a two-fingered robot hand. *Proceedings of the IFAC Symposium on Robot Control*, Capri, 1995, 267-273.

Rissanen, J. Stochastic complexity. *J. R. Statist. Soc. B*, 1987, *49(3)*, 223-239 and 252-265.

Riva, G. and Airoldi, G. Electric transport properties of NiTi thin wires under applied stress. *Journal de Physique IV (Colloque)*, 1995, *5*, C8-623-628.

Shaw, J.A., Kyriakides, S. On the nucleation and propagation of phase transformation fronts in a NiTi alloy. *Acta Materialia*, 45(2), 683-700.

Shi, J.D., Ma, J.L., Gao, Y., Pu, Z.J., Wu, K.H. Fabrication of fine grain size shape memory alloys crystallization of amorphous ribbon. *Proceedings of the Symposium of the Materials Research Society*, 1995, *400*, 221-227.

Stoddard, W.D. and Schiferl, C.M. Robotic applications for shape memory alloy. *Proceedings of of the 10th Robots Conference, Robotics International of SME*, Chicago, 1986, 11/83-86.

Silling, S.A. Dynamic growth of martensitic plates in an elastic material. *Journal of Elasticity*, 1992, *28(2)*, 143-64.

Tamura, H. Fatique properties of Ni-Ti shape memory alloy springs. *Furukawa Review*, 1988, *6*, 123-130.

Trochu, F., Yuan-Yao, Q. Nonlinear finite element simulation of superelastic shape memory alloy parts. *Computers and Structures*, 1997, *5(62)*, 799-810.

Thuillier, S., Favier, D., Canova, G. Micromechanical model of the two way memory effect alloys. *Journal de Physique (Colloque)*, 1995, *IV 5*, 587-592.

Ullakko, K., Hunag, J.K., Kokovin, V.V. and O'Handley, R.C. Magnetically controlled SMA in Ni2MnGa intermetallics. *Scripta Materiala*, 1997, *36(10)*, 1133-1138.

Van Humbeeck, J., Chandrasekaran, M. and Delaey, L. Shape memory alloys: materials in action. *Endeavour, New Series*, 1991a, *15(4)*, 147-154.

Van Humbeeck, J. From a seed to a need: the growth of shape memory applications in Europe. *Shape-Memory Materials and Phenomena – Fundamental Aspects and Applications Symposium*, Boston, 1992, 377-387.

Van Moorleghem, W., Reynaerts, D., Van Brussel, H. and Van Humbeeck, J. General discussion: the use of shape memory actuators. *Proceedings of Actuator 92, 3r4d Intenational Conference on New Actuators*, 1992, Bremen, Germany, 225-227.

Wasilewski, R.J., Butler, S.R. and Hanlon, J.E. On the martensitic transformation in TiNi. *Metal Sci. J.*, 1967, *Vol.1*, 104-110.

Weynant, E., Buffard, L, Charbonnier, P. and Lours, T. Emploi des alliages à mémoire de forme. *Matériaux & Techniques*, 1993, *6-7*, 77-86.

Wu, K., Dalip, S.K., Liu, Y. and Pu, Z. Damping characteristics of R-phase NiTi shape memory alloys. *Smart Structures and Materials SP IE-Int. Soc. Opt. Eng.*, 1995.

Zmuda, J.P. The engine that runs on sunshine. *Popular Science*, April 1974, p. 87,146.

Appendix I. U.S. Patent 5,092,901

Hunter, I.W. and Lafontaine, S. Shape memory alloy fibres having rapid twitch response. US patent 5,092,901, 1992a.

US005092901A

United States Patent [19]

Hunter et al.

[11] Patent Number: 5,092,901

[45] Date of Patent: Mar. 3, 1992

[54] **SHAPE MEMORY ALLOY FIBERS HAVING RAPID TWITCH RESPONSE**

[75] Inventors: **Ian Hunter; Serge R. Lafontaine, both of Montreal, Canada**

[73] Assignee: **The Royal Institution for the Advancement of Learning (McGill University), Montreal, Canada**

[21] Appl. No.: **534,131**

[22] Filed: **Jun. 6, 1990**

[51] Int. Cl.[5] A61F 2/70; A61F 2/08

[52] U.S. Cl. 623/24; 623/14; 60/528; 901/21

[58] Field of Search 623/14, 24, 25, 63–65, 623/58; 60/528, 527; 901/21, 28, 25, 39

[56] **References Cited**

U.S. PATENT DOCUMENTS

3,827,426	8/1974	Page et al.	600/16 X
3,858,141	12/1974	Lackey	219/492 X
4,503,569	3/1985	Dotter	604/8 X
4,556,050	12/1985	Hodgson et al.	600/30
4,655,489	2/1987	Krumme et al.	604/245
4,700,541	10/1987	Gabriel et al.	60/528
4,715,637	12/1987	Hosoda et al.	901/30 X
4,716,731	1/1988	Sakai et al.	60/527
4,838,859	6/1989	Strassman	604/95

FOREIGN PATENT DOCUMENTS

0084427	4/1986	Japan	901/28
1240574	6/1986	U.S.S.R.	901/21
1271738	11/1986	U.S.S.R.	901/25
1278198	12/1986	U.S.S.R.	901/21
1313699	5/1987	U.S.S.R.	901/39

Primary Examiner—Randall L. Green
Assistant Examiner—David H. Willse
Attorney, Agent, or Firm—Bachman & LaPointe

[57] **ABSTRACT**

A modified shape memory alloy fibers exhibits a rapid twitch response under stimulation by an action potential such as the heating effect of an electromagnetic pulse; in particular the relaxation time of the twitch response is considerably shortened as compared with that of the unmodified fibers; the modification is achieved by simultaneous application of a stretching force and a short, powerful electromagnetic pulse effective to bring about contraction resulting from the shape memory and change material properties; this application is carried out a plurality of times.

23 Claims, 2 Drawing Sheets

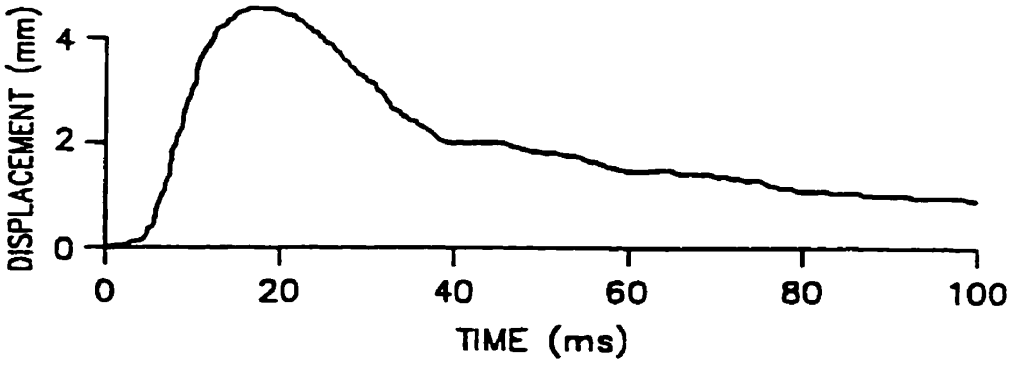

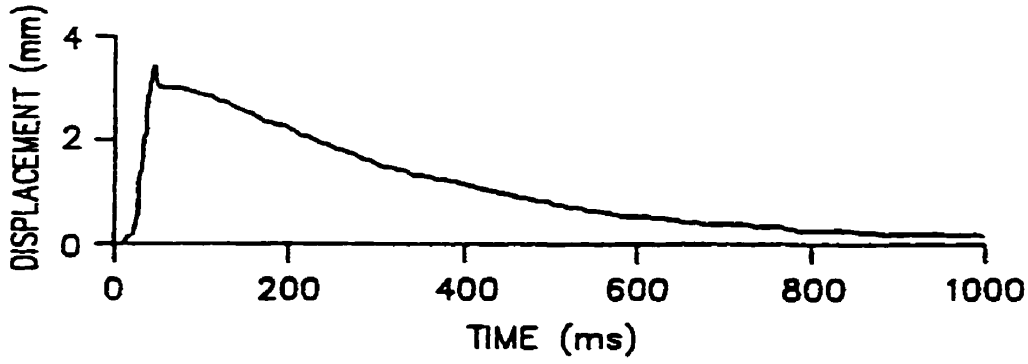

Fig. 1
(PRIOR ART)

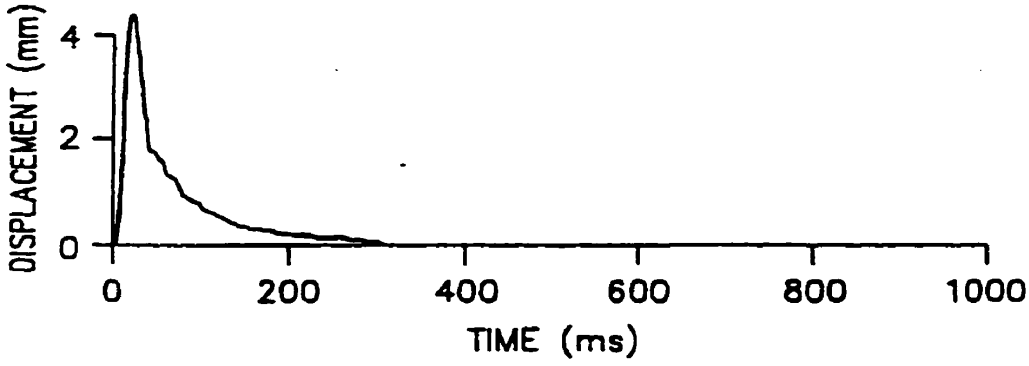

Fig. 2

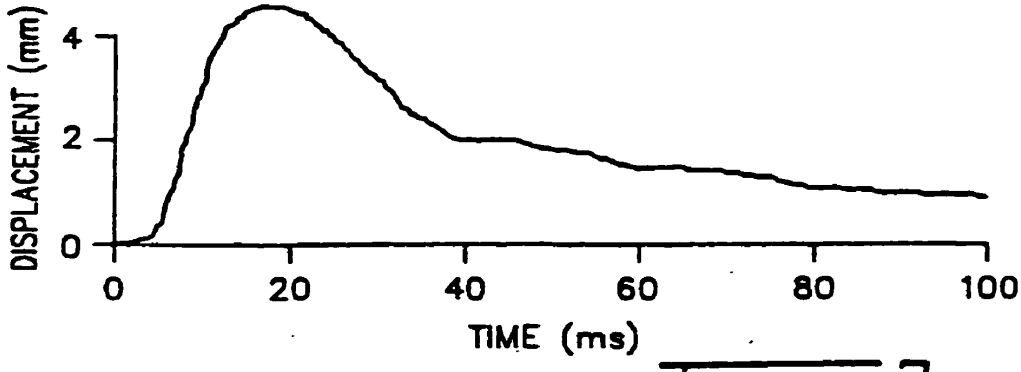

Fig. 3

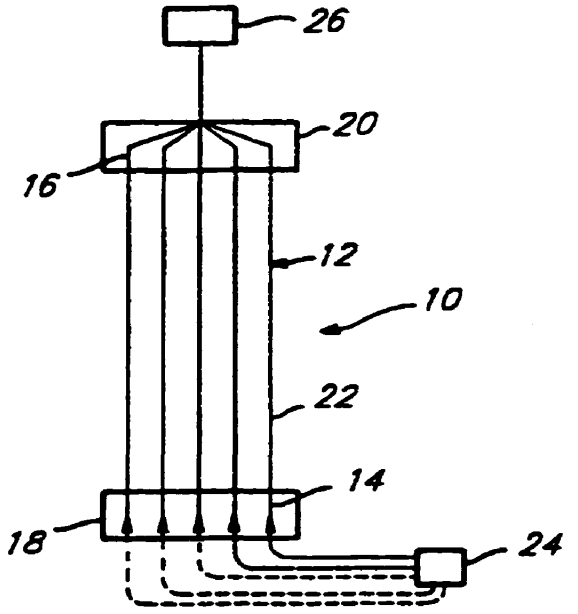

Fig. 4

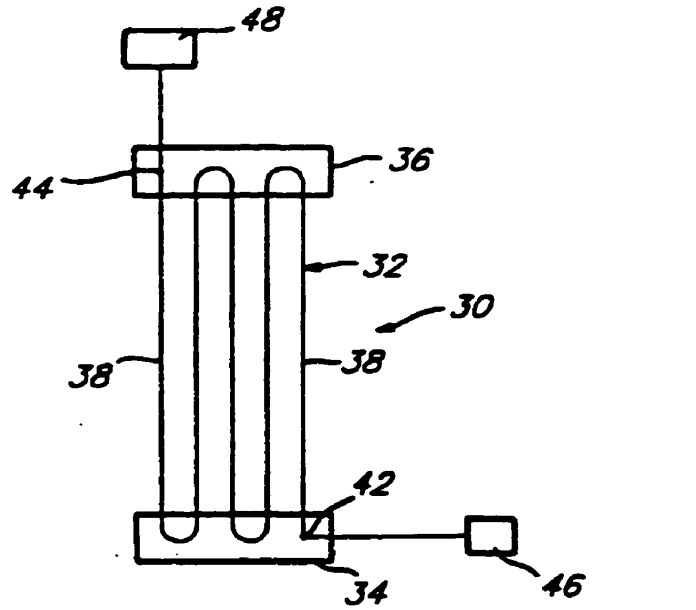

Fig. 5

SHAPE MEMORY ALLOY FIBERS HAVING RAPID TWITCH RESPONSE

BACKGROUND OF THE INVENTION

i) Field of the Invention

This invention relates to modified elongate a fibers of a shape memory alloy, their preparation and use as actuation elements for generation of a working force.

ii) Description of Prior Art

Metal alloys are known which exhibit a shape memory effect. Such alloys exhibit a thermoelastic behavior resulting from transportation from a parent phase stable at an elevated temperature to a martensite phase at a lower temperature. If the alloy is deformed to a first particular shape while in the parent phase and is then shape adjusted while in the martensite phase to a second shape, the first shape is restored when the alloy is heated to the temperature at which transformation from the martensite phase to the parent phase occurs.

In considering the use of shape memory alloys in robotics and prosthesis, it is instructive to compare the properties of shape memory alloys with those of skeletal muscles and the ubiquitous electromagnetic actuators.

In a skeletal muscle of a mammal the tension or maximum force generated per unit cross-sectional area is a substantially constant 350 kN/m^2. In comparison the maximum substainable force generated by commercial high performance linear electromagnetic motors is more than 100 times less. Thus a Bruel & Kjaer linear motor (Model B & K 4810) generates a maximum tension of 2.6 kN/m^2. A short muscle having a muscle length which is the same as the muscle diameter can generate a force per unit mass of about 310 N/kg, whereas Model B & K 4810 generates only 9 N/kg. Muscle usually shortens by more than 20% in a limb, whereas Model B & K 4810 shortens by a maximum of 8%.

A skeletal muscle comprises a bundle of muscle fibers, generally in parallel relationship. More powerful muscles have more fibers, and muscles that must shorten over considerable distances have longer muscle fibers.

Robot limbs have been constructed using elongate Ni-Ti shape memory fibers. A Ni-Ti shape memory fiber having a diameter of 0.8 mm will generate over 100 MN/m^2 tension and shorten by up to 10% of its length. These shape memory fibers suffer a major drawback in that the total contraction and relaxation time is unduly slow and in particular the relaxation time is unduly slow. These shape memory fibers have a total contraction and relaxation time slower than both muscle and most electromagnetic actuators.

SUMMARY OF THE INVENTION

It is an object of this invention to provide an elongate fiber of a shape memory alloy of modified character.

It is a further object of this invention to provide an elongate fiber of shape memory alloy having a short total contraction and relaxation time.

It is a still further object of this invention to provide a method of producing modified elongate fibers of a shape memory alloy.

It is yet another object of this invention to provide an actuator element for generation of a working force, in the form of a modified elongate fiber of a shape memory alloy.

It is a still further object of this invention to provide a motor unit for generation of a working force based on at least one actuator element of the invention.

It has now been found that subjecting an elongate fiber of a shape memory alloy simultaneously to a stretching force and a short, powerful electromagnetic pulse effective to cause contraction of the fiber length and change material properties, results in a modification of the shape memory parameters of the fiber; more especially the modified fiber has a total contraction and relaxation time much shorter than that of the unmodified fiber.

In particular the relaxation time of the modified fiber is much shorter than that of the corresponding unmodified fiber, with the result that the fiber exhibits a rapid twitch response under stimulation by a current pulse (an action potential).

The modified elongate fibers may function as an artificial muscle-like actuator element for generation of a working force in robotics or prosthetics and may form part of a motor unit for generation of a working force in robotics or prosthetics.

DESCRIPTION OF PREFERRED EMBODIMENTS

a) Elongate Fiber

The unmodified elongate fiber employed to produce the modified fiber of the invention is formed from a shape memory metal alloy.

The most widely employed fibers of this type are the Ni-Ti fibers available under the Trade Mark Nitinol. The phase transformation temperatures which are a characteristic of the shape memory are well established and are dependent on the relative proportions of the alloying elements Ni and Ti and the optional inclusion of alloying additives.

Other shape memory alloys include Ag-Cd, Au-Cd, Au-Cu-Zn, Cu-Al, Cu-Al-N, Cu-Zn, Cu-Zn-Al, Cu-Zn-Ga, Cu-Zn-Si, Cu-Zn-Sn, Fe-Pt, Fe-Ni, In-Cd, In-Ti, Ti-Nb and Ti-Ni.

Commercially available fibers typically have a diameter of 0.01 to 10 mm, usually 0.025 to 1 mm, usually greater than 0.1 mm. The length depends on the application.

Ni-Ti fibers are preferred fibers of the invention.

The unmodified fibers typically have a total contraction and relaxation time in excess of 1000 ms for a 0.8 mm diameter fiber. Typically the contraction time is not more than about 50 ms, and the relaxation time is in excess of 950 ms for a 0.8 mm diameter fiber.

b) Modification

The elongate fibers are modified to produce modified fiber exhibiting a change in material properties by the simultaneous application of a stretching force and a short, powerful, electromagnetic pulse.

In order to achieve this the fiber is suitably connected at one end to a linear electromagnetic motor and at the other end to a force transducer. The motor applies a moderate, linear stretching tension (i.e., force/unit cross-sectional area of the fibers), for example, of the order of 40 MN/m^2. A short, very powerful electric potential is applied across the ends of the fiber to produce an electromagnetic pulse effective to achieve a contraction in length of the fiber, while the linear stretching force is maintained.

Suitably this electromagnetic pulse has a current density of 400 to 4000 MA/m^2 and is of short duration so as not to destroy the integrity of the fibers.

In the case of a pulse of 400 MA/m^2 the duration of the pulse is suitably not more than 5 ms, whereas in the case of a 4000 MA/m^2 pulse the duration is suitably not more than 0.5 ms.

For a 0.8 mm diameter fiber, suitably about 75 to 125, preferably about 100 electromagnetic pulses are applied, and the pulses are required to have a high rate of change of current. Thus for a 0.8 mm diameter fiber a rate of change of current of 10,000 A/sec. does not produce a satisfactory modified fiber, whereas a rate of change of current of 200,000 A/sec. does. An optimum rate of change of current in the pulse is 10^6 A/sec.

The modification may conveniently be carried out in a cooling environment to cool the fibre following the temperature increase associated with each pulse. For this purpose the modification is conveniently carried out with the fiber immersed in a bath of liquid coolant, for example, 50% methanol/50% water at −20° C.

c) Modified Fibers

The modified shape memory alloy fibers of the invention exhibit a rapid twitch response under stimulation by an action potential, the twitch being the contraction and relaxation exhibited by the modified elongate fiber in response to the stimulation.

The action potential which serves as stimulation may suitably take the form of a brief current pulse of fixed amplitude and duration, for example, for a 0.8 mm diameter fiber, a pulse of about 50 A for a 1 ms duration. The pulse heats the fiber causing rapid contraction to the memory state which contraction is followed by a rapid relaxation.

The modified fibers more particularly have for a 0.8 mm diameter fiber a twitch response of less than 40 ms, of which the contraction rise time is not more than 10 ms and the relaxation decay time is about 60% completed in 15 ms.

Applications

The modified fibers of the invention find use in applications in which they function as actuator elements for generation of a working force.

Thus the fibers may be employed in motor units to simulate an artificial muscle in robotics or prosthetics.

Such an artificial muscle would consist of a number of motor units arranged in parallel. The number of motor units employed is a function of the total force required by the artificial muscle. The more motor units employed, the greater the total force produce.

Each motor unit may comprise a bundle of discrete elongate modified fibers in side-by-side parallel relationship and electrically insulated from each other along their length. In this case the fibers are electrically in parallel relationship. Alternatively a motor unit may comprise a single elongate modified fiber arranged in a sinusoidal-like path to provide lengths of the fiber in side-by-side parallel relationship; the side-by-side lengths being electrically insulated from each other. In this case the lengths of fiber are electrically in series relationship.

A motor unit containing a bundle of modified fibers may typically contain 5 to 15, more usually 10 fibers. The fibers of different motor units of an artificial muscle may be stimulated independently by separate pulses or pulse sources, more especially sequentially. In this way it is possible to operate the unit while avoiding restimulation of a stimulated fiber which has not completed the relaxation phase; and the working force is generated by a combination of rate and recruitment.

Re-stimulation of a plurality of stimulated fibers during the relaxation phase results in a non-linear summation of the generated forces producing a saturated or constant force level termed the tetanic force.

A pair of artificial muscles each comprising a collection of motor units in parallel may be arranged as an agonist-antagonistic pair which act in opposition but not simultaneously; in this way a working force may be generated by contraction of the fibers of one artificial muscle of the pair for work in one direction, followed by work in the other direction by the other artificial muscle; the agonist-antagonist pair can also be stimulated simultaneously to produce a stiffening effect.

If increased working force is required this can be achieved by employing more fibers, i.e., recruitment, or by stimulating the fibers more rapidly.

BRIEF DESCRIPTION OF DRAWINGS

The invention is further illustrated and explained by reference to the accompanying drawings, in which:

FIG. 1 illustrates graphically the twitch response of a prior art, unmodified shape memory alloy fiber;

FIGS. 2 and 3 illustrate graphically the twitch response of a modified fiber of the invention,

FIG. 4 illustrates schematically a motor unit of the invention in a first embodiment, and

FIG. 5 illustrates schematically a motor unit of the invention in a second embodiment.

DESCRIPTION WITH REFERENCE TO THE DRAWINGS

With further reference to FIG. 1, there is illustrated the twitch response of a conventional Ni-Ti fiber 100 mm in length and 0.8 mm in diameter, heated by passing a pulse current through it of 50 amps for 1 ms. The heating causes the fiber to contract rapidly to the memory state with a displacement of about 3.5 mm in length in a contraction rise time of about 50 ms. The relaxation decay time by cooling after the heating has ceased is slow and is not complete even after 1000 ms.

With further reference to FIG. 2, results are shown for the fiber of FIG. 1, but after modification in accordance with the invention. The modified or altered fiber now has a much shorter twitch response time. As can be seen from FIGS. 2 and 3, the contraction rise time is not more than 10 ms, and the relaxation decay time is considerably shortened being about 60% completed in 15 ms which is markedly shorter than that of the unmodified fiber in FIG. 1.

Further it can be seen from FIG. 2 that the total relaxation decay time of the modified fiber is very much shorter than that of the unmodified fiber of FIG. 1. More especially the relaxation decay time of the modified fiber of FIG. 2, which relaxation decay time comprises a rapid relaxation followed by a slower relaxation, is complete in less than 400 ms. more especially about 300 ms and this is markedly shorter than the more than 1000 ms of the unmodified fiber of FIG. 1.

In reference to FIG. 3 it is clear that whilst the fiber relaxes by 60% very rapidly the final 40% is relatively slow and for this reason it is appropriate to constrict a motor unit with 5 to 15 preferably 10 fibers. Instead of activating all 10 fibers in the motor unit simultaneously it is appropriate to actuate them sequentially. Thus in

the case of a motor unit of 10 fibers a given fibre is not activated again until 10 activation pulses later. Activation of a subsequent fiber will usually take place while the immediately preceding activated fiber is in the rapid phase of the relaxation.

With further reference to FIG. 4, there is illustrated schematically a motor unit 10 for use in an artificial muscle (not shown). Motor unit 10 has a plurality of elongate modified fibers 12, of the invention, in generally parallel side-by-side relationship and having ends 14 and 16 supported in clamps 18 and 20 respectively.

The fibers 12 are insulated along their length by an electrically insulating coating 22.

The ends 14 are insulated from each other in clamp 18, whereas the ends 16 are in electrical contact with each other through clamp 20.

An electromagnetic source 24 provides an electromagnetic pulse to ends 14; the pulse may be applied to one or more of ends 14, sequentially or simultaneously depending on the work force required, as shown in the broken line.

The working force generated by the deformation of the fibers 12 to their memory state is communicated to work element 26.

With further reference to FIG. 5, a motor unit 30 has a single elongate fiber 32 arranged in a sinusoidal like manner between opposed clamps 34 and 36, thereby providing a plurality of side-by-side lengths 38 of the fiber.

The fiber 32 is electrically insulated by an insulating coating 40, and has an input end 42 and an output end 44.

Input end is electrically connected to an electromagnetic source 46 and output end is connected to a work element 48.

Application of an electromagnetic pulse to fiber 32 from source 46 heats the fiber causing return to the memory state and the shape change force generated is communicated to work element 48.

A plurality of the motor units 10 or 30 may be arranged in parallel and employed sequentially. If a low working force is required only some of the motor units may be employed whereas if a high working force is required all of the motor units of the plurality may be employed. The motor units 10 and 30 of the invention permit considerable flexibility in the operation of a prosthesis or robotic.

This invention may be embodied in other forms or carried out in other ways without departing from the spirit or essential characteristics thereof. The present embodiments are therefore to be considered as in all respects illustrative and not restrictive, the scope of the invention being indicated by the appended claims, and all changes which come within the meaning and range of equivalency are intended to be embraced.

We claim:

1. An actuator element for generation of a working force comprising a modified elongate fiber of a shape memory alloy, said modified fiber being derived from an unmodified fiber, said unmodified fiber having been modified by being subjected a plurality of times to a short, very powerful electromagnetic pulse effective to cause contraction of the length of the unmodified fiber and change material properties while under a stretching force serving to elongate said length, said modified fiber exhibiting a twitch response under stimulation by an action potential, said twitch response comprising a contraction time and a relaxation time, said twitch response being rapid as compared with the twitch response of the unmodified fiber.

2. An actuator element according to claim 1, wherein said rapid twitch response is less than 40 ms when subjected to the action potential of an electromagnetic pulse.

3. An actuator element of claim 2, wherein said shape memory alloy is a Ni-Ti alloy and said fiber has a diameter of 0.01 to 10 mm.

4. An actuator element of claim 1, wherein said pulse has a current density of 400 to 4,000 MA/m^2.

5. An actuator element of claim 1, wherein said pulse has a rate of current change of at least 200,000 A/sec.

6. An actuator element of claim 1, wherein said pulse has a current density of 400 to 4,000 MA/m^2 and has a rate of current change of at least 200,000 A/sec.

7. An elongate fiber of a shape memory alloy modified by having been subjected a plurality of times to a short, powerful electromagnetic pulse effective to cause contraction of the length of the fiber and change material properties, while under a stretching force serving to elongate said length, wherein said pulse has a current density of 400 to 4000 MA/m^2, and has a rate of current change of at least 200,000 A/sec.

8. An elongate fiber of claim 7, wherein said shape memory alloy is a Ni-Ti alloy and said fiber exhibits a rapid twitch response having a total contraction and relaxation time of less than 40 ms when subjected to an action potential of an electromagnetic pulse effective to heat said fiber to the shape memory state.

9. An elongate fiber of claim 8, having a diameter of 0.01 to 10 mm.

10. A motor unit for generation of a working force in response to stimulation by an action potential in an artificial muscle comprising;

first and second opposed, spaced apart clamping means,

at least one elongate actuator element comprising an elongate fiber of a shape memory alloy providing a plurality of lengths of fiber in side-by-side, generally parallel relationship extending between said spaced apart clamping means, said lengths being electrically insulated from each other and from said first clamping means,

electrical connection means for connecting said at least one fiber to a source of electromagnetic pulses at said first clamping means, and

connection means at said second clamping means for connecting said at least one fiber to a work element,

said elongate fiber exhibiting a twitch response under stimulation by an action potential, said twitch response comprising a contraction time and a relaxation time and being less than 40 ms.

11. A motor unit of claim 10, wherein said at least one elongate actuator element comprises a plurality of discrete actuator elements in generally parallel side-by-side relationship.

12. A motor unit of claim 10, wherein said at least one elongate actuator element comprises a single actuator element entrained in a generally sinusoidal manner between the clamping means.

13. A motor unit of claim 10, wherein said elongate actuator element is characterized by having been subjected a plurality of times to a short, powerful electromagnetic pulse effective to cause contraction and change material properties, while under a stretching force.

14. A motor unit of claim 13, wherein said pulse has a current density of 400 to 4,000 MA/m^2.

15. A motor unit of claim 13, wherein said pulse has a rate of current change of at least 200,000 A/sec.

16. A process for modifying an elongate fiber of a shape memory alloy comprising subjecting said elongate fiber to a stretching force while applying a plurality of short, very powerful electromagnetic pulses effective to cause contraction and change material properties of the fiber, wherein said electromagnetic pulses have a current density of 400 to 4000 MA/m^2.

17. A process according to claim 16, wherein said fiber is a Ni-Ti fiber having a diameter of 0.01 to 10 mm.

18. A process for modifying an elongate fiber of a shape memory alloy comprising subjecting said elongate fiber to a stretching force while applying a plurality of short, very powerful electromagnetic pulses effective to cause contraction and change material properties of the fiber, wherein said pulses have a rate of current change of at least 200,000 A/sec.

19. A motor unit of claim 18, wherein said pulses have has a current density of 400 to 4,000 MA/m^2.

20. A process for modifying an elongate fiber of a shape memory alloy comprising subjecting said elongate fiber to a stretching force serving to elongate the length of the fiber while applying a plurality of short, very powerful electromagnetic pulses effective to cause contraction and change material properties of the fiber, said fiber being a Ni-Ti fiber having a diameter of 0.01 to 10 mm, wherein said fiber prior to said subjecting has a twitch response comprising a total contraction rise time and relaxation decay time greater than 1000 ms, and said fiber after said subjecting has a twitch response of less than 40 ms.

21. A process according to claim 20, wherein said plurality is up to about 100.

22. A process according to claim 21, wherein said pulses have a rate of current change of at least 200,000 A/sec.

23. A modified elongate fiber derived from an elongate unmodified fiber of a shape memory Ni-Ti alloy, said unmodified elongate fiber having a twitch response, when subjected to an action potential effective to heat said fiber to the shape memory state, with a total contraction and relaxation time greater than 1000 ms, said modified fiber having a twitch response of less than 40 ms and said modified fiber having a diameter of 0.01 to 10 mm, said unmodified fiber having been modified by being subjected a plurality of times to a short, powerful electromagnetic pulse having a current density of 400 to 4,000 MA/m^2, and a rate of current change of at least 200,000 A/sec, effective to cause contraction of the length of the unmodified fiber and change material properties while under a stretching force serving to elongate said length.

* * * * *

Appendix II.

Hunter, I.W. and Lafontaine, S. A comparison of muscle with artificial actuators. *Technical Digest of the Fifth IEEE Solid State Sensor & Actuator Workshop*, 1992a, 5, 178-185.

A Comparison of Muscle with Artificial Actuators

Ian W. Hunter and Serge Lafontaine
Biorobotics Laboratory, Department of Biomedical Engineering,
McGill University, Montreal, Quebec, Canada H3A 2B4

INTRODUCTION

Considerable effort is currently underway to develop a variety of actuator technologies for use in devices such as large walking machines, anthropomorphic robots, micro-robots, micro-surgical robots, prosthetic limbs and artificial organs. The living counterparts of these devices (e.g., elephants, humans, ants, mites, legs and hearts respectively) all utilize muscle for actuation. The "artificial" actuator technologies under development include shape memory alloys, piezoelectric actuators, magnetostrictive actuators, contractile polymers and electrostatic actuators. It is therefore essential to compare the performance of these artificial actuators with nature's actuator, muscle.

In this paper the relevant properties of muscle are outlined and compared with a variety of artificial actuators. These and other actuators, such as regular and superconducting electromagnetic motors, internal combustion engines, hydraulic motors, pneumatic actuators are reviewed and compared with muscle elsewhere (see Hunter, 1990; Hollerbach et al., 1991).

MUSCLE

History

Nature has developed a number of types of actuators. One of the first and smallest is a rotary actuator probably developed about 3,500 million years (Myr) ago which provides some bacteria with a rotating flagellum to enable them to propel themselves about in liquid environments. This submicrometer scale motor, which can rotate at $> 270\ s^{-1}$ (Kudo et al., 1990), and appears to be powered by a flow of protons across a pH gradient, is not employed in larger organisms where muscle, nature's ubiquitous actuator, is used almost exclusively. Unlike the rotary bacterial flagellar motor, muscles are linear actuators which were used 500 Myr ago in early fish and ammonoids. Early dinosaur (300 Myr) and mammalian (120 Myr) muscles were probably essentially the same as those in use today. A wide variety of novel mechanisms using muscle are currently employed in animals although others ceased when dinosaurs, ammonoids and others became extinct about 66 Myr ago.

Mechanism

Whole muscles consist of bundles of muscle fibers. Each muscle fiber is a single cell which can be dissected and maintained functional (alive) in isolation from its parent whole muscle. In comparison with other actuators, muscle cells are all basically of the same design although there are significant differences in performance (e.g., force rise-time and contraction velocity), resulting from small variations in the molecular components, architecture and kinetics.

Mammalian muscle may be broadly separated into two categories, striated and smooth. Smooth muscles are to be found controlling the diameter of various tubes (e.g., veins, arteries, colon, intestines, and the pupil in the eye). Striated muscles (so called because of the sarcomere striations readily apparent under a microscope (see below)) may be further divided into two types, cardiac and skeletal muscle. As the name suggests, cardiac muscle is the actuator from which the heart, a large pump, is constructed. Skeletal muscle is the actuator which drives all limbs as well as the eye, tongue and chest (for breathing).

Whole muscles: A whole skeletal muscle is a bundle of parallel muscle fibers held together by connective tissue. Nerve fibers, blood and lymphatic vessels weave their way throughout the whole muscle. These vessels can lie beside but never inside muscle fibers. The connective tissue (collagen) at the ends of each muscle fiber join together to form the whole muscle tendon which in turn attaches to bone or fascia (connective tissue). The force generated by muscle fibers is transmitted via the tendons to the bones where it appears as a torque about some joint. If the joint torque generated by a muscle is greater than opposing torques (which may result from external loads or from opposing (antagonist) muscles) then the limb will rotate about the joint. Thus contraction of muscles produces angular displacements of limbs about joints.

Muscle fibers: The muscle fibers in large muscles are long but the diameter of muscle fibers in small and large muscles is about the same. Indeed the average muscle fiber diameter in adult humans is about 50 μm whereas 100 μm diameter frog muscle fibers are common. It seems that mammals tend not to grow more muscle fibers as they mature (or do weight lifting) but rather the average muscle fiber diameter increases. While isolated muscle fibers can reversibly contract by over ±50% it seems that in limb movement they only contract by ±10%.

Myofibrils: A muscle fiber is a bundle of even smaller fibers called myofibrils, which are typically about 2 μm in diameter and extend from one end of the muscle fiber to the other. Myofibrils do not have membranes but are separated from each other by a surrounding network of tubes and sacs. This network has two parts, the transverse tubules and the sarcoplasmic reticulum.

Sarcoplasmic reticulum: The sarcoplasmic reticulum (SR) is a network of tubes and sacs which contain intra-cellular fluid having a high Ca^{++} concentration. The voltage pulse which turns on a muscle fiber (called a muscle action potential) travels along the muscle fiber outer membrane (sarcolemma) (at 3 to 5 m/s in typical human skeletal muscle) and down holes into the interior (t-tubules) (at a lower velocity) where it causes Ca^{++} to be released from the lateral sacs of the SR. The Ca^{++} diffuse down into the adjacent myofibrils and turn on the contractile proteins. After the action potential has passed the Ca^{++} is actively pumped back into the SR.

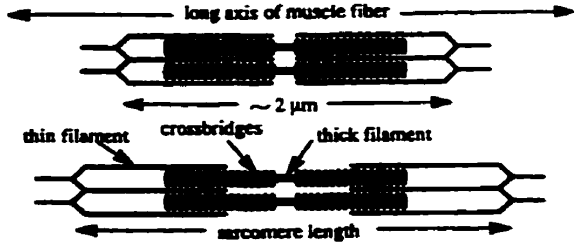

Myofilaments: The myofibril is actually a bundle of even smaller fibers called myofilaments. There are two types of myofilaments, the thick and thin filaments. The thin filament consists largely of the proteins actin, troponin and tropomyosin. The thick filament consists mainly of the myosin protein. The repeating organization of the thick and thin filaments and the way they slide past one another is shown in Figure 1. The basic contractile unit of muscle is the sarcomere (see Fig-

ure 1) which in vertebrate muscle can vary in length from 1.5 to 3.6 μm with a rest length of about 2.2 μm.

Crossbridges: The myosin protein has a large pair of heads which protrude from the thick filament backbone. These myosin heads are called crossbridges because they probably reach across and attach to adjacent thin filaments during muscle contraction. There are about 300 myosin molecules per thick filament. The crossbridges likely periodically attach and detach from the thin filament during contraction (this is called the crossbridge theory of muscle contraction). Each crossbridge probably generates a force of about 1 pN (Ishijima et al., 1991) and after a power stoke of about 12 nm (during which 1 ATP molecule is hydrolyzed) is possibly dragged for at least 28 nm (Higuchi & Goldman, 1991). The rate of this crossbridge cycling appears to be more or less dependent on the type of muscle (it is also highly temperature dependent). For example a single myosin head appears to consume 5 ATP molecules/s during peak filament sliding at 2 μm/s.

Sequence of events during contraction: Figure 2 shows the change in force through time following a single action potential under constant length (isometric) conditions. The muscle twitch data shown in Figure 2 were collected in the authors laboratory from a small bundle of frog muscle fibers at 4 °C. The sequence of events in such a typical single skeletal muscle twitch contraction is still not fully understood. However, the following seems like a probable sequence of events given our current understanding.

The muscle action potential (in turn generated by a single neural action potential) causes a burst of Ca^{++} to be released from the SR. The Ca^{++} binds to troponin which in turn causes the tropomyosin molecule to "move" exposing sites on the actin chain which attract the crossbridge. The crossbridge (initially charged with ATP (adenosine triphosphate)) rotates and generates force from the energy released as ATP splits into ADP (adenosine diphoshate) and P_i (inorganic phosphate). The ADP and P_i are released from the crossbridge head. The crossbridge remains bound to the thin filament until an ATP molecule binds to the crossbridge head to start the cycle over again.

The total force generated by a muscle is determined by the number of crossbridges operating. However, the total number of crossbridges operating at a given instant is in turn dependent on the availability of an adjacent thin filament to attach to (as muscles are stretched the overlap of thick and thin filaments is progressively reduced) and on the availability of Ca^{++} to "turn on" the thin filament (the Ca^{++} concentration increases and decreases dynamically following the passage of an action potential).

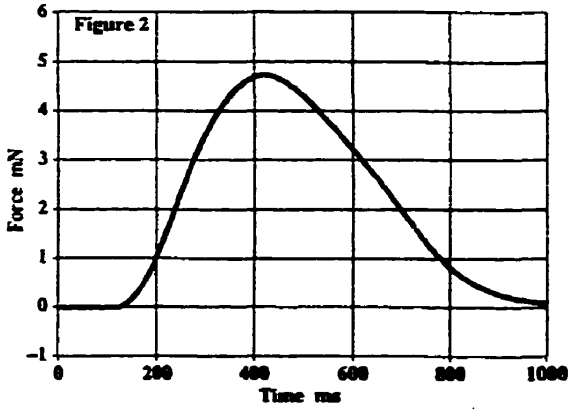

Characteristics

Muscle Model: The relation between imposed length changes (input) and force (output) (or conversely between imposed forces (input) and displacement (output)) is nonlinear. Nonlinear (Hunter & Korenberg, 1986; Korenberg & Hunter, 1986,1990,1992) and time–varying (Nielsen & Hunter, 1991; MacNeil et al., 1992) system identification methods coupled with high performance mechanical testing systems (Hunter et al., 1990) have proved useful in elucidating this relation. A simple mathematical model (Bergel & Hunter, 1979; Hunter et al., 1991) which has been found to account for the behavior of muscle in a wide variety of mechanical experiments is

$$\frac{T(t)-1}{T(t)+a} = \int_0^T k(\tau)\,\lambda(t-\tau)\,d\tau$$

where

$\lambda(t)$ is the extension ratio at time t

$T(t)$ is the tension at time t caused by a single cross–bridge

$k(\tau)$ is the system unit impulse response function

Notice that $T = 1$ when there is no imposed length change on the muscle. This represents the unit force generated by a single active crossbridge. It is found experimentally that the integral of the impulse response function (i.e. the unit step response function) is well represented by the sum of 2 or 3 complex decaying exponentials (Bergel & Hunter, 1979).

The stress, $T_{max}(t)$, generated by a muscle fiber is the sum of the contributions of each cross–bridge operating in parallel. Thus if N is the number of active cross–bridges in parallel per unit fiber cross–sectional area (about $350 \times 10^{15}/m^2$ for vertebrate muscle) and f is the static force generated by a crossbridge ($\sim$ 1 pN), then

$$T_{max}(t) = N f T(t)$$

Thus the peak static tension generated by vertebrate skeletal muscle is about 350 kN/m^2. N is itself a function of the degree of overlap between thick and thin filaments (i.e. sarcomere length) and Ca^{++} concentration. Although $k(\tau)$ above is, in filter terminology, high–pass (i.e. has no static gain) a step change in muscle length can nevertheless result in a static change in muscle tension via the length dependence of N.

Maximum Force generated by muscle: It is interesting to ask if some muscles are stronger than others. The answer is that the maximum static force generated per unit cross–sectional area (i.e. tension, stress) of all vertebrate muscle fibers seems to be remarkably constant at about 350 kN/m^2 (Huxley, 1980). Indeed the maximum force generated by invertebrate muscle is little different (e.g. 800 kN/m^2 for the crayfish). Mammalian cardiac muscle can produce up to 100 kN/m^2 (Hunter et al., 1992). Some invertebrate muscles, such as the muscle responsible for shell closure in certain molluscs, have a catch state in which they can lock themselves so as to produce a sustained force (to hold the shells closed) without energy consumption. In vertebrate muscle there is no such mechanism and the maximum force generated can only be held for a short period of time (muscle "fatigue"). Indeed the maximum sustainable force is usually about 30% of the peak value. For this reason the maximum static sustainable stress generated by muscle is about 100 kN/m^2.

Muscle Power: Unlike maximal force, the maximum power generated by muscle does vary both within the same organism as well as across animals. Power (force × velocity or stress × strain rate) changes because the strain rate to stress relation characteristically produces its maximum power at about 1/3 of its maximum strain rate (which corresponds to a load of about 1/3 of the maximum stress the muscle can gen-

erate). Consequently the maximum power a muscle can generate is roughly 0.1 ×maximum stress ×maximum strain rate. The maximum power per unit mass (in W/kg) is an important figure for robotic and prosthetic actuators, and for vertebrate muscle is roughly 350 kN/m^2 ×strain rate (s^{-1}) ÷ density of muscle (1037 kg/m^3) which equals approximately 35 ×strain rate. Human muscle is typically about 50 W/kg but can be as high as 200 W/kg (certain muscles for brief periods).

Cycle Lifetime of Muscle: An estimate of the cycle lifetime of muscle is readily estimated for cardiac muscle. The heart beats over 3×10^9 times in the life time of an average person.

Muscle Stiffness: One property of muscle which distinguishes itself from all other actuators covered in this review is the large change in stiffness which occurs between resting muscle and maximally activated muscle. While muscle stiffness is highly dependent on length, a large change is also observed under isometric conditions (i.e., fixed length). To illustrate this consider the isometric muscle twitch shown in Figure 2. A small (±0.2%) 800 Hz sinusoidal length change imposed on the muscle during the twitch is shown in Figure 3 where the large change in stiffness is evident.

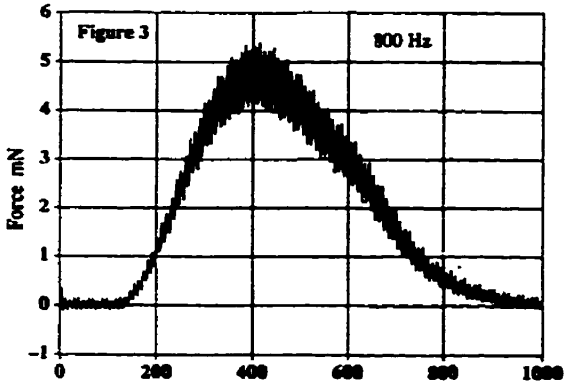

Figure 4 shows the almost linear increase of stiffness with tension which occurs throughout the muscle twitch. The hysteresis evident in Figure 4 is found for a wide variety of muscles using not only sinusoidal but also stochastic length perturbations. The increase in stiffness with force has a simple and probable explanation: the increase and decrease in Ca^{++} concentration in the twitch turns on a corresponding increase then decrease in the number of crossbridges generating force. The crossbridges within a sarcomere are organized in parallel and so force rises and decays in proportion to the number of crossbridges active. However each crossbridge (or the actin–myosin bond) has a stiffness which adds with the other parallel crossbridge stiffnesses with the result that stiffness covaries with force. From Figure 4 it is clear that stiffness increases about 5 times from rest to the peak of the twitch. Independent experiments show that fewer than 50% of the crossbridges are active at the peak of the twitch. Consequently stiffness can vary over more than a 10 fold range from rest to a 100% contraction (which can be achieved by multiple action potentials).

The variation of muscle stiffness with muscle force is in our opinion one of the most important mechanical characteristics of muscle. As muscles can only effectively generate tensile forces (under nondynamic conditions) it is necessary to provide a means to extend them following contraction. This is usually achieved by having opposing muscles operating about a joint. Whereas the forces (or torques) of the two opposing muscles subtract, their stiffnesses add. The result of this is that whereas the stiffness of a single muscle is a linear (neglecting hysteresis) function of the force it generates, the combined stiffness and force of two opposing independently activated muscles are independent. Thus the stiffness of a joint can be varied by the nervous system independently of the torque generated by the limb via co–contraction of the opposing muscles. It is the ability of the nervous system to independently set limb force and stiffness that gives rise to much of a limbs mechanical versatility. Unfortunately, as we will now see, it is one of the characteristics that will be most difficult for artificial actuators to replicate (although a possible solution is given in the Conclusion).

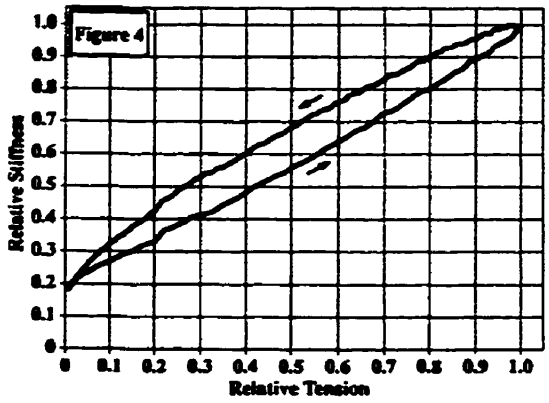

SHAPE MEMORY ALLOY ACTUATORS

History

Chang and Read discovered in 1951 that an alloy of gold and copper would return to its undeformed state when heated after being deformed. A few years later Basinski and Christian (1954) observed the same effect in Indium–Titanium alloy. The effect was again observed by Buehler, Gilfrich and Wiley (1963) in a Nickel–Titanium (50% Ni, 50%Ti) alloy. These researchers coined the term "Shape Memory Effect" to describe the phenomenon. Numerous SMAs have been studied (see Funakubo, 1987). The most extensively studied SMA is the NiTi alloy (typically 50% Ni). NiTi fibers and springs have been frequently proposed for use as artificial muscles (Hashimoto et al., 1985; Bergamasco et al., 1989; Hirose et al., 1985,1989; Homma et al., 1989; Ikuta, 1990; Hunter et al., 1990,1991) because of its favorable material properties, nontoxicity and reasonable cost.

Mechanism

Otsuka and Shimizu (1970) showed that the shape memory effect was caused by a martensite to austenite phase transition. This phase transition occurs progressively over a band of temperatures. At low temperatures (i.e. below the phase transition temperature band) the NiTi has low crystal symmetry and can be readily plastically deformed. This state is alternatively called the martensite phase or the R–phase (because rhombohedral crystalline structures predominate). When heated to temperatures above the phase transition band the NiTi transforms to a higher symmetry crystalline structure, called the parent or austenite phase, has the same distribution of atoms as that found before the plastic deformation.

Fibers can be "trained" to contract as they undergo a martensite to austenite phase transition with heating. Expansion to the original fiber length then occurs when the SMA is cooled to its martensitic phase again.

Characteristics

The contraction time of NiTi is governed by the amplitude of the current pulse (and hence the heating time) passed through it. By using large current pulses this contraction time can be made very short (Hunter et al., 1991). The rate limiting part of the NiTi contraction and expansion cycle is in the relatively long time required for NiTi to cool and return back to its original length. The cooling time is governed by thermal diffusion and the fact that in both heating and cooling the usual thermal capacity has to be considered as well as the latent heat involved in the phase change between the austenite and martensite phase (Ikuta, 1990).

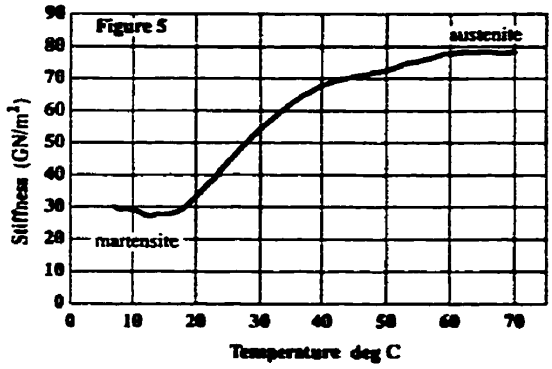

NiTi Fibers: Figure 5 shows results from the authors laboratory where an almost 3–fold change in stiffness (as measured by a 10 Hz tensile force) is obtained from a 0.8 mm NiTi fiber as its is cooled from 70 to 8 °C. If the fiber is immersed in a coolant and then rapidly heated by a brief current pulse passed through it, the fiber will contract and then expand again in < 100 ms. The contraction velocity (strain rate) of the NiTi fibers is a function of externally imposed load as shown in Figure 6. Notice that the peak strain rate (at zero load) is about 3 s^{-1} which is similar to mammalian muscle. The peak generated stress extrapolated to zero velocity (i.e., isometric conditions) is > 200 MN/m^2. This is nearly 1000 times greater than muscle.

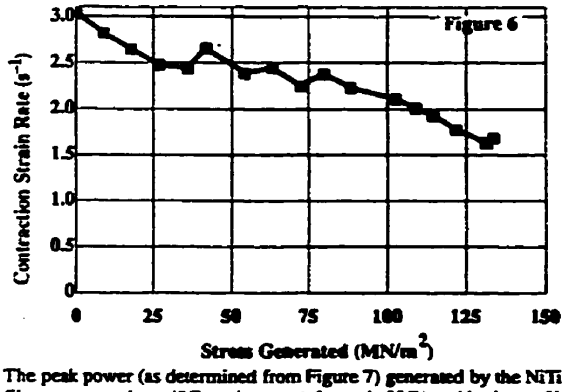

The peak power (as determined from Figure 7) generated by the NiTi fiber occurs at about 40% peak stress (cf muscle 33%) and is almost 50 kW/kg. This is about 1000 times larger than muscle. However it must be remembered that the peak power/mass and peak generated stress values mentioned do not include the mass or volume of the cooling system in which the fiber is immersed. A fair comparison with muscle requires this.

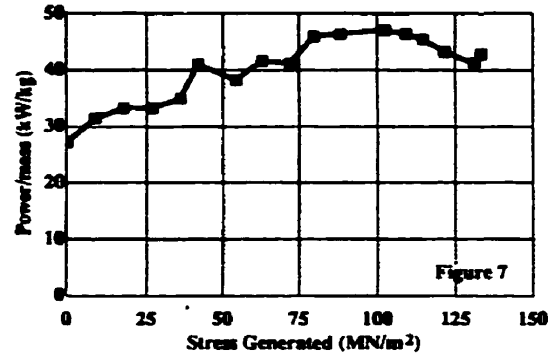

The efficiency with which NiTi converts thermal energy to mechanical energy has been considered by McCormick (1987) and varies from <2% to >3%, when there is full recovery of the heat associated with the thermal capacity. At present no method has been devised to recover this heat while retaining fast cycling. This is because current methods for producing relatively fast NiTi cycling involve continuous flow of a coolant over the NiTi.

POLYMERIC ACTUATORS

History

The study of polymeric actuators dates back 40 years to the work of Kuhn and Katchalsky (Kuhn, 1949; Kuhn et al., 1950; Katchalsky & Oplatka, 1965) who observed substantial, and reversible, chemically induced changes in the dimensions of synthetic polyelectrolyte gels.

Mechanism

Various synthetic polymers are known to convert chemical or electrochemical energy into mechanical energy. They include polyelectrolyte gels, natural and synthetic rubber and cross–linked collagen (see review by Tatara, 1987).

Polyelectrolyte gels: Currently one of the most studied contractile polymer is the polyacrylic acid – polyvinyl alcohol (PAA–PVA) gel which swells in dilute salt solution when a voltage is applied across it (De Rossi et al., 1986; Chiarelli et al., 1987; Chiarelli & De Rossi, 1988). De Rossi et al. (1986) have proposed that the contraction is largely a result of pH gradients (established by the electrode reactions) which propagate through the gel by electrodiffusion resulting in perturbations in the electrostatic interactions between polyelectrolyte ionized groups which in turn cause mechanical deformation of the gel.

Rubber: When natural and synthetic rubbers are immersed in certain organic solvents (e.g., chloroform, toluene, benzene) they expand in volume (up to 300%). When the solvent evaporates the rubber contracts to its original dimensions.

Collagen: When collagen fibers (e.g., from animal tendons) are immersed in CH_2O they become cross–linked and will contract (up to 40%) and expand again in high and low concentration salt solutions respectively (Katchalsky & Oplatka, 1965).

Characteristics

Polymer Gels: Caldwell (1990) has investigated the characteristics of PVA–PAA thin film strips (100 μm thick) which contract when immersed in acetone and expand (swell) when immersed in water. Caldwell (1990) has measured the relation between externally imposed

loads on the PVA–PAA strips and contraction velocity (strain rate). The resulting curve is almost identical in shape to that found for muscle. The peak strain rate which occurs at zero load was 0.1 s^{-1} which is 10 to 100 times slower than muscle. The peak stress generated by the PVA–PAA strips under isometric conditions (i.e., 0 velocity) was 300 kN/m^2 which is similar to mammalian muscle (350 kN/m^2). Caldwell also determined the peak power to be 5.8 W/kg. This is about 10 to 30 times less than human muscle peak power.

Using 10 μm thick polymer gel films Suzuki (1991) has reported 200 ms contraction times with acetone activation. De Rossi et al. (1986) predict that 1 μm thick PVA–PAA gels should be able to achieve strain rates of 5 to 10 s^{-1} which would place them in the range of muscle.

Conducting Polymers: Recent work on electrically conducting polymers (e.g., polyaniline, polyphenylene, polythiophene, polyacetylene, polypyrrole) having low ionization potentials or high electron affinities to permit doping with electron donors or acceptors (see Baughman et al., 1991) has yielded some very promising materials which can be activated with low voltages (< 1 V). Baughman et al. (1991) calculate that doped polyaniline fibers and polyacetylene film should be able to produce stresses of 180 and 450 MN/m^2 respectively. These values are about 1000 times greater than muscle and comparable with shape memory alloys. Although it remains to be seen how quickly such electrically conducting polymers can contract it seems likely that contractions of < 100 ms should be readily achievable.

PIEZOELECTRIC ACTUATORS

History

In 1880 Pierre Curie and his brother discovered that when forces were applied to certain crystals they generated a charge which they found to be roughly proportional to the applied mechanical stress (force). It was quickly realized that the same crystals should show the converse of this effect, namely that an applied voltage should generate deformation of the crystal. Cady (1964) has reviewed the early history of this area.

Mechanism

A simplified model of ceramics (see Uchino, 1986) involves the notion of anions (–) and cations (+) connected by springs forming a crystal lattice. Cations move in the direction of an applied electric field while the anions move in the opposite direction. The forces thereby generated cause lattice deformation. Piezostrictive materials have both high and low stiffness ionic bonds (i.e. are noncentrosymmetric crystals) and have an induced strain, x, which is roughly proportional to the applied electric field, E. The electromechanical coupling is direction–dependent and so is specified by a material dependent piezoelectric tensor d. Thus $x = dE$. Electrostrictive materials are centrosymmetric crystals and have an induced strain which is proportional to the square of the electric field. Thus $x = mE^2$ where m is a material dependent tensor. Other phenomena complicate this simplified view. In particular, additional nonlinear strain changes resulting from crystalline domain reorientation cause the ubiquitous hysteresis seen in piezoelectric materials during changes in electric field.

Characteristics

Of the actuators considered in this paper, piezoelectric actuators follow muscle as being the most ubiquitous. A huge range of piezoelectric actuators have been developed. The small strains (usually < 0.1%) and high stresses (e.g., 35 MN/m^2) generated by piezoelectric materials have spawned a diverse range of displacement amplifying mechanisms such as bimorphs, cantilevers, inchworms, vibromotors, microsteppers and surface–wave motors.

Piezoelectric ceramics: The properties of various piezoceramics are amply documented elsewhere (e.g., Jaffe et al., 1971; Uchino, 1986). A number of interesting actuators involving piezoelectric materials are under development. For example Yano and Takahashi (1989) have developed a novel differential mechanical amplifier coupled to a multilayer piezoelectric ceramic NEPEC–10 ($0.5Pb(Ni_{1/3}Nb_{2/3})O_3$–$0.35PbTiO_3$–$0.15PbZrO_3$). The device amplifies the small strain of the piezoelectric element 50 times, with a corresponding decrease in stiffness, while maintaining overall electro–mechanical efficiencies in the order of 30%. We have instrumented and used this piezoelectric actuator in a number of applications and have achieved very high displacement bandwidths. The device indicates that by coupling piezoelectric elements with novel mechanical amplifiers it should be possible to create modular and muscle–like actuators.

Piezoelectric polymers: Piezo– (or ferro–) electric polymers such as poly–vinylidene fluoride (PVDF) have been proposed for applications requiring an artificial muscle–like actuator (e.g., Lee & Marcus, 1981; Lovinger, 1983). The peak reversible stress and strain developed by PVDF is about 3 MN/m^2 and 0.1% respectively. Unfortunately this latter value is rather small and like piezoelectric ceramics and magnetostrictive materials mechanical amplifiers are needed to produce the larger displacements required by many applications. We have constructed experimental actuators using PVDF and have found the peak stress to be too low for many applications requiring muscle–like performance. For example a 200–fold mechanical amplification is required to make its peak strain similar to muscle. The resulting peak stress is then at best a meager 15 kN/m^2.

MAGNETOSTRICTIVE ACTUATORS

History

In 1840 James Joule discovered that a nickel rod contracted in the presence of a longitudinal magnetic field. In saturating magnetic fields, Ni achieves peak magnetostrictive strains of -0.033×10^{-3}. In 1972 Clark and Belson discovered that when certain rare–earth metals such as terbium and dysprosium are combined with iron, the resulting alloys, $TbFe_2$ (Terfenol) and $DyFe_2$, show very high maximum (magnetic saturation) magnetostrictive strains (specifically $TbFe_2$ at 2.46×10^{-3} and $DyFe_2$ at 1.26×10^{-3}). Unlike Ni and Fe, $TbFe_2$ and $DyFe_2$ show positive magnetostrictive strains and so expand in a magnetic field. Recently an alloy containing both terbium and dysprosium, $Tb_{0.27}Dy_{0.73}Fe_{1.9}$, called Terfenol–D has been developed which has a high magnetostrictive strain (2.0×10^{-3}).

Mechanism

The effect known as magnetostriction is due to magnetic domains in the material aligning themselves with the direction of the magnetic field, with a consequent change in material dimensions (see Clark, 1980). The magnetic field is usually generated by a coil wound around a rod of the magnetostrictive material (e.g., Terfenol–D). By changing the current in the coil the magnetic field is changed and hence the rod changes length.

Characteristics

Some of the properties of Terfenol–D are a function of the technique used to grow the material. Recently (see Clark et al., 1989) techniques have been developed to produce highly grain–oriented rods which result in maximal strains.

Similar to piezoelectric actuators such as PZT, the maximum strain declines roughly linearly with increased force output (load). Terfenol–D has a very high energy density of 14 to 25 kJ/m^3 compared with 0.7 to 1.3 kJ/m^3 for PZT.

Class	SubClass	Example	Density kg/m³	Stress MN/m²	Stiffness GN/m²	Δ	Strain %	Strain Rate s⁻¹	Power W/kg	Energy kJ/m³	Life Cycles	Eff. %
Muscle	skeletal	human	1,037	0.35	0.06	5	> 40	5	>100	0.8	$> 10^9$	>35
	cardiac	h. heart	1,037	0.1	0.05	5	> 40	4	>100	0.8	$> 10^9$	>35
Piezo-electric	ceramic	NEPEC-10	7,500	35	40	1.1	0.09	> 10	>1000	> 10	$> 10^8$	> 30
	polymer	PVDF	1,780	3	3	>1.2	0.1	> 1	>100	> 1	$> 10^6$	< 1
SMA	NiTi	fiber	6,450	> 200	78	3	> 5	3	>1000	> 10	$> 10^5$	> 3
Polymer	gel	PVA-PAA	~1,300	0.3	< 0.1	10	> 40	0.1	> 5	0.4	$> 10^5$	30
	conducting	polyaniline	~1,500	180	5	1.7	> 2	> 1	>1000	> 1	$> 10^5$	> 30
Magneto strictive	rare-earth	Terfenol-D	9,250	70	35	1.4	0.2	1	>1000	> 10	$> 10^5$	< 30
Electro-static	polyimide	SVCMA	1,061	0.04	< 0.01	?	> 10	> 1	> 10	1	?	> 20

Table 1. Properties of a variety of contractile materials. The various quantities shown are peak values and will not in general occur at the same operating point or time. Stress and strain refer to actively generated quantities. The ratio between peak stiffness (shown) and minimum stiffness (not shown) is denoted by Δ . These values are distilled from a wide variety of sources and many will change as better materials types and architectures are developed. In the cases of muscle, piezoelectric, and electrostatic actuators the values presented include the entire actuator size and mass. For the other actuators the required accessories (e.g., NiTi cooling system) are not included in the calculations. Fair comparisons between the latter and former actuators will require such inclusions (which in many cases have not been optimized yet).

Terfenol-D based actuators are limited to peak strains of 0.2%. For displacements larger than 0.2% "inch-worm" type linear stepping actuators (sometimes called magnetoelastic wave motors) have been developed (Kiesewetter, 1988). These motors, which move in small steps (e.g., 10 μm) can move over substantial displacements although at rather low velocities (e.g., 0.01 m/s).

We have built a number of magnetostrictive actuators using Terfenol-D. Unlike piezoelectric actuators, magnetostrictive actuators require bulky coils whose crossectional area is invariably many times greater than that of the magnetostrictive rod. To achieve strains in the order order of 0.2 % requires magnetic fields of over 100 kA/m. Such fields are attained with considerable resistive losses in the coils with the consequent thermal dissipation problems. Coil inductance prevents both high strains and the potentially high strain rates of Terfenol-D being attained in a single design.

ELECTROSTATIC ACTUATORS

History

The history of electrostatic actuators dates back over 150 years. A number of electrostatic motors have been developed (e.g., Bollée, 1969; Jefimenko, 1973) and more recently electrostatic micro-motors have been successfully demonstrated (e.g., Trimmer & Gabriel, 1987; Jacobsen et al., 1989; Tai et al., 1989; Egawa & Higuchi, 1990; Branebjerg & Gravesen, 1992; Sato & Shikida, 1992). The first electrostatic actuator with immediate potential for artificial muscle applications was recently developed by Niino et al., (1992). These researchers have termed their actuator a stacked variable capacitance motor with active slider (SVCMA).

Mechanism

Many electrostatic actuators involve the repulsive force generated between electrodes charged with equal polarities. The SVCMA actuator built by Niino et al., (1992) has multiple stator and slider sheets which slide over each other in a fashion reminiscent of the muscle sarcomere (though about 50,000 times larger). Each sheet is a composite including polyimide film with multiple Cu electrodes fabricated on it. By switching appropriate voltages on the electrodes (e.g., ± 800 V) the stator and slider move relative to each other in 80 μm steps (cf muscle < 50 nm steps).

Characteristics

The SVCMA has a density similar to muscle and can generate peak stresses of 35 kN/m² (about 10% of muscle) and peak strains of > 10% (similar to muscle). The contraction strain rate vs imposed stress relation has the same shape as muscle with peak strain rates similar to slow muscle (i.e., 1 s^{-1}). The peak power of 17 W/kg (cf 200 W/kg for brief muscle contractions) occurs at an imposed stress of about 10% (cf muscle 33%) of maximum. Just as a whole muscle has length and velocity transducers lying in parallel with muscle fibers, the SVCMA has an inbuilt displacement transducer. This is clearly a very promising actuator technology whose only disadvantage may be the high voltages required.

CONCLUSIONS

Comparisons

Table 1 shows the characteristics of examples of the various contractile materials discussed in previous sections. Except for number of cycles to failure (life cycles) muscle is equalled or outperformed in each characteristic by other actuators. However muscle does possess some features not yet achieved by other technologies. Muscle is able to grow and modify itself as a function of imposed stresses and strains. Muscle is also able to repair itself. Indeed the dominant proteins in human muscle are renewed every few months. Muscle is also good to eat !

Stiffness Modulation

One of the most remarkable characteristics of muscle is the large range over which the stiffness of a whole muscle and hence joint can be controlled. For example in a series of studies Kearney and Hunter (see review 1990) have measured up to 50-fold changes in human ankle stiffness resulting from triceps surae activation. The stiffness of one of the authors leg muscles (triceps surae as measured about the ankle joint) is shown in Figure 8. There is almost a 40 fold change in stiffness from rest to maximum contraction. This is much greater than the change found for single muscle fibers (see Table 1). It is important to speculate how this large change can occur at the whole muscle level but not at the single fiber level. In particular other contractile materials may be able to utilize the same mechanism to achieve comparable modulation of stiffness.

The difference between whole muscles and single fibers is most likely due to a significant percentage of whole muscle fibers being slack at "rest" with a progressive decrease in this percentage as contraction level increases. By having a sufficiently large number of fibers in parallel (e.g. 1 million in a human biceps muscle) smooth recruitment of slack fibers can be achieved.

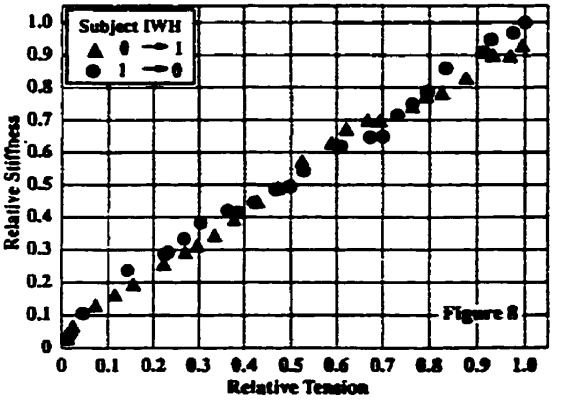

Traditional Actuators

Traditional actuators such as internal combustion, electromagnetic, hydraulic and pneumatic actuators have been extensively studied and developed. While it is true that the development of these technologies has been driven by non-robotic and non-prosthetic applications and that there is room for incremental improvements when they are optimized for particular robotic applications, it is also clear that radical improvements are unlikely in the near future. If nature's experience is relevant, then actuators that can be scaled by parallel configurations of small unit actuators (modularity), as in muscles, is highly desirable. It seems unlikely that in the near future any of the traditional actuator technologies will provide this modularity.

Novel Actuators

A number of novel actuator technologies show great promise. Polymeric, shape memory alloy and electrostatic actuators have the ability to be built in modular form and scaled according to force and displacement requirements. Shape memory alloy actuators have poor efficiencies at present. However, it seems that their efficiency is not constrained theoretically to be so low and consequently future work may be able to increase it substantially. Other novel actuators, such as those involving photostriction (i.e., contract upon application of light), have not been discussed in this paper but also hold considerable promise.

Research Directions

At present the number of research laboratories in the world undertaking research on new actuator technologies is alarmingly small. The prospects of such research making significant advances toward the goal of achieving fast, lightweight, dexterous robots and prosthetic limbs is very high. In particular, work must proceed on the polymeric, electrostatic and shape memory alloy actuator technologies to achieve muscle-like performance. We feel that without substantial emphasis and progress in the development of such novel actuator technologies robotics will flounder and prosthetic limb development will remain moribund.

Finally it must be asserted that there is the very real possibility of fabricating real muscles with specific characteristics. We (like many other groups) have grown fully functioning muscle cells using cell culture techniques and kept them alive for a few weeks. Work is under way in a few laboratories (e.g., Dr. Lee Sweeney, University of Pennsylvania) to synthesize muscle cells with a wide variety of preselected properties. Although this work is difficult and long-term, when successful such "designer muscle" will have vast applications.

ACKNOWLEDGEMENTS

This work was supported by the Medical Research Council (MRC) of Canada, the Canadian Natural Sciences and Engineering Research Council (NSERC) and the Institute for Robotics and Intelligent Systems (IRIS) a Canadian Network of Centres of Excellence. IWH would like gratefully to acknowledge personal support by a General Motors – Canadian Institute for Advanced Research (GM–CIAR) Fellowship. We thank Dr. Bob Kirsch for collecting the muscle data shown in Figures 3 and 4. We also thank Dr. Rob Kearney in whose laboratory the data shown in Figure 8 where collected. Finally special thanks go to Dr. John Hollerbach who has on many occasions provided us with substantial encouragement.

REFERENCES

Basinski, Z.S. and Christian, T. *Acta Metallurgica*, 1954, 2, 101.

Baughman, R.H., Shacklette, L.W., Elsenbaumer, R.L., Plichta, E.J. and Becht, C. Micro electromechanical actuators based on conducting polymers. In P.I. Lazarev (ed.), *Molecular Electronics*, Kluwer: Netherlands, 1991, pp 267–289.

Bergamasco, M. Salsedo, F. and Dario, P. A linear SMA motor as direct–drive robotic actuator. *1989 IEEE International Conference on Robotics and Automation*, May, 1989, Scottsdale, Arizona, 618–623.

Bergamasco, M. Salsedo, F. and Dario, P. Shape memory alloy micromotors for direct–drive activation of dexterous artificial hands. *Sensors and Actuators*, 1989, *17*, 115–119.

Bergel, D.A. and Hunter, P.J. The mechanics of the heart, Chapter 4 in *Quantitative Cardiovascular Studies: Clinical and Research Applications of Engineering Principles*. Edited by N.H.C. Hwang, D.R. Gross and D.J. Patel. University Park Press, Baltimore, 1979. pp 151–213.

Bollée, B. Electrostatic motors. *Philips Technical Review*, 1969, 30, 178–194.

Branebjerg, J. and Gravesen, P. A new electrostatic actuator providing improved stroke length and force. *Proceedings IEEE Micro Electro Mechanical Systems*, 1992, 5, 6–11.

Buehler, W.J., Gilfrich, J. and Wiley, K. *Journal of Applied Physics*, 1963, *34*, 1465.

Cady, W.G. *Piezoelectricity*. McGraw–Hill, New York, 1946. Revised edition by Dover Publications, New York, 1964.

Caldwell, D.G. Pseudomuscular actuator for use in dextrous manipulation. *Medical and Biological Engineering and Computing*, 1990, 28, 595–600.

Chang, L.C. and Read, T.A. *Transactions of the American Institute of Mechanical Engineers*, 1951, *189*, 47.

Chiarelli, P. and De Rossi, D. Determination of mechanical parameters related to the kinetics of swelling in an electrically activated contractile gel. *Progress in Colloid and Polymer Science*, 1988, *78*, 4–8.

Chiarelli, P., Genuini, G. and De Rossi, D. Electrochemically driven muscle–like actuators. *IEEE 9th Annual Conference of the Engineering in Medicine and Biology Society*, 1987, *9*, 1089–1091.

Clark, A.E. and Belson, H.S. Giant room–temperature magnetostrictions in $TbFe_2$ and $DyFe_2$. *Physical Review*, 1972, *B5*, 3642–3644.

Clark, A.E. Magnetostrictive rare earth–Fe_2 compounds. In *Ferromagnetic Materials Vol. 1*, edited by E.P. Wohlfarth, North–Holland, 1980, pp. 531–589.

Clark, A.E., Teter, J.P., Wun–Fogel, M., Moffett, M. and Lindberg, J. Magnetomechanical coupling in Bridgman grown $Tb_{0.3}Dy_{0.7}Fe_{1.9}$ at high drive levels. *34th Conference on Magnetism and Magnetic Materials*, Boston, 1989, *34*, 1–12.

De Rossi, D., Chiarelli, P., Buzzigoli, G., Domenici, C. and Lazzeri, L. Contractile behavior of electrically activated mechanochemical

polymer actuators. *Transactions of the American Society for Artificial Internal Organs*, 1986, 32, 157–162.

Egawa, S. and Higuchi, T. Multi-layered electrostatic film actuator. *Proceedings IEEE Micro Electro Mechanical Systems*, 1990, 3, 166–171.

Funakubo, H. (ed.) *Shape Memory Alloys*. Gordon and Breach: New York, 1987.

Hashimoto, M. Takeda, M. Sagawa, H. Chiba, I. and Sato, K. Application of shape memory alloy to robotic actuators. *Journal of Robotic Systems*, 1985, 2, 3–25.

Higuchi, H. and Goldman, Y.E. Sliding distance between actin and myosin filaments per ATP molecule hydrolysed in skinned muscle fibers. *Nature*, 1991, 352, 352–354.

Hirose, S., Ikuta, K. and Umetani, Y. Development of shape–memory alloy actuators. Performance assessment and introduction of a new composing approach. *Advanced Robotics*, 1989, *3*, 3–16.

Hirose, S., Ikuta, K. and Umetani, Y. A new design method of servo–actuators based on the shape memory effect, in *Theory and Practice of Robots and Manipulators, Proceedings of RoManSy '84, the 5th CISM–IFToMM Symposium*, Hermes Publishing, 1985, 339–349.

Hirose, S., Ikuta, K. and Sato, K. Development of a shape memory alloy actuator. Improvement of output performance by the introduction of a s–mechanism. *Advanced Robotics*, 1989, *3*, 89–108.

Hollerbach, J.M., Hunter, I.W. and Ballantyne, J. A comparative analysis of actuator technologies for robotics. In The Robotics Review 2, O. Kahatib, J.J. Craig and T. Lozano–Perez, eds., MIT Press, Cambridge, Mass., 1991, 301–345.

Homma, D., Miwa, Y. and Iguchi, N. Micro robots and micro mechanisms using shape memory alloy. *The 3rd Toyota Conference Integrated Micro Motion Systems: Mircomachining, Control and Application. Nissin, Aichi, Japan*, October, 1989, 22, 1–21.

Hunter, I.W. Novel Actuators For Use in Robotics And Tele–Robotics, Report Prepared for the US Office of Naval Research, 1990, 88p.

Hunter, I.W., Lafontaine, S., Doukoglou, T.D., Jones, L.A., Korenberg, M.J., Nielsen, P.M.F., Kirsch, R.F. and Kearney, R.E. Micro–robotics and the study of muscle: special problems in control, system identification and modelling. *IFAC Symposium on Identification and System Parameter Estimation*, 1991, Budapest, Hungary, pp. 197–202.

Hunter, I.W., Lafontaine, S. and Hollerbach, J.M. Artificial muscle prototype for use in robotic and prosthetic limbs. *Proceedings of the 16th Canadian Medical and Biological Engineering Conference*, 1990, *16*, 35–36.

Hunter, I.W., Lafontaine, S., Hollerbach, J.M. and Hunter, P.J. Fast reversible NiTi fibers for use in microrobotics. *Proceedings IEEE Micro Electro Mechanical Systems*, 1991, 2, 166–170.

Hunter, I.W., Lafontaine, S., Nielsen, P.M.F., Hunter, P.J. and Hollerbach, J.M. Manipulation and dynamic mechanical testing of microscopic objects using a tele–micro–robot system. IEEE Control Systems Magazine, 1990, *10*, 3–9.

Hunter, I.W. and Korenberg, M.J. The identification of nonlinear biological systems: Wiener and Hammernein cascade models. Biological Cybernetics, 1986, *55*, 135–144.

Hunter, P.J., Nielsen, P.M.F., Smaill, B.H., LeGrice, I.J. and Hunter, I.W. An anatomical heart model with applications to myocardial activation and ventricular mechanics. Accepted for publication in High Performance Computing in Biomedical Research (Ed. Theo Pilkington) CRC Press, October 1992.

Huxley, A.F. *Reflections on muscle*. Princeton University Press: Princeton, New Jersey, 1980.

Ikuta, K. Micro/miniature shape memory alloy actuator. *Proceedings IEEE Micro Electro Mechanical Systems*, 1990, *3*, 2156–2161.

Ishijima, A., Doi, T., Sakurada, K., and Yanagida, T. Sub–piconewton force fluctuations of actomyosin *in vitro*. *Nature*, 1991, *352*, 301–306.

Jacobsen, S.C., Price, R.H., Wood, J.E., Rytting, T.H. and Rafaelof, M. The wobble motor: an electrostatic planetary–armature, micro-actuator. *Proceedings IEEE Micro Electro Mechanical Systems*, 1989, 2, 17–24.

Jaffe, B., Cook, W.R. and Jaffe, H. *Piezoelectric ceramics*. Academic Press, London, 1971.

Jefimenko, O.D. Electrostatic motors. In A.D. Moore (ed.) *Electrostatics and its applications*, Wiley: New York, 1973, 131–147.

Katchalsky, A. and Oplatka, A. Mechanochemical engine. Proceedings of the 4th International Congress on Rheology. E.H. Lee and A.L. Copley (eds.). Interscience, New York, 1965, 73.

Kearney, R.E. and Hunter, I.W. System identification of human joint dynamics. *CRC Critical Reviews of Biomedical Engineering*, 1990, *18*, 55–87.

Kiesewetter, L. The application of Terfenol in linear motors. *Proceedings of the 2nd International Conference on Giant Magnetostrictive and Amorphous Alloys for Sensors and Applications*, 1988, 2, 1–18.

Korenberg, M.J. and Hunter, I.W. The identification of nonlinear biological systems: LNL cascade models. Biological Cybernetics, 1986, *55*, 125–134.

Korenberg, M.J. and Hunter, I.W. The identification of nonlinear biological systems: Wiener kernel approaches. Annals of Biomedical Engineering, 1990, *18*, 629–654.

Korenberg, M.J. and Hunter, I.W. The identification of nonlinear biological systems: Volterra kernel approaches. *Annals of Biomedical Engineering*, 1992, submitted.

Kudo, S., Magariyama, Y. and Aizawa, S–I. Abrupt changes in flagellar rotation observed by laser dark–field microscopy. *Nature*, 1990, *346*, 677–679.

Kuhn, W. Artificial muscle model. *Experientia*, 1949, *5*, 318

Kuhn, W., Hargitay, B., Katchalsky, A. and Eisenberg, H. Mechanochemical system. Nature, 1950, 165, 514

Lee, J.K. and Marcus, M.A. The deflection–bandwidth product of poly(vinylidene fluoride) benders and related structures. *Ferroelectrics*, 1981, *32*, 93–101.

Lovinger, A.J. Ferroelectric polymers. *Science*, 1983, *220*, 1115–1121.

MacNeil, J.B., Kearney, R.E. and Hunter, I.W. Identification of time–varying biological systems from ensemble data. *IEEE Transactions on Biomedical Engineering*, 1992, submitted.

McCormick, P.G. On the practical efficiency of shape memory engines. *Scripta Metallurgica*, 1987, *21*, 99–101.

Nielsen, P.M.F. and Hunter, I.W. Identification of the time–varying properties of the heart. In L. Glass, P.J. Hunter and A. McCulloch (eds.), *Theory of heart: biomechanics, biophysics, and nonlinear dynamics of cardiac function*, Springer–Verlag, 1991, 77–86.

Niino, T., Egawa, S., Nishiguchi, N. and Higuchi, T. Development of an electrostatic actuator exceeding 10N propulsive force. *Proceedings IEEE Micro Electro Mechanical Systems*, 1992, *5*, 122–127.

Otsuka, K. and Shimizu, K. *Scripta Metallurgica*, 1970, 4, 469.

Sato, K. and Shikida, M. Electrostatic film actuator with a large vertical displacement. *Proceedings IEEE Micro Electro Mechanical Systems*, 1992, *5*, 1–5.

Suzuki, M. Amphoteric polyvinyl alcohol hydrogel and electrohydrodynamic control method for artificial muscles. In D. De Rossi (ed.) *Polymer Gels*, Plenum Press: New York, 1991, pp. 221–236.

Tai, Y.C., Fan, L.S. and Muller, R.S. IC–processed micro–motors: design, technology, and testing. *Proceedings IEEE Micro Electro Mechanical Systems*, 1989, 2, 1–6.

Tatara, Y. Mechanochemical actuators. *Advanced Robotics*, 1987, 2, 69–85.

Trimmer, W.S.N. and Gabriel, K.J. Design considerations for a practical electrostatic micro–motor. *Sensors and Actuators*, 1987, *11*, 189–206.

Uchino, K. Electrostrictive actuators: materials and applications. *Ceramic Bulletin*, 1986, *65*, 647–652.

Yano, T. and Takahashi, S. Utilization of piezoelectric stiffened effects on impact printer heads. *Electronics and Communications in Japan*, 1989, 72, 19–32.

Appendix III.

Lafontaine, S.R., Hunter, I.W. and Jones, L.A. NiTi artificial muscles for micro-robotics and medical applications. *Proceedings of the International Conference on Industrial Applications of Shape Memory Alloys*, Quebec City, July, 1994.

NiTi Artificial Muscles for Micro–Robotics and Medical Applications.

Serge R. Lafontaine, Ian W. Hunter and Lynette A. Jones
Department of Mechanical Engineering,
Massachusetts Institute of Technology, Cambridge, Massachusetts, U.S.A.

Introduction

New smart materials are required in micro–robotics and medical devices for actuation, control, energy supply, and fabrication. Muscle–like actuators which combine large power–to–mass ratios, high forces per unit area and wide bandwidths are needed to actuate small and micro–mechanisms. We are currently investigating two classes of smart materials: NiTi alloys and synthetic metals, i.e. electrically conducting, contractile polymers. At present, the research with synthetic metals is at the level of basic science. New "muscle–like" actuators are being developed, however, from fast contracting NiTi fibers (Hunter et al., 1991) which are also being used for new high–performance parallel drive mechanisms for master–slave tele–micro–robots and endoscopic devices. This research and its future directions will be summarized in this paper.

Artificial Muscle Actuators

Muscle as an actuator

Muscle has been used as a standard against which the performance and characteristics of other actuators has been compared (see Table 1 derived from Hollerbach et al., 1991; Hunter 1990; Hunter & Lafontaine, 1992). An important characteristic of muscle is its ability to generate both relatively high tensions (350 kN/m^2) as well as large and rapid changes in length (> 20%). Muscle is also a light actuator which is an important property for autonomous robots (or androids). In other respects such as in its power/mass ratio, muscle is in the low to average range of performance. Another important feature of muscle not listed in Table 1 is its very long life time which exceeds 10^9 cycles.

There are indications that the composition of muscles has not changed appreciably from early dinosaurs to present day mammals. Muscles consist of a bundle of fibers arranged in parallel and held together by connective tissue. The maximum force per unit area remains fairly constant across mammals as does the maximum strain. The force generated by a muscle is controlled using a combination of two mechanisms: recruitment, which is the capacity to change the number of muscle fibers activated at a particular instant, and rate coding, which refers to the frequency with which these fibers are stimulated or activated by repetitive pulses.

Large changes in stiffness occur in muscle as a function of the force generated. These changes are in the order of a ten–fold range from rest to maximum force (Hunter et al, 1993). The stiffness of a joint about which a pair of agonist and antagonist muscles insert can be changed by varying the forces produced by the two groups of muscles. It is possible for the net torque to remain constant while the stiffness of the joint varies over a considerable range of values.

Actuator	Max. Strain	Max. Strain Rate	Max. Power/ Mass	Max. Stress	Max. Torque/ Mass	Mech. Efficiency
	%	/s	W/kg	M N/m^2	N.m/kg	%
Muscle	20	2	50	0.35	20	35
NiTi	>6%	3	>1,000	>150	~700	<6
Polymer	?	>1	>1,000	180	?	>30
Electro–static	>10	>1	>10	.04	<1	>20
Magneto–strictive	0.2	1	>1,000	70	7	>80
Piezo–electric	0.21	>10	>1,000	35	2.6	>80

Table 1. Properties of different actuators. Some of these figures are estimates and more accurate figures will become available as research progresses or new materials are developed. These values do not represent fair comparisons between actuators as the required accessories are not included in the calculations. The torque–to–mass ratio for linear actuators is estimated as the peak torque in a simple lever mechanism which rotates by 60 degrees.

NiTi as an artificial muscle actuator

Actuators consisting of a number of NiTi fibers arranged in parallel, as opposed to coil–like configurations, are considered here. NiTi artificial actuators exceed by a factor of 35 the maximum torque/mass ratio of muscle. This figure does not, however, include the weight of associated control circuitry and ancillary power sources. The high peak tension (stress) generated by NiTi fibers (about 800 times greater than muscle) is effectively much less when the area around the fibers required for cooling is considered.

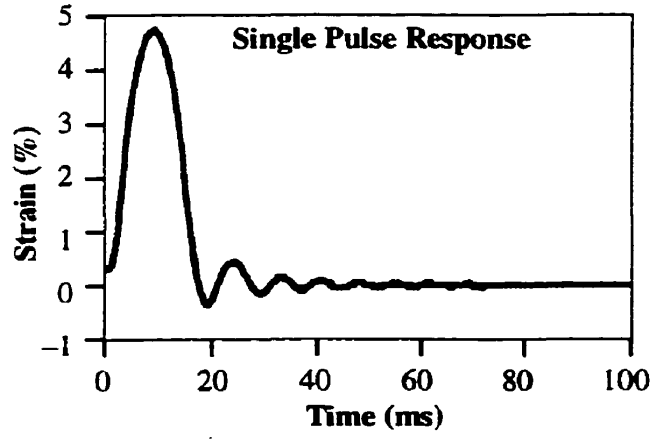

Figure 1. NiTi fiber twitch response.

NiTi actuators are usually considered slow devices. They can contract quickly but their relaxation time is considerably longer. We have found that when NiTi fibers are submitted to brief, very large current pulses, after a period of training, the fibers return to their original length much

more rapidly (Hunter et al, 1991). Figure 1 shows the twitch response of a NiTi shape memory actuator where the response is completed in less than 20 ms.

Figure 2 shows the stiffness of NiTi fibers as a function of temperature cycling. These results indicate that very large changes in stiffness occur in NiTi fibers. This phenomenon has been observed using two different experimental setups and different types of analysis. The change in stiffness can vary by a factor of 10 as revealed by linear analysis and impulse response estimation. The mechanisms responsible for these changes in stiffness are not as yet known. These results indicate, however, that like muscle, the stiffness of NiTi artificial muscle actuators can be controlled over a large range of values.

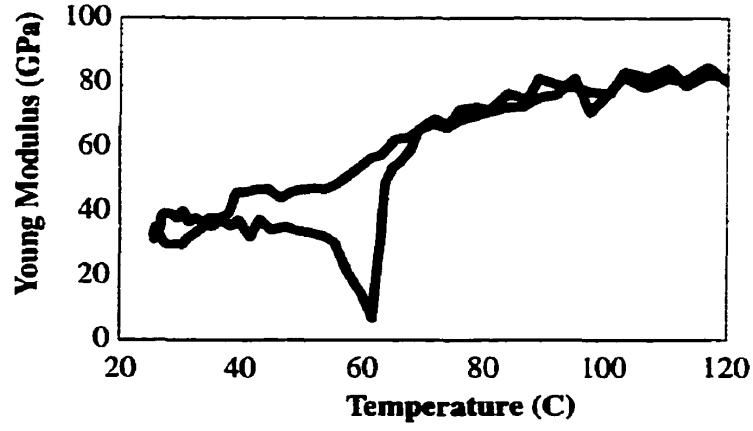

Figure 2. Example where NiTi stiffness changes by a factor of 10.

The maximum strain of NiTi fibers is about one third that of muscle. As a consequence, in order to make the same angular movement as a muscle controlling a limb, the lever arm controlled by the NiTi actuator would be one third the size and much larger stresses would be produced at the end of the fibers where they are mechanically secured.

NiTi actuators cannot compete with muscle when compared on the basis of life cycles or efficiency. Applications of NiTi actuators are therefore severely limited at present in situations where power consumption is of primary importance or where long life times are required. An example of the latter would be in an artificial heart.

High Performance Parallel Drive Mechanisms

Parallel Drive Mechanisms

In micro–robotics, both micro–motion robots and autonomous micro–robots have their applications. We have developed a number of very high performance micro–motion robots for applications in biology, engineering (micro–machining and micro–fabrication) (see Hunter et al., 1990, Olivier et al., 1993) and medicine (master–slave robot for retinal surgery) (see Hunter et al, 1993). In order to maximize the bandwidth of the mechanical systems, it is essential that all actuators operate independently (i.e. in parallel) rather than rely on serial configurations where one actuator is mounted on a limb moved by another actuator. In many of our designs (Hunter et al, 1990)

molecular hinging in flexure elements has been used to couple together movements from several motors which still maintains micro–motion accuracy.

Superelastic NiTi flexure elements

Although parallel drive systems with flexure elements have been used successfully in micro–motion robots, there are problems associated with using them in medical robots where large ranges of motion are required. The large changes in angular displacements at flexure elements introduce strains beyond the limits of elasticity of conventional materials (e.g. 0.2%) which fail after a short period of use. We have been experimenting successfully with using super–elastic NiTi wire as flexure elements. NiTi can undergo strain changes exceeding 6% which permits very large ranges of angular displacements at flexure joints.

New developments in fabrication of micro–actuators

One major difficulty that must be faced when using NiTi shape memory alloys is the considerable problems associated with attaching NiTi alloys mechanically to other structures and with making reliable electrical connections. Standard welding or soldering techniques cannot be used with NiTi alloys. Recently CO_2 laser butt welding has been successfully used and it has been shown that there are no significant changes in stress–strain curves or residual strain in welded specimens (Araki et al., 1989; Hirose et al, 1990).

We have recently developed a new and simple technique which permits soldering as well as conventional welding techniques for electrically and mechanically connecting NiTi shape memory alloys. It is now possible to attach NiTi shape–memory alloys or super–elastic fibers directly to other structures. This technique lends itself easily to parallel processing of a large number of fibers. Furthermore it intrinsically preserves all of the NiTi shape memory or super–elastic properties of the alloys except at the location where the fibers are attached. This new technique permits fabrication of micro–actuators in micro–robots which was previously not feasible because of difficulties in mounting the fibers.

Micro–mechanisms

A unique micro–fabrication and micro–machining center has been developed in the laboratory (Madden et al, 1994). Microscopic parts (such as micro–springs) have been fabricated and eventually the fabrication center will be used to construct micro–mechanisms. In conjunction with the new welding, soldering and mechanical attachment techniques described above, it will soon be possible to build, for the first time, micro–actuators and micro–robots using NiTi fibers.

Medical Simulators

A number of medical simulators are being developed for use in training surgeons and for rehearsing surgical procedures. A laparoscopic simulator consisting of a physical model of the human torso with surgical instruments has been built in conjunction with a complete virtual environment which includes a finite element models of the organs inside the torso. The surgeon either wears a heads up display or special glasses for stereoscopic viewing of the virtual tools and organs. Surgical tools are held by the surgeon which are instrumented so that their positions are known exactly and virtual forces exerted by the tools are solved by the finite element model and fed back to the surgeon via force reflecting multi–degree–of–freedom interfaces. The use of fast contracting NiTi actuators and NiTi super–elastic hinges in these force reflecting interfaces holds great promise.

Internet Experiment: A Virtual Laboratory

The traditional process of publishing scientific results is somewhat incompatible with the scientific method. One paradigm of science consists of an iterative process in which experiments are performed, data gathered, a model formulated and the validity of the model tested by simulation and quantitative comparison with the experimental data. Typically new experimental results are reproduced independently by other teams of researchers who test the reliability and validity of the experiments.

In scientific publications it is usually not possible, economical or practical to include raw experimental data, except in the form of plots and graphs. Consequently testing alternate models is extremely difficult for researchers who have access only to printed publications. Often experiments other than those performed for the publication are required to verify a new model. We have therefore proposed that not only journals, but experimental data and the experimental apparatus itself should be made available to other research groups through high speed networks (Lafontaine et al., 1994).

For this experiment we have decided to use Mosaic/WWW as the basis of our virtual laboratory for the following reasons: World Wide Webb (WWW) provides fast dissemination of available services; it is developed around a hypertext documentation system with optional viewers for postscript high quality hardcopies; images, sound and movies can also be displayed with external viewers and which will permit remote inspection of the experimental setup; and has access to FTP for transfer of raw binary data.

This service will be made publicly available later this year. At that point after obtaining the authorization via email, any researcher using X–Windows and Mosaic will be able remotely to repeat experiments, such as those in which the stiffness of NiTi fibers was investigated (Fig. 2), to inspect data and use different numerical techniques to check results.

Conclusion

Although NiTi shape memory alloys have a number of limitations as actuators, including being highly inefficient in their energy conversion and having short life–times, their potential for application is large in micro–robotics and in a number of areas in medicine. Other types of smart materials, such as polymeric actuators, offer greater advantages but research is only starting in this area and it will be many years before practical applications can be considered.

Acknowledgements

We wish to gratefully acknowledge the support provided by grants from the U.S. Office of Naval Research and the Natural Sciences and Engineering Research Council of Canada.

References

Araki, T., Hirose, A., Uchihara, M., Kohno, W., Honda, K., and Kondoh, M. Characteristics and fracture morphology of Ti–Ni type shape memory alloy and its laser weld joint. Journal of the Society of Materials Science, 1989, Japan, 38,. 428, 478–483

Hirose, A., Uchihara, M., Araki, T., Honda, K., and Kondoh, M. Laser welding of Ti–Ni type shape memory alloy, Journal of the Japan Institute of Metals, 1990, 54, 3, 262–269.

Hollerbach, J.M., Hunter, I.W. and Ballantyne, J. A comparative analysis of actuator technologies for robotics. In the Robotics Review 2, O. Kahatib, J.J. Craig and T. Lozano–Perez, eds., MIT Press, Cambridge, Mass., 1991, 301–345.

Hunter, I.W. Novel Actuators for use in robotics and tele–robotics. Report prepared for the US Office of Naval Research, 1990, 88p.

Hunter, I.W. and Lafontaine, S. A comparison of muscle with artificial actuators. Technical Digest of the Fifth IEEE Solid State Sensor & Actuator Workshop, 1992, 5, 178–185.

Hunter, I.W., Lafontaine, S., Nielsen, P.M.F., Hunter, P.J. and Hollerbach, J.M. Manipulation and dynamic mechanical testing of microscopic objects using a tele–micro–robot system. IEEE Control Systems Magazine, 1990, 10, 3–9.

Hunter, I.W., Lafontaine, S., Hollerbach, J.M. and Hunter, P.J. Fast reversible NiTi fibers for use in microrobotics. Proceedings IEEE Micro Electro Mechanical Systems, 1991, 2, 166–170.

Hunter, I.W., Jones, L.A., Sagar, M., Doukoglou, T., Lafontaine, S., Charette, P.G., Mallinson, G.D. and Hunter, P. (1993). A teleoperated microsurgical robot and associated virtual environment for eye surgery. Presence, 1993, 2, 265–280.

Lafontaine, S. and Hunter, I.W. Muscles for Robots: Internet/Mosaic Experiment, IRIS/PRECARN Annual Conference IV, Toronto, June 1994.

Madden, J., Hunter, I.W., Madden, P.G., Brenan, C.J.H. and Lafontaine, S. Spatially constrained electrodeposition. Engineering Foundation Conferences: Nanofabrication and biosystems: frontiers and challenges, Keauhou–Kona, Hawaii, May, 1994.

Olivier, M., Hunter, I.W., Lafontaine, S., Brenan, C.J.H., Laferriere, A. and Patterson, L.R.B. A tele–nano–positioning–robot for micro–fabrication and micro–assembly. IARP Workshop on Micro–Machines, Japan, October 1993.

Appendix IV. List of Material Properties for NiTi

Constant	Units	Alloy	Austenite	R	martensite	Source
Resistivity	μΩ·m		.82		.76	5
			.77	.91	.76	2
			.76	.98	.87	6
				1.1	.5	3
			1		.8	8
			.6		.75	9
Resistivity Sensitivity	μΩ·m/°C		8×10^{-4}	0	$7.\times10^{-4}$	6
Thermal Expansion	$°C^{-1}$		11×10^{-6}		6.6×10^{-6}	7,8
Sensitivity of transition temperatures	°C/Pa			8.8×10^{-8}	2.3×10^{-7}	6
Annealing	°C	400-600				5
Melting		1300				5,9
Heat Capacity	kJ/kg/°C	.322				5
		.883				7,8,9
Latent Heat	kJ/kg	24.2				7,8
Poisson Ratio		.33				9
Young's Modulus	Gpa		75		28	5
		95				3
			23	15	20	6
			83		28-41	8
Magnetic Permeability		<1.002				8
Magnetic Susceptibility			3.8		2.5	
			2.1		3.0	9
Thermal Conductivity	W/m/°C		18		8	5
		18				3
			18		8.6	8
		30				9
Density	kg/m^3	6450				7, 8, 9
Yield strength	MPa		600			5
			195-690		70-140	8
Tensile Strain	%				50	3
		25-50				8
Tensile Strength	MPa	1000				5
		895-1900				8
Efficiency	%	5				5
		3				2
Velocity of sound	m/s	5100-5300				
Max. Strain	%	8				5
Hardness	R_B	80				9
Abrasion Resistance	m^3/cycle	$8x10^{-17}$				9
Work output	kW/kg	1000				5
		100				2

Data From:

(1) Funakubo (1987)

(2) From experimental work in this thesis.

(3) Van Humbeck (1991)

(4) Duerig *et al.* (1990)

(5) Gilbertson (1994)

(6) Ikuta et al. (1991)

(7) Flexinol Inc.

(8) SMA Inc.

(9) Innovative Technology International, Inc.